N_2O Production in the Global Ocean: Controls by Nitrification and Denitrification Pathways

by

Rebecca Pierce

B.Eng., B.Sc., Queen's University, 2020

A Thesis Submitted in Partial Fulfillment of the Requirements for the Degree of

MASTER OF SCIENCE

In the School of Earth and Ocean Sciences

We acknowledge and respect the lək̓ʷəŋən peoples on whose traditional territory the university stands and the Songhees, Esquimalt and W̱SÁNEĆ peoples whose historical relationships with the land continue to this day.

N_2O Production in the Global Ocean: Controls by Nitrification and Denitrification Pathways

By

Rebecca Pierce

B.Eng., B.Sc., Queen's University, 2020

Supervisory Committee

James Christian, Co-Supervisor
School of Earth and Ocean Sciences

Roberta Hamme, Co-Supervisor
School of Earth and Ocean Sciences

Tetjana Ross, Committee Member
School of Earth and Ocean Sciences

Abstract

Nitrous oxide (N_2O) is a potent greenhouse gas with a high global warming potential, but the underlying processes behind N_2O production and consumption are not well understood. The ocean is known to be a strong source of N_2O to the atmosphere, yet ocean N_2O production is poorly constrained at anywhere from 10 to 53% of the total N_2O atmospheric source. In order to narrow down estimates of net N_2O production in the ocean, I have created a steady state model to explore the uncertainties involved in the biological processes that contribute to N_2O production and consumption (nitrification and denitrification). Model results show that oxygen and organic matter supply strongly control N_2O production and consumption rates, and also demonstrate strong dependence on parameters such as the oxygen threshold for oxic versus suboxic remineralization, the oxygen concentration dependence of N_2O reduction to N_2, the proportion of suboxic and oxic remineralization in relation to oxygen, and the attenuation length scale of sinking organic matter. Additionally, I find that global net N_2O production rates are heavily influenced by the oxygen data input into the model: interpolation of oxygen data or averaging of monthly oxygen data to an annual mean can lead to underestimation of denitrification. As suboxic conditions are required for denitrification to produce (and consume) N_2O, precise and accurate oxygen data is integral to constraining estimates of global ocean N_2O production.

The results of the base case scenario of the model, as well as from a number of sensitivity experiments, indicate that the source and sink terms for N_2O production are larger than suggested by many past models. N_2O production and consumption by denitrification are high in oxygen deficient zones (19.2 Tg-N y^{-1} and 8.37 Tg-N y^{-1}, respectively) while global total nitrification production is low (0.740 Tg-N y^{-1}). N_2O production by denitrification is primarily responsible for generating relatively high net N_2O production rates in the global ocean (11.5 Tg-N y^{-1} for the base case scenario), and likely provide a greater proportion of global N_2O emissions to the atmosphere than many previous estimates. Model representation of denitrification production and consumption rates is highly sensitive to changes in oxygen concentration and parameters related to oxygen, suggesting that altered ocean environments due to future climate change may have a large effect on N_2O production in the ocean. This research isolates the uncertainties that most impact N_2O production and consumption processes and suggests pathways of future research to narrow down these uncertainties. In particular, I recommend more in-situ oxygen sampling with high precision and accuracy (especially in oxygen deficient zones), experimental research to constrain important parameters, and separation of N_2O production by nitrification, N_2O production by denitrification, and N_2O consumption by denitrification in future model development (as in this model).

Table of Contents

List of Figures

List of Tables

Dedication

I'd like to thank my supervisors and family for being patient, supportive, and understanding throughout the course of this research – especially as it took place during the course of the COVID19 pandemic. This thesis is dedicated to all students who kept up their studies during the pandemic and lockdown.

"I wish it need not have happened in my time," said Frodo.

"So do I," said Gandalf, "and so do all who live to see such times. But that is not for them to decide. All we have to decide is what to do with the time that is given us."

-J.R.R. Tolkien, The Fellowship of the Ring

I'd also like to thank my friends and neighbours, who helped me stay sane when we were isolated and whose positive thinking ensured that this thesis reached its completion.

1 Introduction

Nitrous oxide (N_2O) is a potent greenhouse gas that has a high Global Warming Potential and can contribute to anthropogenic climate change and ozone depletion, despite occurring in trace concentrations (Ravishankara et al. 2009, Portmann et al. 2012, Ciais et al. 2013, Müller et al. 2021). N_2O's Global Warming Potential is 265-298 times that of carbon dioxide for a 100-year timescale, and N_2O gas emitted to the atmosphere can remain there for more than 100 years (Ciais et al. 2013, Makowski 2019). An estimated 10-53% of total N_2O sources are from ocean contributions (Anderson et al. 2010, Freing et al. 2012, Ciais et al. 2013, Bange et al. 2019). This large range of estimates demonstrates how global and regional N_2O emissions from the ocean are still not well constrained. This is in part due to a fundamental lack of understanding of the nitrogen cycle processes involved – particularly the contributions of nitrification and denitrification to N_2O production.

The extent of nitrification and denitrification in the ocean remains a subject of contention, as do rates of N_2O production and subsequent efflux from the ocean (Yool et al. 2007, Freing et al. 2012, Babbin et al. 2015, Battaglia and Joos 2018, Bange et al. 2019). Nitrification is known to occur in oxic waters, with reaction rates decreasing in suboxic concentrations while N_2O yield from nitrification increases as O_2 decreases (Nevison et al. 2003, Grundle et al. 2012, Ji et al. 2018). Denitrification only occurs in suboxic waters, where N_2O is produced at a certain suboxic range of O_2 but is consumed at extremely low, near-anoxic O_2 concentrations (Dalsgaard et al. 2014, Babbin et al. 2015, Kelly et al. 2021). *In situ* measurements of N_2O production and consumption rates by these processes report a wide range of values that are affected by both oxygen and organic matter supply, making the degree to which these reactions are controlled by environmental conditions and substrate availability difficult to determine. Researchers have found some success in estimating a range of global net N_2O production rates using modelling and laboratory data, but the scale at which each process contributes to the global ocean's production of N_2O is not completely understood and so resulting production rates are often poorly defined (Zamora and Oschlies 2014, Babbin et al. 2015, Battaglia and Joos 2018, Tian et al. 2020). In a changing climate, the magnitude and distribution of nitrification or denitrification in various regions of the ocean may change (Codispoti 2010, Martinez-Rey et al. 2015, Battaglia and Joos 2018). This could mean a substantial change in the outgassing of greenhouse gases in some regions.

This research models the contributions to N_2O production from nitrification and denitrification in order to clarify what changes in environmental conditions will most affect ocean N_2O emissions. In doing so, the key controls and uncertainties of these processes will be identified, highlighting the missing observational data most crucial to improving understanding of N_2O production. The results from this model, corroborated by quantifications of additional uncertainties, aim to improve accuracy of future Earth System Models.

The marine nitrogen cycle controls the ocean's productivity though nutrient availability (Gruber and Galloway 2008, Lam and Kuypers 2011), but the ongoing discovery of new processes and organisms complicates mathematical representation of the processes involved (Capone et al. 2008, Kalvelage et al. 2011, Thamdrup 2012). As anthropogenic change affects biogeochemical processes in new and often unexpected ways, understanding the existing nitrogen cycling pathways and mechanisms of N_2O production will become increasingly important (Codispoti et al. 2001, Bange et al. 2019). To better anticipate the future ecosystem our society will inhabit it

is imperative that marine scientists understand what nitrogen cycling pathways occur, the relevant reaction rates, and how they may change in the future.

Nitrogen cycling processes that impact N_2O production are shown in Figure 1 below, although the representation of these processes in the mathematical model will be condensed and simplified (especially in the case of denitrification). Remineralization of organic nitrogen (N_{org}) produces ammonium (NH_4^+), which can then undergo nitrification to produce nitrate (NO_3^-) and, as a by-product, nitrous oxide (N_2O). In low oxygen conditions (O_2 less than approximately 6 μmol-O_2 L^{-1}), denitrification occurs through reduction of nitrate and nitrite (NO_2^-) to nitrous oxide as well as reduction of nitrous oxide itself to dinitrogen (N_2).

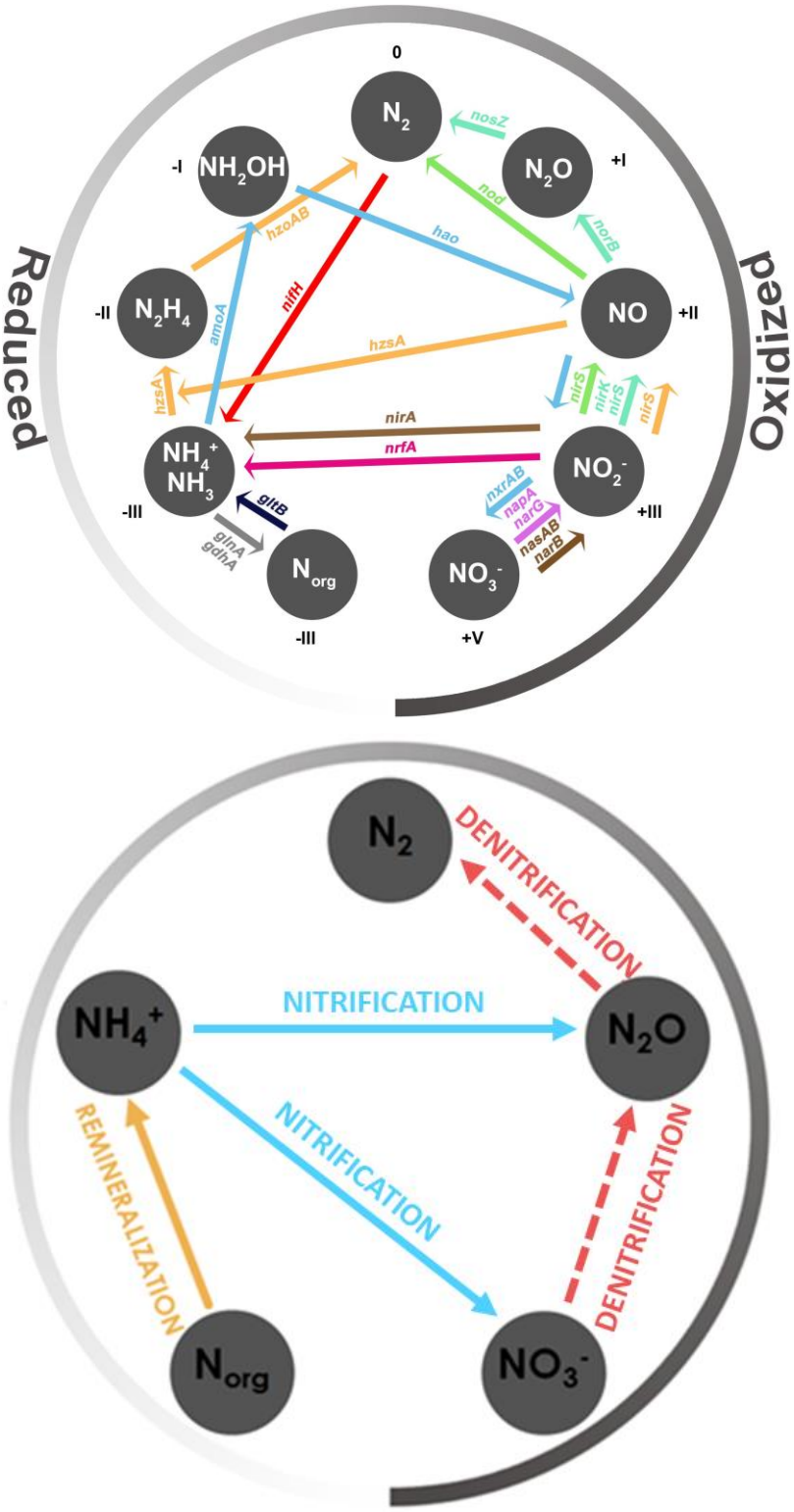

Figure 1: Nitrogen Cycle Diagrams. Top image shows the full scope of the nitrogen cycle from Pajares & Ramos 2019, while the bottom image is processes that are directly relevant to N_2O and that are included in this model.

Nitrification and denitrification pathways will be the emphasized for the purpose of this study due to their direct contributions to N_2O production, although there are other as-yet unverified biological sources or sinks for N_2O that are neglected here due to lack of concrete information. Some of these processes include anaerobic ammonium oxidation (anammox) (Dalsgaard et al. 2012) and dissimilatory nitrate reduction to ammonium (DNRA, or nitrate/nitrite ammonification) (Lam and Kuypers 2011). Additionally, recent research suggests that there may be a substantial difference in the reaction kinetics and controls on nitrification between bacteria and archaea (Löscher et al. 2012, Casciotti et al. 2018, Santoro et al. 2021, Kelly et al. 2021), indicating that models may need to parameterize different pathways for bacterial and archaeal nitrification. Unfortunately, current lack of information on these processes has made it difficult to approximate their relative importance in global estimates of N_2O production.

As an example, pathways for N_2O production by nitrification by bacteria versus archaea might differ in O_2 tolerance and reaction kinetics. This would directly affect the amount of N_2O produced by nitrification, but the degree to which these organisms differ - and the manner in which they differ – is not yet confirmed or fully quantified (Trimmer et al. 2016, Casciotti et al. 2018, Santoro et al. 2021). In addition to NH_4^+ oxidation by bacteria and archaea, other N-removal pathways could affect N_2O production. While anammox and DNRA do not directly produce N_2O, they affect substrate availability (NH_4^+, NO_3^-) and occur in suboxic waters where there is strong production and consumption of N_2O by denitrification. However, although anammox and DNRA have been observed *in situ*, the data needed for parameterizing reaction pathways and establishing the relative importance of these processes (compared to nitrification and denitrification) in the ocean nitrogen cycle and N_2O production are still lacking.

Nitrification is the oxidation of ammonium to nitrate through two phases – ammonium oxidation and nitrite oxidation – and can produce N_2O as a by-product (Yool et al. 2007, Capone et al. 2008, Rassamee et al. 2011, Lam and Kuypers 2011). Nitrification only occurs in oxygenated conditions; however, at low O_2 concentrations the yield of N_2O (as opposed to NO_3^-) increases substantially. Below a certain O_2 concentration *denitrification* also occurs to both produce and consume N_2O depending on how far the reaction progresses. Because of this, N_2O is an intermediate product of the denitrification reaction while it is a by-product of the nitrification reaction. Denitrification is also controlled by O_2: if O_2 concentrations are suboxic but not anoxic then denitrification may be halted or severely hindered at the intermediate step before N_2O reduction to N_2 (Dalsgaard et al. 2012, Babbin et al. 2015, Ji et al. 2018, Sun et al. 2021).

As most N_2O production and consumption reactions are heavily affected by O_2 concentration, regions in and at the boundaries of oxygen deficient zones (ODZs) are highly relevant in researching the individual contributions of these reactions to N_2O production. Maximum N_2O concentrations and production rates have been recorded at the boundaries of ODZs and are considered to be caused by a combination of nitrification and denitrification processes occurring concurrently (Babbin et al. 2015, Trimmer et al. 2016, Sun et al. 2017, Ji et al. 2018, Rees et al. 2021). As ODZs are projected to expand due to anthropogenic climate change (Keeling et al. 2010, Schmidtko et al. 2017, Breitburg et al. 2018), the N_2O produced in these regions is also anticipated to change – perhaps drastically (Codispoti 2010, Martinez-Rey et al. 2015, Battaglia and Joos 2018). The reactions relevant to N_2O production and consumption are shown in relation to O_2 concentration in ODZs in Figure 2.

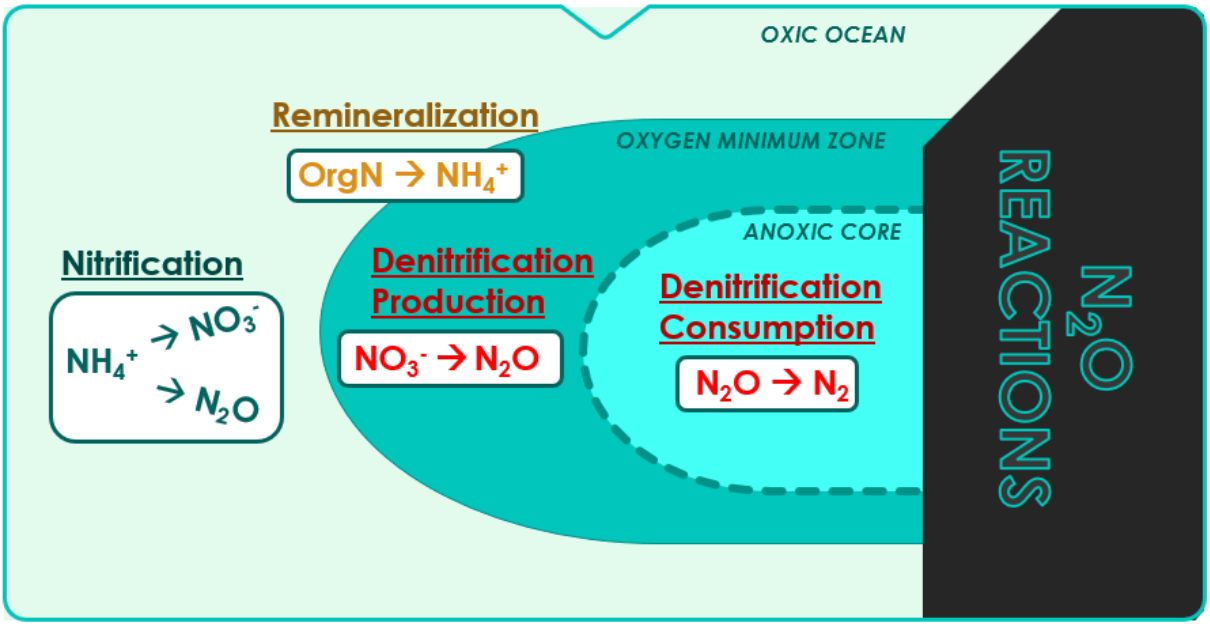

Figure 2: Illustrations of where relevant N_2O reactions (remineralization, nitrification, and denitrification) occur in relation to dissolved O_2 concentrations in the ocean, with a focus on oxygen deficient zones (ODZs).

In addition to O_2 availability, N_2O production is affected by environmental conditions such as temperature, irradiance, and substrate supply (Babbin et al. 2015, Laufkötter et al. 2017, Ji et al. 2018, Battaglia and Joos 2018). By using computer model simulations to generate N_2O production rates, the sensitivity of nitrification and denitrification to O_2 and these environmental conditions can be investigated. Improving the detail and accuracy of these simulations will aid in generating a more complex, realistic representation of the nitrogen cycling system and N_2O production from the ocean.

Due to the relevance of O_2 in relation to N_2O production – especially in terms of denitrification – the size and intensity of oxygen deficient zones has substantial control over global N_2O production rates. ODZs are naturally occurring regions in the ocean where O_2 reaches suboxic concentrations, even reaching near-zero concentrations in the cores of the ODZ. Often referred to as 'shadow zones,' ODZs are thought to originate from a combination of physical processes (such as weak ventilation) and biological processes (such as high productivity in surface waters) and typically occur near the western coastlines of continents at depths of around 200-1500 (Paulmier and Ruiz-Pino 2009, Ulloa et al. 2012). The strongest ODZs are in the Eastern Tropical North Pacific off the western coast of North America, the Eastern Tropical South Pacific off the coast of Peru, and in the Northern Arabian Sea. While ODZs are formed by natural processes, they are projected by global Earth System Models to expand due to effects of anthropogenic climate change (Stramma et al. 2008, Ciais et al. 2013).

Aside from oxygen, environmental conditions such as irradiance and temperature can control N_2O production reactions. Solar irradiance can inhibit nitrification, and the degree to which light permeates the ocean subsurface determines the depths at which nitrification can occur. The attenuation of light to < 1% occurs at depths of approximately 100 m in clear waters, and below this depth the effects of irradiance on nitrification are minimized (Dore and Karl 1996).

Temperature is another relevant environmental condition within the scope of N_2O production processes. Remineralization of organic matter is dependent on temperature and provides the initial reactants used in nitrification and denitrification reactions. Temperatures tend to be highest at the ocean's surface and vary regionally and seasonally, though similar to solar irradiance the variations in temperature greatly decrease below a certain depth.

Existing N_2O production models have been developed and adapted to account for new data and observations over the past few decades, though there is no consensus on parameterization methods. Table 1 highlights global estimates from some of these models, where the wide range of global net N_2O production rates illustrates how insufficient data impedes identification of uncertain parameters, contributing to poorly constrained estimates of N_2O production in the ocean.

Table 1: Global Net N_2O Production Rates

Author & Date	**Global Net N_2O Production Rate**
Capone 1991	~10.5 Tg-N y^{-1}
Suntharalingam, Sarmiento, and Toggweiler 2000	~3.85 Tg-N y^{-1} (2.7-8.0 Tg-N y^{-1})
Codispoti et al. 2001	~6 Tg-N y^{-1}
Nevison et al. 2003	~4 Tg-N y^{-1} (5.8 $\pm$ 2 Tg-N y^{-1})
Bianchi et al. 2012	6.2 $\pm$ 3.2 Tg-N y^{-1}
Freing et al. 2012	3.1-3.4 $\pm$ 0.9 Tg-N y^{-1}
Zamora and Oschilies 2014	1.6-11.7 Tg-N y^{-1}
Babbin et al. 2015	~4 Tg-N y^{-1} from ODZs alone (no global estimate)
Battaglia and Joos 2017	~4.5 Tg-N y^{-1} (3.0-6.1 Tg-N y^{-1})
Ji et al. 2018	1.7-4.4 Tg-N y^{-1}
Buitenhuis et al. 2018	2.4-2.5 $\pm$ 0.8 Tg-N y^{-1}
Sun et al. 2021	3-5 Tg-N y^{-1}

Uncertainties in reaction mechanisms are also highlighted by studies on genomics and gene expression (e.g., Ulloa et al. 2012, Newell et al. 2013, Jayakumar et al. 2017, Pajares and Ramos 2019), both in recognizing major reaction pathways and determining community composition in varying marine environments. Microbial community structure in coastal environments is very different from that in the open ocean, and differs between the low-oxygen core of ODZs and the region near the oxycline (Sun et al. 2017, Coates and Wyman 2017, Rees et al. 2021).

Overall, the global ocean nitrogen budget remains poorly constrained – especially regarding N_2O as produced by nitrification and denitrification. Currently, the best available global budgets estimate the ocean N_2O source at approximately 2.5-4.3 Tg N y^{-1} for the decade of 2007-2016 (Figure 3) (Ciais et al. 2013, Tian et al. 2020), although the estimates by various models and observational studies can vary anywhere between approximately 2 to 12 Tg N y^{-1} (Table 1).

Comparing the estimated 2.5-4.3 Tg N y^{-1} produced by the ocean to the total sum of natural sources of N_2O (8.0-17.0 Tg-N y^{-1}) and anthropogenic sources (4.7-11.4 Tg-N y^{-1}) over the same time period (Ciais et al. 2013) reinforces the idea that marine N_2O emissions comprise a sizable portion of the global N_2O budget and should be better defined to project global climate and effects of anthropogenic change (Battaglia and Joos 2018, Bange et al. 2019).

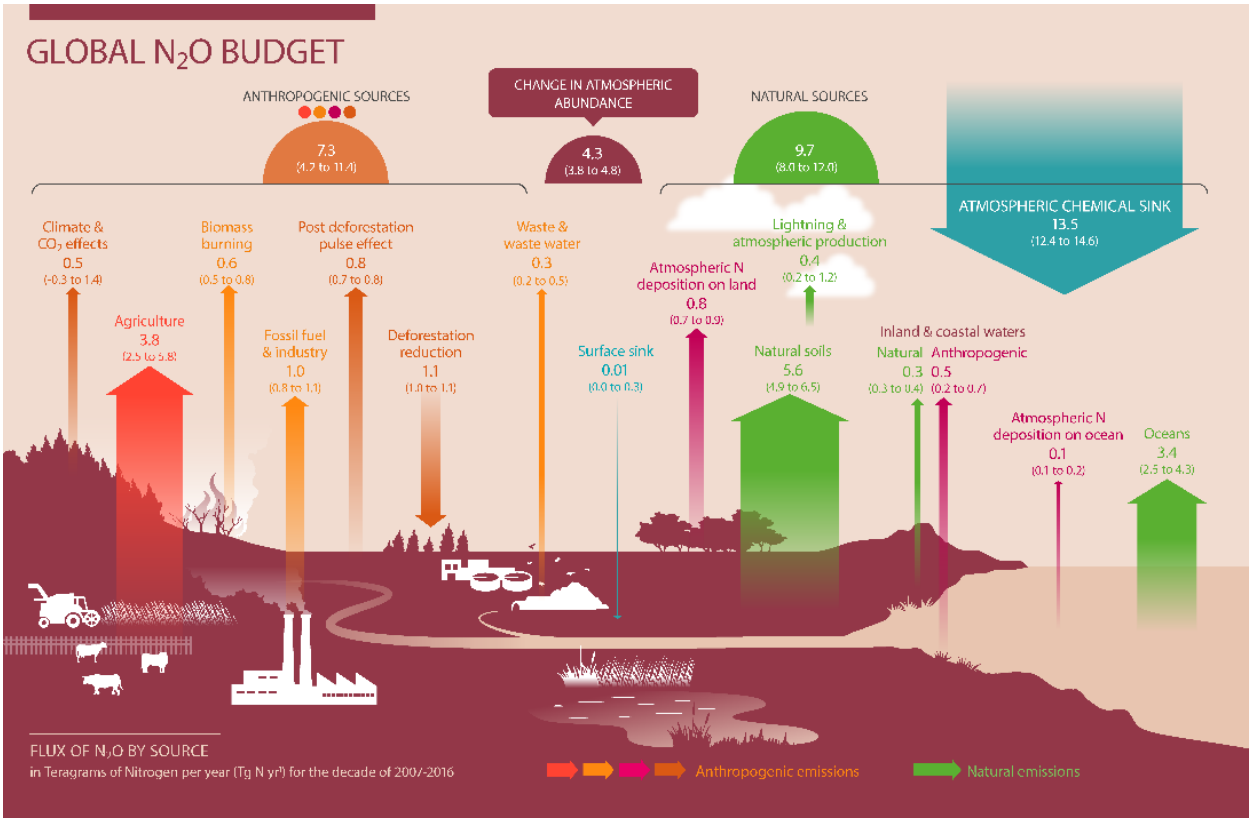

Figure 3: Global N_2O budget with sources and sinks (from Tian et al. 2020)

In addition to a dearth of data on N_2O reaction mechanisms, ongoing discoveries force scientists to adapt and update their understanding of the nitrogen cycle itself. As an example, nitrification has historically been attributed to bacterial nitrifiers in oxic environments while denitrification has been attributed to bacterial denitrifiers in anoxic environments. In recent years, however, novel pathways – such as anammox, ammonium oxidation by archaea, and anaerobic nitrogen fixation (Dalsgaard et al. 2005, Könneke et al. 2005, Dekas et al. 2009, Löscher et al. 2012) – have revealed new nitrogen cycling pathways that compound the need for a re-examination of the nitrogen cycle (Thamdrup 2012, Voss et al. 2013). Furthermore, discovery of atypical *nosZ* genes – the genes responsible for nitrous oxide consumption (Figure 1) – existing in environments with unexpectedly high oxygen concentrations has led to scrutiny of established

ideas about oxygen inhibitions of denitrification processes (Sun et al. 2017, 2021, Rees et al. 2021).

These new nitrogen cycling processes affect the ongoing debate over the magnitude of nitrification and denitrification occurring globally, as well as over the comparative strength of regional N_2O production (Thamdrup 2012, Kriest and Oschlies 2015, Ji et al. 2018, Tian et al. 2020). The consumption of nitrogen species to produce N_2O and N_2 influences nutrient availability and so is directly relevant to ocean productivity. Moreover, the emission of N_2O gas from the ocean's surface provides a substantial portion of global atmospheric concentrations, contributing to the intensifying effects of greenhouse gases.

Yet despite its environmental importance, N_2O is often ignored in both biogeochemical models and sustainable development goals (Kanter et al. 2020). The current lack of data on microbial community structure, reaction rates, and oxygen inhibition impedes quantification of both novel and well-established processes; therefore, this research employs computer models to simulate and investigate possible scenarios over the whole range of pelagic marine environments.

Research Questions & Scope of Research

The goal of this project is to generate a computer simulation model representing the nitrification and denitrification pathways leading to ocean N_2O production to better identify the key uncertainties that control these reactions. In creating this simulation, the sensitivity of N_2O production rates to environmental conditions are investigated in a portable mathematical model that can be integrated into global Earth System Models to support projections of future ocean N_2O emissions. By isolating these reactions in a controlled virtual environment, the questions and uncertainties concerning O_2 inhibition of various processes, representations of rate equations, and the relative contribution of each reaction can be better defined. This provides more robust nitrification and denitrification biogeochemical pathway representation, particularly in quantifying the relative contribution of these individual reactions to N_2O production and emissions from the ocean. The computer model is designed to answer the following research questions and ultimately provide a road map of the most important "missing quantities" in our understanding of N_2O dynamics that will need to be improved in future observational studies.

- When parameterizing N_2O production and consumption, what are the key uncertainties and how strongly do these uncertainties affect net N_2O production?
- How do key uncertainties affect how much N_2O production occurs in the oxic ocean compared to the suboxic ocean? In the global ocean, is more N_2O produced by nitrification or denitrification?
- What are the main controls on N_2O production by nitrification and denitrification?
- How do environmental conditions and substrate availability affect the partitioning of N_2O production between nitrification and denitrification?
- What is the relationship between organic matter remineralization, oxygen, and maximum N_2O production in, and at the boundary of, oxygen deficient zones? In oxygen deficient zones, how does the rate of denitrification production of N_2O compare to denitrification consumption of N_2O?
- How might anthropogenic changes to environmental conditions affect global ocean N_2O production?

The model will answer these questions by constructing a global 3D representation of how net N_2O production rates and individual production and consumption rates by nitrification and/or denitrification vary in various environments. By maintaining a relatively simple framework, the controlling elements on N_2O production and consumption rates can be investigated without considering the full spectrum of biogeochemical processes that occur *in situ*. Past models (Babbin et al. 2015, Ji et al. 2018, Sun et al. 2021) have used similar modelling techniques using a steady state framework, which assumes that reaction rates do not change over time. Such models have found success in using this assumption to develop a plausible range of net N_2O production rates despite known uncertainties in parameters and parameterizations, and as such provide the basis for the model created here. The model developed in this research has an increased level of detail compared to existing steady-state N_2O production models and models that have been embedded in global 3D ocean models (e.g., Suntharalingam et al. 2000; Zamora and Oschlies 2014, Battaglia and Joos 2018), with a greater biological focus on individual reaction pathways and the influence of a wider range of environmental conditions (temperature, irradiance, substrate availability) on these reactions. This model's novelty arises from its incorporation of a full, global 3D distribution of environmental conditions, allowing investigation into reaction controls and testing of parameters and parameterizations without necessitating the complexity of a complete Earth System Model.

This 3D model is based on a uniform 2^o x 2^o latitude/longitude grid over 33 depth layers (Locarnini et al. 2010). Five Earth System Models, CanESM5 (Christian et al. 2022), CanESM5-CanOE (Christian et al. 2022), CNRM-ESM2-1 (Séférian et al. 2019), GFDL-ESM4 (Stock et al. 2020), and UKESM1-0-LL (Yool et al. 2021), were also interpolated to this grid. Parameters and parameterizations used in this model will be a combination of the most recent advances in the literature and the most reasonable best-estimates as determined according to model results and sensitivity. These quantities will be evaluated for their validity in relation to global net N_2O production rates and used to generate a list of uncertain terms that have the strongest influence on global N_2O production rates, in the hope that it will highlight the more important gaps to be filled. The finalized parameterization of N_2O production in the ocean is designed to be utilized in the context of future Earth System Models, and so aims for simplicity and adaptability.

As this project focuses on how O_2 concentrations affect N_2O production pathways, yield, and magnitude by individual processes, particular attention will be paid to regions with ODZs where O_2 may vary sharply over relatively small distances. Partitioning between nitrification and denitrification is known to be one of the greatest sources of uncertainty in N_2O modelling, and so particular attention is paid to the relative strength of these processes in and around ODZs. By comparing variation of the N_2O production rates across these regions of disparate O_2 concentrations, the magnitude of control by O_2 on nitrification, denitrification, and remineralization is better elucidated. Investigating the nature of this O_2 control allows for development of more accurate model estimates of how much N_2O production occurs in oxic waters compared to suboxic waters, and so determine the proportion of N_2O provided by each in the global total estimates. This is also of particular importance in analyzing the contribution by denitrification production in relation to denitrification consumption, where O_2 concentrations that reach as low as 1-2 $\mu mol\text{-}O_2\ L^{-1}$ can affect partitioning between N_2O production or consumption.

N_2O production rates' relation to O_2 concentrations are established by quantifying multiple processes: the yield of N_2O from nitrification, the partitioning of denitrification's production and consumption pathways, and the tolerances of denitrification processes to the presence of O_2. Once the base case scenario for each of these qualities is established, their sensitivity is examined by varying parameters individually and assessing the change in the N_2O production rates. Production rates' sensitivity to other environmental conditions (temperature, solar irradiance, substrate availability) are similarly determined: observing independent interactions between rates and varying environmental conditions narrows down a reasonable base case, and sensitivity of each reaction to these environmental conditions is explored by changing the representative parameters.

Parameters are altered within a range that is reasonable given available literature data or using best estimates in the scheme of the model if there is little or no available data. In this way, the degree of control by known uncertain qualities can be analyzed to determine the most relevant parameters that need more elucidation in future observational and laboratory research. Best estimates of uncertain parameters are generated by comparing the output global net production rates to past model estimates from literature.

N_2O concentrations (instead of rates) are not a reliable measure of model credibility as concentrations can not be compared to in situ data without considering ocean circulation and other complexities of ocean biogeochemical cycling. However, a general awareness of the magnitude of concentrations in the ocean and in the model are useful in discerning if regional patterns are comparable. For example, elevated N_2O production is observed in and around oxygen deficient zones in observational data, which is also represented in this model at the same locations.

In addition to existing environmental conditions, the model's sensitivity to projected environmental conditions as a result of anthropogenic climate change is evaluated using data from Earth System Models: CanESM5 (Christian et al. 2022), CanESM5-CanOE (Christian et al. 2022), CNRM-ESM2-1 (Séférian et al. 2019), GFDL-ESM4 (Stock et al. 2020), and UKESM1-0-LL (Yool et al. 2021). The N_2O production rates that arise from using these different models as input environmental conditions help project possible changes in N_2O cycling and N_2O emitted from the ocean to the atmosphere, and so aid understanding of greenhouse gas emissions in a future ocean with different biogeochemical properties.

Thesis Outline

The following Methodology section (Section 2.0) will summarize how the computer model was created and how it uses steady state conditions through use of a 'virtual chemostat' to simulate real world N_2O production and consumption rates. It will also list the relevant inputs to the model and their derivations and detail the source material for data products generated outside the scope of the model. The basic model framework is described in Section 2.1, with process equations and equations for environmental conditions provided in Sections 2.1.1 and 2.1.2, and explanation of relevant data sets in Section 2.1.3. The nature of the steady state model or "virtual chemostat" will be explained in Section 2.2, with Section 2.2.1 describing the model initialization.

The Results section (Section 3.0) will begin with evaluation of the characteristics of global and regional N_2O production and consumption rates in Section 3.1 and will analyze sensitivity of N_2O production and consumption rates to oxygen (Section 3.2), remineralization of organic matter (Section 3.3) and to environmental conditions (Section 3.4). An in-depth investigation of how all individual parameters, environmental conditions, and data product inputs affect N_2O production rates will be presented in Section 3.5, and Section 3.6 will provide projections of N_2O production and consumption rates in relation to future ocean conditions for O_2, organic matter, and temperature as generated by five Earth System Models.

The Discussion (Section 4.0) will explain the significance of the uncertain parameters, environmental conditions, and data products that have the greatest influence on N_2O production in the ocean in Section 4.1 and will evaluate the model validity in relation to past literature in Section 4.2. Model significance and an estimation of potential future effects of climate change on N_2O production will be discussed in Section 4.3.

The conclusion (Section 5.0) will summarize the scope of the model and its relevance to science and society.

2 Methodology

This research uses a computer model as a 'virtual laboratory' to investigate how N_2O production rates can be estimated from mathematical representations of relevant processes and environmental conditions, using observed data and computer simulations. In this section the process equations for reaction pathways of N_2O production will be described, as well as environmental conditions such as solar irradiance, temperature, oxygen, and substrate concentrations.

2.1 Model Description

To simplify the full spectrum of reactions related to N_2O production and nitrogen cycling, five state variables will be used in representing remineralization, nitrification, and denitrification. These are *oxygen* (O_2), *detritus* (organic nitrogen – orgN), *ammonium* (NH_4^+), *nitrate* (NO_3^-), and *nitrous oxide* (N_2O). These five state variables are affected by five process equations depicting their rate of change, which are described here and followed by a table of parameter values. Process reactions are represented as rates of change of the state variables in the form *d*[X]*/dt*, where [X] is the concentration of the state variable and *d/dt* is the rate of change.

The state variables, parameters, and equations used to depict relevant N_2O production processes concern three main reactions: remineralization (by both oxic and denitrification processes), ammonium oxidation (part of the nitrification process that can produce N_2O), and N_2O consumption by denitrification. N_2O production processes are primarily controlled by oxygen availability, but also by first order rate constants, substrate concentration, and environmental conditions such as temperature and irradiance. Parameterizations of environmental conditions will be detailed in the section following the main process equations and table of values.

While it is possible to parameterize these processes with more chemical species and with a wider variety of environmental conditions, the following equations represent the most essential factors known to affect these reactions. Avoiding unnecessary complications allows a deeper investigation into the main controls on N_2O production and consumption processes.

2.1.1 Process Equations

The equation for the rate of change of the first state variable, detritus (*D*), is depicted in *Equation 1*, detailing how detrital organic matter is remineralized by both oxic and suboxic processes. The partitioning between oxic and suboxic remineralization is represented by Ω, which will be described in *Equation 3*.

$$\frac{d}{dt}[\mathrm{D}] = -(1-\Omega)k_{remin}T_g[\mathrm{D}] - (\Omega)fNO_{3,remin}k_{remin}T_g[\mathrm{D}]$$

(Equation 1)

Temperature affects remineralization rates according to the Arrhenius Equation (Burdige and Komada 2011, Laufkötter et al. 2017) using a reference temperature (T_{ref}) of 12ºC (285.15 K), the activation energy required for remineralization of organic matter (E_a = 5.4 x 10^3 J mol^{-1}) (Medlyn et al. 2002, Bunce 2019), and the gas constant (R = 8.31447 J K^{-1} mol^{-1}). The term T_g describes the Arrhenius equation and the effect temperature has on the remineralization rate (*Equation 2*).

$$T_g = e^{\frac{-E_a}{R}\left(\frac{1}{T}-\frac{1}{T_{ref}}\right)}$$

(Equation 2)

Lower temperatures decrease the reaction rate of remineralization processes while higher temperatures increase the reaction rate (Figure 4). Most of the world's ocean below the euphotic zone (100 m) is cold, with a mean temperature of approximately 5°C (Locarnini et al. 2018). The interactions between the spatial patterns of temperature in relation to spatial patterns of organic matter supply can alter the magnitude of remineralization rates throughout the global ocean (Rahmstorf 2002, Burdige and Komada 2011, Laufkötter et al. 2017).

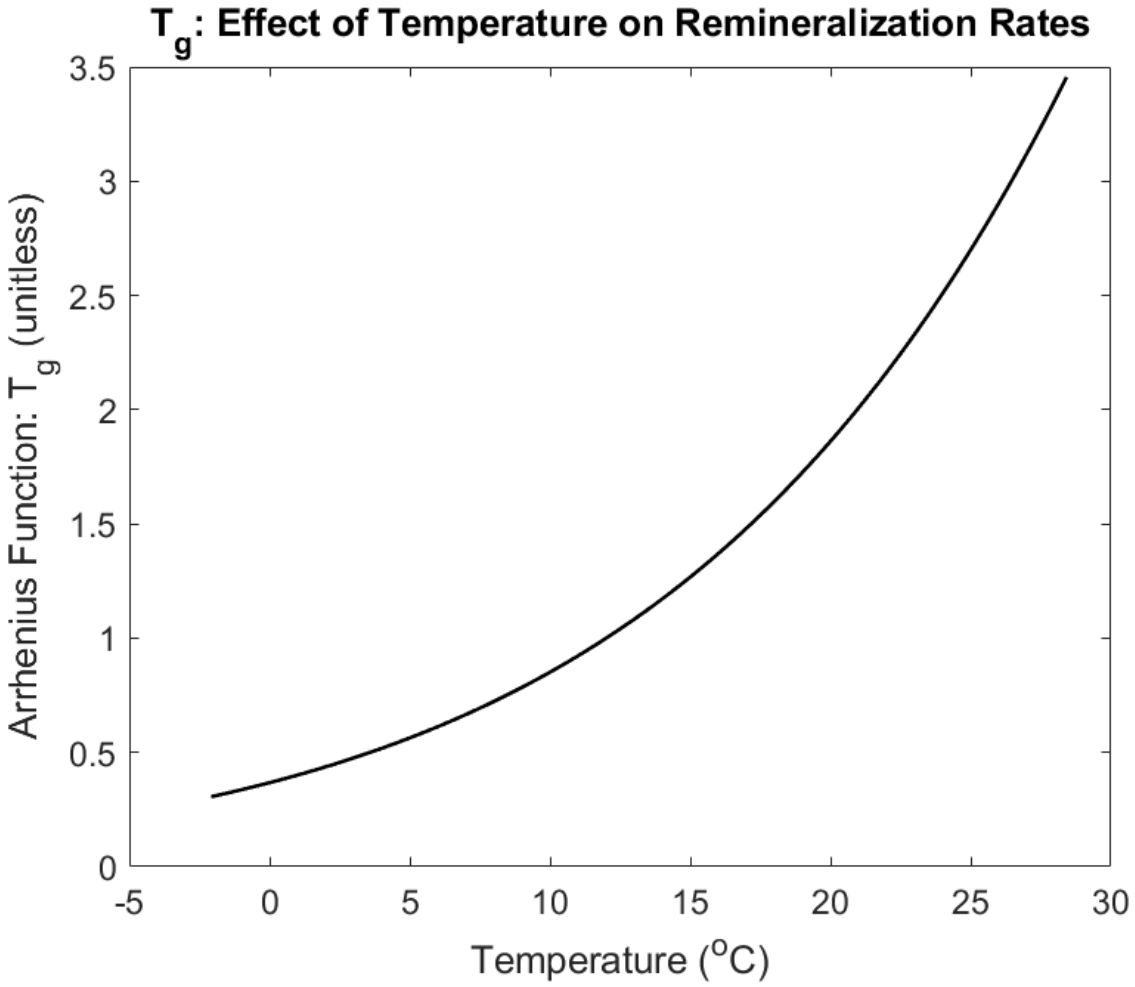

Figure 4: Effect of temperature on remineralization using the Arrhenius function (T_g)

As most of the world's ocean lies around the mean of 5°C, the average effect T_g has on remineralization rates is decreasing the base rate by up to 50-60% relative to the reference temperature of 12°C, although as mentioned above this is subject to small changes. The higher temperature range of 20-28°C rarely occurs below 100 m, so it is rare that the T_g exceeds 2 as shown in Figure 4. As this model does not include depths shallower than 100 m, the focus is on cooler temperatures.

In *Equation 1*, detritus is only consumed as this model does not include processes that occur in the euphotic zone that generate organic matter. Instead, organic matter produced at the surface that has reached depths past 100 m is consumed through oxic remineralization (1-Ω) and suboxic remineralization (Ω), which is the first step of denitrification (*Equation 3*). Both oxic and

suboxic remineralization are affected by temperature according to T_g and a remineralization rate constant, k_{remin} = 0.25 d^{-1}, common to both.

$$\Omega = \left(\frac{thr_{O2,remin} - \min\{[O_2], thr_{O2,remin}\}}{thr_{O2,remin}} \right)^c$$

(Equation 3)

Equation 3 details the partitioning between oxic and suboxic remineralization according to O_2 concentrations, where Ω represents the fraction of suboxic remineralization and (1-Ω) represents the fraction of oxic remineralization. The O_2 threshold where suboxic remineralization begins, thr_{O2}, is set at 6 µmol-O_2 L^{-1} – a median of estimates from 2-10 µmol-O_2 L^{-1} (Codispoti et al. 2001, Devol et al. 2008, Dalsgaard et al. 2014) - and the exponent *c* controls how quickly oxic remineralization declines and suboxic remineralization increases with decreasing O_2. For the base case scenario of the model, *c* = 3, so that Ω takes the shape depicted in Figure 5 (red) and 1-Ω takes the shape depicted in blue.

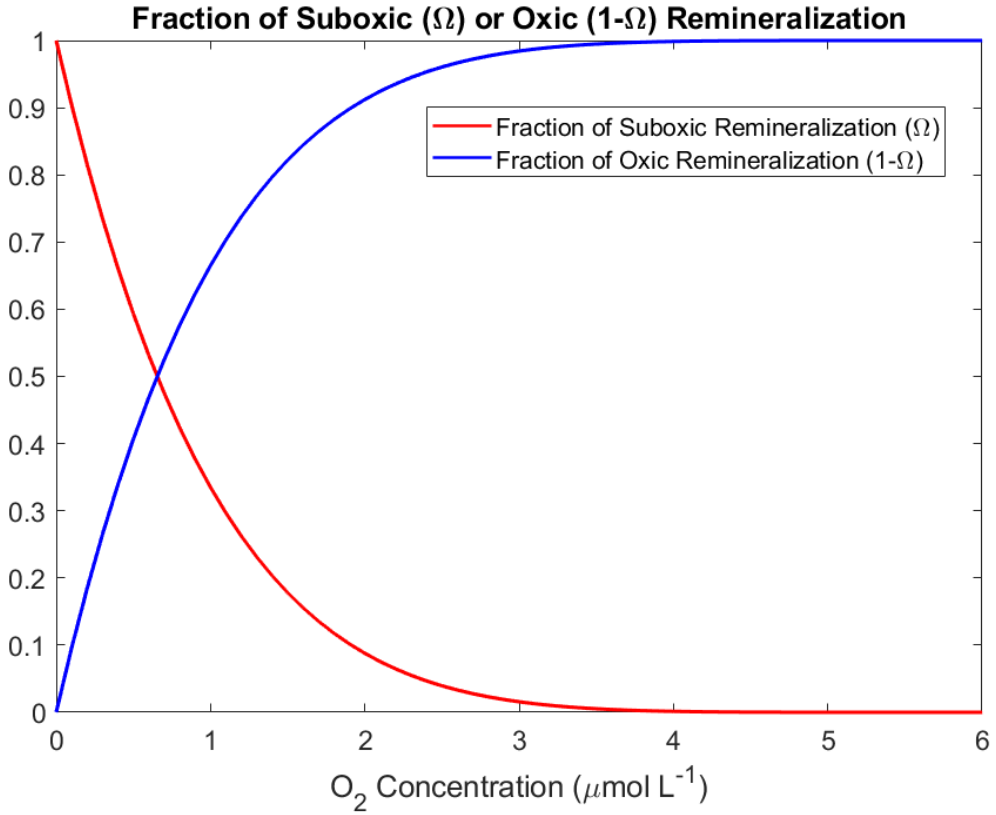

Figure 5: Fraction of suboxic remineralization, Ω (red), and oxic remineralization, 1-Ω (blue), at O_2 concentrations in the suboxic range from 0-6 µmol-O_2 L^{-1}.

Figure 5 shows how the portion of oxic and suboxic remineralization changes gradually according to O_2 and the exponent *c*. While suboxic remineralization can only begin to occur starting at $O_2 \leq$ 6 µmol-O_2 L^{-1}, oxic remineralization still occurs in the suboxic O_2 range from 0-6 µmol-O_2 L^{-1} though it decreases rapidly as O_2 approaches zero. The parameter *c* was chosen to mimic the shape of the Ω curve of increasing denitrification with decreasing O_2 according to Devol (1978) and Dalsgaard et al. (2012, 2014).

Suboxic remineralization (Ω) is also controlled by the term $fNO_{3,remin}$ (*Equation 4*) according to NO_3^- concentrations – this is because NO_3^- is used as the electron acceptor in suboxic remineralization, instead of O_2 as the electron acceptor in oxic remineralization. If NO_3^- concentrations are very low, then the rate of suboxic remineralization will be restricted according to a Michaelis-Menten-style curve using a half-saturation constant $K_{NO3,remin}$ = 5 μmol-NO_3^-.

$$fNO_{3,remin} = \frac{[NO_3^-]}{[NO_3^-] + K_{NO3,remin}}$$

(Equation 4)

The Michaelis Menten curve of $fNO_{3,remin}$ versus NO_3^- in *Equation 4* is depicted in Figure 6 (top), and the proportion of suboxic remineralization in relation to NO_3^- and O_2 is visualized in Figure 6 (bottom) by multiplying $fNO_{3,remin}$ and Ω.

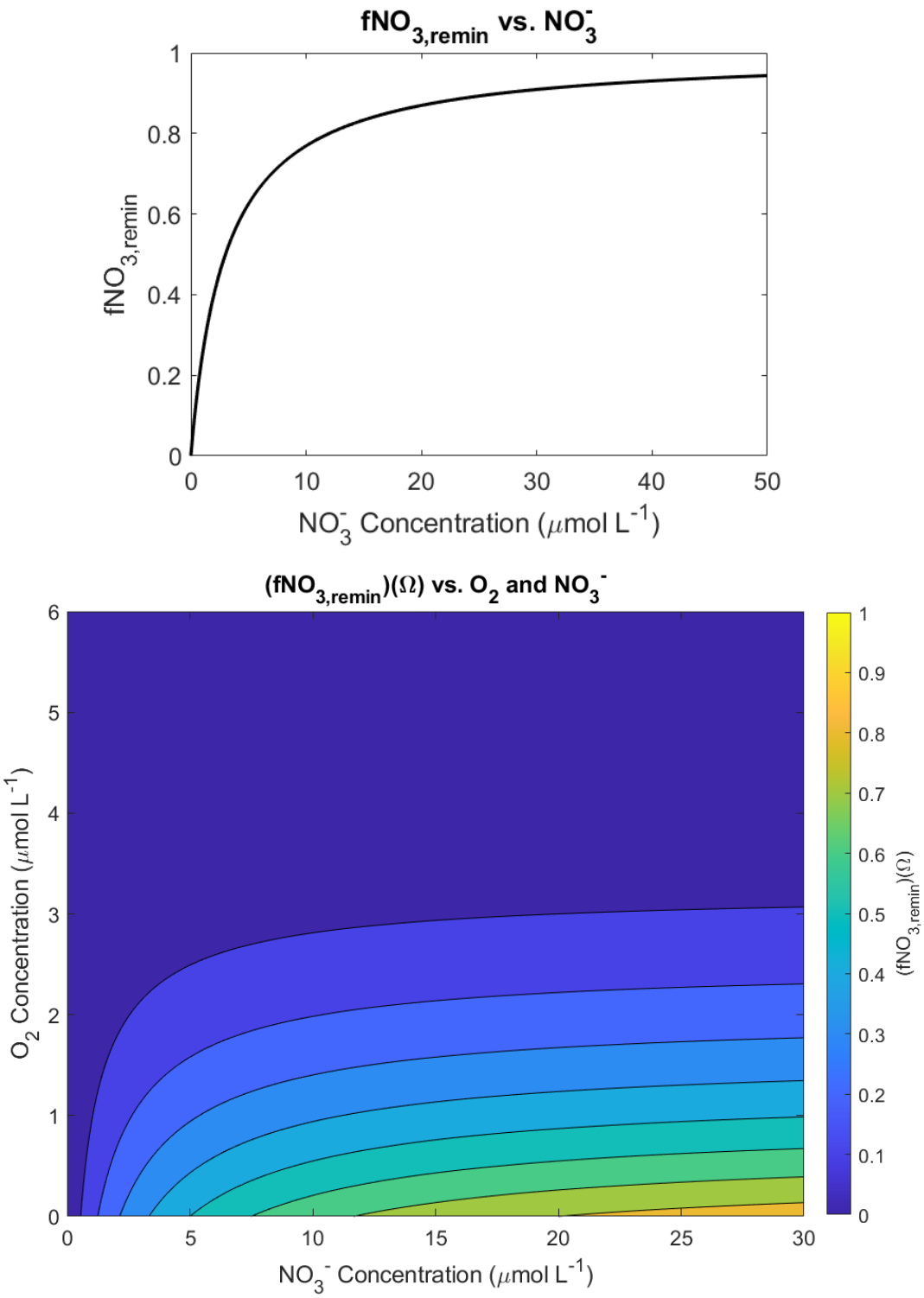

Figure 6: *fNO*$_{3,remin}$ versus NO_3^- (top), and relationship of (*fNO*$_{3,remin}$)(Ω), NO_3^-, and O_2 (bottom).

In the top panel of Figure 6, *fNO*$_{3,remin}$ decreases with NO_3^-, especially below concentrations of approximately 10 μmol-NO_3^- L^{-1}. In the bottom panel, there is a greater change of Ω along the vertical O_2 axis rather than the horizontal NO_3^- axis. This is because the rate of suboxic remineralization (denitrification) is more strongly regulated by O_2 than by NO_3^-.

The second main process equation concerns the rate of change of ammonium, NH_4^+, and is described by *Equation 5*.

$$\frac{\boldsymbol{d}}{\boldsymbol{dt}}[\mathbf{NH_4}^+] = (\mathbf{1}-\Omega)\boldsymbol{k_{remin}T_g}[\mathbf{D}] + (\Omega)\boldsymbol{fNO_{3,remin}k_{remin}T_g}[\mathbf{D}] - (\boldsymbol{\gamma})\boldsymbol{fO_{2,AmOx}k_{AmOx}}[\mathbf{NH_4}^+]\left(\frac{\boldsymbol{E_x}}{\boldsymbol{E_x}+\boldsymbol{E_z}}\right) - (\mathbf{1}-\boldsymbol{\gamma})\boldsymbol{fO_{2,AmOx}k_{AmOx}}[\mathbf{NH_4}^+]\left(\frac{\boldsymbol{E_x}}{\boldsymbol{E_x}+\boldsymbol{E_z}}\right)$$

(Equation 5)

Equation 5 details how NH_4^+ is both produced by remineralization of detritus (first two terms) and consumed by ammonium oxidation through nitrification (second two terms). Nitrification is a multiple-step process that involves NH_2OH and NO_2^- as intermediates, but for the purposes of this model it is being represented as a single step reaction. The remineralization terms are the same as those in *Equation 1*.

The nitrification terms consume NH_4^+ to produce both NO_3^- and N_2O as a by-product using the partitioning term γ. γ represents the yield of N_2O from ammonium oxidation, while *1*-γ represents the yield of NO_3^- (*Equation 6*).

$$\gamma = 0.01\left(\frac{a}{[O_2]} + b\right)$$

(Equation 6)

Equation 6 uses O_2 concentrations to determine the yield of N_2O in relation to NO_3^-, where a = 0.2 μmol-O_2 L^{-1} and b = 0.08 (Ji et al., 2018). This equation was first used by Nevison et al. (2003) and was later revised by Ji et al. (2015, 2018) to better represent in-situ observational yields. Figure 7 provides a visualization of how the percent yield of nitrification changes with O_2; note that the equation for γ that is used within the model includes multiplication by 0.01, while the figure below removes this 0.01 to depict yield as a percent.

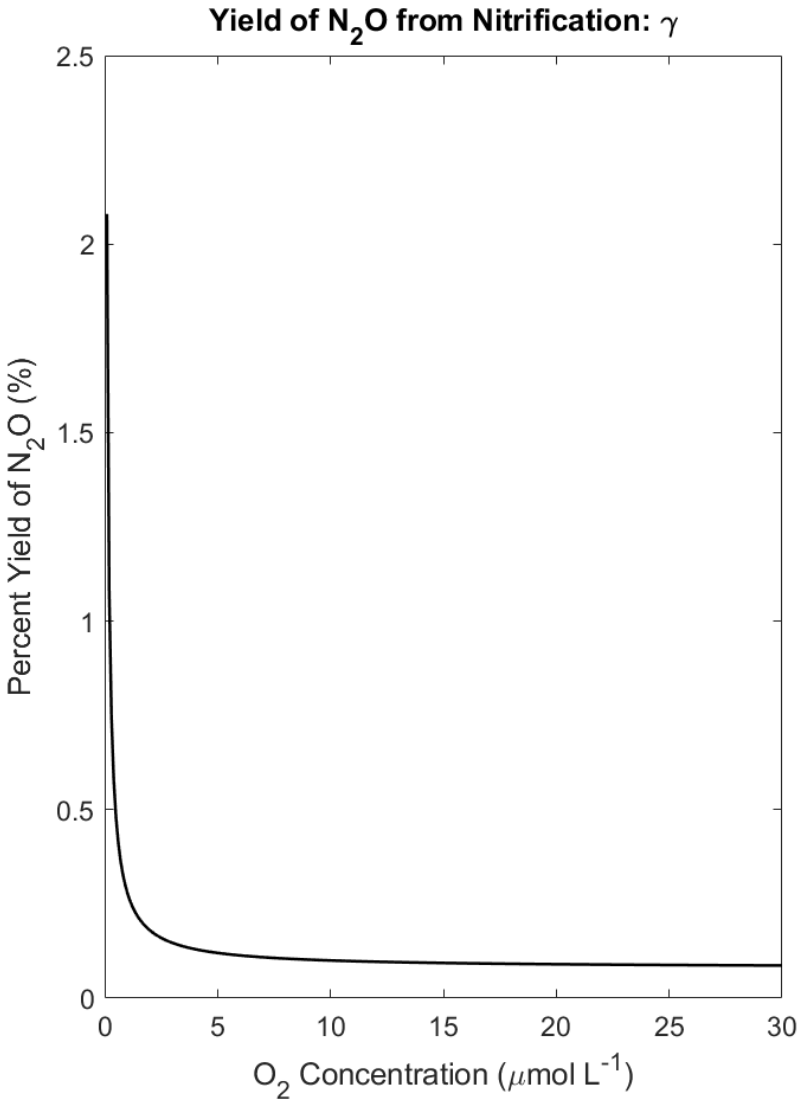

Figure 7: Percent yield of N_2O from nitrification versus O_2 concentrations.

In Figure 7, the percent yield of N_2O (vertical axis) is very low at higher O_2 concentrations but increases exponentially as O_2 reaches suboxic and anoxic concentrations. Because of this, the yield of N_2O from nitrification in oxic waters is very low (approx. 0.04%) despite higher overall nitrification rates, while the yield of N_2O in suboxic waters is higher while nitrification rates become quite small.

This relationship between yield of N_2O and O_2 is integral to understanding how much N_2O is produced in the oxygenated waters, which comprise most of the global ocean, versus the suboxic waters that are mostly only present in ODZs. Despite most of the world's seawater being oxygenated and therefore capable of N_2O production through nitrification, the yield of N_2O is often so low that very little of the global total may be produced through this pathway.

In addition to γ, the nitrification rate is controlled by a rate constant, $k_{AmOx} = 0.8\ d^{-1}$, a solar irradiance inhibition factor, $E_x/(E_x+E_z)$, and O_2 according to $fO_{2,AmOx}$. Solar irradiance affects nitrification rates – light inhibits the nitrification process, such that increased irradiance will result in lower nitrification rate. Since the model does not include the euphotic zone, the

influence of solar irradiance on nitrification is small but not negligible. The light inhibition term, $E_x/(E_x+E_z)$, requires a depth-dependent irradiance, E_z. E_z and its parameterization is discussed further in Section 2.1.2. The effect of irradiance on nitrification at various depths and latitudes is depicted in Figure 8, with E_z (irradiance at depth) discussed further in Section 2.1.2 (*Equation 11*).

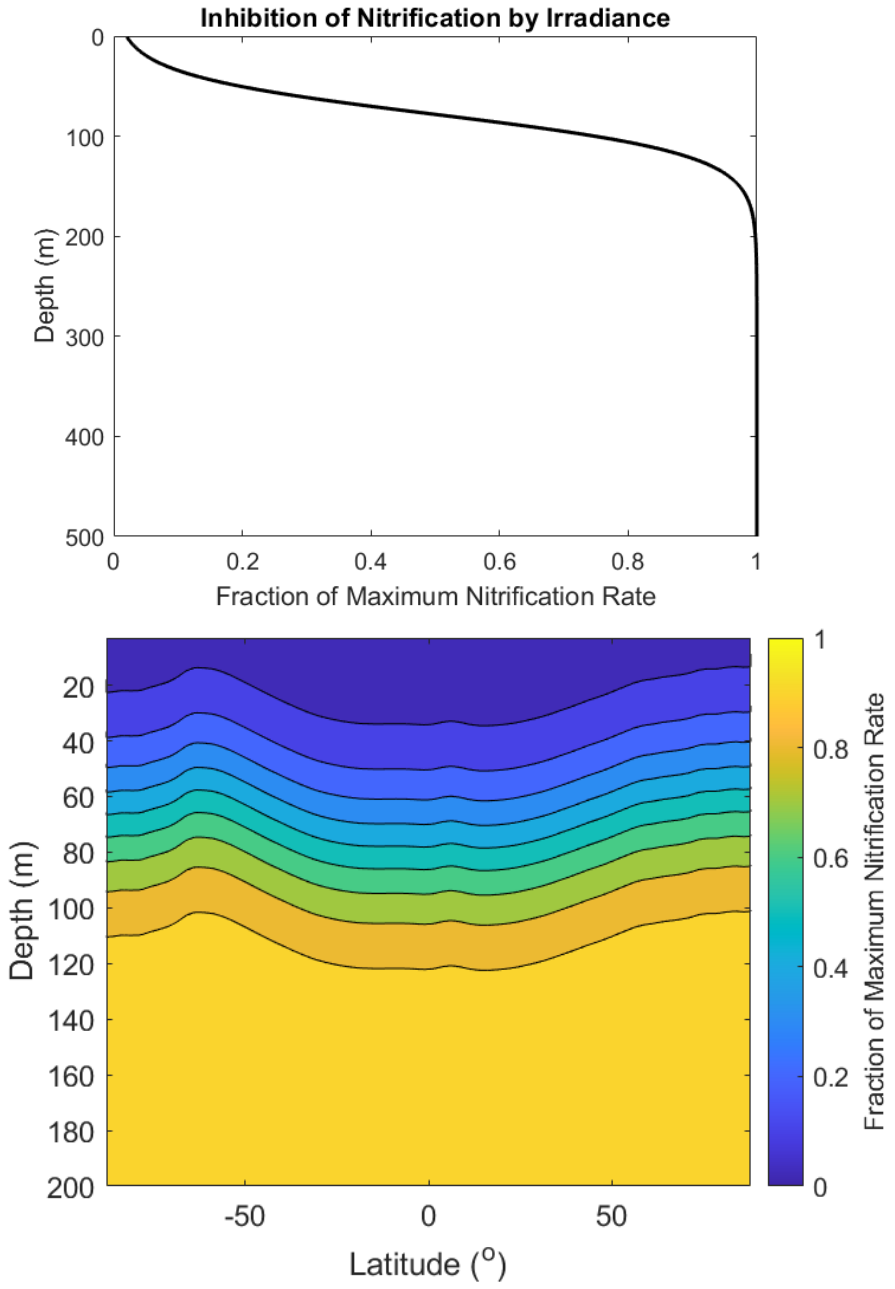

Figure 8: Inhibition of nitrification by solar irradiance. Top panel shows a one-dimensional depth profile using annually and globally averaged surface solar irradiance (E_0), bottom panel uses annually averaged zonal mean surface solar irradiance across various latitudes.

In the real world, the euphotic zone depth is correlated with the light attenuation coefficient a_c; however, within the scope of this model a constant a_c and euphotic zone depth are assumed. This

means that the inhibitory effect of solar irradiance does not reach far past the set depth of the euphotic zone (100 m) and so does not have a strong influence on nitrification except at depths of approx. 100-125 m (Figure 8). In the real world, light attenuation and euphotic zone depth vary strongly by location across the globe; however, for the purposes of N_2O production via nitrification such a simplification is expected to have very little effect on results (see Sections 3.4.2, 3.4.3).

$fO_{2,AmOx}$ is another Michaelis-Menten-style parameter that limits the rate of nitrification as O_2 decreases. While the rate of ammonium oxidation is reduced with decreasing O_2 (*Equation 7*), the yield of N_2O (in relation to NO_3^-) is *increased* with decreasing O_2 (*Equation 6*). This unique relationship with O_2 is what necessitates two individual O_2-dependent parameterizations: $fO_{2,AmOx}$ and γ.

$$fO_{2,AmOx} = \frac{[O_2]}{[O_2] + K_{O2,AmOx}}$$

(Equation 7)

$fO_{2,AmOx}$ uses O_2 concentrations and a half-saturation constant, $K_{O2,AmOx}$ = 5 μmol-O_2 L^{-1}, to limit nitrification rates with decreasing O_2. This differs from γ, which does not affect the rate of nitrification itself but the yield of N_2O from nitrification. $fO_{2,AmOx}$ is illustrated in Figure 9 in relation to O_2 concentration.

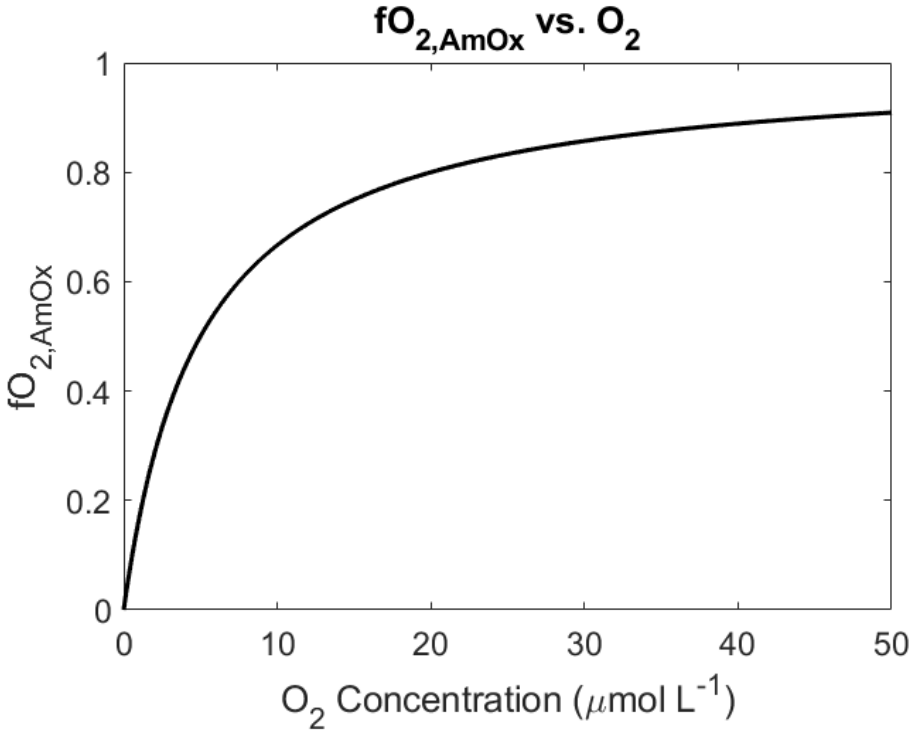

Figure 9: $fO_{2,AmOx}$ versus O_2. $fO_{2,AmOx}$ decreases the rate of nitrification as O_2 decreases, especially below approximately 10 μmol-O_2 L^{-1}.

Similar to the depiction of $fNO_{3,remin}$ in Figure 6, Figure 9 shows how $fO_{2,AmOx}$ follows a Michaelis-Menten curve, decreasing the rate of nitrification at low O_2 concentration.

The third main process equation is the rate of change of NO_3^-, where NO_3^- is increased through nitrification and consumed through denitrification production of N_2O (suboxic remineralization) (*Equation 8*).

$$\frac{d}{dt}[NO_3^-] = (1-\gamma) fO_{2,AmOx} k_{AmOx} [NH_4^+] \left(\frac{E_x}{E_x + E_z}\right) - (\Omega) fNO_{3,remin} k_{remin} T_g R_{NO3:OrgN} [D]$$

(Equation 8)

NO_3^- is produced by nitrification (first term) and consumed by suboxic remineralization, or denitrification (second term). In the first term, *1-γ* is the yield of nitrification to NO_3^- instead of N_2O, and is identical to the last term in the NH_4^+ process equation (*Equation 5*). The second term is similar to the previous representations of remineralization with one notable change – a Redfield ratio, $R_{NO3:orgN}$. $R_{NO3:orgN}$ is used to convert from moles of detritus (orgN) consumed to the proportionate amount of moles of NO_3^-, where $R_{NO3:orgN}$ = (106 mol C : 16 mol N)(4 mol NO_3^- : 5 mol C) = 5.3 (Redfield 1958, Froelich et al. 1979).

The next main process equation concerns O_2 and is described in *Equation 9*. O_2 is only consumed in this model for the same reason detritus is only consumed – the model only concerns the regions below the euphotic zone, and so sources of O_2 like photosynthesis or gas exchange with the atmosphere are not considered.

$$\frac{d}{dt}[O_2] = -(\gamma) fO_{2,AmOx} k_{AmOx} [NH_4^+] \left(\frac{E_x}{E_x + E_z}\right) - 2(1-\gamma) fO_{2,AmOx} k_{AmOx} [NH_4^+] \left(\frac{E_x}{E_x + E_z}\right) - (1-\Omega) k_{remin} T_g R_{O2:OrgN} [D]$$

(Equation 9)

The rate of consumption of O_2 is governed by three terms – the first term is consumption by ammonium oxidation to produce N_2O (*γ*), the second term is consumption by ammonium oxidation to produce NO_3^- (1-*γ*), and the third term is consumption of detritus by oxic respiration (Ω). 2 moles of O_2 are required to oxidize the 2 moles of NH_4^+ used to produce 1 mole of N_2O. Similarly, 2 moles of O_2 are consumed when producing 1 mol of NO_3^- by nitrification. The third term includes the Redfield ratio, $R_{O2:OrgN}$ = (106 mol O_2: 16 mol N), that refers to the moles of O_2 needed to remineralize 1 mole of organic nitrogen. This $R_{O2:OrgN}$ is a simplification, as deviations from the 106:16 ratio can arise depending on the area of study and the community composition of phytoplankton. Such nuances were not taken into consideration for this project, and so the $R_{O2:OrgN}$ is smaller than the 163:22 ratio posited by more modern studies (Martiny et al. 2014).

The final process equation is for the rate of change of N_2O and is the primary focus of the model results (*Equation 10*).

$$\frac{d}{dt}[N_2O] = 0.5(\gamma) fO_{2,AmOx} k_{AmOx} [NH_4^+] \left(\frac{E_x}{E_x + E_z}\right) + 0.5(\Omega) fNO_{3,remin} k_{remin} T_g R_{NO3:OrgN} [D] - k_{cons} [N_2O] e^{\left(-\frac{[O_2]}{K_{O2,cons}}\right)}$$

(Equation 10)

Equation 10 contains three terms: production of N_2O as a by-product from nitrification, production of N_2O as an intermediate in denitrification (suboxic remineralization), and

consumption of N_2O as the final step of denitrification. The first and second terms are multiplied by 0.5 to reflect that 0.5 moles of N_2O are produced by oxidation of 1 mol of NH_4^+ through nitrification or by remineralization of detritus using 1 mol of NO_3^-.

The last term detailing N_2O consumption by denitrification uses the N_2O produced by both nitrification and denitrification as a substrate, a rate constant (k_{cons} = 0.8 d^{-1}), and an exponential term that is controlled by O_2 and an O_2 inhibition factor, $K_{O2,cons}$ = 0.3 μmol-O_2 L^{-1} (Dalsgaard et al. 2014; Babbin et al. 2015). This consumption term is illustrated in Figure 10, which shows how O_2 inhibits consumption of N_2O even at very low O_2 concentrations.

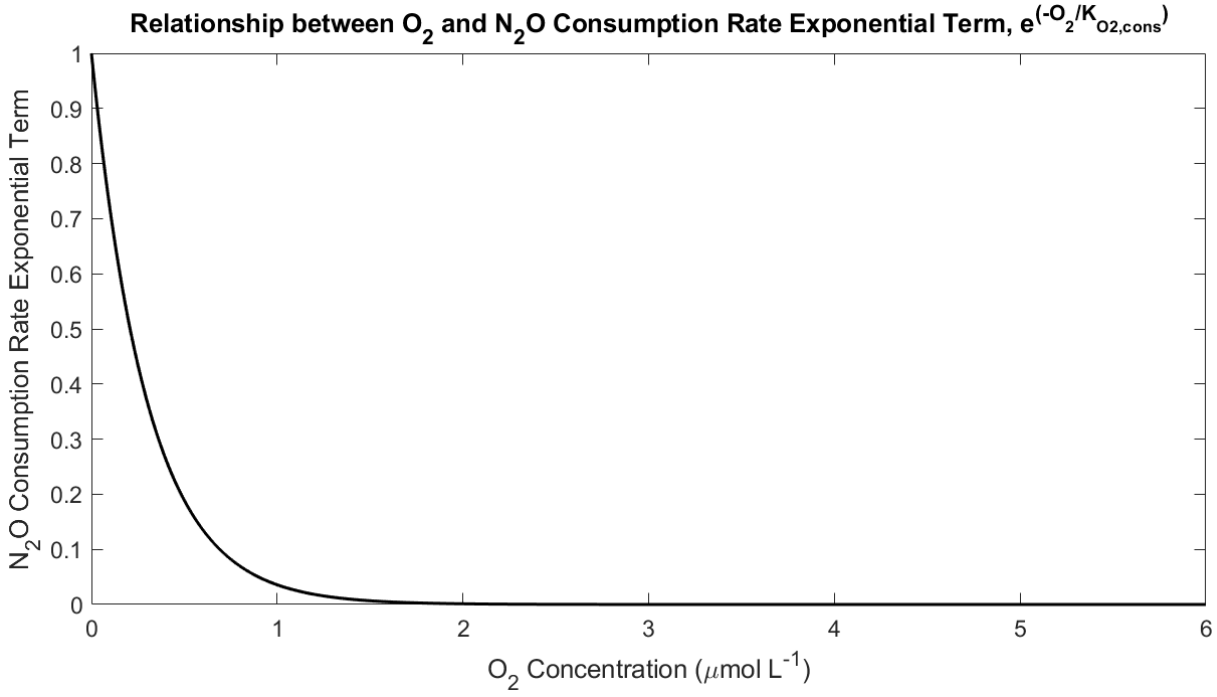

Figure 10: Relative N_2O consumption rate vs. O_2 concentration.

While the O_2 inhibition factor, $K_{O2,cons}$, is set at 0.3 μmol-O_2 L^{-1}, the exponential nature of the N_2O consumption term is such that N_2O is consumed up to O_2 concentrations of approximately 1.5 μmol-O_2 L^{-1}. In this way, $K_{O2,cons}$ is different than the thr_{O2} for suboxic and oxic remineralization in Ω (*Equation 3*) as it isn't a strict threshold but a limiting term.

Table 2 details the model parameter values.

Table 2: Table of Parameters for Model Process Equations

Name	Label	Value	Reference	Level of Confidence
Nitrification dependence on O_2 half saturation constant	$K_{O2,AmOx}$	5 μmol-O_2 L^{-1}	Martens-Habbena et al. 2009, Babbin et al. 2015	Medium
Suboxic Remineralization dependence on NO_3^- half saturation constant	$K_{NO3,remin}$	5 μmol-NO_3 L^{-1}	Babbin et al. 2015	Medium
N_2O consumption O_2 inhibition term	$K_{O2,cons}$	0.3 μmol-O_2 L^{-1}	Dalsgaard et al. 2014, Babbin et al. 2015	Low
Rate constant for ammonium oxidation	k_{AmOx}	0.8 d^{-1}	-	ǂ
Rate constant for remineralization	k_{remin}	0.25 d^{-1}	-	ǂ
Rate constant for N_2O consumption	k_{cons}	0.8 d^{-1}	-	ǂ
Implicit irradiance parameter	E_x	1.00 mol m^{-2} d^{-1}	-	Christian et al. 2022
Nitrification yield constant	a	0.2 μmol-O_2 L^{-1}	Ji et al. 2018	Medium
Nitrification yield constant	b	0.08 (n.d.)	Ji et al. 2018	Medium
Reference Temperature	T_{ref}	285.15 K		ǂ
Activation Energy	E_a	54,000 J mol^{-1}	Raven and Geider 1988	Medium
Gas Constant	R	8.31447 J K^{-1} mol^{-1}	J K^{-1} mol^{-1}	ǂ
Oxygen threshold for oxic vs. suboxic remineralization	thr_{O2}	6 μmol-O_2 L^{-1}	-	Low
Redfield ratio of oxygen to nitrogen	$R_{O2:OrgN}$	(106:16), or 6.625 (mol O_2/mol N)	Redfield 1958	Medium
Redfield ratio of nitrate to organic nitrogen	$R_{NO3:OrgN}$	(106:16)*(4:5), or 5.300 (mol C/mol N) x (mol NO_3^-/mol C)	Redfield 1958	Medium
Redfield ratio of organic carbon to organic nitrogen	$R_{C:OrgN}$	(106:16) or 6.625 (mol C/mol N)	Redfield 1958	Medium
Dilution Rate[+]	DR	0.25 d^{-1}	-	ǂ

[+]*Dilution Rate to be discussed in Section 2.2.*

ǂ *Parameter is intrinsic to model structure or is arbitrary (T_{ref}) or a known physical constant (R).*

2.1.2 Environmental Conditions

In addition to the process equations described above, there are also environmental conditions that influence the state variables' rates of change. Namely, temperature, *T*, which influences remineralization rates, and solar irradiance. Also relevant is how detritus (D) concentrations are generated and input to the system. The source data for detritus uses the flux of particulate carbon exported from the euphotic zone from Earth System Model simulations, and so the parameterization for how exported organic matter is attenuated with depth will affect detritus concentrations.

As mentioned above, the effect of solar irradiance on nitrification is described using $E_x/(E_x+E_z)$, where E_z is calculated from surface solar irradiance, E_0, and attenuated exponentially with depth (z) according to a light attenuation coefficient, $a_c = 0.05$ m^{-1} (*Equation 11*) (Arst et al. 1997).

$$E_z = E_0 e^{-a_c z}$$

(Equation 11)

To relate surface solar irradiance, E_0, to biological processes, PAR (Photosynthetically Active Radiation: W m^{-2} or mol m^{-2} d^{-1}) is often used to represent light energy at the ocean's surface in terms of the wavelengths of light energy that are accessible to photosynthetic organisms (Hall and Rao 1999). The PAR fraction of total surface solar irradiance is set at 0.5 (Kirk 1994). Nitrification rates are limited by light, but how much of this is actual inhibition of the process and how much is indirect (due to competition with phytoplankton with ammonium) is not well understood (Smith et al. 2014). PAR is representative of the wavelengths that penetrate the depths where nitrification occurs, and so using this fraction of total irradiance helps simulate how certain wavelengths of light are most responsible for nitrification rate limitation. Surface PAR is depicted in Figure 11, where the top image shows annually averaged PAR at various latitudes and the bottom image shows temporal variations in PAR at various latitudes.

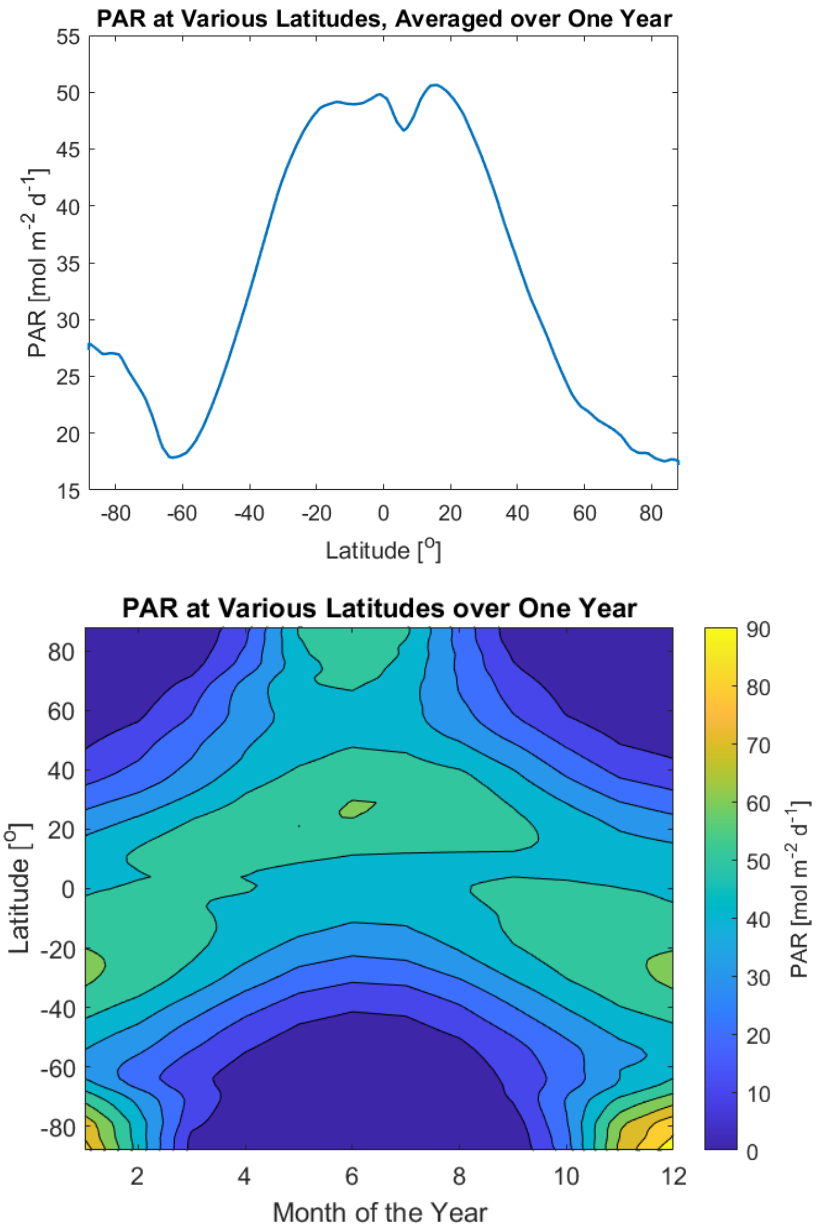

Figure 11: Surface PAR across varying latitudes. Top figure depicts annual averages, while bottom figure depicts monthly variations in PAR over the course of one year. Data from ISCCP (Bishop et al. 1997).

Temperature affects remineralization according to the Arrhenius Equation (T_g) (*Equation 2*), and while spatial variations in temperature are only strong in shallow waters, the circulation of water masses can also cause temperature differences at depth (Figure 12).

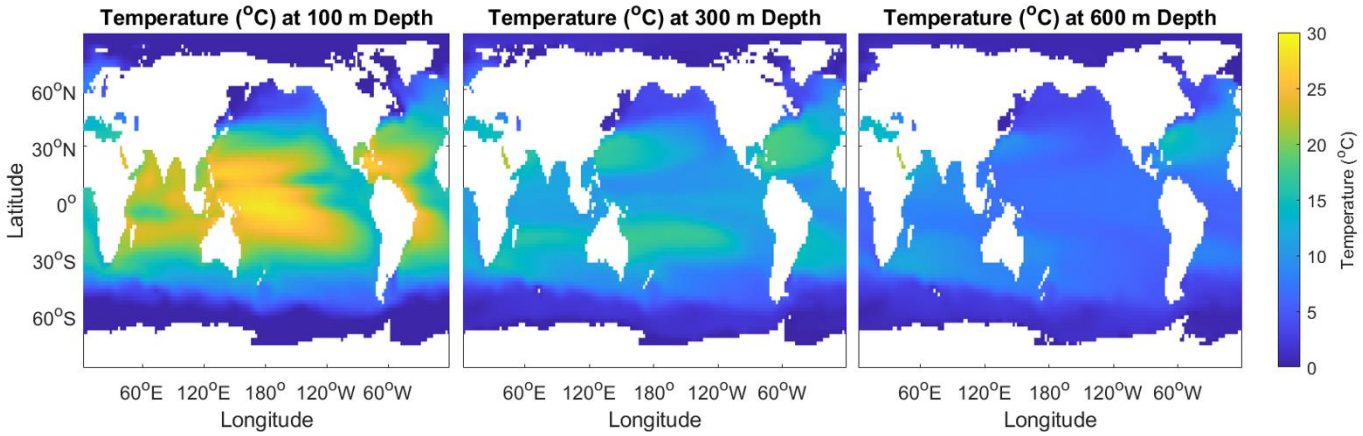

Figure 12: Regional variations in annual mean temperature at depths of 100 m (left), 300 m (middle), and 600 m (right). Data from World Ocean Atlas (Locarnini et al. 2018).

The temperature variation at 100 m is much greater than at 600 m or more (Figure 12), so the effect of temperature on remineralization will be more substantial in shallower waters.

The attenuation of organic matter flux with depth is a strong control on the remineralization rates that affect all N_2O production and consumption mechanisms. Detritus flux from the euphotic zone at 100 m is attenuated exponentially according to *Equation 12* to calculate detritus flux at depth (F_z) (Marsay et al. 2015). F_{eu} is the flux of detrital organic matter (orgN) from the euphotic zone, α_{RLS} = 0.003 m^{-1} is the inverse remineralization length scale, z is depth (m), and z_{eu} is the euphotic zone depth (100 m).

$$F_z = F_{eu} e^{-\alpha_{RLS}\,(z - z_{eu})}$$

(Equation 12)

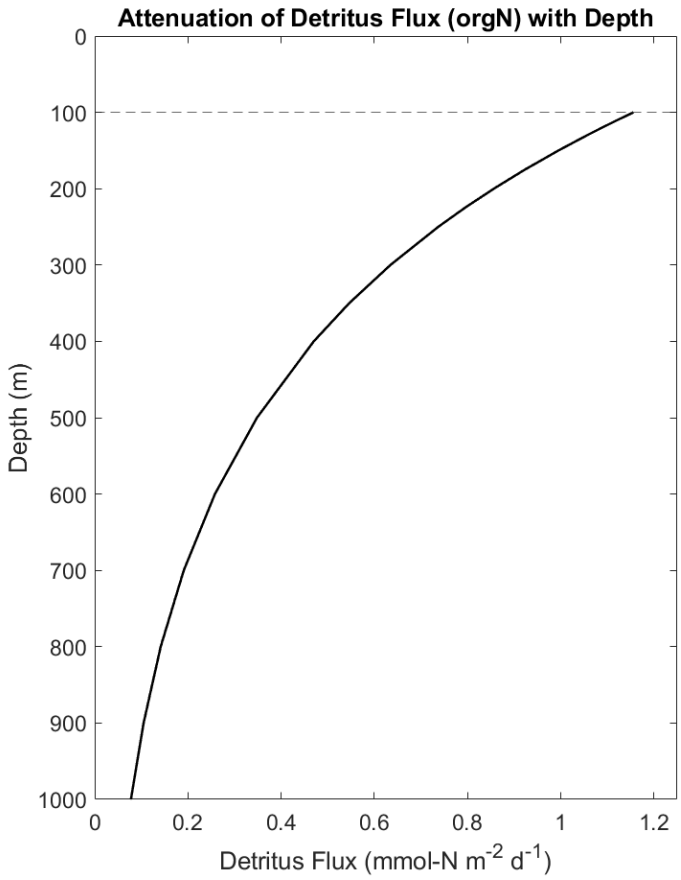

Figure 13: Detritus flux (F_z) with depth using export from the euphotic zone (F_{eu}) and an inverse remineralization length scale (a_c) of 0.003 m^{-1}

The shape of the attenuation curve dictates how much detritus is input into the model at a specific depth, reflecting decreasing concentrations of organic nitrogen with depth (Figure 13). Modelling the availability of organic matter in the ocean is complex and involves many additional parameterizations that are not represented in this model for the sake of simplicity. Including the flux attenuation with depth according to a constant remineralization length scale permits at least a preliminary investigation into how detrital availability affects related N_2O production and consumption processes.

Table 3 provides a list of the sources and conversion factors used for generating input of environmental conditions.

Table 3: Environmental Conditions

Name	Label	Value	Units	Reference	Level of Confidence
Light Attenuation coefficient	a_c	0.05	m^{-1}	Austin and Petzold 1981	Medium
Irradiance at surface	E_0	-	mol m^{-2} d^{-1}	Bishop et al. 1997	High
PAR fraction of total surface solar irradiance	-	0.5	-	Kirk 1994	High
Detritus Flux from Euphotic Zone (100 m)	F_{eu}	-	mol-N m^{-2} d^{-1}	CMIP6 models (see text) global totals normalized to estimates by Resplandy et al. 2019, Nowicki et al. 2022	Medium
Inverse Remineralization Length Scale	α_{RLS}	0.003	m^{-1}	Marsay et al. 2014	Medium
Temperature	T	-	K	Locarnini et al. 2018	High
Oxygen	O_2	-	μmol-O_2 L^{-1}	Garcia et al. 2018a	Low (suboxic)/Medium (oxic)
Nitrate	NO_3^-	-	μmol-NO_3^- L^{-1}	Garcia et al. 2018b	Medium

2.1.3 Data Sets

A series of data sets were used as inputs into this model for temperature, solar irradiance, O_2, NO_3^-, and detritus (in the form of EPC – export of particulate carbon from the euphotic zone). The data are gridded on a 2 x 2^o latitude/longitude using 33 depth layers to generate 3D global output of net N_2O production rates, as well as the individual contributions by nitrification N_2O production, denitrification N_2O production, and denitrification N_2O consumption. The vertical levels are those used in earlier (through 2009) versions of the World Ocean Atlas (e.g., Locarnini et al. 2010).

The 2018 World Ocean Atlas (Locarnini et al. 2018, Garcia et al. 2018a, 2018b) provides temperature as well as NO_3^- and O_2 data products (monthly climatology) in the base case scenario, while model-generated temperature, O_2, and EPC are used in sensitivity analyses. In addition to the O_2 data products provided by the World Ocean Atlas, O_2 data products collated by Kwiecinski and Babbin (2021) are also used. The Kwiecinski and Babbin O_2 data is not gridded, but rather consists of a set of individual profiles (see below Section 3.2). O_2 data is adjusted using a correction scheme by Bianchi et al. (2012), which is discussed further in Section 3.2.

Surface solar irradiance data are taken from the International Satellite Cloud Climatology Project (ISCCP) data set (Bishop et al. 1997) and gridded at the same 2 x 2^{o} resolution. To generate input detritus concentrations, EPC (export production of carbon at 100 m) was taken from Earth System Model simulations using CanESM5 and CanESM5-CanOE (Christian et al. 2022), CNRM-ESM2-1 (Séférian et al. 2019), GFDL-ESM4 (Stock et al. 2020), and UKESM1-0-LL (Yool et al. 2021), with CanESM5-CanOE as the base case. All of the EPC data products are interpolated to the same grid resolution as the World Ocean Atlas and ISCCP data, and the detrital organic matter is translated from units of carbon to units of nitrogen using the same Redfield ratio as for O_2 (see Table 2) All ESM data for present climate are climatologies of the years 1986-2005 of the CMIP6 historical experiment and for future climate years 2081-2100 of the ssp585 experiment (Eyring et al. 2016).

2.2 Chemostat: A Virtual Laboratory

A *virtual chemostat* was created to simulate the above biogeochemical processes. A chemostat is essentially a bioreactor that maintains chemical composition at a controlled level – influent is continuously added and effluent removed at a fixed rate until a constant chemical composition is obtained. A useful metaphor is a beaker filled with active bacterial cultures capable of a known set of chemical reactions. Initially, reactants are added to the beaker to undergo these reactions and be converted into products, with some reactants remaining as 'leftovers' in the effluent (Figure 14). When there is no change in output concentrations of the state variables, steady state conditions are met. For the base case scenario of the model (using the parameterizations and constants listed above), the model takes about 40 days to reach steady state.

To generate these steady state conditions, each *d*[X]*/dt* process equation is appended with an additional dilution term as represented by *Equation 13*. The dilution term takes the input concentration of the state variable, $[X]_{in}$, and subtracts the steady state concentration at each daily time step, [X], then multiplies this by the dilution rate: $DR([X]_{in}-[X])$. Source and sink terms refer to those presented in *Equations 1, 5, 8-10.*

$$\frac{d[\mathrm{X}]}{dt} = Source_X - Sink_X + DR([\mathrm{X}]_{in} - [\mathrm{X}]) = 0$$

(Equation 13)

The chemostat can then be applied to a global 3D framework by running the experiment at every grid point on a global 3D grid. The model uses a uniform 2 x 2^{o} resolution grid with 33 depth levels that range up to 6000 m. There is no physical movement of water or solutes between grid points. As mentioned previously, depths shallower than 100 m are not included because the reactions most relevant to N_2O occur below the euphotic zone.

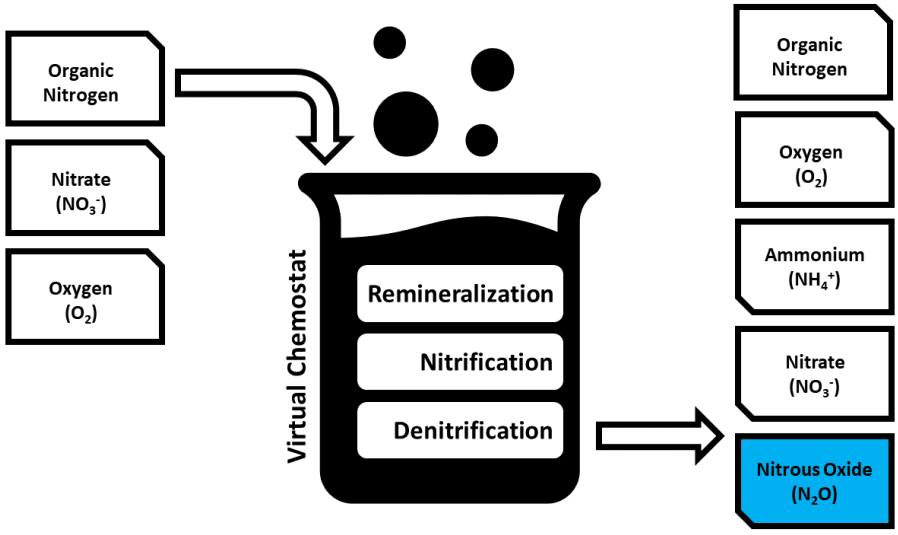

Figure 14: A schematic of the chemostat, illustrating input and output variables and reaction processes.

The chemostat includes remineralization, nitrification, and denitrification reactions using an initial input of detritus (organic nitrogen), NO_3^-, and O_2, with initial and influent NH_4^+ and N_2O concentrations set to zero. The output comprises all five state variables including NH_4^+ and N_2O. N_2 is not included as an explicit state variable as it is not the primary focus of this research; however, conservation of nitrogen was confirmed by calculating N_2 produced as the reaction product of N_2O consumption by denitrification. This method allows individual processes that cannot be separated in situ to be studied independently though computer simulation in a controlled environment. Production from nitrification and denitrification less the consumption in denitrification provides the net N_2O production rate that can then be globally integrated to estimate the global net N_2O production rate.

2.2.1 Chemostat Initialization

The five state variables used are O_2, NO_3^-, NH_4^+, N_2O, and detritus (organic N). O_2 and NO_3^- influent concentrations are provided by 2018 World Atlas data (Locarnini et al. 2018, Garcia et al. 2018a, 2018b), while NH_4^+ and N_2O initial concentrations are set to zero. Organic N is calculated from export of particulate carbon from the euphotic zone (100 m), as provided by five Earth System Models: CanESM5, CanESM5-CanOE, CNRM-ESM2-1, GFDL-ESM4, and UKESM1-0-LL (Christian et al. 2022, Séférian et al. 2019, Stock et al. 2020, Yool et al. 2021). The global total sum of carbon exported from the euphotic zone is normalized to 20 Pg-C y^{-1} – this is a high estimate, compared to the commonly accepted estimate of 9 Pg-C y^{-1} (Resplandy et al. 2019, Nowicki et al. 2022), as only about half of the input of organic matter is remineralized before the system reaches steady state.

Export of particulate carbon is converted to organic N using a Redfield ratio of 106 mol-C:16 mol-N (Redfield 1958) and attenuated with depth using exponential decay at a specified remineralization length scale (see *Equation 12* and Figure 13) and converted from flux into an input concentration by dividing by the chemostat dilution rate.

3 Results

The model results are presented in this section, where the chemostat was run until steady state for all locations in a global 3D grid. The output from the chemostat generates reaction rates, which are integrated over each grid box (2^o latitude, 2^o longitude, varying depth layer thickness) to estimate global production of N_2O in Tg-N y^{-1}. Both net N_2O production rates and N_2O production and consumption rates for individual processes (nitrification production, denitrification production, and denitrification consumption) are generated from this model.

To analyze the sensitivity of ocean N_2O production to input concentrations, environmental conditions, and mathematical parameterizations, changes in the global estimates of N_2O production rates are calculated according to changes in the model input. The base case scenario is presented first in Section 3.1, where global and regional N_2O production rates are established, with the following sections identifying how different data products and varying model parameterizations can affect results.

3.1 Global and Regional N_2O Production

The global and regional N_2O production rates using the base case scenario for the model are presented here. The base case scenario uses the input conditions described in Section 2, which are then altered individually in the following sections to assess model sensitivity. Instead of attempting to align the base case scenario model output with previous models' estimates of global N_2O production rates, the base case is established according to the most modern and widely accepted parameters, parameterizations, and data products. Since model sensitivity is quantified by comparing global N_2O production rates to the output base case scenario, it is also imperative to provide a clear view of N_2O production rates in both suboxic ($O_2 \leq 6$ μmol-O_2 L^{-1}) and oxic conditions ($O_2 > 6$ μmol-O_2 L^{-1}) to better understand how different production pathways influence the global net total.

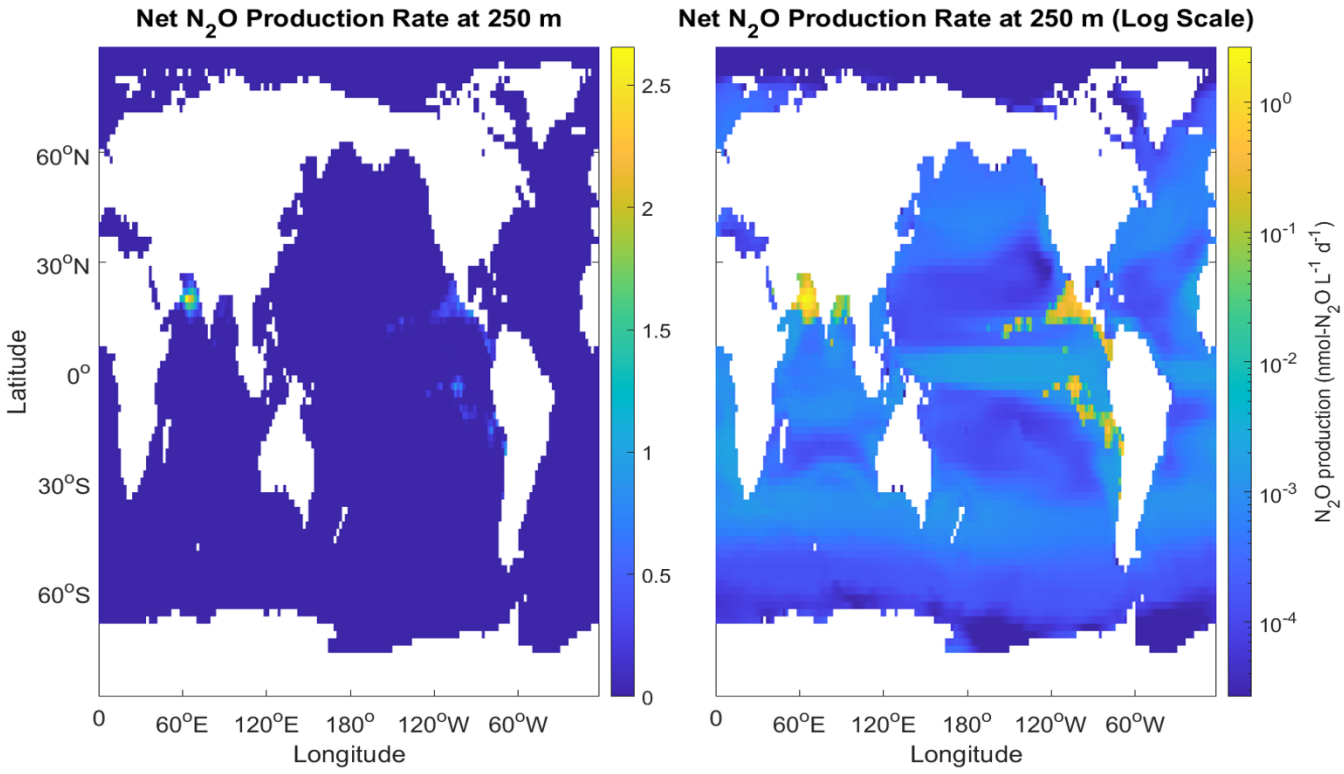

Figure 15: Global Net N_2O Production Rates at 250 m, on a linear (left) and logarithmic (right) colour scale.

Global maps of N_2O production rates at 250 m are shown in Figure 15, using both linear and logarithmic colour scales, and in Figure 16, where N_2O production rates are shown for multiple depth layers between 150 and 1000 m using a logarithmic colour scale.

The oxygen deficient zones can be easily identified as hotspots of N_2O production: N_2O production rates are visibly higher in ODZs, such as in the Arabian Sea, the subtropical Northeast Pacific, and the subtropical Southeast Pacific (Figure 15). Figure 15 (left) highlights the strong difference between these regions, while the logarithmic scale (Figure 15, right) also depicts the spatial variability in the oxygenated ocean. These ODZ 'hotspots of production' are to be expected, as N_2O production rates from denitrification tend to be much higher than from nitrification, and because denitrification takes place in suboxic waters.

Net N_2O production in ODZs is large because N_2O *production* rates by denitrification tend to dominate N_2O *consumption* rates by denitrification, as N_2O consumption only occurs in a very narrow range of suboxic O_2 concentrations (approx. 0-2 μmol-O_2 L^{-1}) while production occurs in a wider range of O_2 from 0-6 μmol-O_2 L^{-1}.

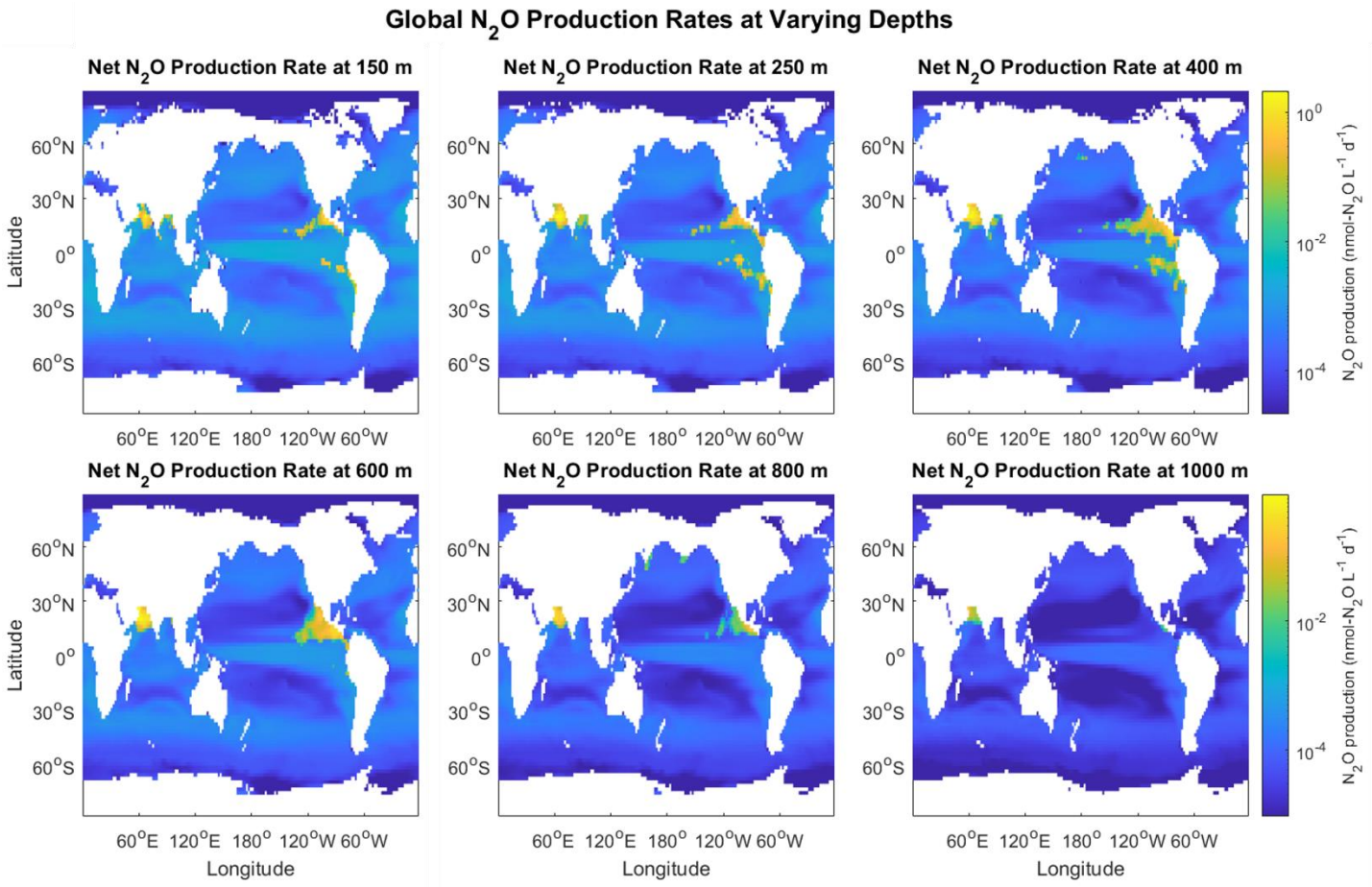

Figure 16: Global Net N_2O Production rates across multiple depth layers from 150 m to 1000 m, using a logarithmic colour scale. Top panels (150-400 m) share a common color scale range, which is different from the color scale range used for the bottom panels (600-1000 m).

The general shape of the ODZ can be observed as the production 'hotspots' change in size and intensity (Figure 16) between depth layers. Net N_2O production rates are higher in the upper depth ranges than in the lower depth ranges, but the ODZs remain visible even at depths up to 800 m. Total N_2O production rates by nitrification and denitrification and N_2O consumption rates by denitrification are depicted in Figure 17 and Table 4. Denitrification production is greater than denitrification consumption in ODZs (Figures 15-17) and denitrification production of N_2O in ODZs is much greater locally than nitrification production in suboxic waters (Figure 20).

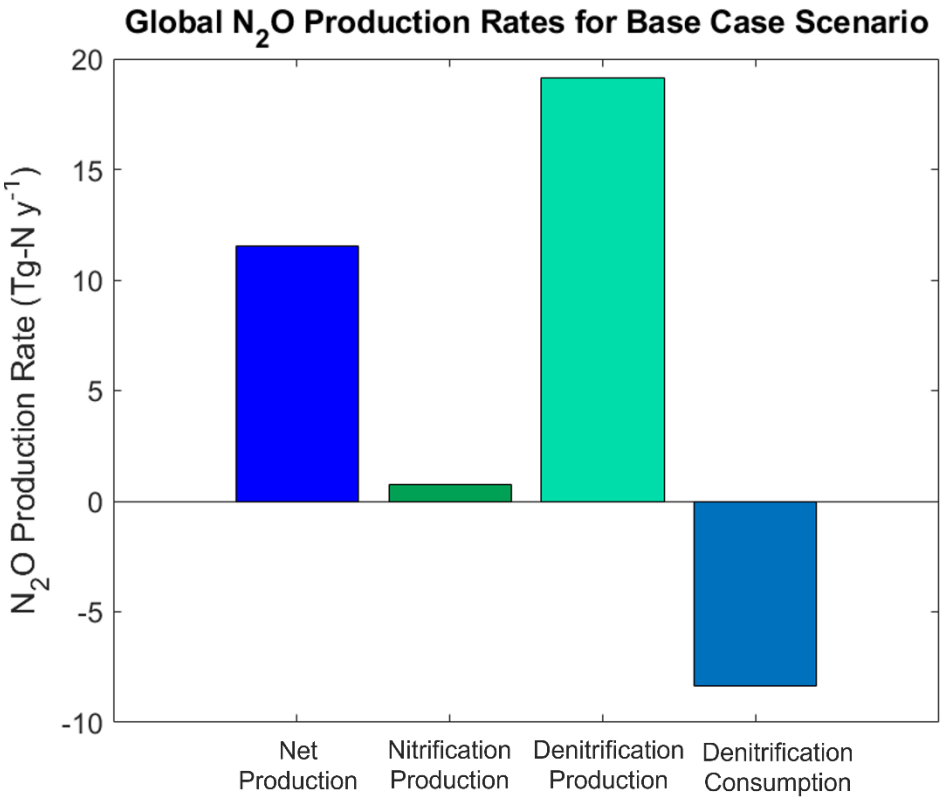

Figure 17: Global N_2O production rates from the base case scenario of the model, including net production, production from nitrification, production from denitrification, and consumption by denitrification. Net production is 11.5 Tg-N y^{-1}, with production by denitrification comprising the majority of global net production.

In the base case scenario, denitrification production is the dominant N_2O production pathway in the global ocean, over 25 times greater than production by nitrification despite denitrification occurring over a much smaller volume of water. Even accounting for denitrification consumption of N_2O, which removes close to half of the N_2O produced from denitrification, the net N_2O production rate from denitrification is over 15 times greater than by nitrification.

Table 4: Model global total N_2O production and consumption rates for base case scenario

Global Net N_2O Production Rate	11.5 Tg-N y^{-1}
Global Nitrification Production Rate	0.740 Tg-N y^{-1}
Global Denitrification Production Rate	19.2 Tg-N y^{-1}
Global Denitrification Consumption Rate	-8.37 Tg-N y^{-1}

To take a more detailed look at regional differences (particularly between ODZs and the oxic ocean), Figures 18 and 19 depict cross-sections of net N_2O production rates in the North Pacific ODZ along 120°W (Figure 18) and the oxygenated North Atlantic along 30°W (Figure 19). The 'hotspot' of high N_2O production is easily observed in the North Pacific as it mirrors the shape of the ODZ in this region but does not appear in the oxygenated North Atlantic.

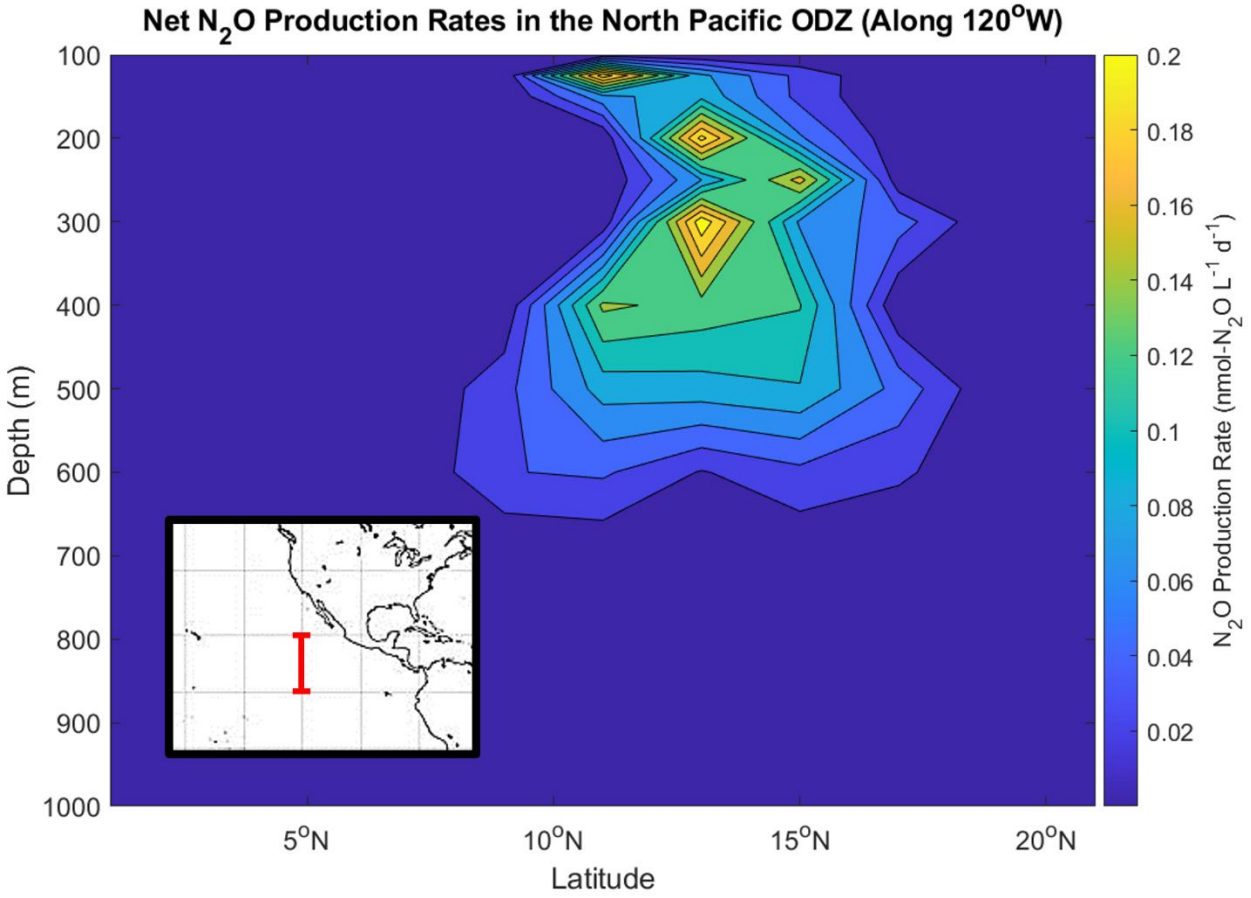

Figure 18: Net N_2O production rates in the North Pacific, along 120°W.

Net N_2O production rates range as high as 0.2 nmol-N_2O L^{-1} d^{-1} in the North Pacific when O_2 reaches the suboxic conditions present in the ODZs but drop rapidly to approx. 0.02 nmol-N_2O L^{-1} when denitrification can no longer occur due to elevated O_2 concentrations.

While there is regional variation in production of N_2O by nitrification in oxic waters, the range of nitrification N_2O production rates is very small relative to the difference between nitrification and denitrification production rates, and so is not easily seen in the depiction of the North Pacific in Figure 18 (note that Figures 15-16 use logarithmic colour scales, while Figures 18-19 do not). This regional variation is more easily seen in Figure 19, which presents net N_2O production rates in the subtropical North Atlantic – as with most of the oxygenated ocean, only nitrification N_2O production takes place as denitrification requires suboxic O_2 concentrations, and the highest rates are several orders of magnitude less than in the ODZs.

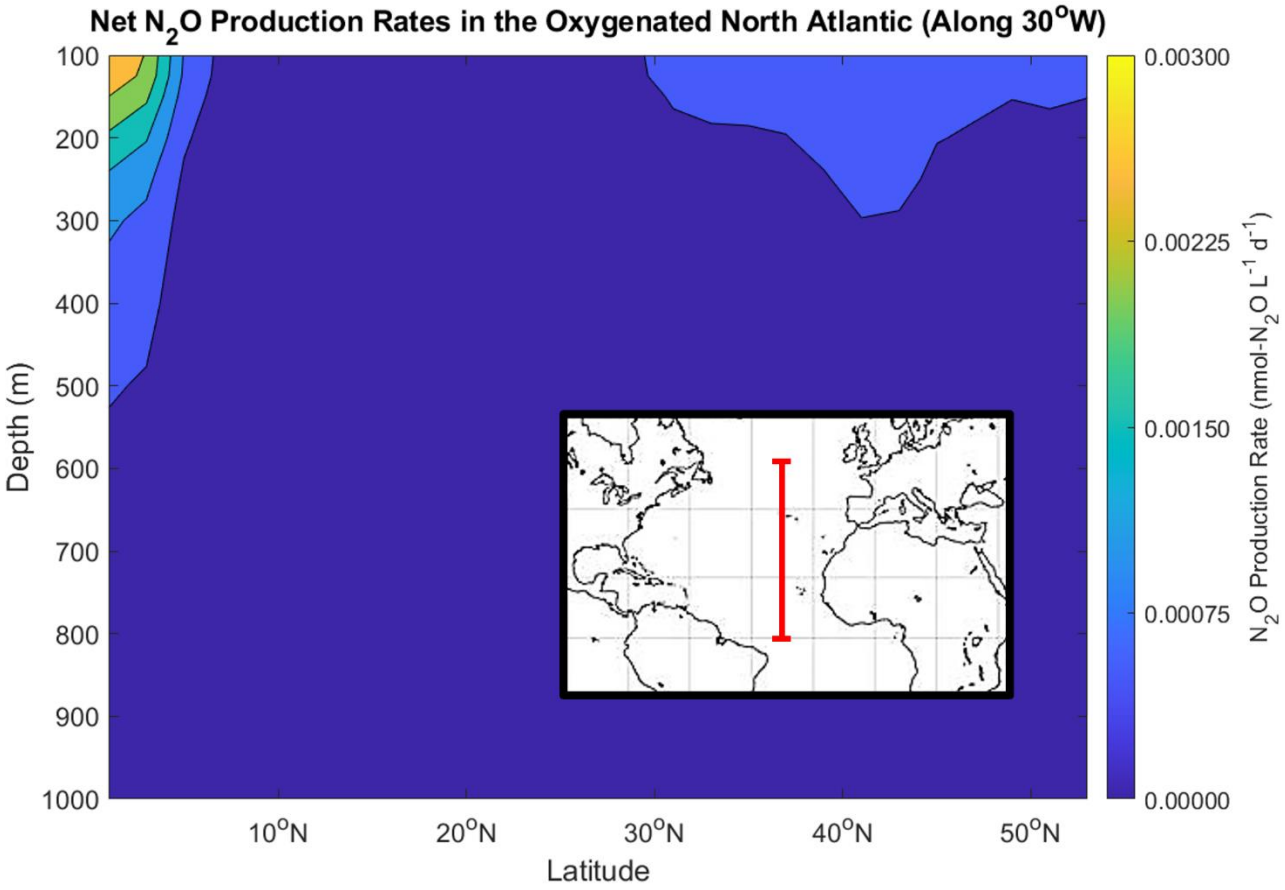

Figure 19: Net N_2O production rates in the North Atlantic, along 30ºW. Note that the colour scale range is smaller than in Figure 18, as N_2O production rates in oxic waters are much lower than those in suboxic waters.

The net N_2O production rates in the oxic waters of the North Atlantic do show some variation that is mostly determined by rates of organic matter remineralization, as well as by O_2 concentrations (Figure 19). Greater availability of detritus and O_2 near the surface allows higher nitrification rates and so greater nitrification N_2O production rates, even though the higher O_2 concentrations decreases *yield* of N_2O (see *Equation 5* and Figure 8). As this model allows no physical exchange of water between grid cells, these differences evolve from the O_2 and detritus data products rather than from movement of water masses.

The highest net N_2O production rates in the North Atlantic reach 0.003 nmol-N_2O L^{-1} d^{-1} (Figure 19), while rates at the boundaries of the North Pacific ODZ (where O_2 is near 6 nmol-O_2 L^{-1} d^{-1}) range between 0.02-0.04 nmol-N_2O L^{-1} d^{-1}. This indicates that net N_2O production rates are higher not only in the core of the ODZs, but also at the boundaries where both nitrification and denitrification reactions occur.

The higher net N_2O production rates at ODZ boundaries could be due to increased yield of N_2O from nitrification at lower O_2 concentrations, despite the lower overall nitrification rates, or due to denitrification production rates that remain high even within the upper suboxic range (5-6 μmol-O_2 L^{-1}) at the ODZ boundaries. To determine which of these reaction mechanisms dominates, a comparison of nitrification and denitrification production rates in the North Pacific ODZ is presented in Figure 20. Note the difference in scale for the colour bars for nitrification versus denitrification – nitrification production rates are three to four orders of magnitude smaller than denitrification production rates.

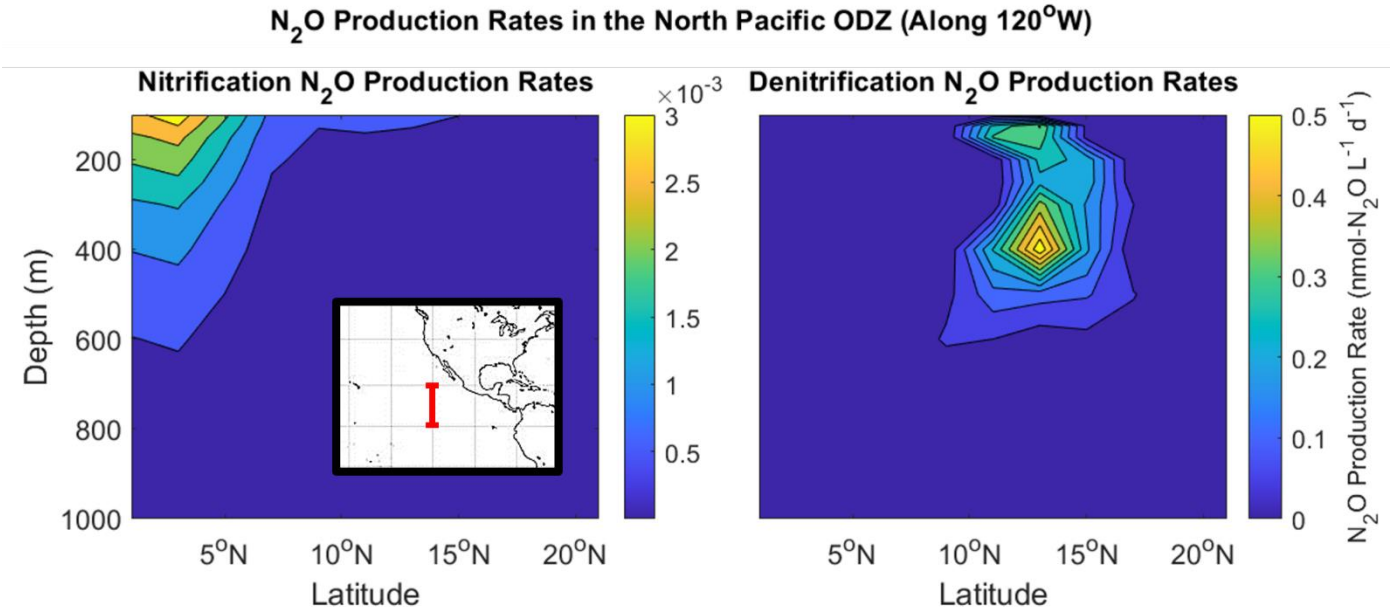

Figure 20: N_2O production rates by nitrification (left) and denitrification (right) for a transect along 120°W.

Nitrification N_2O production rates (Figure 20, left) are more strongly controlled by organic matter supply through remineralization than by O_2 concentrations, such that the ODZ 'hotspot' seen in denitrification N_2O production rates (Figure 20, right) is not present. Nitrification N_2O production rates increase at the surface and towards the equator where there is a greater supply of detritus. Nitrification N_2O production rates are also much lower than denitrification rates for the ODZ region (10°N to 18°N), emphasizing that denitrification production in ODZs – even at the upper suboxic O_2 range - has more control over the net N_2O production rates than nitrification production of N_2O.

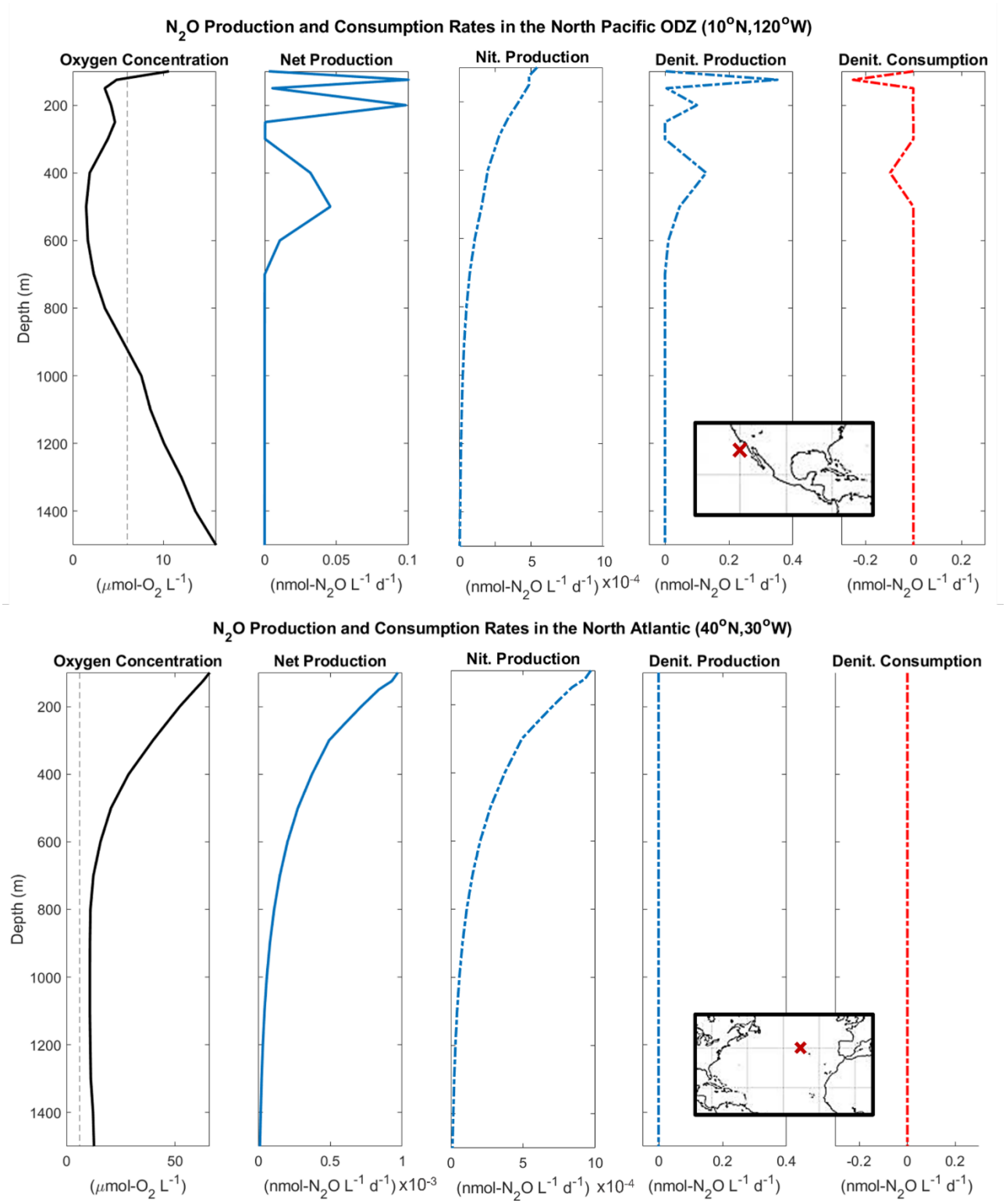

Figure 21: Depth profiles for the North Pacific oxygen deficient zone (10ºN, 120ºW) (top) and the oxygenated North Atlantic (40ºN, 30ºW) (bottom). Vertical dashed line in oxygen concentration plots represent the O_2 threshold for suboxic remineralization at 6 µmol-O_2 L^{-1}.

The regional differences between waters in and at the boundaries of ODZs and in oxic waters far from ODZs can also be illustrated using depth profiles for each of these areas (Figure 21). The rates of N_2O production by denitrification are much higher than by nitrification in ODZs, and rates of N_2O consumption by denitrification tend to be substantially smaller than denitrification production rates as N_2O consumption requires even lower O_2 concentrations than denitrification production. Peaks in the top panel of Figure 21 for denitrification production and consumption occur when O_2 decreases to near-anoxic concentrations, where peaks are larger in shallower waters due to a greater supply of organic matter.

The upper boundaries of the North Pacific ODZ are at approximately 150 m depth, where O_2 concentrations reach below 6 μmol-O_2 L^{-1} and denitrification reactions begin (Figure 21, top). Lower boundaries are less defined but appear to reach approx. 1000 m depth. In the North Atlantic O_2 concentrations do not reach below 6 μmol-O_2 L^{-1}. Therefore, there is no denitrification and N_2O production is entirely from nitrification, leading to lower net N_2O production rates. Nitrification production of N_2O follows the shape of the attenuation of detrital flux (decreasing exponentially with increasing depth) and has much smaller N_2O production rates than in the ODZ (Figure 21, bottom).

Despite the fact that ODZs occupy a relatively small volume of water compared to the oxygenated ocean, global net N_2O production rates by denitrification are higher than global N_2O production rates by nitrification (Table 3). This reaffirms the conclusion that denitrification is the dominant pathway for N_2O production – both on a regional scale within ODZs and on a global scale.

3.2 Sensitivity to Oxygen

This section details the model's sensitivity to input of O_2. Effects of spatial and temporal averaging are analyzed alongside variations in the O_2 and detritus data products input to the model. As discussed in the introduction, O_2 is one of the most fundamental controls on N_2O production rates, especially at the suboxic O_2 concentrations that allow denitrification. This means that data products must be as accurate as possible, especially in the lower O_2 range. Flaws in O_2 data that may generate small differences in other biogeochemical models can have a much more substantial effect on N_2O production.

3.2.1 Deficiencies in Data Products

The first significant problem in the accuracy of O_2 concentrations arises from the collection of interpolated data from the 2018 World Ocean Atlas (WOA) (Locarnini et al. 2018, Garcia et al. 2018). While WOA provides easily accessible global data products, the interpolation involved tends to 'smear out' low O_2 concentrations in a given region, making suboxic concentrations appear higher than observed in individual profiles. Furthermore, early suboxic O_2 measurements have historically been biased high by an average of 5-6 μmol-O_2 L^{-1} yet are still frequently incorporated in modern data sets (Fuenzalida et al. 2009, Ulloa and Pantoja 2009, Naqvi et al. 2010). This was identified and described by Bianchi et al. (2012), who created a simple linear correction method to lower O_2 concentrations to better resemble observations (*Equation 14*). In Equation 14 O_2 is in μmol L^{-1} and any concentrations that become negative as a result of this correction are set to zero.

$$[O_{2,\text{corrected}}] = \max\{1.009[O_{2,\text{WOA}}] - 2.523, 0\}$$

(Equation 14)

Bianchi et al. (2012) used this method to correct the 2005 WOA data set (Garcia et al. 2006), while this model uses the 2018 WOA data set (Garcia et al. 2018a). The Bianchi correction method provides more data points at low O_2 concentrations in the 2018 WOA data set. The difference is illustrated in Figure 22 using a histogram of the number of suboxic data points ($O_2 \leq 6$ μmol-O_2 L^{-1}) using original WOA data and the corrected WOA data.

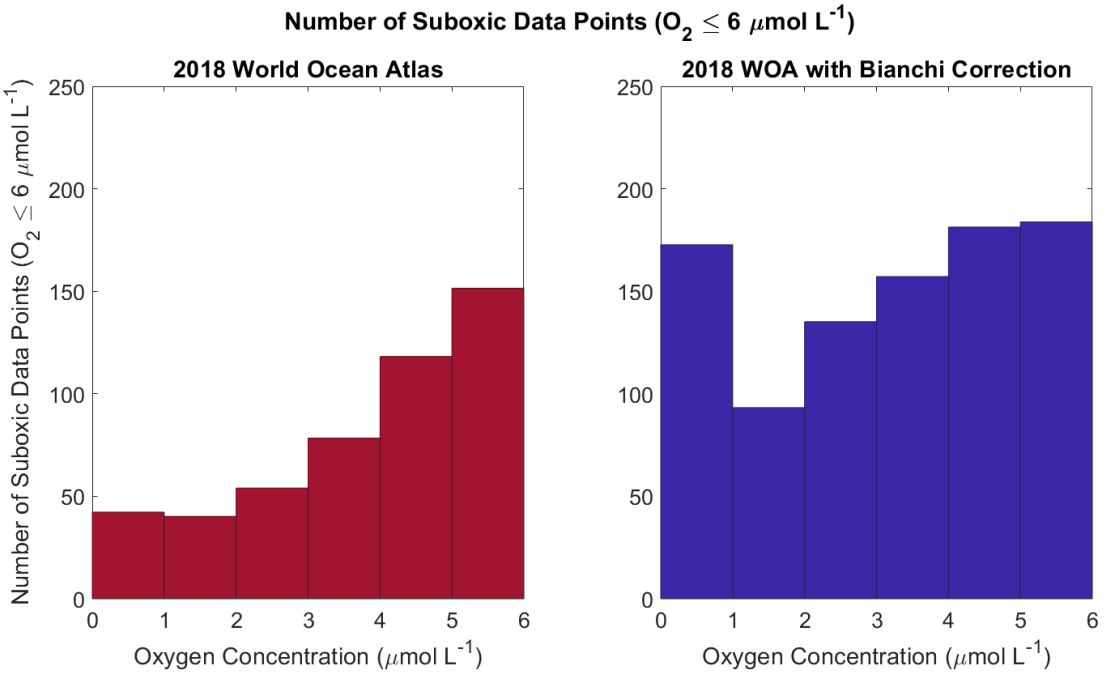

Figure 22: The number of suboxic O_2 data points (0-6 μmol-O_2 L^{-1}) for the unaltered 2018 World Ocean Atlas O_2 data (left), as well as the corrected O_2 data using a linear correction method from Bianchi et al. (2012) (right), where $[O_{2,corrected}] = 1.009*(O_{2,WOA}]-2.523$ (μmol-O_2 L^{-1}). If $[O_{2,corrected}] < 0$, concentration is set to zero.

Applying Bianchi's linear O_2 correction method increases the number of data points for each suboxic concentration range (0-1 μmol-O_2 L^{-1}, 1-2 μmol-O_2 L^{-1}, etc.). The total number of suboxic data points increases from 485 to 923 (0.008% to 0.014% of all data points) and provides a larger range of low-O_2 data to be input into the model. The correction method also adds a much larger amount of data points in the near-anoxic range (0-1 μmol-O_2 L^{-1}). This is because all O_2 concentrations that become negative as a result of the correction are set to zero. O_2 concentrations that reach zero (or close to zero) have been measured *in situ* (Revsbech et al. 2009, Ulloa and Pantoja 2009, Bianchi et al. 2012, Thamdrup et al. 2012, Ji et al. 2018), but the volume of water in the 0-1 μmol-O_2 L^{-1} range is not known due to lack of data and difficulty of measuring O_2 accurately at extremely low concentrations.

The difference in regional O_2 concentrations can be seen in Figure 23, below, which compares O_2 at a location within the North Pacific ODZ (15°N, 110°W) for the original WOA 2018 data and the Bianchi-corrected WOA 2018 data.

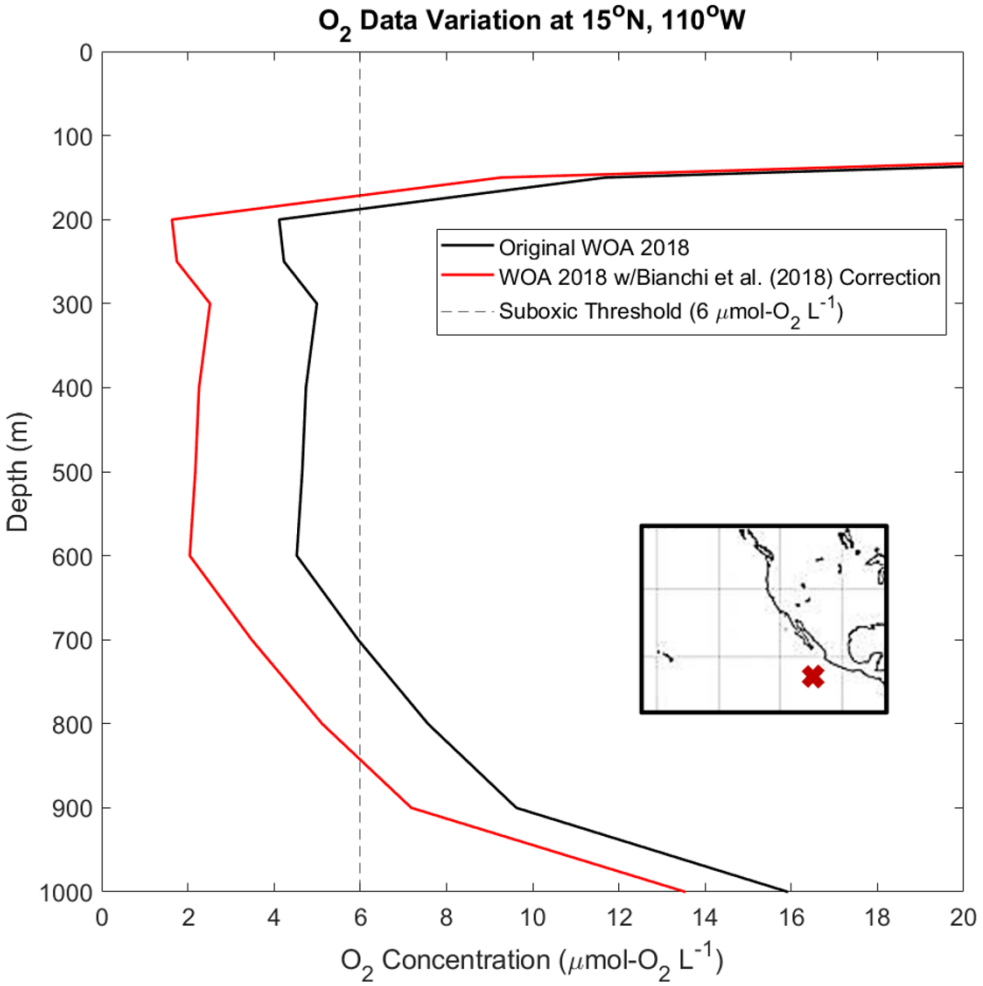

Figure 23: Depth profiles of O_2 concentration in the North Pacific ODZ (15°N, 110°W), with original WOA 2018 data and WOA 2018 data with Bianchi et al. (2012) correction method.

As the Bianchi correction method is linear, the altered data slightly decreases the O_2 concentrations while maintaining the shape of the curve and overall regional trends in O_2. Although the Bianchi correction method generates negligible changes to the model in oxic waters, changes within suboxic waters can be substantial – in this location, it provides double the number of suboxic data points than available in the unaltered data set (Figure 22). For this reason, the Bianchi correction method was applied when establishing the base case model scenario.

3.2.2 Temporal Averaging

To establish whether seasonal variation in O_2 data affects global N_2O production rates averaged over one year, the monthly O_2 concentrations were first compared to each other and then to the global average to determine if O_2 varies substantially enough across the seasons to affect global net N_2O production rates (Figure 24). No substantial difference was found. While O_2 concentrations can vary seasonally in surface waters, this model starts at depths of 100 m.

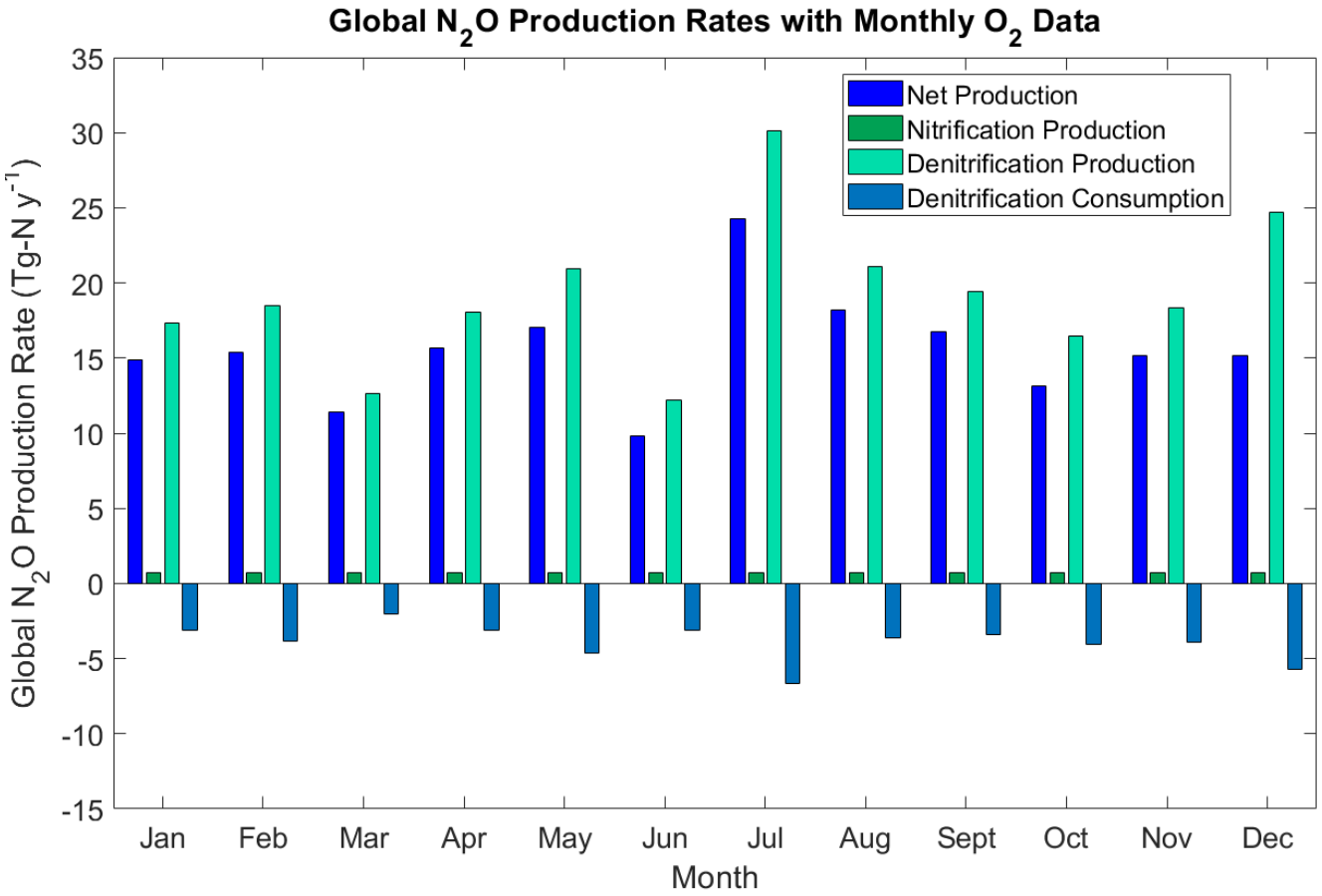

Figure 24: Monthly variation in global N_2O production rates with monthly O_2 data (Garcia et al. 2018a).

While there are variations in N_2O production rates according to monthly input of O_2, there are no discernable trends that follow seasonal cycles (e.g., increased production in March-May for the spring bloom in the Northern Hemisphere and in August-October for the spring bloom in the Southern Hemisphere; seasonal upwelling in April-July from the Eastern Boundary Current (Schwing et al. 1998)). Instead, monthly variation can be attributed to gaps in data collection rather than reflecting true seasonal trends.

However, in the same way that WOA interpolation of data underestimated suboxic O_2 concentrations, leading to high-biased O_2 in ODZs, averaging the O_2 data over the year 'smoothed out' many of the low O_2 concentrations that are important for N_2O production (Figure 25).

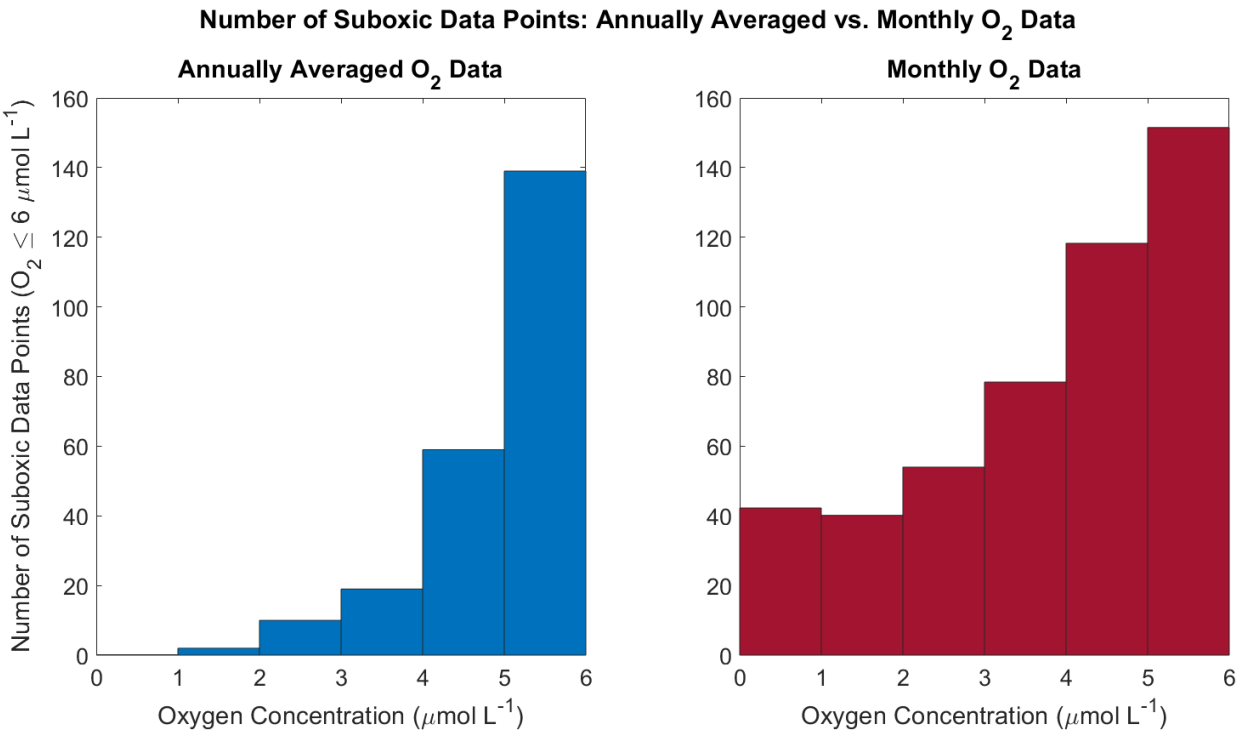

Figure 25: Histogram of the number of suboxic oxygen data points (0-6 μmol-O_2 L^{-1}) for the 2018 World Ocean Atlas data for annually averaged data (blue) and monthly data (red). Monthly data are normalized to the same number of data points as for the annually averaged data.

The histograms in Figure 25 demonstrate how much O_2 data with concentrations below 6 μmol-O_2 L^{-1} is lost when taking an annual average (Figure 25, left) compared to using monthly data (Figure 25, right). Concentrations between 0-4 μmol-O_2 L^{-1} are especially affected, where temporal averaging removes 75-100% of the suboxic data points. When the annually averaged O_2 data products are input into the model, they generate very low denitrification production rates even in the cores of the ODZs, and zero denitrification consumption as O_2 does not reach low enough concentrations.

To further illustrate this point, Figure 26 shows global annual N_2O production rates from the model when using the annually averaged O_2 data or using monthly O_2 data.

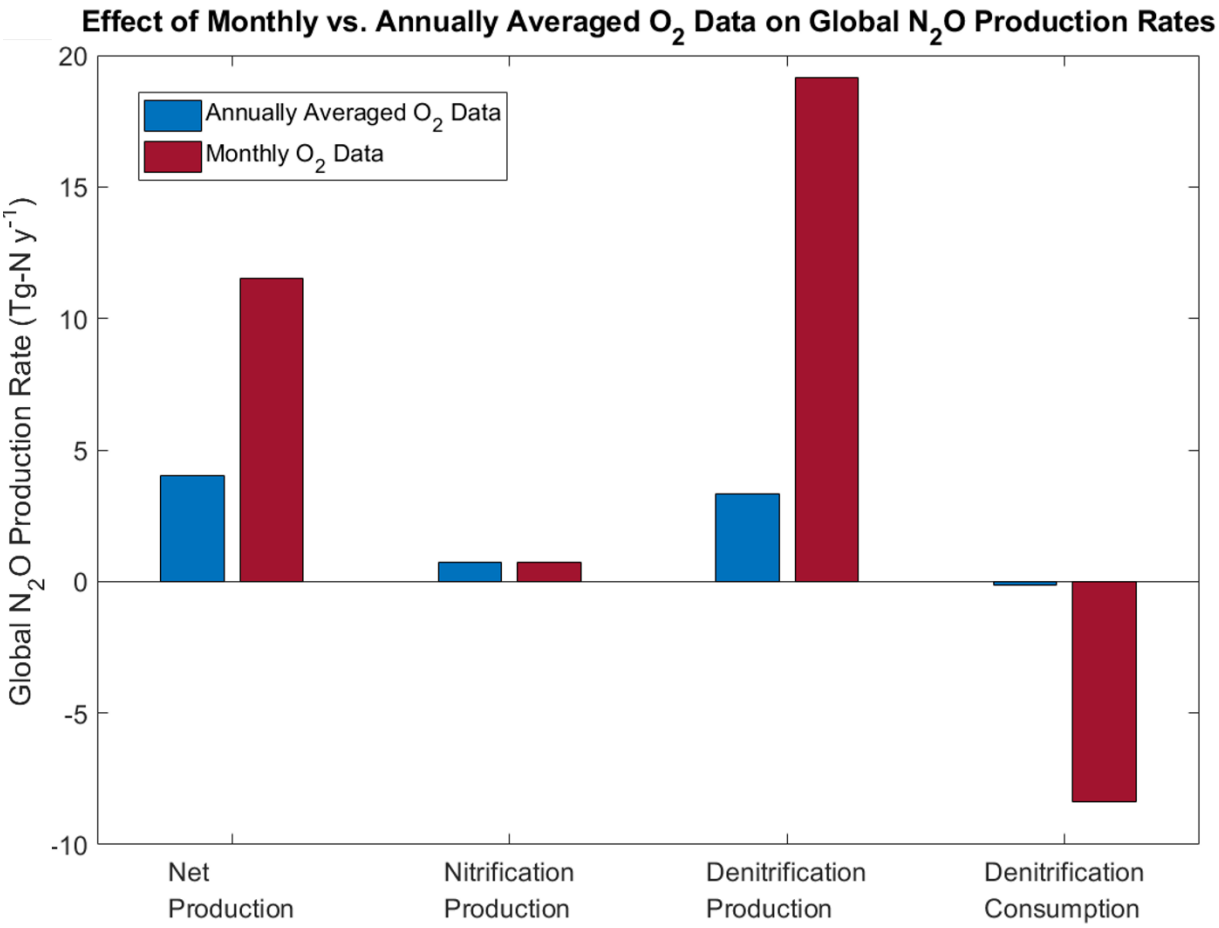

Figure 26: Global total N_2O production rates using annually averaged O_2 data (blue) compared to using monthly O_2 data (red).

The net global N_2O production rates as well as individual reaction rates – especially denitrification production and consumption of N_2O – are massively affected by temporal averaging of O_2 data products (Figure 26). Net production rates decrease by 65% when using annually averaged O_2 instead of monthly data, as denitrification production rates become greatly reduced by 83%, and denitrification consumption rates reach near zero due to removal of the lowest suboxic data points (<1% of the magnitude of consumption rates when using monthly O_2). Nitrification N_2O production rates see negligible effects as annual averaging of data products does not substantially change the O_2 at higher concentrations. Using the annually averaged O_2 (averaged before being input into the model) causes the proportion of nitrification N_2O production to rise in relation to the denitrification N_2O production, since denitrification production rates become much smaller and more comparable to nitrification production rates. For this reason, the monthly O_2 climatology data was used for the base case scenario of the model.

It is important to note that the Bianchi correction method was originally used on annually averaged O_2 data from the 2005 WOA data set, and so applying it to the more recent monthly 2018 WOA data set may produce its own set of uncertainties. Bianchi et al. (2012) were attempting to correct loss of suboxic data points that were in part a result of annual averaging of

WOA data, as compared to instantaneous O_2 concentrations collected *in situ*. Therefore, applying the correction to 2018 O_2 data may be an over-correction of monthly data that no longer suffers from annual averaging. Unfortunately, it is difficult to tell if the 2018 WOA data is more accurate with the correction method or without it. It may be that increasing the amount of suboxic data points, even with a redundant correction method, produces a data set that is more accurate to real world conditions. For this reason, and because Kwiecinski and Babbin's (2021) data set does not yet provide an interpolated O_2 data set for the complete global ocean, the Bianchi correction method was maintained and applied to the 2018 WOA data. The assumption here is that, despite improvements from the 2005 to 2018 WOA data sets, the 2018 WOA data still underestimates O_2 concentrations in suboxic waters and so is improved by the increased number of suboxic data points from the Bianchi correction method.

3.2.3 Regional Averaging and Newly Available O_2 Data Products

Interpolation of observational O_2 data is necessary to creating a global 3D data product, but as detailed in the sections above, it can also cause O_2 concentrations to become biased towards higher concentrations. This is especially true if the observational data are sparse and must be averaged across a large region. Although interpolation techniques have improved, the 2^o x 2^o resolution used here necessitates losing some of the more-extreme-suboxic O_2 concentrations so that low O_2 data may be 'smeared out' in a similar fashion to temporal averaging.

A new method has been proposed that improves understanding of O_2 in suboxic waters – in particular, the size, shape, and intensity of ODZs. Kwiecinski and Babbin (2021) (hereafter referred to as Kwiecinski and Babbin) produced a more precise and accurate representation of the Eastern Tropical Pacific oxygen deficient zone using 0.5^o x 0.5^o resolution by finding the vertical gradient of O_2 ($d[O_2]/dz$). In other words, rather than identifying ODZs by O_2 concentrations, Kwiecinski and Babbin defined the cores as regions where $d[O_2]/dz$ collapse to zero – this allows regions with very low O_2 to be identified without the instrumentational issues that affect absolute concentrations. Tens of thousands of data points are analyzed using this method using data provided by both CTD sensors and Argo floats, generating detailed high 3D resolution of the ODZs in the North and South Pacific. The result is a more highly resolved spatial structure of the ODZ than in previously developed data sets, with more O_2 data in the suboxic range. This method has great promise in understanding the shape and intensity of ODZs, but there is still work to be done in order to produce an accurate, high-resolution gridded data set for O_2 concentrations (as opposed to $d[O_2]/dz$ gradients). The primary benefit of using the Kwiecinski and Babbin data set for O_2 concentrations is a much greater amount of data points, primarily collated from both CTD and Argo float profiles; however, the O_2 concentrations still suffer from the sensor calibration errors inherent to these sampling techniques.

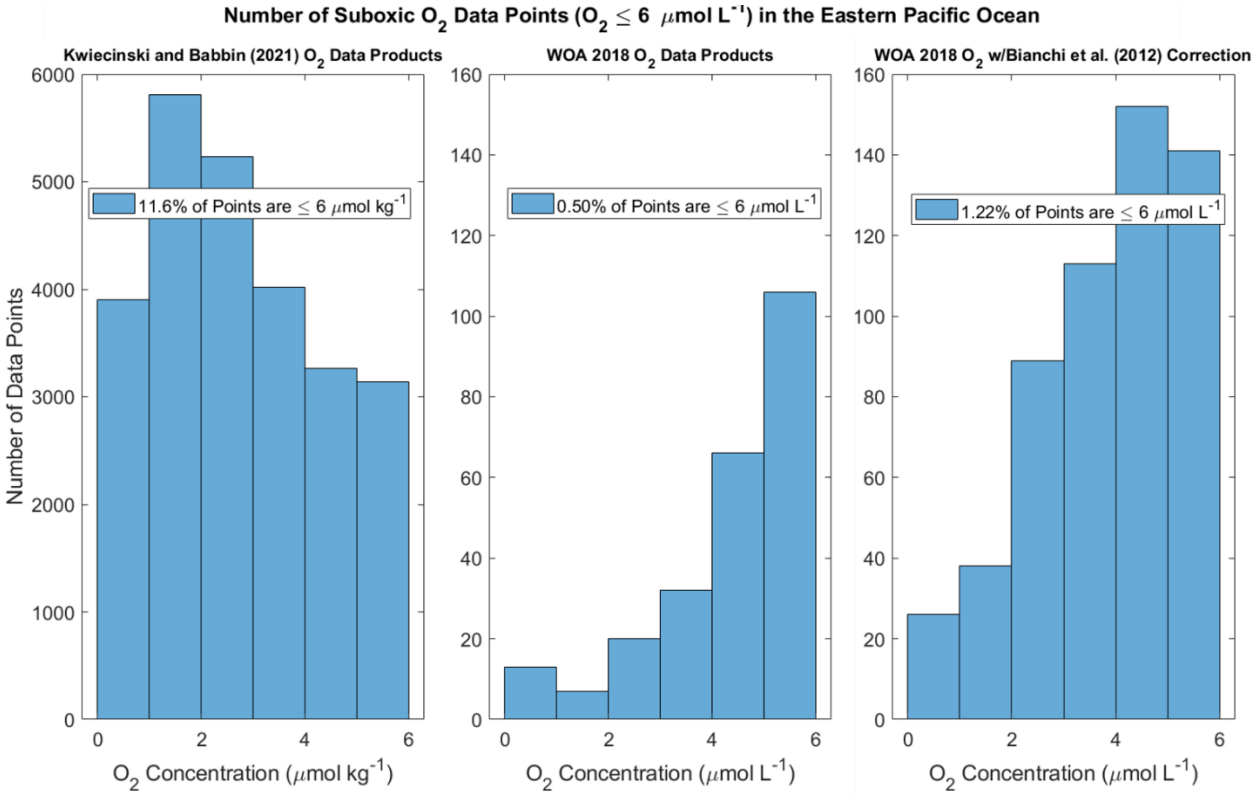

Figure 27: Number of suboxic O_2 data points ($O_2 \leq 6$ μmol kg^{-1}) in the Eastern Pacific Ocean (50°S to 50°N, 180° to 80°W) uses three types of O_2 data products: Kwiecinski and Babbin (2021), WOA2018, and WOA2018 with Bianchi et al. (2012) correction.

The original 2018 WOA data has 0.50% of total data points as suboxic O_2, applying the Bianchi correction method increases that to 1.22%, while the Kwiecinski and Babbin data has nearly ten times that at 11.6% of all data points (Figure 27). This comparison between the interpolated WOA data (with and without the Bianchi correction) and the Kwiecinski and Babbin data is not a perfect 'apples-to-apples' analogy. Firstly, Kwiecinski and Babbin's O_2 concentrations are not interpolated to a uniform gridded data set and so do not suffer from the 'smearing' of data inherent in the interpolated WOA data. Secondly, the individual profiles considered by Kwiecinski and Babbin for their O_2 analysis were located only in the North and South Pacific ODZ regions and therefore may be biased towards suboxic waters. This is not to say that the suboxic data gathered is inaccurate, but that the amount of data collected in low-O_2 waters may be disproportionate compared to a global data set. It remains difficult to determine whether concentrations at specific locations for any of the three data sets are truly accurate – however, the much greater fraction of suboxic O_2 data points provided by the Kwiecinski and Babbin data products suggests that both the original 2018 WOA and the Bianchi-corrected 2018 WOA data products underestimate the amount of suboxic water in the Pacific ODZs.

A comparison between O_2 and resulting net N_2O production rates is provided in the Figure 28, which presents depth profiles at multiple locations for all three O_2 data products – Kwiecisnki and Babbin (2021), original 2018 WOA data, and Bianchi-corrected WOA data. All of these locations are within the geographic scope of the Kwiecinski and Babbin data set (50°S to 50°N, 180° to 80°W).

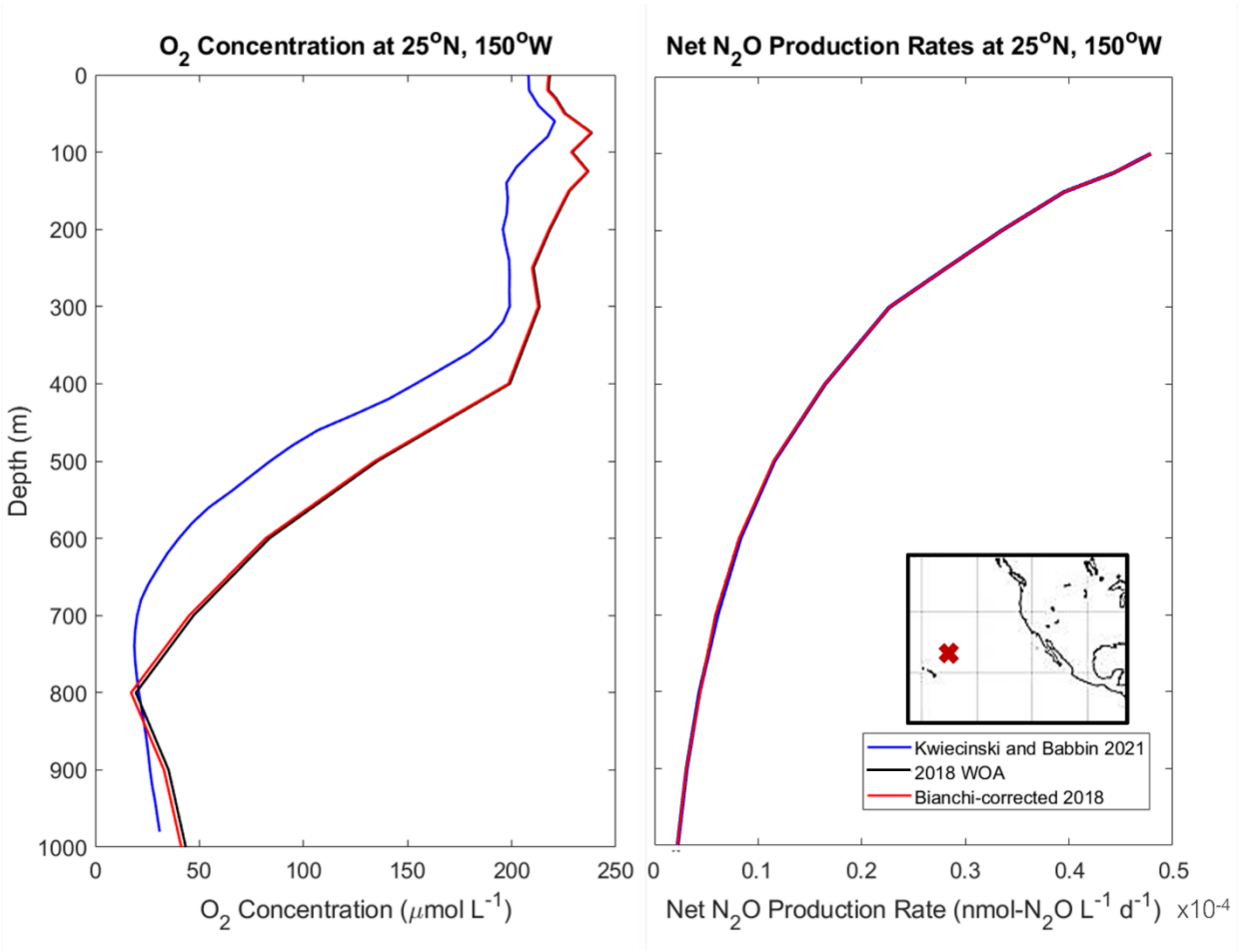
O2 Concentration at 25°N, 150°W
Depth (m)
0
100
200
300
400
500
600
700
800
900
1000
0
50
100
150
200
250
O2 Concentration (μmol L-1)
Net N2O Production Rates at 25°N, 150°W
0
0.1
0.2
0.3
0.4
0.5
Net N2O Production Rate (nmol-N2O L-1 d-1) x10-4
Kwiecinski and Babbin 2021
2018 WOA
Bianchi-corrected 2018

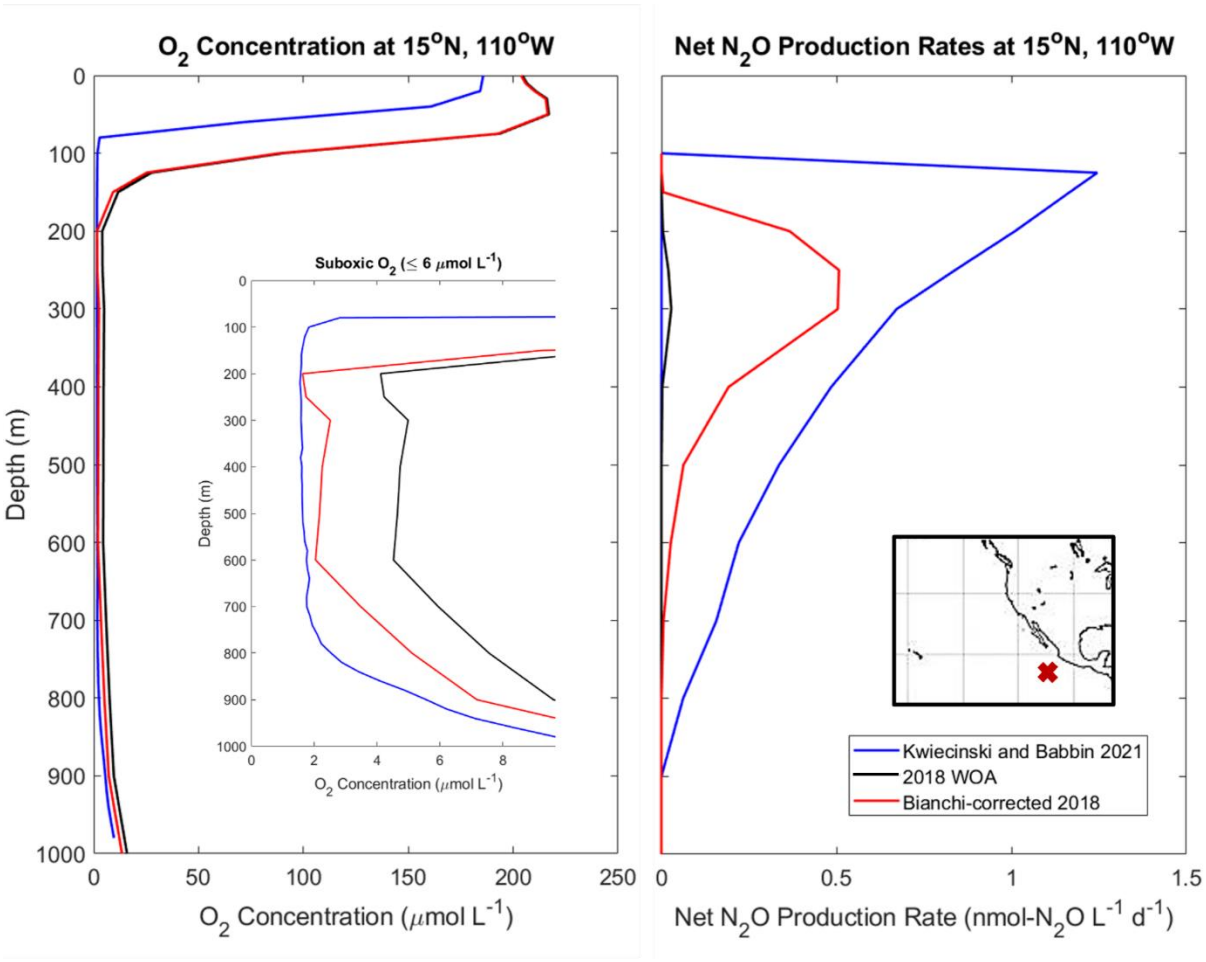
O2 Concentration at 15°N, 110°W
Depth (m)
O2 Concentration (μmol L-1)
Suboxic O2 (≤ 6 μmol L-1)
Net N2O Production Rates at 15°N, 110°W
Net N2O Production Rate (nmol-N2O L-1 d-1)
Kwiecinski and Babbin 2021
2018 WOA
Bianchi-corrected 2018

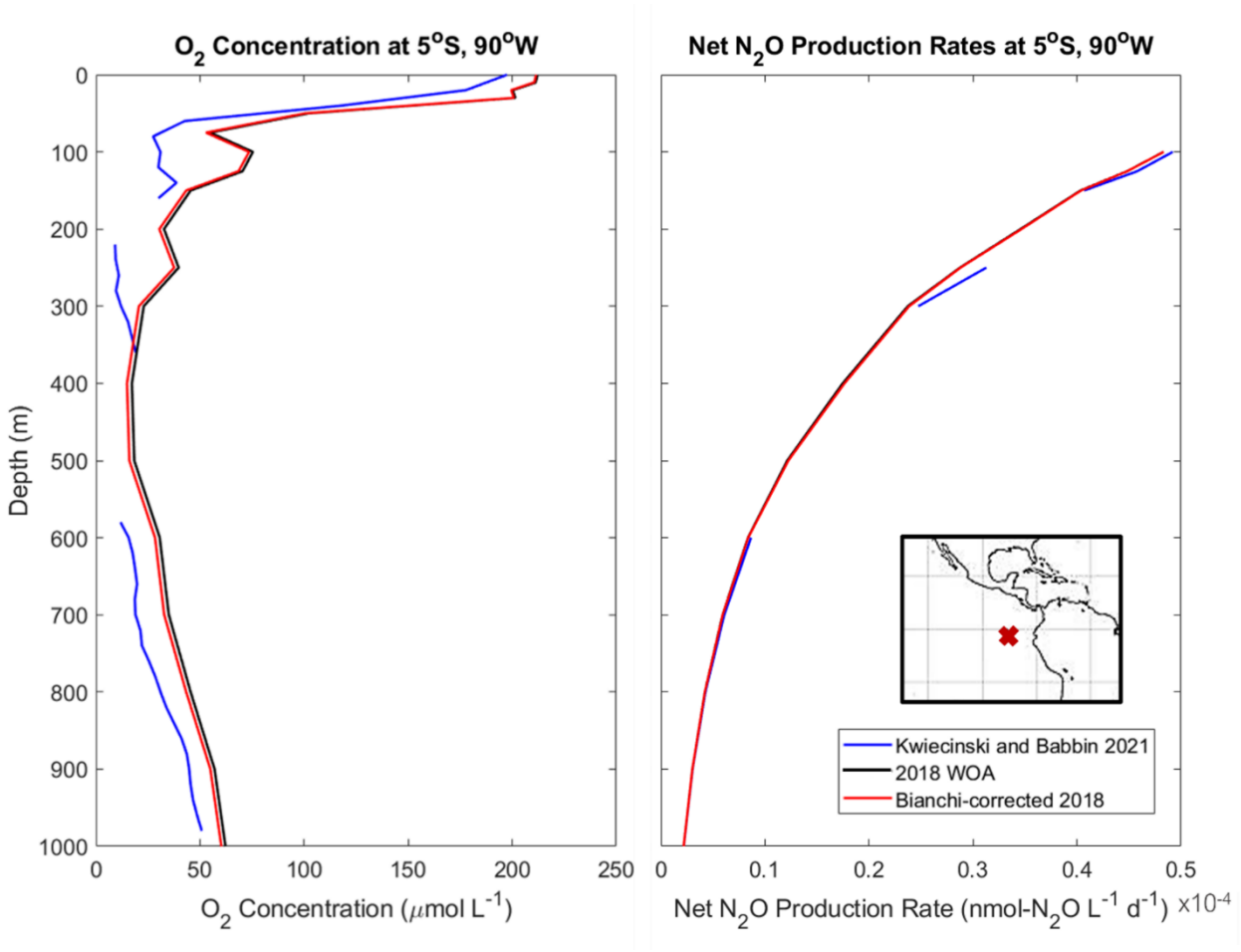
O2 Concentration at 5°S, 90°W
Depth (m)
0
100
200
300
400
500
600
700
800
900
1000
0
50
100
150
200
250
O2 Concentration (μmol L-1)
Net N2O Production Rates at 5°S, 90°W
0
0.1
0.2
0.3
0.4
0.5
Net N2O Production Rate (nmol-N2O L-1 d-1) x10-4
Kwiecinski and Babbin 2021
2018 WOA
Bianchi-corrected 2018

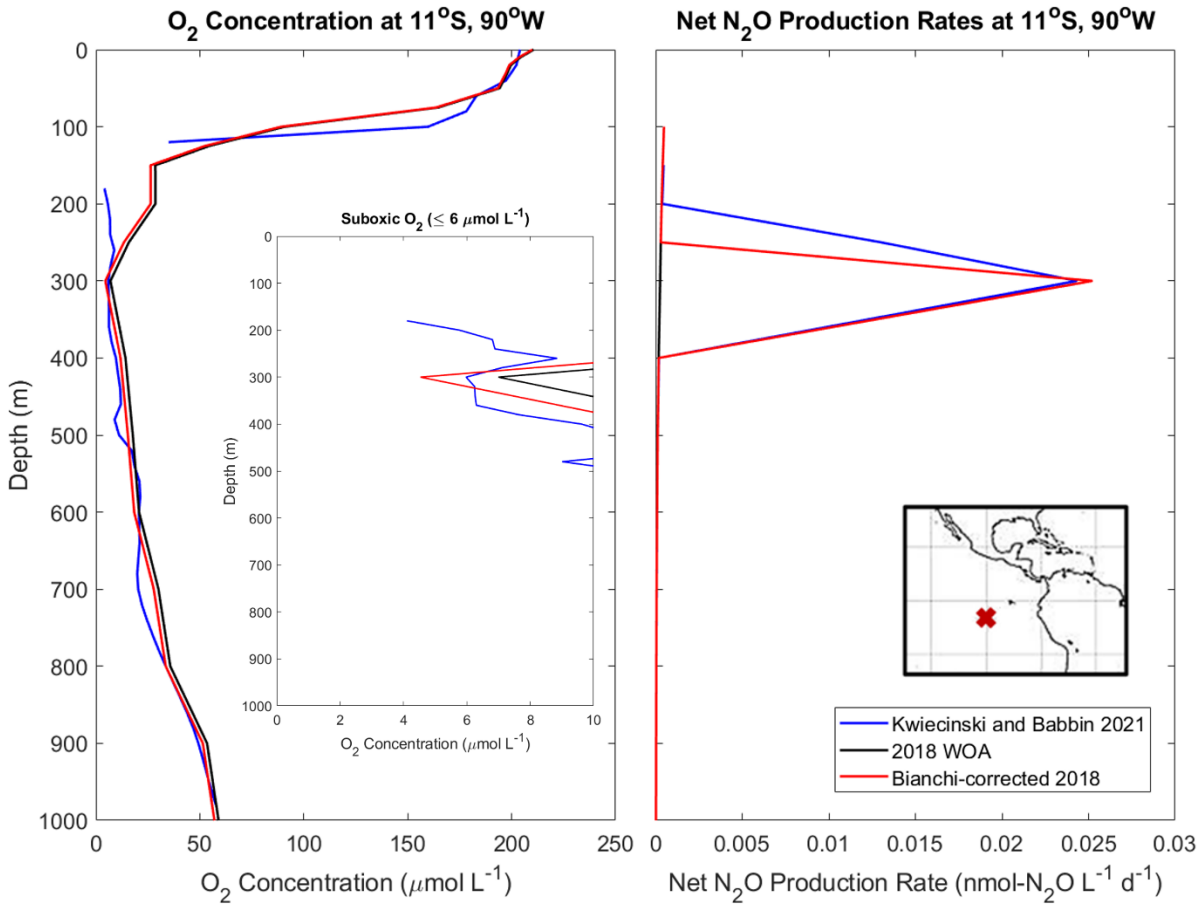

Figure 28: O_2 Concentrations using three different data sets - Kwiecinski and Babbin 2021 (blue), 2018 WOA (black), and Bianchi-corrected WOA2018 (red) - and net N_2O production rates using these O_2 data products. When the difference between WOA2018 and Bianchi-corrected WOA2018 is negligible, the black WOA2018 line may not be visible.

Examples of how the new Kwiecinski and Babbin O_2 data products may affect net N_2O production rates in different regions are depicted above in Figure 28. The first two locations are in the North Pacific although only the location at 15°N, 110°W is located in the North Pacific ODZ. The second two locations are in the South Pacific, and while both are located in the South Pacific ODZ, only the location at 11°S, 90°W reaches suboxic concentrations low enough for denitrification to occur. When O_2 is lower than 6 μmol-O_2 L^{-1}, denitrification production of N_2O increases net N_2O production rates over 3-4 times in magnitude (note the x-axis range for net N_2O production rate) to display peaks of N_2O production. The other two locations have lower N_2O production rates due to nitrification being the only N_2O production process and have rates several orders of magnitude less than the denitrification production rates.

The difference in O_2 depth profiles between the WOA data (and Bianchi-corrected WOA data) and the Kwiecinski and Babbin data is immediately apparent. While the Bianchi correction slightly decreases O_2 from the original WOA while maintaining the same shapes of the curves, the Kwiecinski and Babbin data products generate substantially lower O_2 concentrations for all locations. The shapes of the curves are generally maintained, though to a lesser degree than the

difference between Bianchi-corrected and original WOA data, but the depth of the oxic-anoxic interface is substantially shallower – especially in ODZ locations.

The WOA and Bianchi-corrected WOA data shows an oxycline that is anywhere from 25-100 m deeper than in Kwiecinski and Babbin's data for the North Pacific, though it is only slightly deeper (<25 m) for the South Pacific. The emergence of the oxic-anoxic interface and ODZs at shallower depths can have a substantial effect on the net N_2O production rates. At shallow depths closer to the euphotic zone there is a greater input of organic matter and substrates to be used in N_2O production reactions – combining this with low O_2 at shallow depths will permit N_2O production by denitrification to occur at greater rates than would be possible at deeper locations.

In addition to a generally shallower oxic-anoxic interface, the gradient in the oxycline is much sharper in the Kwiecinski and Babbin data set than in the WOA data sets, reaching low O_2 concentrations more quickly and providing a larger region of suboxic O_2 waters capable of supporting denitrification and high N_2O production rates. Increased volumes of suboxic waters combined with a greater supply of detrital organic matter at shallower depths therefore can result in higher net production by denitrification, where denitrification production rates that are already much higher than rates of production from nitrification are further increased.

This can be seen in the North Pacific ODZ (15^{o}N, 110^{o}W; Figure 28b) where net N_2O production rates are greatly increased when using the Kwiecinski and Babbin data set compared to either of the WOA data sets. The N_2O profile mirrors the shape of O_2 concentrations where the ODZ is visible at a shallower depth and at lower concentrations for Kwiecinski and Babbin data compared to WOA and Bianchi-corrected WOA data. The suboxic O_2 concentrations for the Kwiecinski data set are sustained over a greater range of depths than for WOA, which causes sustained high denitrification N_2O production. This leads to an increase in maximum net N_2O production rates at this location when using Kwiecinski and Babbin's data (1.25 nmol-N_2O L^{-1} d^{-1}) rather than the original WOA data (0.028 nmol-N_2O L^{-1} d^{-1}) – nearly 45 times different in magnitude. Interestingly, this is not true for all locations with suboxic O_2, as the location in the South Pacific (11^{o}S, 90^{o}W) has fairly similar O_2 concentrations across all data sets.

If the Kwiecinski and Babbin data set were applied to regional or global estimates of N_2O production rates, its likely that similarly higher rates would occur across ODZ regions. However, for the time being these water column N_2O production and consumption rates are available only for depth profiles at specific locations.

The effect of higher N_2O production rates due to denitrification processes is restricted to ODZs and suboxic waters that permit denitrification – while the O_2 in oxygenated waters sees similar trends between the Kwiecinski and Babbin data sets and the WOA data sets, the effect on N_2O production rates is negligible. For all regions where O_2 remains > 6 μmol-O_2 L^{-1}, nitrification is the only N_2O production process, and nitrification is less affected by O_2 than denitrification. Even the large differences in O_2 between the Kwiecinski and Babbin data and the WOA data sets produce negligible differences in N_2O production rates.

It should also be noted that while the vertical gradient of O_2 ($d[O_2]/dz$) and its related term *fODZ* used by Kwiecinski and Babbin have been interpolated to create a 3D data set, the actual O_2 concentrations have not been similarly reconciled. Interpolation of the O_2 concentrations and reconciliation with the resolution of other existing data products was determined to be outside the scope of this study and so the Bianchi-corrected WOA data products were maintained for the base case scenario of the model. However, future N_2O models will benefit from the Kwiecinski

and Babbin (2021) data, and so this section provides a brief analysis of the impact of using this O_2 scheme compared to original 2018 WOA and Bianchi-corrected 2018 WOA.

3.3 Sensitivity to Organic Matter Remineralization

Detritus (D) is the substrate for remineralization: oxic remineralization of organic matter provides the NH_4^+ used in nitrification that is subsequently converted into both N_2O and NO_3^-, while suboxic remineralization uses organic matter as a substrate alongside NO_3^- for the first step of denitrification (reduction of NO_3^- to N_2O). While NO_3^- data products are provided by WOA to be used as the model initial conditions, the influent concentration of NH_4^+ is set to zero and so NH_4^+ availability is entirely controlled by the supply of detritus.

The data products used to provide influent detritus concentrations are the export of particulate carbon (EPC) from the euphotic zone as generated by five Earth System Models – CanESM5, CanESM5-CanOE, CNRM-ESM2-1, GFDL-ESM4, and UKESM1-0-LL (see Sections 2.1 and 2.2). The base case scenario of the model uses CanESM5-CanOE. To determine how differences in EPC among models affects N_2O production and consumption rates, spatial and temporal variation are analyzed, as well as differences in the parameterization of detrital flux attenuation with depth (Equation 12).

3.3.1 Temporal Variation

Organic matter can vary seasonally as well as spatially, and unlike O_2 the effects of seasonal changes remain recognizable at well depths below 100 m (Figure 29). To determine how temporal variation affects global N_2O production rates, monthly EPC data was used to generate global N_2O production rates, which can then be compared to global N_2O production rates using annually averaged EPC from the base case scenario (Figure 30).

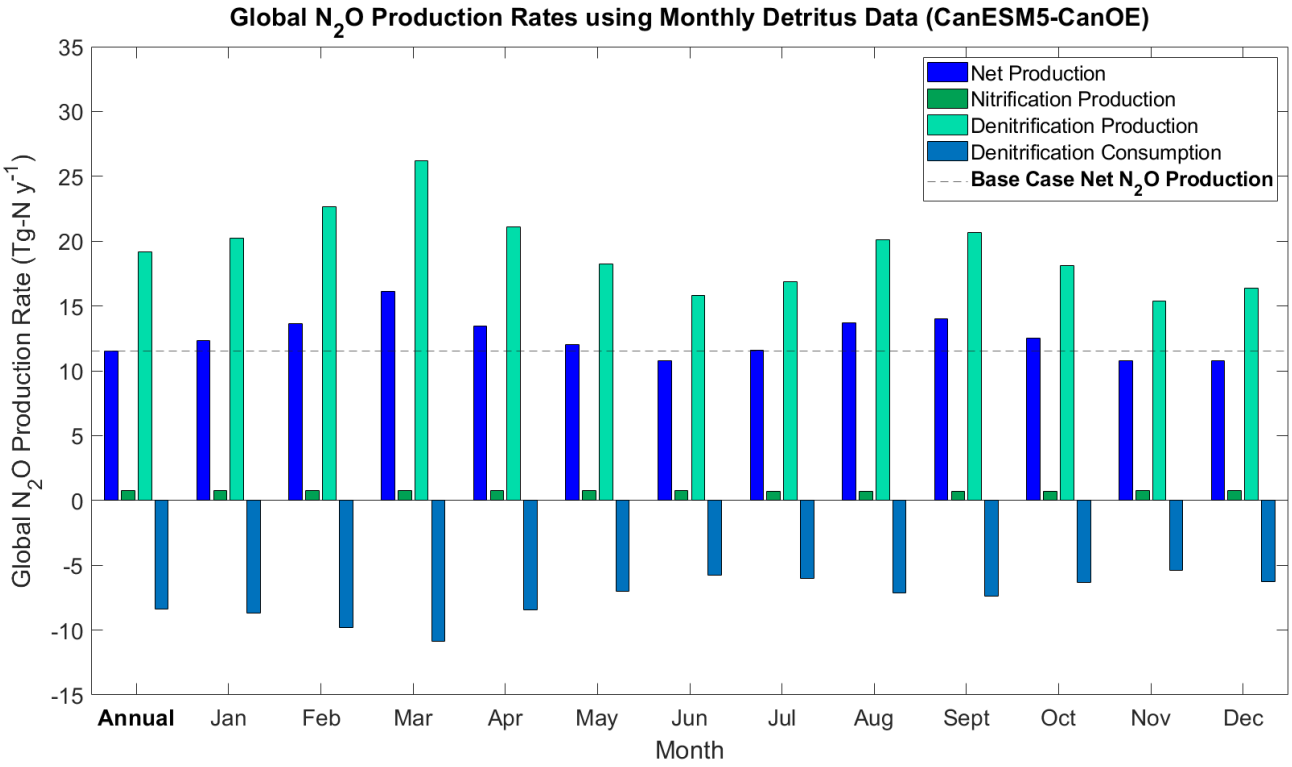

Figure 29: Global N_2O production rates using monthly or annually averaged export production (CanESM5-CanOE). The base case scenario (annually averaged export) is in bold.

The temporal variation in detritus does match seasonal trends of a large spring bloom in February-April from the Northern Hemisphere, followed by a smaller bloom in August-October from the spring bloom in the Southern Hemisphere (Figure 29). However, the difference between using monthly data and annually averaged data is relatively small in terms of global net N_2O production rates. Using the annually averaged EPC only varies slightly from using the monthly data, with a relatively small change in global net N_2O production rates (Figure 30).

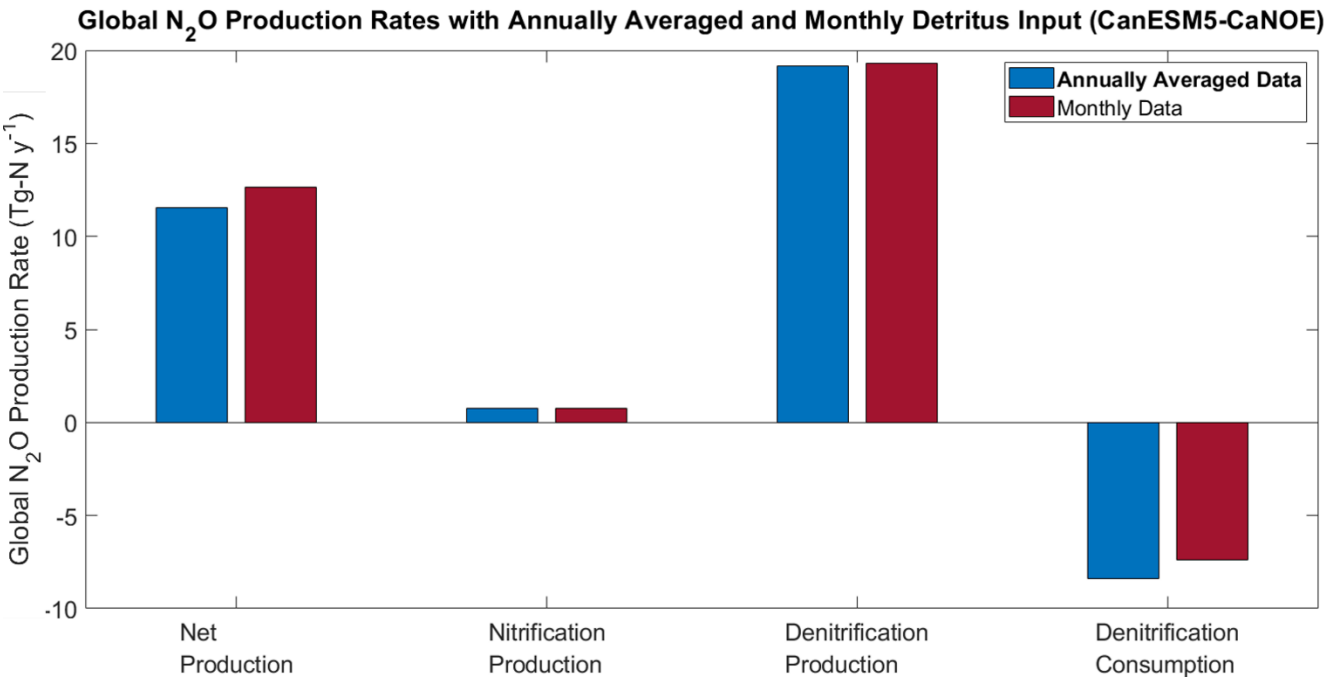

Figure 30: Global N_2O production rates using monthly or annually averaged export production (CanESM5-CanOE).

There is a slight change in denitrification production rates accompanied by a larger change in denitrification consumption rates, but the effect on net N_2O production rates remains small at only an 8.9% difference. This implies that the model is not strongly sensitive to the seasonality of detritus flux.

3.3.2 Spatial Variation

To determine the effects of spatial variation among the EPC data from the five models, the global total of exported carbon from each is first normalized to 20 Pg-C y^{-1} (as in the base case scenario). This allows only regional variation between models to be assessed without discrepancies in the total amount of export affecting the results (Figure 31).

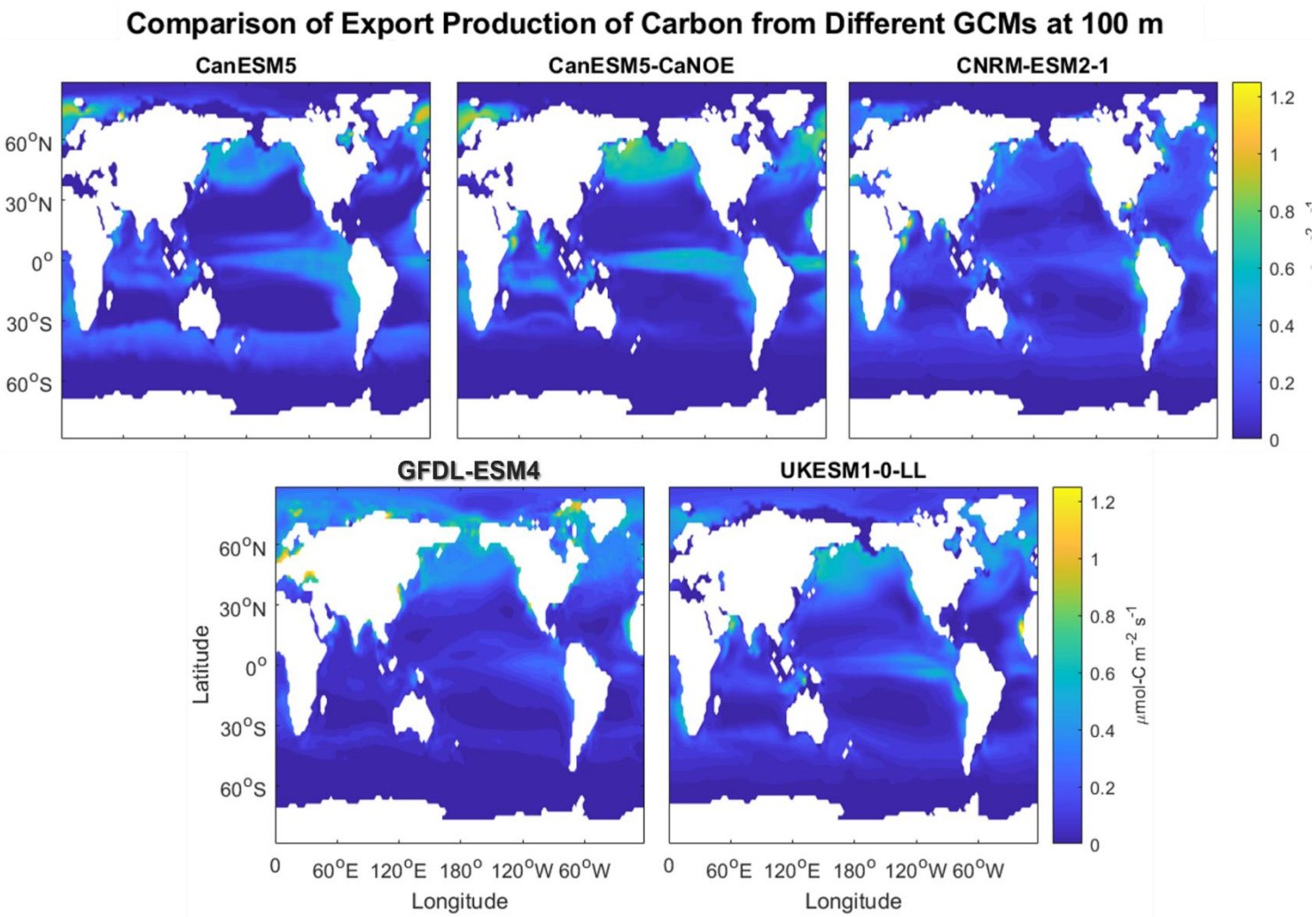

Figure 31: Export production of carbon from the euphotic zone as generated by five Earth System Models: CanESM5, CanESM5-CanOE, CNRM-ESM2-1, GFDL-ESM4, and UKESM1-0-LL.

Figure 31 provides a visualization of the spatial variation of particulate carbon flux from the euphotic zone. Figure 32 shows how this affects the N_2O production rates from the model. The interactions among detritus, O_2, NO_3^-, temperature, and solar irradiance all combine to influence N_2O production and consumption rates, but keeping the global total EPC constant allows for estimation of the sensitivity to spatial distribution of EPC among models.

The choice of EPC data products substantially affects global N_2O production even when the data products use the same global total EPC (Figure 32). Denitrification production and consumption in particular are the most affected.

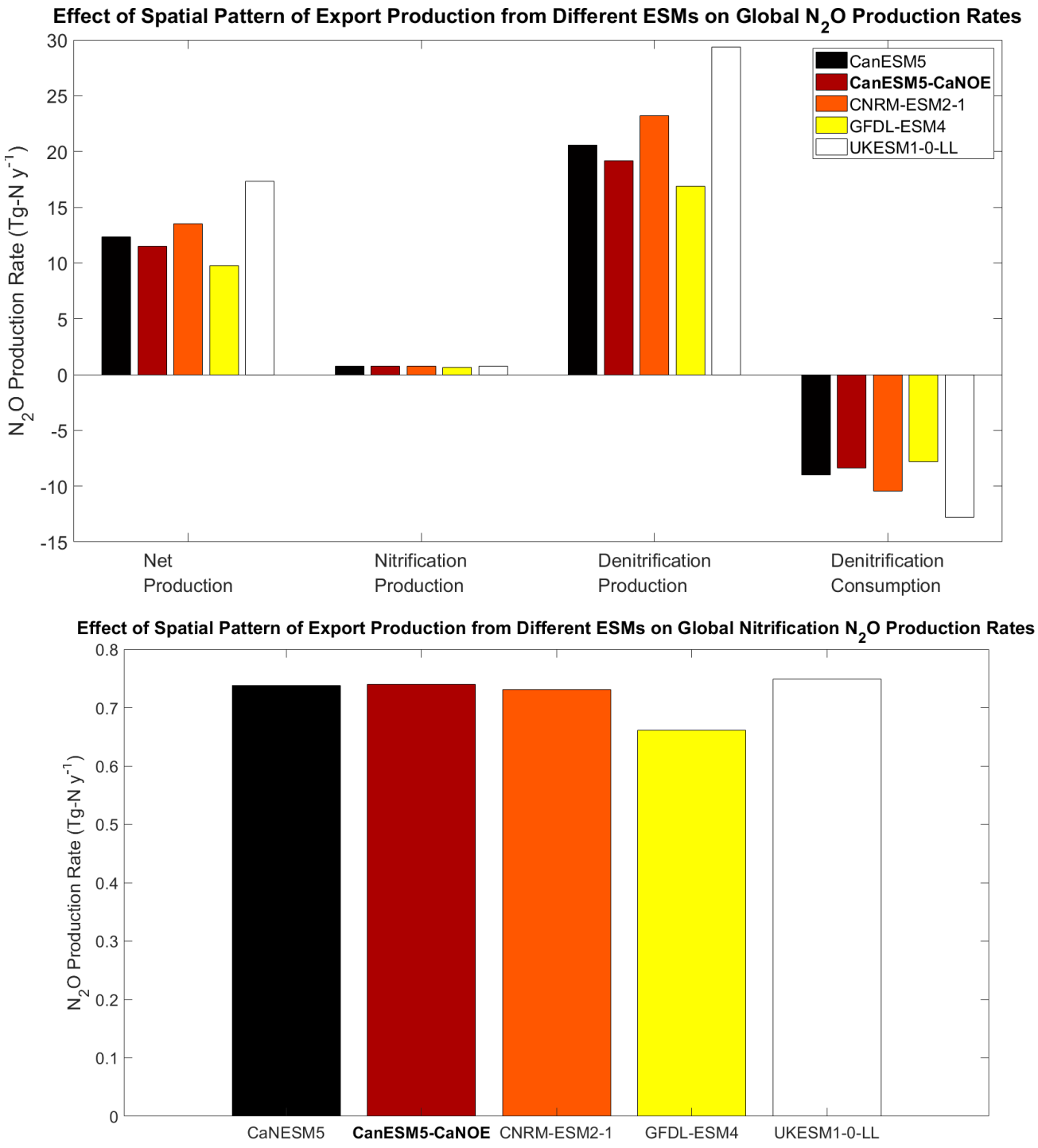

Figure 32: Global N_2O production and consumption rates using export production of particulate organic matter from the euphotic zone from different Earth System Models. Bottom panel depicts the nitrification production rates in the top panel at a larger scale. Base case (CanESM5-CanOE) is in bold.

When there is higher EPC overlying the ODZs, there tends to be higher net N_2O production rates due to greater substrate supply for use in denitrification reactions. If there is more organic matter available in the regions overlying ODZs, then there will be more reactants to fuel denitrification in suboxic waters. Differences between the spatial distribution of EPC from choice of Earth System Model have a moderate effect on net N_2O production rates of up to 43.7%.

3.3.3 Detrital Flux Attenuation with Depth

Detritus attenuates with depth exponentially according to *Equation 12*, where organic matter flux from the euphotic zone decreases with depth according to a constant remineralization length scale (α_{RLS}). For the base case scenario, detrital flux is calculated using CanESM5-CanOE model output and attenuated with an inverse remineralization length scale, α_{RLS} = 0.003 m^{-1}. To determine how strongly the remineralization parameterization affects global net N_2O production rates, α_{RLS} is varied between 0.001 and 0.02 m^{-1} to see how flux attenuation with depth affects the input of detritus to the model, and so the remineralization rate and N_2O production (Figure 33).

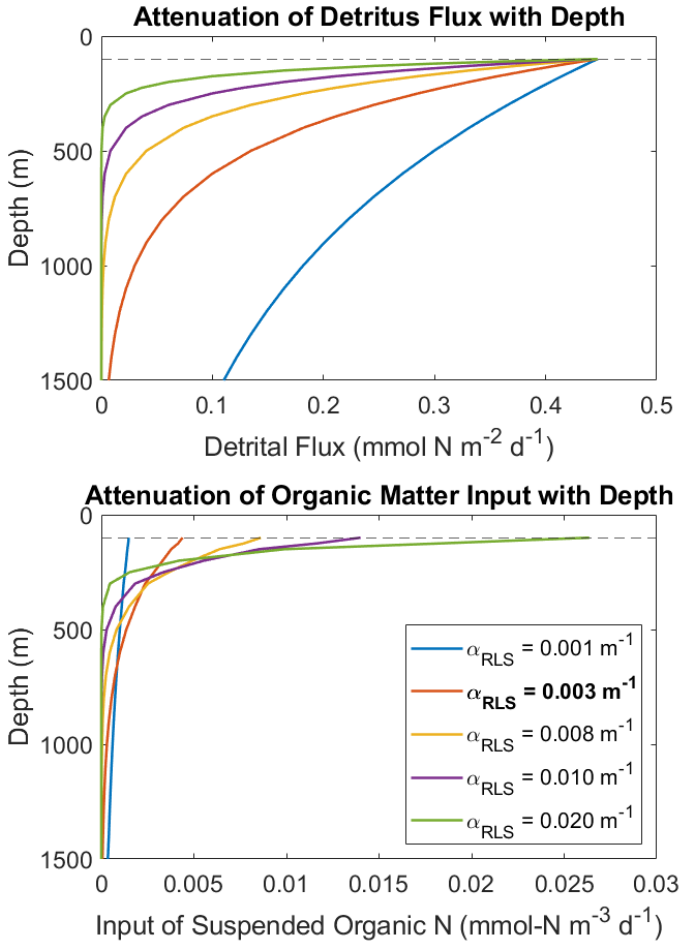

Figure 33: Effect of changing the remineralization length scale on the attenuation of detritus flux with depth (top) and the rate of detritus input into each model layer (bottom). Base case scenario (α_{RLS} = 0.003 m^{-1}) is in bold.

The value of α_{RLS} affects the shape of the curve of flux attenuation with depth (Figure 33, top), where a low α_{RLS} creates very slow attenuation with depth of the detritus input into the model and a higher α_{RLS} implies a rapid detritus concentration decay with depth (Figure 33, bottom). The

bottom panel depicts the detritus input into the model as derived from integration across depth layers using the attenuation of detritus flux from the top panel.

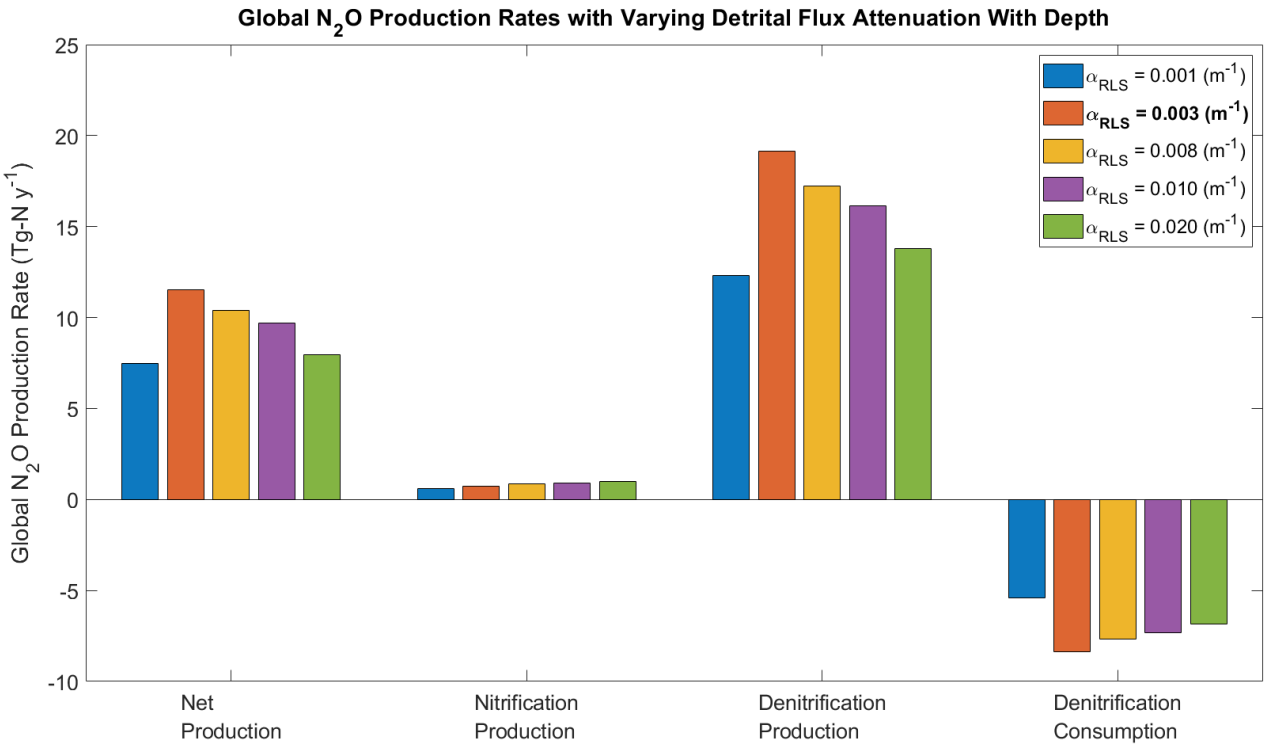

Figure 34: Effect of changing the inverse remineralization length scale (α_{RLS}) on global N_2O production rates (using export production from CanESM5-CanOE).

The global N_2O net production rate decreases with increasing remineralization length scale (α_{RLS}), except at the lowest value of 0.001 m^{-1} (Figure 34). The decrease in net N_2O production rates from α_{RLS} = 0.003 – 0.020 m^{-1} is likely because there is decreasing availability of detritus in the regions where O_2 is low enough for denitrification production and consumption of N_2O. Higher α_{RLS} provides a greater amount of organic matter at shallower depths and attenuates much more quickly in the 300-600 m region where ODZs occur (Figure 33). The total integrated remineralization of organic matter for the water column may not be small itself, but the depth at which organic matter supply is high will affect N_2O production. When α_{RLS} = 0.001 m^{-1}, much of the detritus is transported to greater depths that are well oxygenated and so unlikely to undergo denitrification to produce (and consume) N_2O.

While there are lower net N_2O production rates, this is due to the strong influence from the denitrification reactions. Denitrification production and consumption rates increase and decrease alongside each other, since high denitrification production of N_2O provides higher N_2O concentrations to be consumed by the completion of the denitrification reaction. In contrast to the generally lower denitrification rates with higher α_{RLS}, nitrification N_2O production rates increase with higher α_{RLS}. This is due to the proportion of organic matter that reaches the seafloor without undergoing remineralization and consequent nitrification, rather than interactions between O_2 and nitrification yield of N_2O. Higher α_{RLS} leads to greater total detritus concentrations input into the model – over three times in magnitude for the range of α_{RLS} tested. Overall, this can lead to net N_2O production rates changing up to 35% when varying α_{RLS}.

3.4 Sensitivity to Temperature and Solar Irradiance

Remineralization (both oxic and suboxic) is affected by temperature, and nitrification is affected by solar irradiance. In this section, these properties will be investigated to determine how strongly they affect N_2O production rates.

3.4.1 Seasonal Variations in Temperature

Spatial variations in temperature are accounted for by applying World Ocean Atlas temperature data to remineralization rates using the Arrhenius equation (see Section 2.1); however, temperature does not vary strongly at depths below 100 m. Nevertheless, seasonal variations may affect remineralization processes – namely, remineralization of detritus to NH_4^+ and suboxic remineralization of organic matter reducing NO_3^- to N_2O (denitrification). Figure 35 depicts global net N_2O production rates using annually averaged and monthly temperature data.

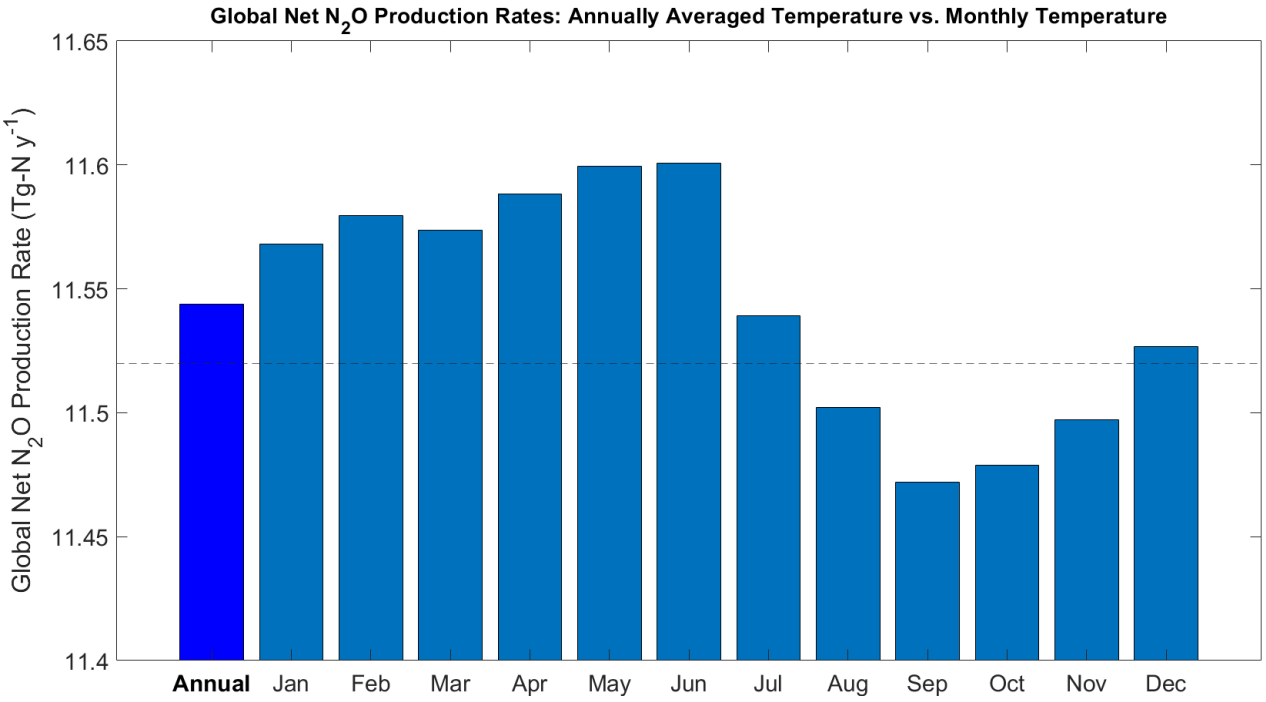

Figure 35: Global net N_2O production rates using annually averaged and monthly temperature data. Base case scenario (annually averaged temperature data) is in bold. Note the small range on the y-axis scale.

While there is temporal variation in global net N_2O production rates over the course of the year, the effect is not substantial as rates range from approximately 11.5 to 11.6 Tg-N_2O y^{-1}, resulting in a maximum total difference of 1.1%. The difference between using an annual average of temperature data and using the average of simulations using monthly data is only a 0.21% difference. For this reason and to decrease processing time, the base case scenario of using annually averaged temperature data products was maintained.

3.4.2 Seasonal Variations in Solar Irradiance

As with the temperature experiment above, sensitivity to seasonal solar irradiance is also evaluated here. Since solar irradiance inhibits nitrification, nitrification N_2O production rates are the primary quantity affected. As with seasonal trends in temperature, temporal changes in solar irradiance produce very little effect on global nitrification N_2O production rates (Figure 36), where the difference between the maximum rates (June) and the minimum rates (January) amounted to 0.20% of the total. The effect on global *net* N_2O production rates is even smaller, with a maximum difference of 0.014%.

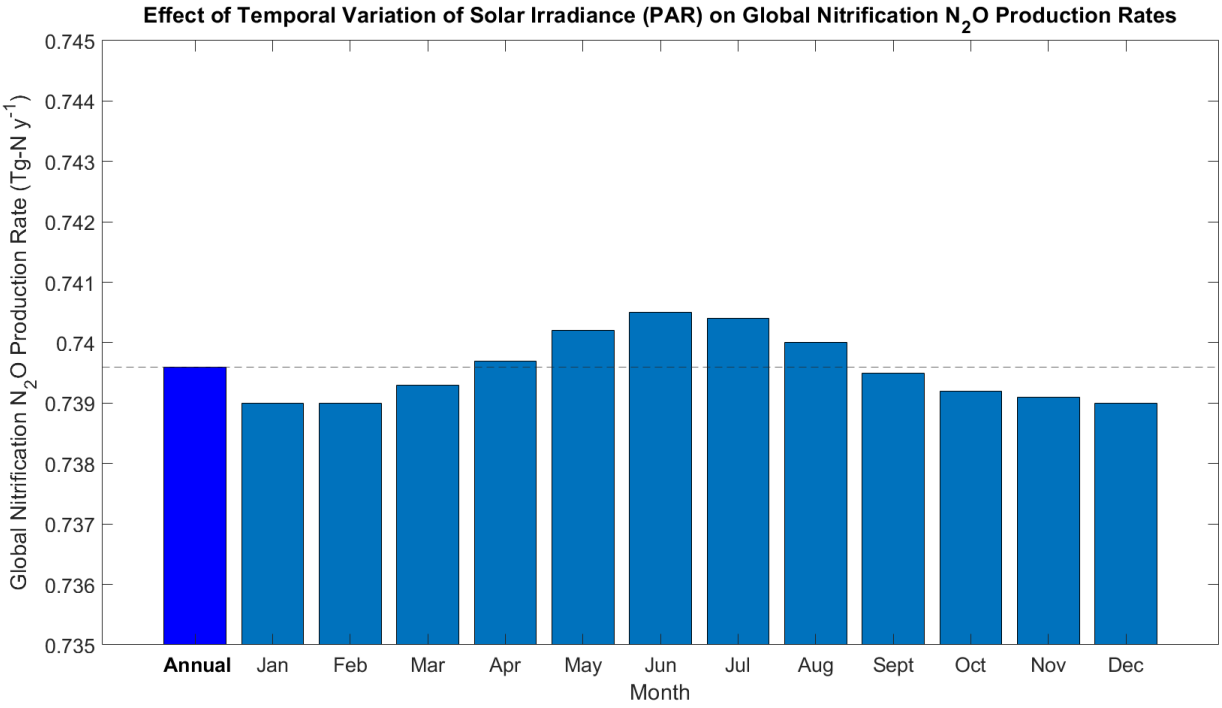

Figure 36: Global N_2O production rates by nitrification using location-specific, monthly data for solar irradiance (PAR) from ISCCP (Bishop et al. 1997). Base case scenario (annually averaged irradiance) is in bold. Note the small range on the y-axis scale.

A quantitative comparison between using all months of solar irradiance data products and taking an annual average of the output nitrification N_2O production rates, versus using a pre-generated annual average also resulted in negligible differences - less than a 0.1% change in global nitrification N_2O production rates and a near-zero change in global net N_2O production rates (Figure 36).

The small influence of temporal changes in solar irradiance on N_2O production rates is to be expected. The penetration of solar irradiance past depths of approximately 100 m is limited and

so only influences a small region of the global model, and nitrification production of N_2O is minor compared to denitrification.

3.4.3 Solar Irradiance Light Penetration Depth

While there is very little change in global net N_2O production rates when using monthly solar irradiance data products, it is possible that a greater effect could be seen if the light penetration depth was altered. This model uses a constant light attenuation coefficient (a_c) that does not fully represent how water clarity in different regions would influence how much solar irradiance penetrates the ocean's depths. To determine the effect on global net and nitrification N_2O production rates, a_c was varied from its base case (0.05 m^{-1}) across a range of values: 0.01, 0.05, 0.10, 0.25, and 0.50 m^{-1}. These a_c coefficients were then applied to the irradiance inhibition factor $E_x/(E_x+E_z)$ (see Equations 11-12) and observed with depth across varying latitudes (Figure 37, 38).

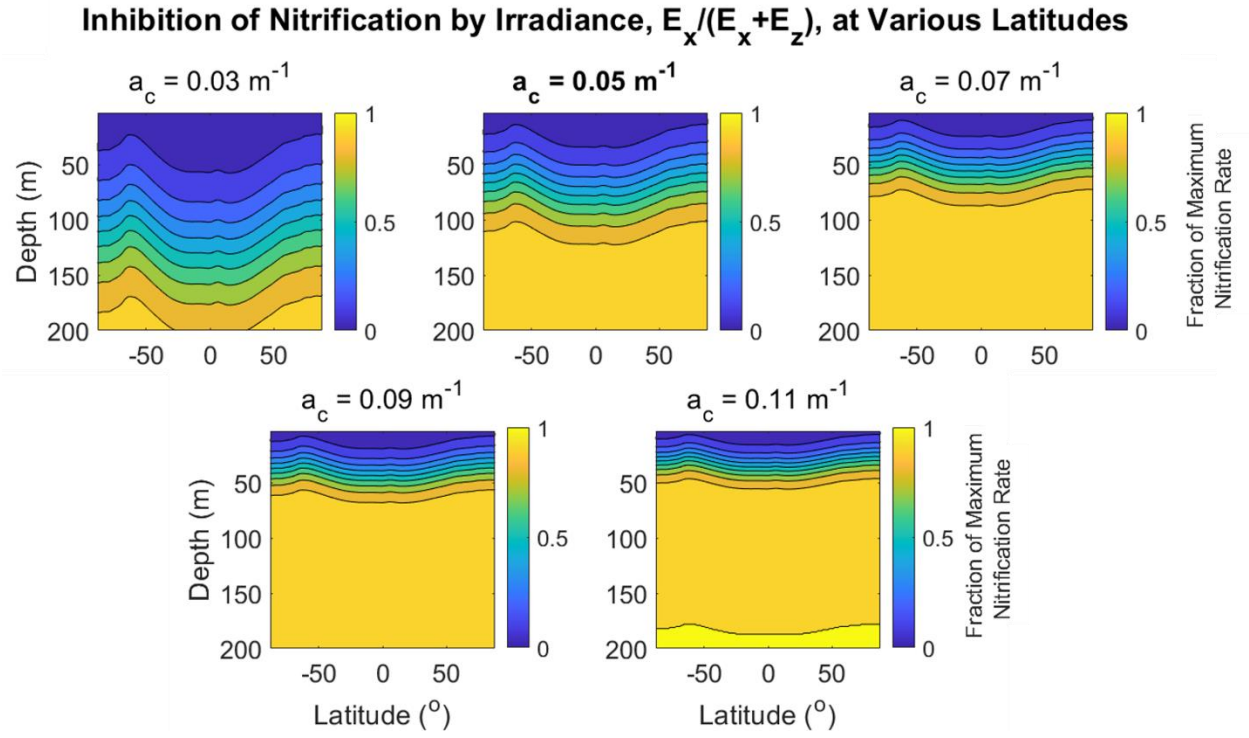

Figure 37: Inhibition of nitrification by irradiance at various latitudes using a range of light attenuation coefficients, a_c. Calculated using zonally and annually averaged surface solar irradiance. Base case scenario (a_c=0.05 m^{-1}) is in bold.

Increasing a_c effectively decreases the depth of the region affected by solar irradiance – with a_c greater than the base case of 0.05 m^{-1} irradiance has almost no effect on nitrification in the model as $E_x/(E_x+E_z)$ remains close to 1 at depths greater than 100 m (Figure 37). Decreasing a_c to 0.03 m^{-1} increases the inhibition of nitrification by solar irradiance as the light permeation depth increases to approximately 200 m (Figure 37). To gain another perspective on how a_c controls the nitrification inhibition factor over depth, a series of depth profiles was created using a constant PAR of 50 mol m^{-2} d^{-1} (Figure 38).

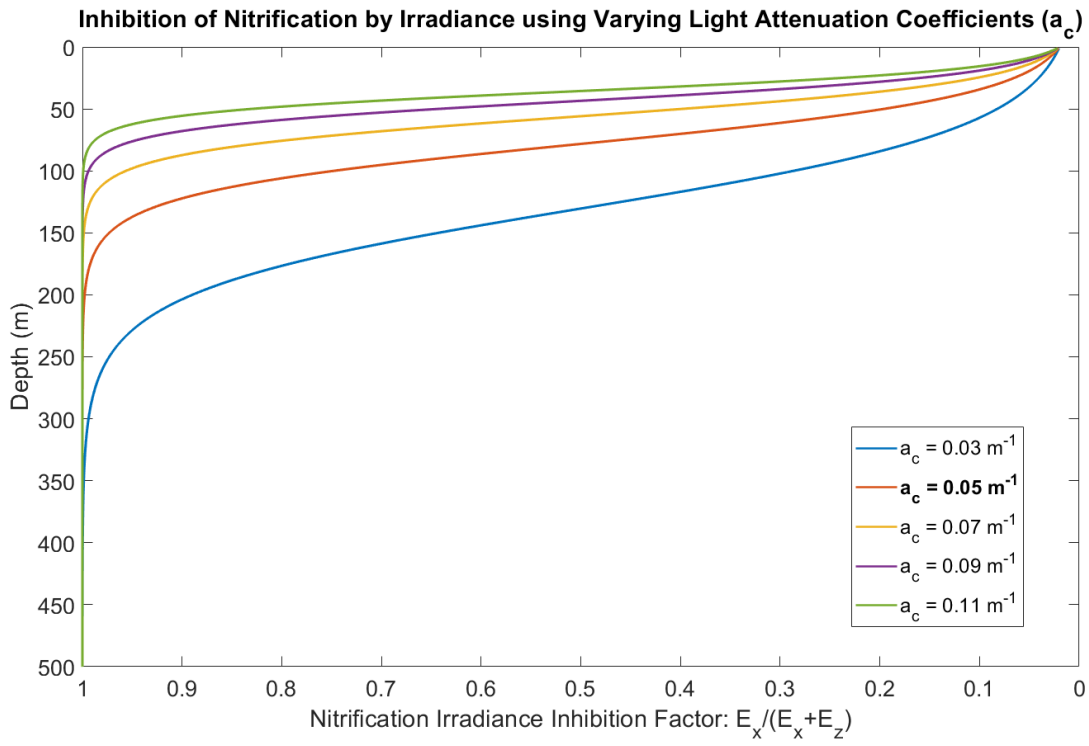

Figure 38: Effect of varying the light attenuation coefficient (a_c) on the irradiance inhibition factor, $E_x/(E_x+E_z)$, using a common surface PAR = 50 mol m^{-2} d^{-1}. Base case scenario (a_c=0.05 m^{-1}) is in bold.

Increasing the light attenuation coefficient, a_c, decreases the depth at which solar irradiance, and so the irradiance inhibition factor, $E_x/(E_x+E_z)$, will affect nitrification within the model. A very low a_c of 0.01 m^{-1} would cause inhibition of nitrification due to solar irradiance to occur at depths up to 1000 m, while a large a_c of 0.50 m^{-1} means that nitrification will not be inhibited by irradiance past approximately 10 m (Figure 38). Since this model does not account for depths above 100 m, this would mean that there would be no effect by solar irradiance on nitrification or nitrification N_2O production rates.

To see how varying the light penetration effect may change global nitrification N_2O production rates, the model was run using the range of a_c light attenuation coefficients (Figure 39). Global net N_2O production rates and denitrification N_2O production and consumption rates show negligible change and so are not depicted.

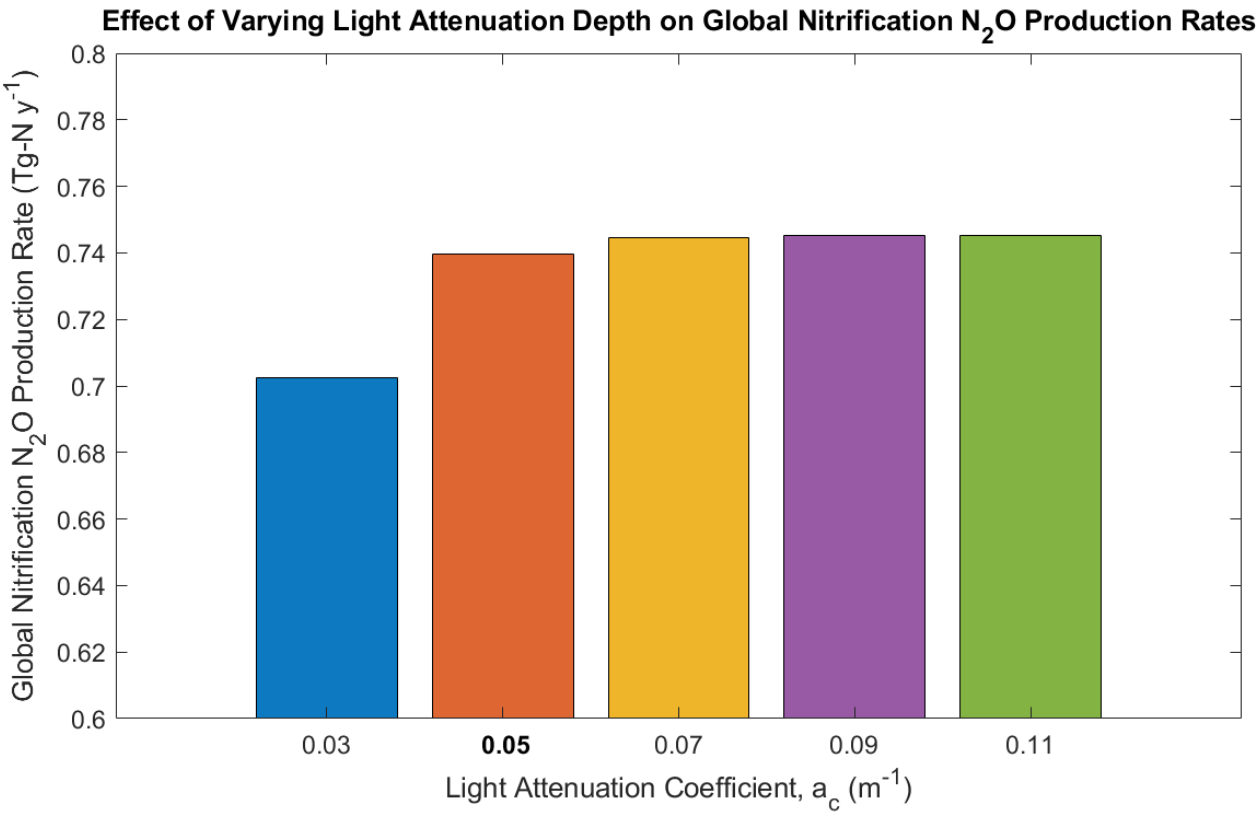

Figure 39: Global nitrification N_2O production rates using varying light attenuation coefficients (a_c). Base case scenario (a_c=0.05 m^{-1}) is in bold.

The effect of changing the light attenuation coefficient on global nitrification N_2O production rates is quite small, as is expected given that the model only involves reactions below the euphotic zone (100 m). Even an a_c of 0.03 m^{-1} will only result in a relatively small effect on global nitrification N_2O production.

However, global models include nitrification within the euphotic zone may see a stronger effect on global N_2O production rates with varying a_c. For the purposes of this model, which only considers N_2O-relevant reactions below the euphotic zone, the base case coefficient of 0.05 m^{-1} was maintained and sensitivity to this parameter is considered to be weak.

3.5 Parameter Sensitivity Analysis

The following parameterizations use specific parameters that are either poorly quantified in literature, have a wide range of possible values, or have no literature basis at all. The sensitivity of the model will generate a better idea of which parameters have the most control over global N_2O production rates, as well as the values that best produce results in line with past literature estimates.

3.5.1 Half-Saturation Constants for Nitrification and Suboxic Remineralization ($fO_{2,AmOx}$ and $fNO_{3,remin}$)

Two key parameterizations control nitrification and remineralization processes through availability of the electron acceptors required for the reaction to proceed. $fO_{2,AmOx}$ determines the nitrification rate as a function of availability of O_2, while $fNO_{3,remin}$ ensures that suboxic remineralization/denitrification rates are limited by the availability of NO_3^-. As the half-

saturation constants for each of these equations are not well established in literature, the model's sensitivity to these qualities is evaluated here to determine how strongly these constants affect global N_2O production rates.

$fO_{2,AmOx}$

The nitrification reaction rate is directly affected by availability of O_2 and NH_4^+ (*Equation 5*), and indirectly affected by how detritus concentrations and temperature affect remineralization of detritus to NH_4^+. The effects of changing the half-saturation constant ($K_{O2,AmOx}$) on $fO_{2,AmOx}$ are shown in Figure 40. For this experiment, the tested $K_{O2,AmOx}$ values were 0.1, 1, 3, 5, 10, and 30 µmol-O_2 L^{-1}.

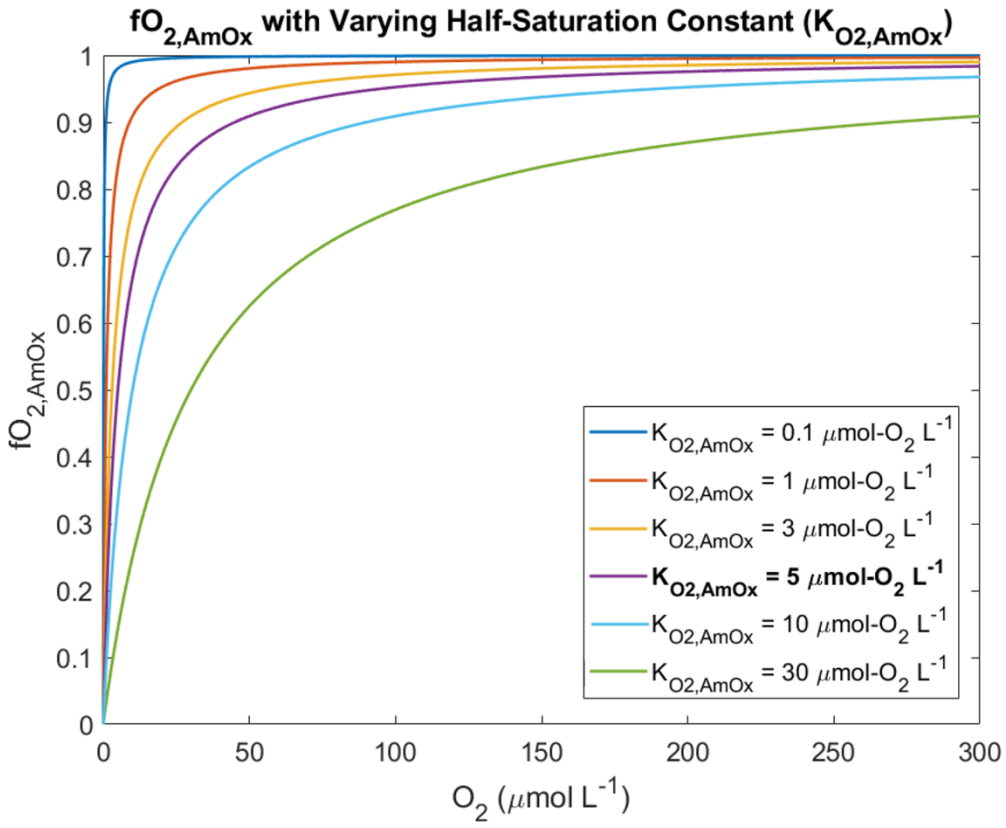

Figure 40: Relative rate of ammonium oxidation vs. O_2 using varying half-saturation constants ($K_{O2,AmOx}$). Base case scenario ($K_{O2,AmOx}$=5 µmol-O_2 L^{-1}) is in bold.

A higher $K_{O2,AmOx}$ generates a more gradual decrease in $fO_{2,AmOx}$ as O_2 decreases, while a lower $K_{O2,AmOx}$ produces a sharper curve such that O_2 has little control on nitrification except at very low O_2 concentrations. It is worth noting that nitrification rates are affected by O_2 through $fO_{2,AmOx}$, but nitrification *N_2O production* rates are also affected by O_2 as O_2 concentrations affect the yield of N_2O from nitrification, which is discussed below.

It is important to maintain nitrification in the lower O_2 range, as there is evidence of nitrification occurring at low O_2 (Bristow et al. 2016, Ji et al. 2018). If $K_{O2,AmOx}$ is too large, nitrification will be strongly inhibited under low O_2. For this reason, the base case scenario uses a $K_{O2,AmOx}$ value of 5 µmol-O_2 L^{-1} to help represent the variability of nitrification rates in the oxygenated ocean as

well as near the boundaries of ODZs – however, this remains an uncertain quantity and will be discussed more in the following Discussion section (Section 4.1).

To determine how this assumption of $K_{O2,AmOx}$ = 5 µmol-O_2 L^{-1} lies in relation to other half-saturation constants in terms of global N_2O production, the range of $K_{O2,AmOx}$ values were applied to the model to observe the resultant range of global N_2O production rates by nitrification (Figure 41).

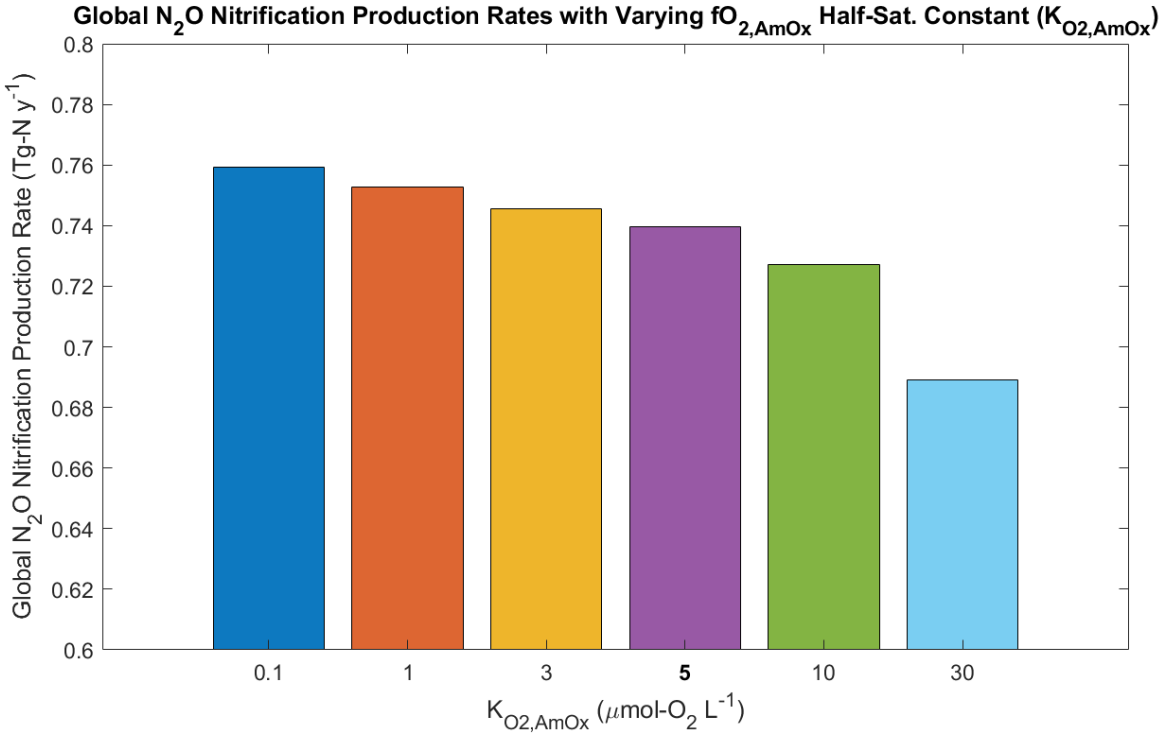

Figure 41: Global N_2O production rates from nitrification with varying $fO_{2,AmOx}$ half-saturation constant ($K_{O2,AmOx}$). Base case scenario ($K_{O2,AmOx}$=5 µmol-O_2 L^{-1}) is in bold.

While changing the half-saturation constant $K_{O2,AmOx}$, does have an effect on global nitrification production rates (Figure 41) – namely, that increased $K_{O2,AmOxi}$ results in lower nitrification N_2O production – the effect is negligible in terms of global net N_2O production rates. Global net N_2O production rates with varying $K_{O2,AmOx}$ only vary between approximately 11.4-11.6 Tg-N_2O y^{-1} for a maximum 1.0% difference.

$fNO_{3,remin}$

$fNO_{3,remin}$ uses a half-saturation constant ($K_{NO3,remin}$) and a Michaelis Menten-styled parameterization similar to *$fO_{2,AmOx}$*, but refers to decreasing suboxic remineralization rates with decreasing availability of NO_3^-. Both suboxic and oxic remineralization pathways consume organic matter (detritus), but the oxic pathway uses O_2 as an electron acceptor while the suboxic pathway uses NO_3^- as an electron acceptor. Suboxic remineralization approaches 100% of total remineralization at low O_2, so *$fNO_{3,remin}$* is used to ensure that suboxic remineralization rates decrease to zero as NO_3^- approaches zero.

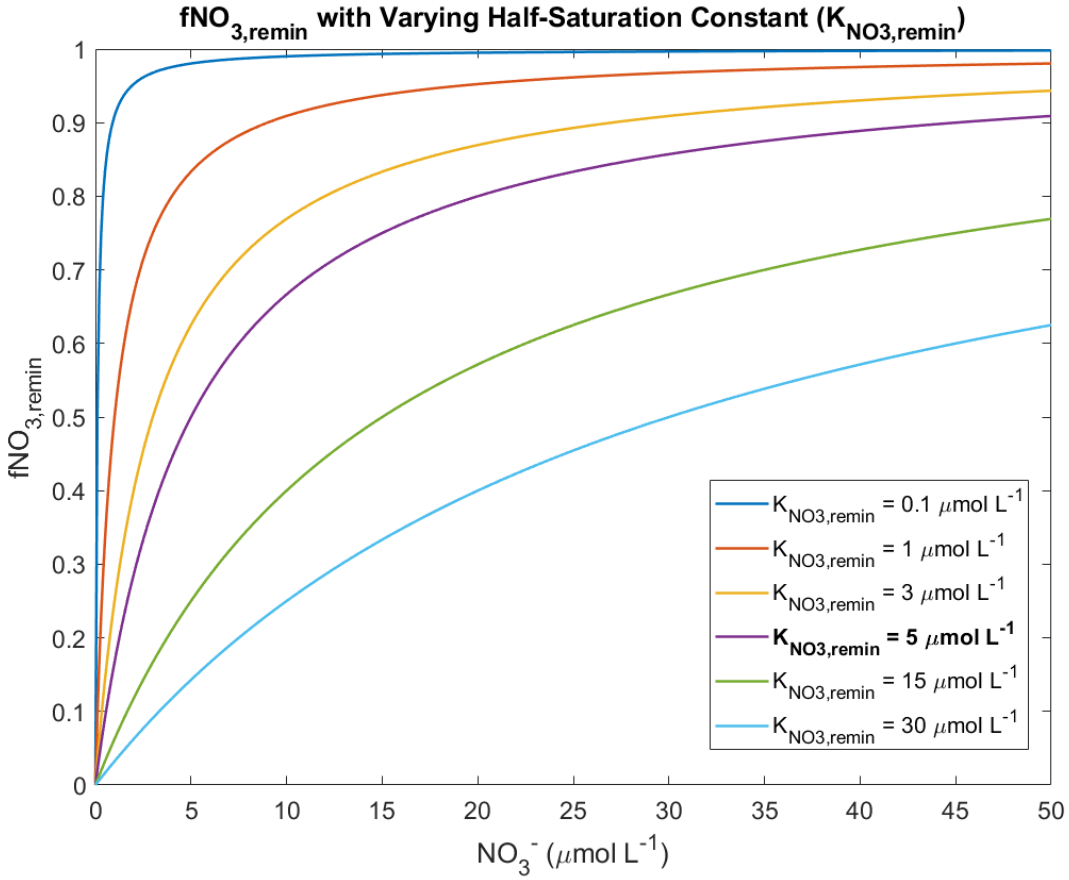

Figure 42: Relative rate of denitrification vs. NO_3^- with varying half-saturation constant ($K_{NO3,remin}$). Base case scenario ($K_{NO3,remin}$=5 μmol-NO_3^- L^{-1}) is in bold.

Unfortunately, there are very few literature estimates of the dependence on NO_3^- in terms of a half-saturation constant, and so $K_{NO3,remin}$ was set to be equal to 5 μmol-NO_3^- L^{-1}. To determine how strongly this half-saturation constant may affect global N_2O production rates and global net N_2O production rates, a range of $K_{NO3,remin}$ values were tested: 0.1, 1, 3, 5, 10, and30 μmol-NO_3^- L^{-1}. These half-saturation constants were then plotted against various NO_3^- concentrations to see how the reaction rate decays with limited NO_3^- availability (Figure 42).

The base case $K_{NO3,remin}$ half-saturation constant was chosen to be 5 μmol-NO_3^- L^{-1} as it shows a more gradual reaction rate decay in the 'medium' range of NO_3^-. When NO_3^- concentrations are between 20-50 μmol-NO_3^- L^{-1} there is approximately a 20% decrease in reaction rates, while lower NO_3^- concentrations see a much greater rate decay. Higher half-saturation constants show very strong decreases in rates even in the 'medium' range of NO_3^-, and along with the requirement of suboxic remineralization occurring in the 0-6 μmol-O_2 L^{-1} this was deemed too strong. The lower values of the half-saturation constant show little change in the reaction rate in the 'medium' range of NO_3^-.

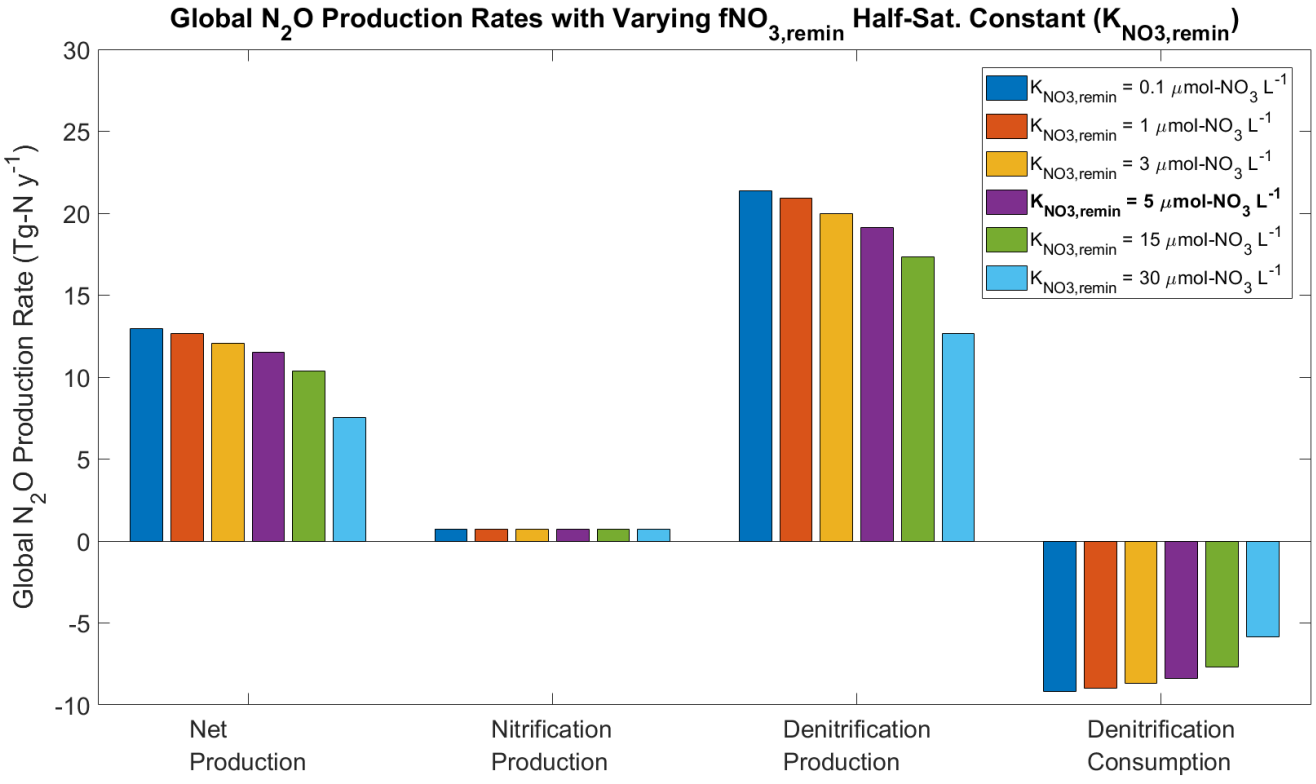

Figure 43: Global N_2O production rates with varying $fNO_{3,remin}$ half-saturation constant ($K_{NO3,remin}$). Base case scenario ($K_{NO3,remin}$=5 μmol-NO_3^- L^{-1}) is in bold.

To see how strongly this choice affects global N_2O production, the model was run using each $K_{NO3,remin}$ and comparing the output global N_2O production (and consumption) rates alongside each other (Figure 43). The impact of varying $K_{NO3,remin}$ on net N_2O production rates is moderate, amounting to up to a maximum 41.7% difference.

3.5.2 Nitrification N_2O Yield Parameterization

Another key parameterization is the yield of N_2O from nitrification. The equation representing this, *Equation 6*, was introduced by Nevison et al. (2003) and was further developed by Ji et al. (2015, 2018) – however, the parameterization itself is functionally the same. To understand how these changes in constants might affect N_2O production by nitrification, different combinations of *a* and *b* were input into the model to determine the effects on nitrification N_2O production.

Table 5: Parameterizations for N_2O yield from nitrification (γ)

Yield Formula	***a* and *b* constants**
(Nevison et al. 2003): $\gamma = 0.5(a/[O_2] + b)$	
Nevison et al. parameterization A	a = 0.26 μmol-O_2 L^{-1}, b = -0.0006
Nevison et al. parameterization B	a = 0.20 μmol-O_2 L^{-1}, b = -0.0004
(Ji et al. 2015, 2018): $\gamma = 0.01(a/[O_2] + b)$	
Ji et al. parameterization A (base case scenario)	a = 0.20 μmol-O_2 L^{-1}, b = 0.08
Ji et al. parameterization B	a = 0.07 μmol-O_2 L^{-1}, b = 0.04
Ji et al. parameterization C	a = 0.33 μmol-O_2 L^{-1}, b = 0.12

Applying these parameterizations across a range of O_2 concentrations gives the results shown in Figure 44. The main differences between Nevison et al. (2003) and Ji et al. (2015, 2018)'s formulations are that Nevison parameterization are more sensitive to O_2 at higher concentrations, and that the maximum yield at suboxic concentrations is much higher than in the Ji parameterization (Figure 44). This is likely because Nevison et al. (2003) based their research off laboratory studies conducted by Goreau et al. (1980) that produced higher N_2O yields from nitrification than the in-situ studies conducted by Ji et al. (2015, 2018). The more recent research by Ji et al. (2015, 2018) included *in situ* studies that show a much lower yield of N_2O by nitrification than the laboratory culture studies by Goreau et al. (1980) that were used for Nevison et al. (2003)'s original yield parameterization. Therefore, while it was important to compare Ji et al. (2015, 2018)'s parameterizations with the parameterizations by Nevison et al. (2003), the newer version was taken as the more reasonable scenario. The base case of a = 0.2 μmol-O_2 L^{-1}, b = 0.08 is based on the recommendation by Ji et al. (2018).

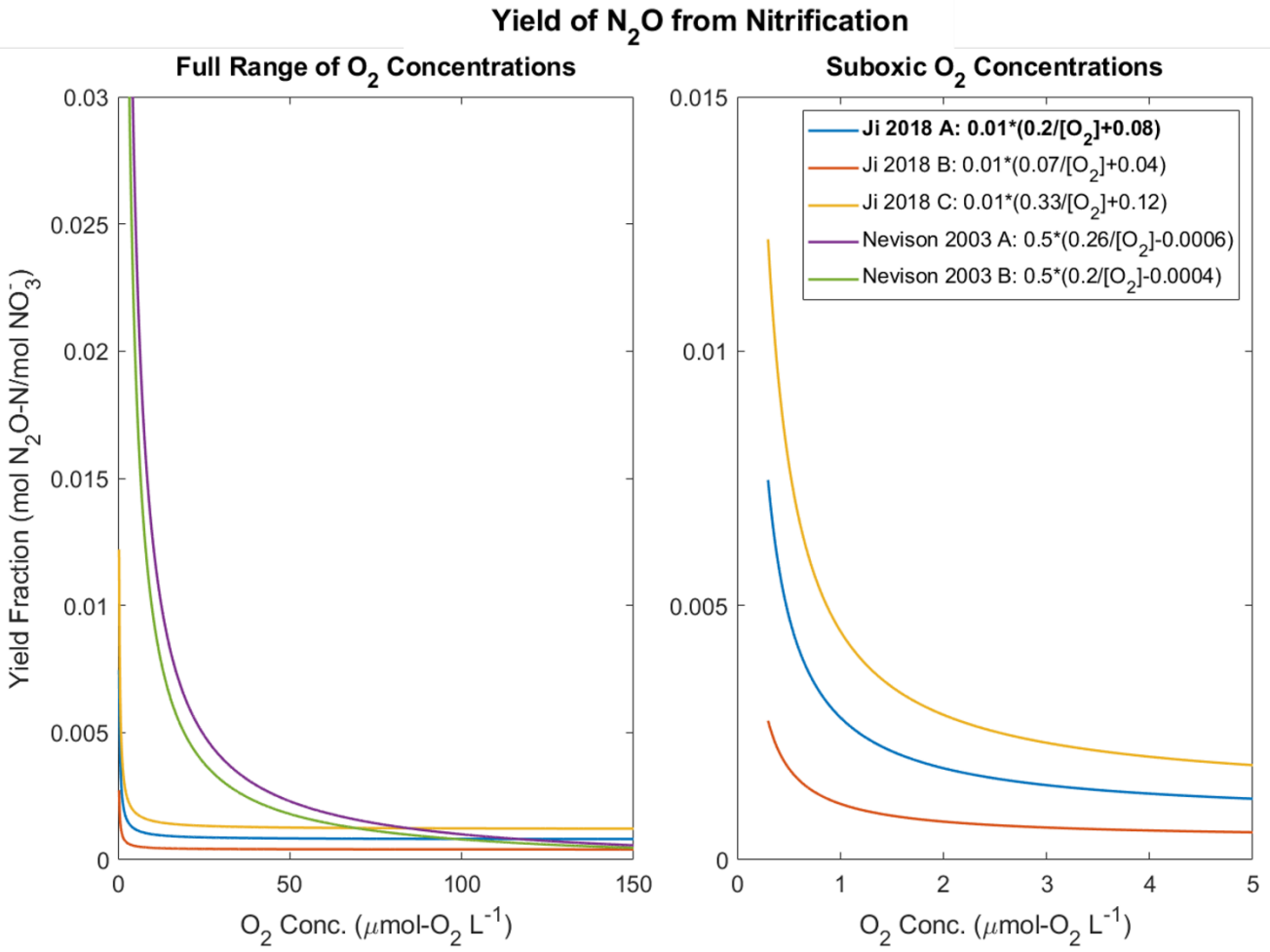

Figure 44: Yield of N_2O from nitrification (γ) with different parameterizations across a range of O_2 concentrations. Left panel shows a wider range of O_2 concentrations and all five yield parameterizations, while the right panel shows suboxic O_2 concentrations and highlights differences between the different Ji et al. (2018) parameter estimates. Base case scenario (Ji 2018 A) is in bold.

From Figure 44 it is obvious that the amount of N_2O by nitrification will be greatly affected by the parameterization choice. Previous studies have reported a wide range of global nitrification N_2O production rates and these estimates tend to be much higher than those produced by this model (see Table 1; also discussed further in Section 4.2). However, most of these models have not implemented the newer Ji et al. (2015, 2018) parameterizations that would substantially decrease the yield of N_2O by nitrification in the higher O_2 concentration range and so decrease the global nitrification N_2O production rate. When compounded with the higher denitrification N_2O production rates generated by newer and more accurate O_2 data products (see Section 3.3), this would result in the much smaller proportions of N_2O produced by nitrification than by denitrification seen in this model in comparison to past estimates.

To see how strongly the yield parameterization affects global N_2O production rates from nitrification, the combinations listed above were compared using model output of global nitrification production rate estimates (Figure 45). The substantial difference in yield parameterizations in Figure 44 (left) is also seen in Figure 45, where the range of global nitrification N_2O production rates can differ by up to 74.1%. Despite this large difference in

nitrification N_2O production, the relatively small influence of nitrification production rates compared to denitrification production and consumption rates means that the effect from different yield parameterizations has a low effect on the global net N_2O production rate. For perspective, the difference between the smallest (Ji 2018 B) and largest (Nevison 2003 A) global nitrification N_2O production rates amounts to a maximum 8.4% difference in global *net* N_2O production rates (Figure 46).

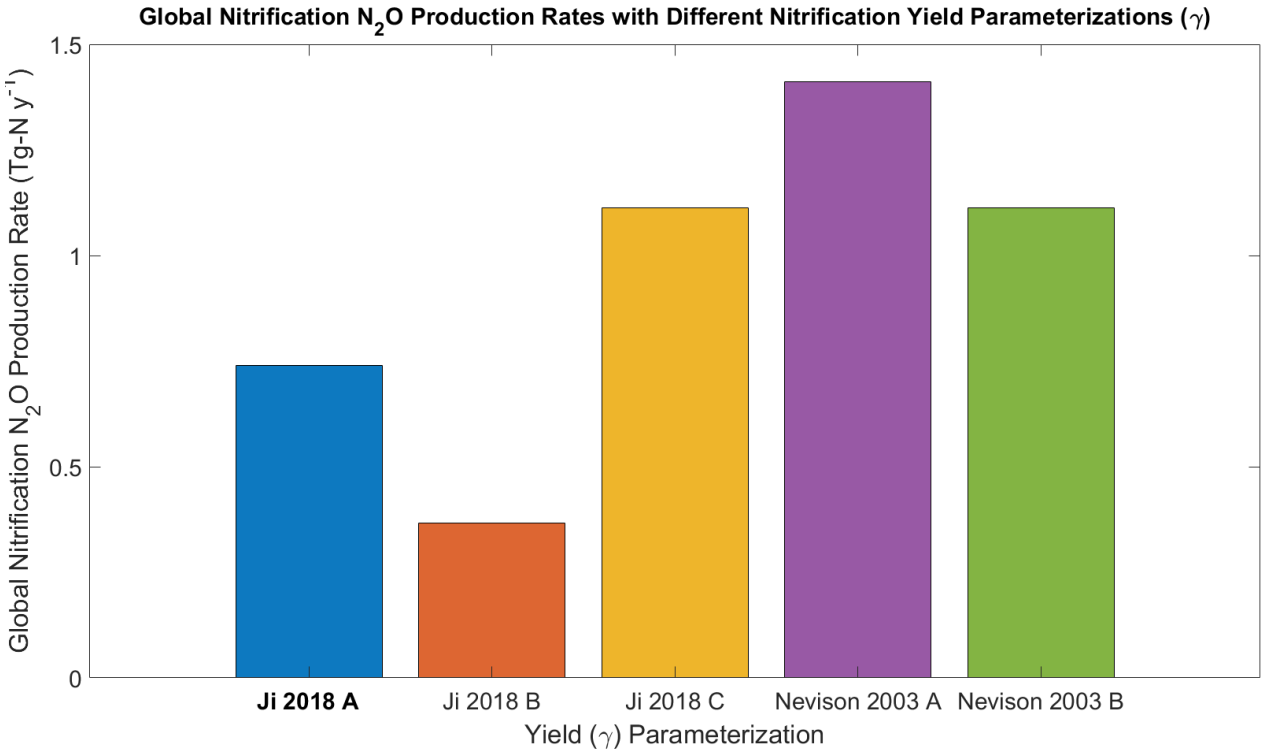

Figure 45: Global N_2O production rates by nitrification with different parameterizations for yield (γ) of N_2O from nitrification. Base case scenario (Ji 2018 A) is in bold.

Nitrification N_2O production rates are greatly increased when using the Nevison et al. (2003) formulation, which is understandable given the overall higher yield of N_2O by nitrification by this parameterization (Figure 44). Notably, the Nevison parameterization "B" was comparable to the Ji parameterization "C", implying that even using the older Nevison yield parameterization it may be possible to generate similar global N_2O production rates by nitrification. However, even with the higher yields by the Nevison parameterizations the global N_2O production rates by nitrification are still lower than most past estimates (Figure 46).

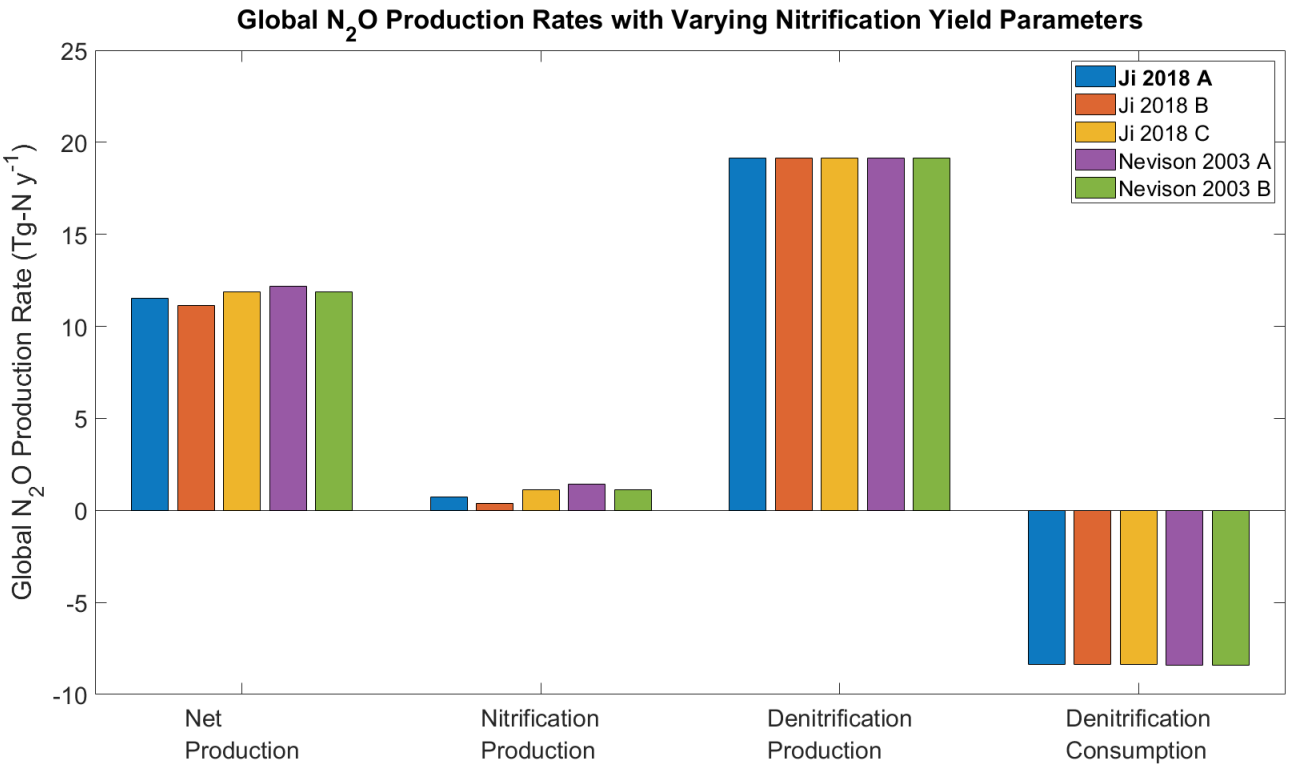

Figure 46: Global N_2O production rates with varying parameterizations for yield (Υ) of N_2O from nitrification. Base case scenario (Ji 2018 A) is in bold.

The yield parameterization is notable in that it is one of the few parameters that affects the proportion of global N_2O production rates by nitrification substantially enough to affect global net N_2O production rates. However, different parameterizations still produce relatively low N_2O production rates by nitrification relative to denitrification.

This is reasonable in the scope of our model – while nitrification production of N_2O is mostly determined by the yield of nitrification to N_2O instead of NO_3^-, it is also reliant on the nitrification rates themselves which are in turn directly reliant on organic matter input from detritus remineralization rates. This, combined with O_2 limitations from $fO_{2,AmOx}$, means that low nitrification N_2O production rates are only moderately influenced by changes in the yield parameterization.

3.5.3 O_2 Threshold for Oxic vs. Suboxic Remineralization

The proportion of suboxic remineralization (denitrification) is controlled by availability of O_2. The commonly cited O_2 threshold at which oxic remineralization ends and suboxic remineralization begins has been widely debated due to discrepancies between model, laboratory, and in-situ research (Paulmier and Ruiz-Pino 2009, Bianchi et al. 2012, Babbin et al. 2015, Sun et al. 2021). The commonly used 6 μmol-O_2 L^{-1} threshold is maintained as the base case in this model – however, a sensitivity experiment was conducted to highlight how additional research on this threshold could improve models. In this experiment, the O_2 threshold, thr_{O2}, was varied between 3, 6, 10, and 20 μmol-O_2 L^{-1}.

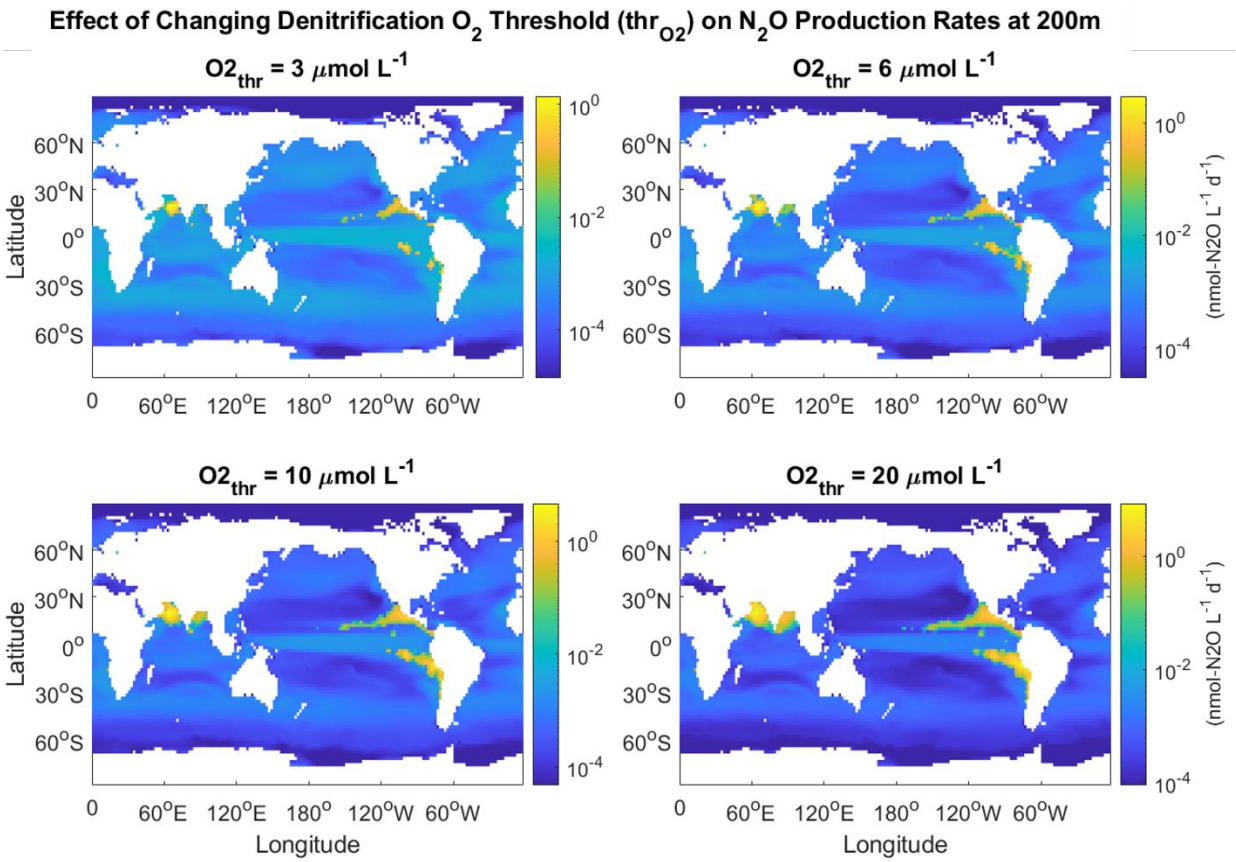

Figure 47: Effect of O_2 concentration threshold for denitrification (thr_{O2}) on global net N_2O production rates at 200 m.

The O_2 threshold for suboxic remineralization affects the amount of N_2O from denitrification production and consumption, which is shown in Figure 47 for a depth of 200 m. The hotspots of high production rates that occur in ODZs increase in size with increasing thr_{O2}. This affects the global total N_2O production rate very strongly as the volume of water with N_2O production by denitrification expands.

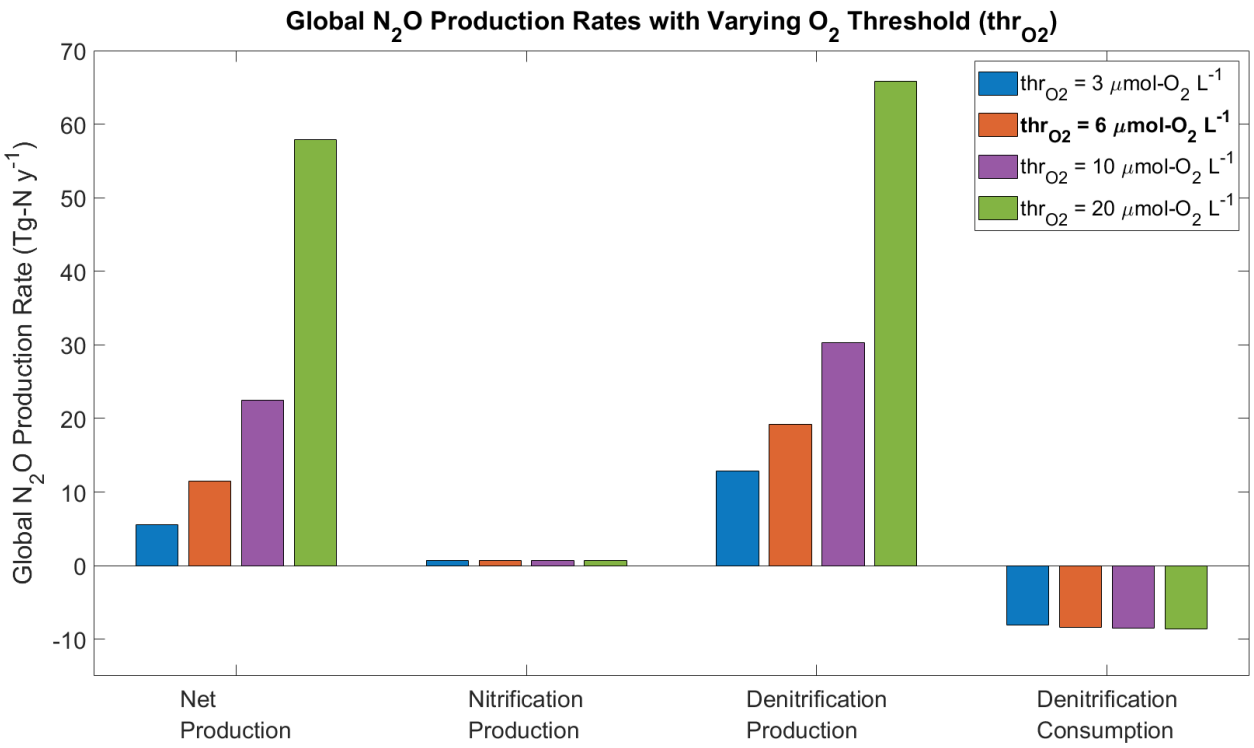

Figure 48: Global N_2O production rates with varying thr_{O2}. Base case scenario (thr_{O2} = 6 µmol-O_2 L^{-1}) is in bold.

As it is often common practice to use 6 µmol-O_2 L^{-1} for thr_{O2}, a much higher threshold of 20 µmol-O_2 L^{-1} seems unlikely despite its use in some models (Sun et al. 2021). This is highlighted by the high global N_2O production rates seen in Figure 48. However, if true it would have important repercussions for the global nitrogen budget and can increase net N_2O production rates by over ten times.

3.5.4 Exponent *c* in Ω

As with changes in thr_{O2}, the exponent *c* in the partitioning term between oxic and suboxic remineralization (Ω) also affects the proportion of N_2O production from denitrification. Increasing *c* results in smaller denitrification (and associated production and consumption of N_2O) rates. As Ω is a term created for this model, *c* does not have any literature values to compare – instead, the base case scenario where *c* = 3 was chosen to approximate observed relationships between denitrification rate and O_2 (e.g., Devol 1978, Dalsgaard et al. 2012). Figure 49, below, shows how varying *c* affects the proportion of oxic remineralization in relation to denitrification.

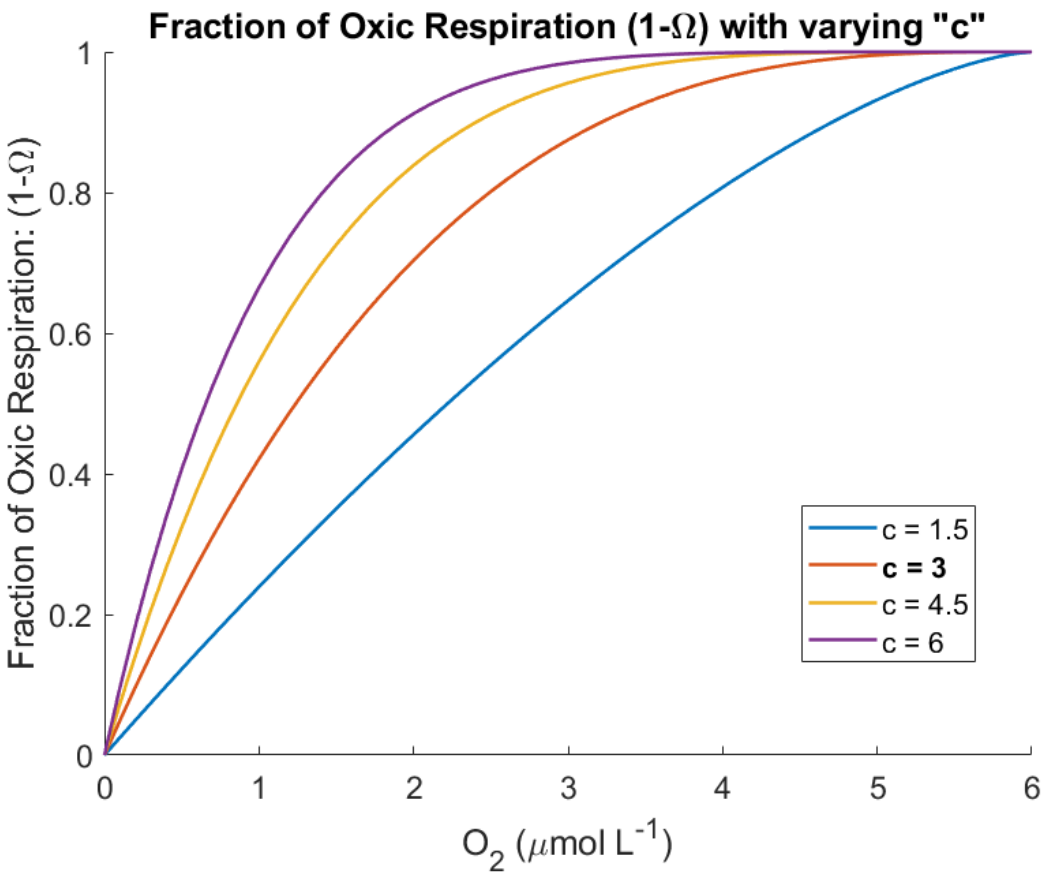

Figure 49: Fraction of oxic respiration (1-**Ω**) with varying exponent *c*. Base case scenario (*c* = 3) is in bold.

When $c > 1$, the oxic respiration curve has high oxic respiration at the upper end of suboxic concentrations (3-6 μmol-O_2 L^{-1}), which is what best represents the trends shown by Devol (1978) and Dalsgaard et al. (2012) in their laboratory experiments on bacterial oxygen uptake kinetics in ODZs. When $c < 1$ the opposite is true – oxic respiration rapidly declines, even at O_2 concentrations near the thr_{O2} of 6 μmol-O_2 L^{-1}, which is not consistent with existing literature. Because of this, this model uses only values > 1 (Figure 49). A higher *c* implies that the fraction of oxic respiration remains high for a wider range of the upper suboxic O_2 concentrations.

The effect of changing *c* on net N_2O production rates can be seen using a depth profile in the North Pacific ODZ (Figure 50). As *c* increases, net denitrification N_2O production rates (denitrification production minus consumption) decrease.

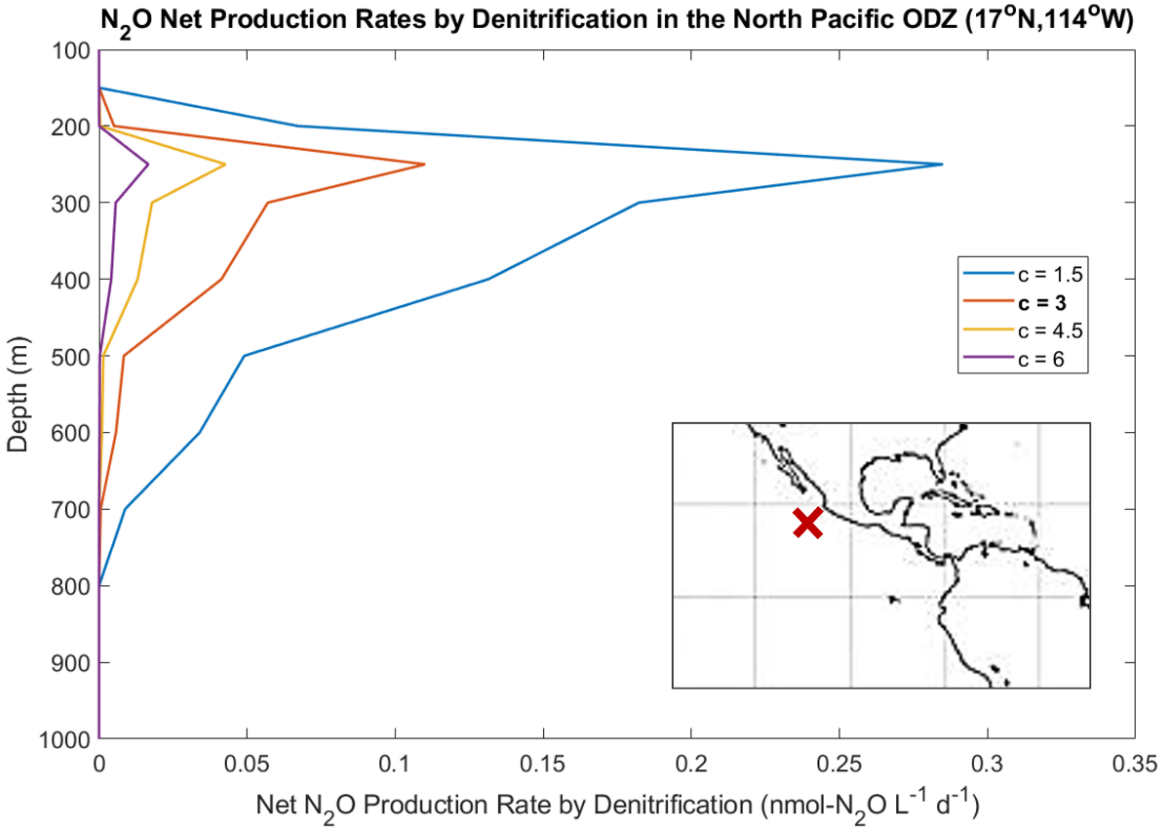

Figure 50: Effect of changing exponent *c* on net N_2O production rates by denitrification in the North Pacific ODZ at 17°N, 114°W. Base case scenario (*c* = 3) is in bold.

This is also reflected in the global N_2O production rates (Figure 51); however, the strong difference seen in the ODZ is diminished in global totals due to the relatively small region ODZs occupy in the global ocean.

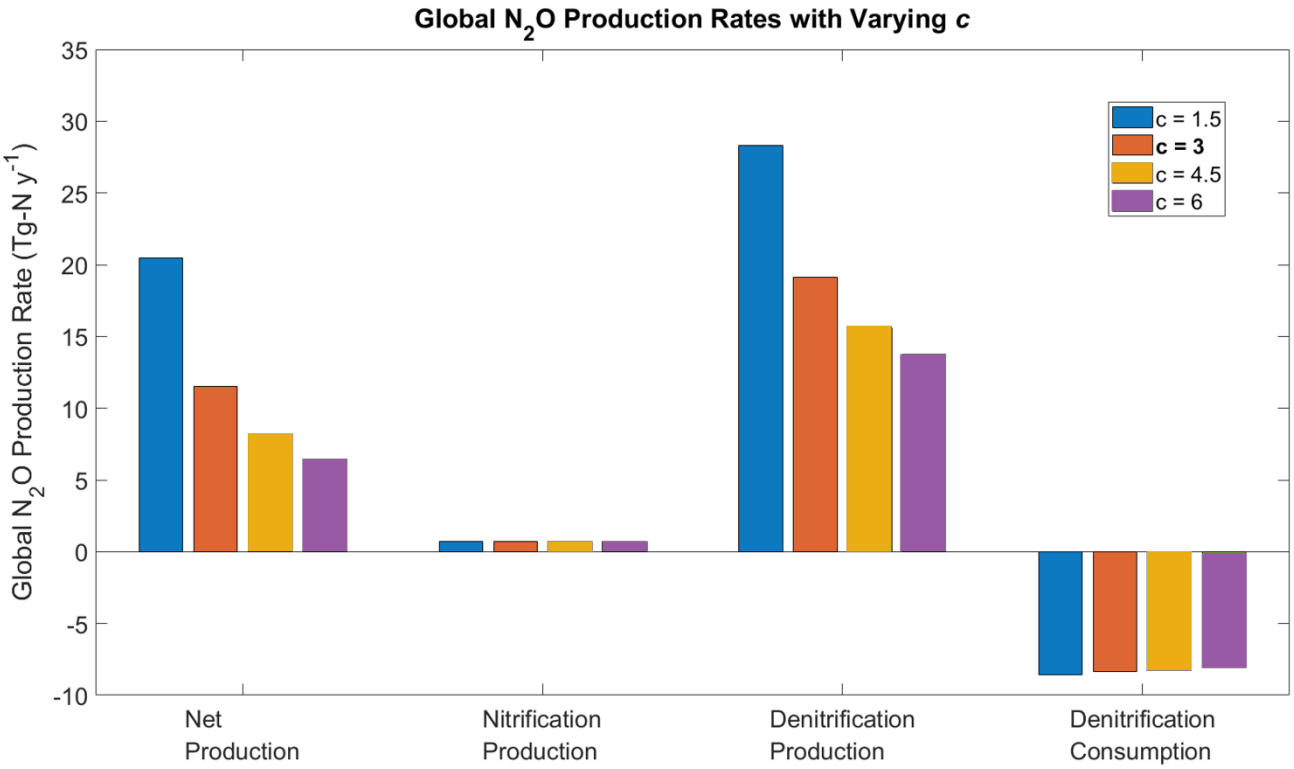

Figure 51: Effect of varying exponent *c* in Ω on global N_2O production rates. Base case scenario (*c* = 3) is in bold.

Although *c* does have substantial influence over the global net N_2O production rates through control of global denitrification production and consumption rates, it is not as strong as the influence of thr_{O2}. A smaller *c* of 1.5 generates larger net N_2O production rates of 20.5 Tg-N y^{-1} while a larger *c* of 6 generates smaller net N_2O production rates of 6.4 Tg-N y^{-1} – less than a third of rates produced by *c* = 1.5. The base case scenario, *c* = 3, leads to net N_2O production rates of 11.5 Tg-N y^{-1} and was selected mainly due to its 'middling' status. Lowering the value of *c* can result in net N_2O production rates that increase over three times from the lowest to highest tested values.

As Ω itself is a newly introduced term and involves both these parameters, the combination of both thr_{O2} and *c* will have a strong effect on how global N_2O production rates are calculated. These two quantities are highly influential to N_2O production rates as well as highly uncertain and require more quantification in both laboratory and *in situ* studies.

3.5.5 Denitrification Consumption O_2 Inhibition Term ($K_{O2,cons}$)

While the first step of denitrification (production of N_2O by reducing NO_3^-) begins at 6 µmol-O_2 L^{-1}, the second step (consumption of N_2O by reducing N_2O to N_2) largely occurs at much lower O_2 concentrations. The exact concentration and the relationship between N_2O consumption rates by denitrification with O_2 are not well understood, mainly due to these two steps being combined in modelling studies and the difficulty of measuring reactions in extremely low O_2 waters in observational and laboratory studies.

The parameterization used in this model uses a rate constant, N_2O concentration, and an exponential relationship with O_2 according to an O_2 'poisoning' term (*Equation 10*). The exponential parameterization means $K_{O2,cons}$ is not a 'hard' O_2 threshold like thr_{O2} in Ω

(partitioning between oxic and suboxic remineralization), but still reflects the near-anoxic O_2 concentrations required for reduction of N_2O.

To see how $K_{O2,cons}$ affects the relationship between N_2O consumption and production by denitrification, as well as total global N_2O production rates, $K_{O2,cons}$ was varied between 0.3, 1.0, 3.0, and 4.5 μmol-O_2 L^{-1} (Figure 52). This allows investigation into denitrification consumption only occurring in anoxic environments as well as in environments where O_2 concentrations are much higher.

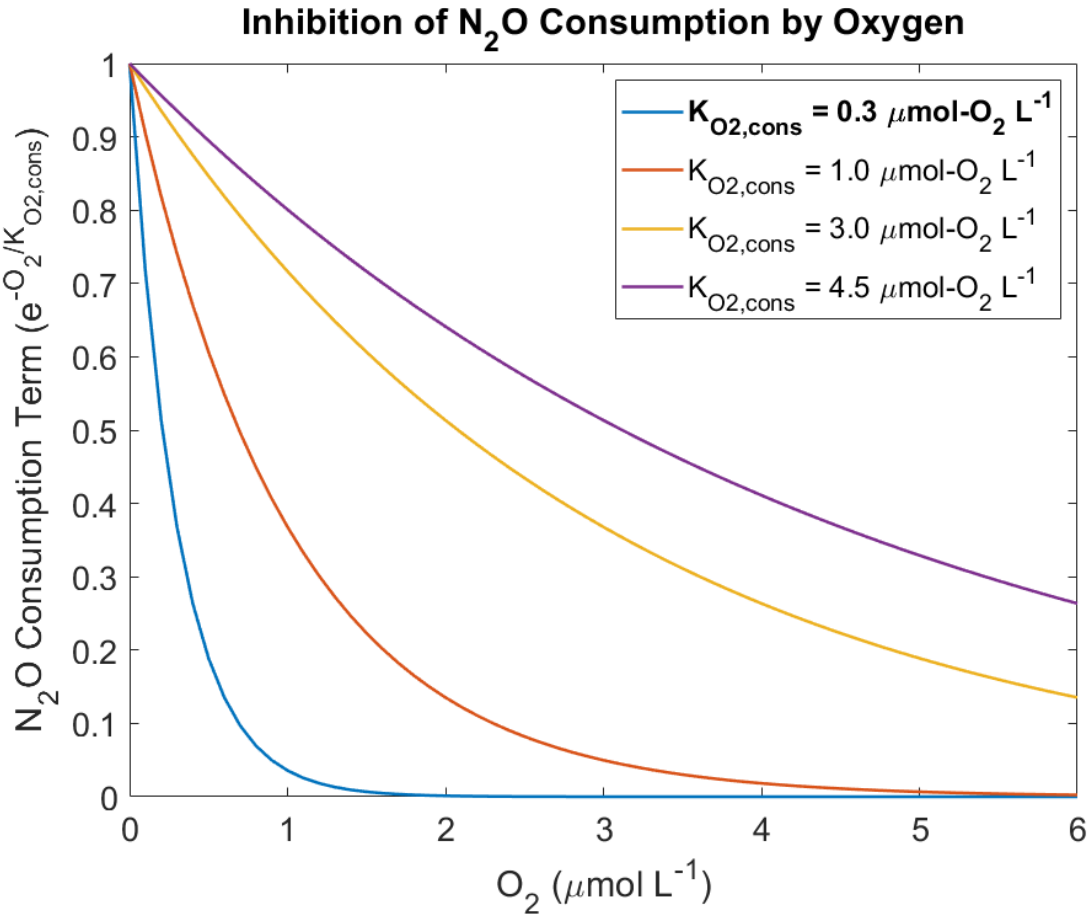

Figure 52: Effect of varying $K_{O2,cons}$ on N_2O consumption within suboxic range of O_2 concentrations. Base case scenario ($K_{O2,cons}$ = 0.3 μmol-O_2 L^{-1}) is in bold.

The base case scenario, $K_{O2,cons}$ = 0.3 μmol-O_2 L^{-1} (blue), demonstrates how N_2O consumption begins at below approximately 2 μmol-O_2 L^{-1} but is limited except at << 1 μmol-O_2 L^{-1}. When $K_{O2,cons}$ is lower than this, N_2O consumption will remain very low even when O_2 is less than 0.5 μmol-O_2 L^{-1}.

When $K_{O2,cons}$ is higher than 0.3 μmol-O_2 L^{-1}, N_2O consumption begins at higher O_2 concentrations. Even increasing $K_{O2,cons}$ to 1.0 μmol-O_2 L^{-1} (red) causes N_2O consumption near the thr_{O2} of 6 μmol-O_2 L^{-1}, while a $K_{O2,cons}$ higher than 3.0 μmol-O_2 L^{-1} (yellow, purple) results in N_2O consumption occurring outside the suboxic region, which is not plausible.

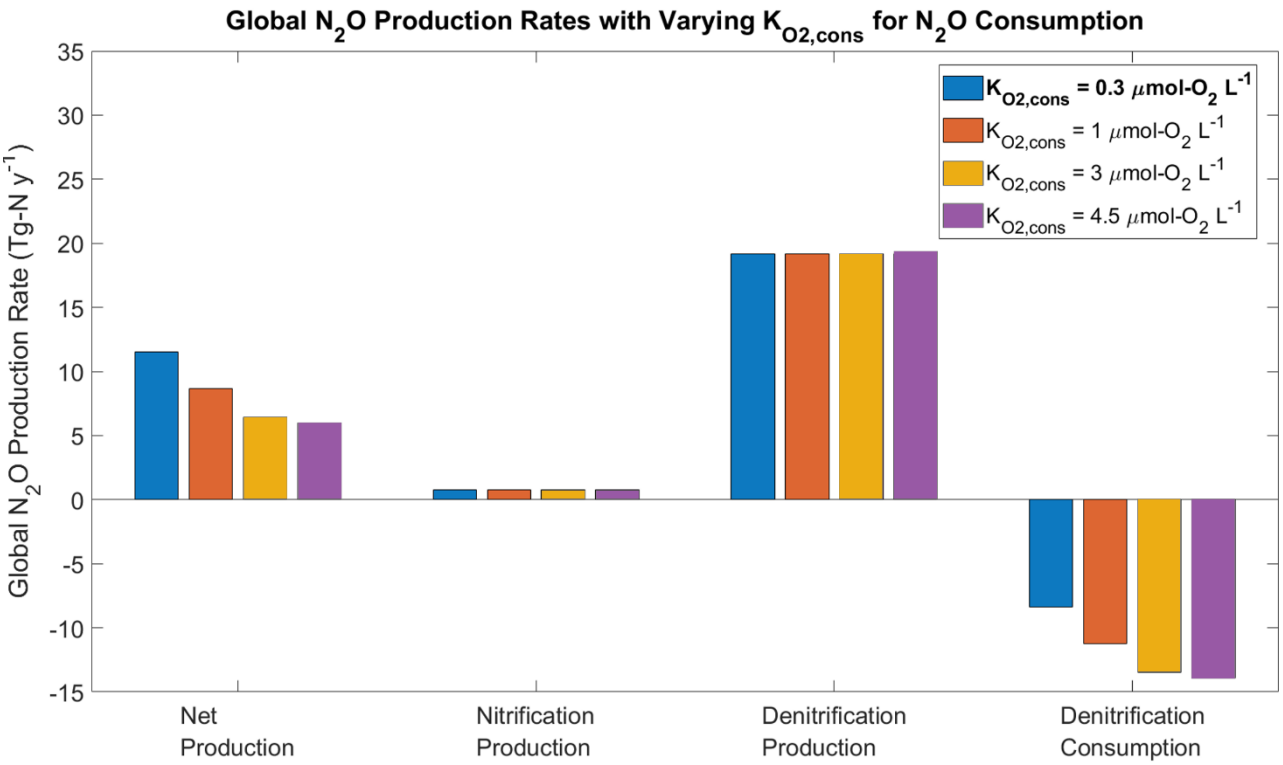

Figure 53: Global N_2O production rates with varying $K_{O2,cons}$ for N_2O consumption by denitrification. Base case scenario ($K_{O2,cons}$ = 0.3 μmol-O_2 L^{-1}) is in bold

Figure 53 shows N_2O consumption and production by denitrification by using varying $K_{O2,cons}$ to generate global N_2O production rates. Nitrification and denitrification production rates are unaltered by changes in $K_{O2,cons}$, but the net N_2O production rates are substantially affected. The large amount of N_2O produced by denitrification causes strong N_2O consumption rates, with higher $K_{O2,cons}$ creating higher N_2O consumption rates – varying $K_{O2,cons}$ between 0.3 and 4.5 μmol-O_2 L^{-1} can lead to consumption rates between 8.4 and 13.9 Tg-N y^{-1} (maximum 40% difference), with the lower consumption rate a result of a lower $K_{O2,cons}$. This is reflected in the net N_2O production rates, as a low $K_{O2,cons}$ and low consumption rate will lead to increased net N_2O production when N_2O production rates remain the same.

The strong correlation between global net N_2O production rates and $K_{O2,cons}$ combined with the uncertainty of the nature of the consumption pathway – i.e., the O_2 concentration at which it begins and the shape of the curve as O_2 changes – implies that this quantity is one of the more important parameters to be investigated by future research. Gaining more information on $K_{O2,cons}$ and the best form of N_2O consumption rate parameterization will be of paramount importance in determining the proportions of global N_2O produced and consumed by the three pathways.

3.6 Effects of Projected Future Climate Change

The five global Earth System models (ESMs) discussed above (CanESM5, CanESM5-CanOE, CNRM-ESM2-1, GFDL-ESM4, UKESM1-0-LL) are used in this section to provide historical and future estimates of O_2, detritus flux, and temperature. Historical data are averages for 1986-2005, whereas future data are averages for 2081-2100. The *delta* data are created by taking the projected future minus historical data from the five ESMs and, in the case of ΔO_2, adding this to

the present-day data from the World Ocean Atlas. The intent here is to determine whether any changes in global N_2O production rates using varying data product inputs are a result of differences between models or differences between past and future data. As the five ESMs use different parameterizations to generate data, changes in the magnitude and spatial resolution of the data products can be better compared from historical to future projections when accounting for the differences in the model. For example, if a certain model consistently predicts lower O_2 concentrations than the others, it might look as if the amount of deoxygenation in future projections is also stronger for this model than for the other ESMs. However, by using the delta data only the *difference* between past and future is compared between models – since that specific model has lower O_2 for both past and future, the delta data may show that the amount of O_2 loss projected for the future is in fact weaker than for the other ESMs.

In all tested scenarios, ESM EPC or temperature was input to the model for historical simulations and future projections, so that the final result is the model output of future projections of N_2O production and consumption rates minus the historical projections of N_2O production and consumption rates. For O_2, the difference of historical and projected O_2 (delta) was added to the WOA O_2 data ($\Delta O_2 + O_{2,WOA}$) to better compare global N_2O production and consumption rates to the base case scenario. Adding the delta data to the WOA data is necessary for O_2 due to biases in the ESM distribution of O_2.

3.6.1 Oxygen

To analyze how global N_2O production rates will be affected by future changes in O_2, namely anticipated global deoxygenation due to anthropogenic influences, O_2 data from the five ESMs is input into the model – this includes O_2 for the historical climate, for the future climate, as well as delta O_2 (future minus historical data products) added to the observation-based base case.

Historical O_2 Data

The historical O_2 data generated by the five ESMs (as opposed to the 2018 World Ocean Atlas data used in the base case scenario of the model) have varying spatial distributions as depicted in Figure 54. The size and intensity of the ODZs in the eastern North Pacific, eastern South Pacific, and the Arabian Sea are of particular importance as they strongly influence the amount of N_2O produced and consumed by denitrification in suboxic waters.

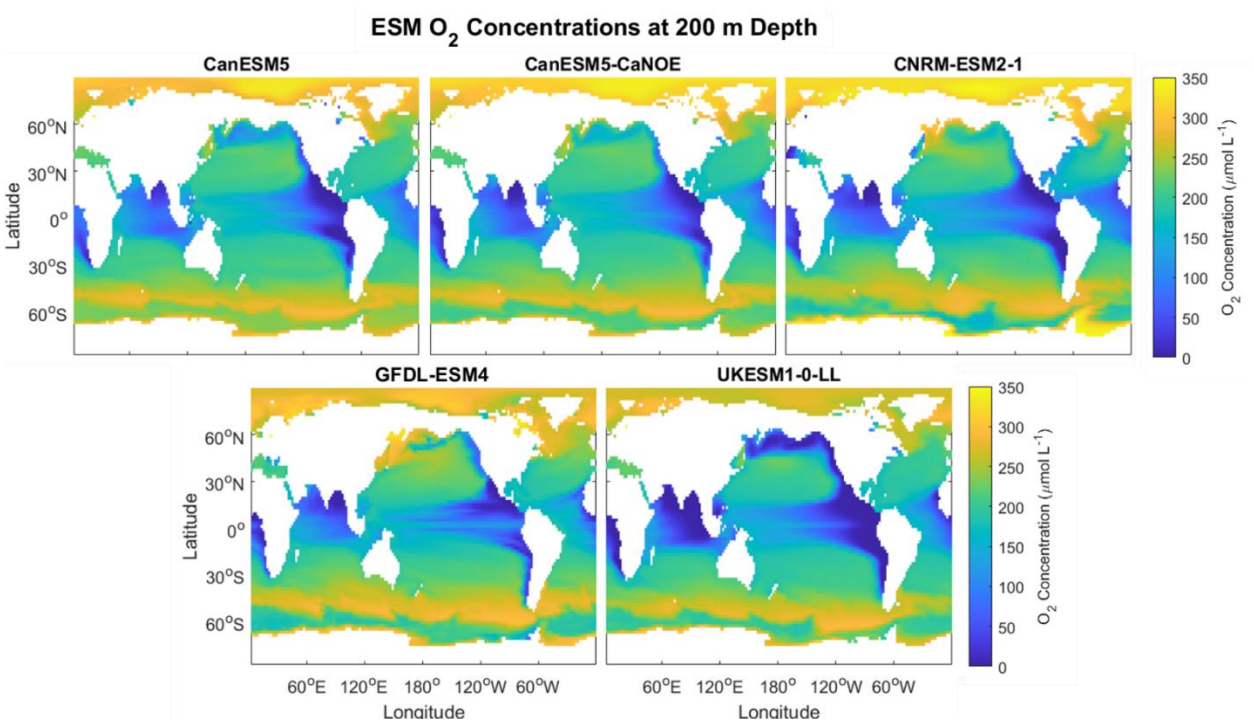

Figure 54: Historical (1986-2005) ESM O_2 concentrations at 200 m depth.

Applying these data products to the model produces rates of N_2O production and consumption shown in Figure 55 (top: all production and consumption pathways, bottom: nitrification production rates from top panel depicted at a larger scale). Figure 55 (top) displays how global net N_2O production rates vary using the five different O_2 model data products from 1986-2005 as well as the base case scenario for this model using O_2 data products from the 2018 World Ocean Atlas.

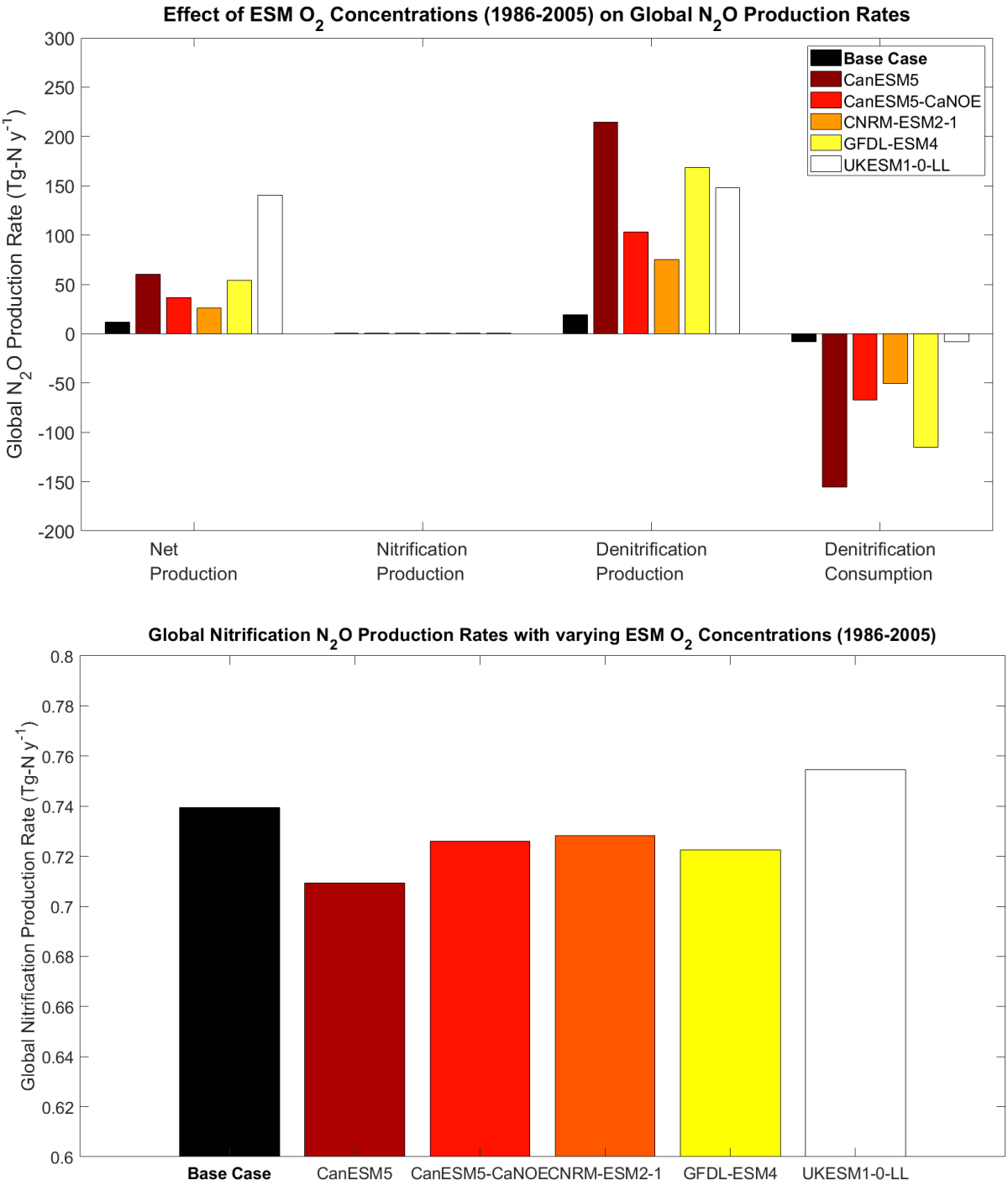

Figure 55: Effect of O_2 distribution from five ESMs on global N_2O production and consumption rates

The first notable difference in using ESM O_2 data, rather than the base case scenario of using WOA data, is a substantial increase in net N_2O production rates due to a large increase in denitrification N_2O production and consumption rates (Figure 55, top) that is not seen in the nitrification N_2O production rates (Figure 55, bottom). Nitrification production rates for the base

case are slightly higher than the average of all five ESMs, though lower than the highest N_2O production rates by nitrification for UKESM1-0-LL. Denitrification production rates also remain higher than denitrification consumption rates, especially in the case of the UKESM1-0-LL data – net N_2O production rates are over twice as large as for the other ESMs because denitrification consumption rates are extremely low. Conversely, CanESM5 has high denitrification production rates but also has high denitrification consumption rates. Because of this, the net N_2O production rates for CanESM5 are substantially lower than UKESM1-0-LL despite having much larger N_2O production rates by denitrification.

Both CanESM5 and UKESM1-0-LL have the largest net N_2O production rates by denitrification, but the difference lies in the magnitude of the production and consumption rates by denitrification. UKESM1-0-LL has more denitrification production occurring without simultaneous denitrification consumption that would lower the net N_2O production rates. In comparison, CanESM5 has global denitrification production rates that are larger than for UKESM1-0-LL but has substantial denitrification consumption rates that lower the net N_2O production rates (discussed further in Discussion, Section 4.1).

Future Projections of O_2

Global maps of the future projections of O_2 data at 200 m from the five ESMs is depicted in Figure 56. Visually, there is very little difference between future and historical O_2 projections, but slight variation results in different global N_2O production rates, as shown in Figure 56.

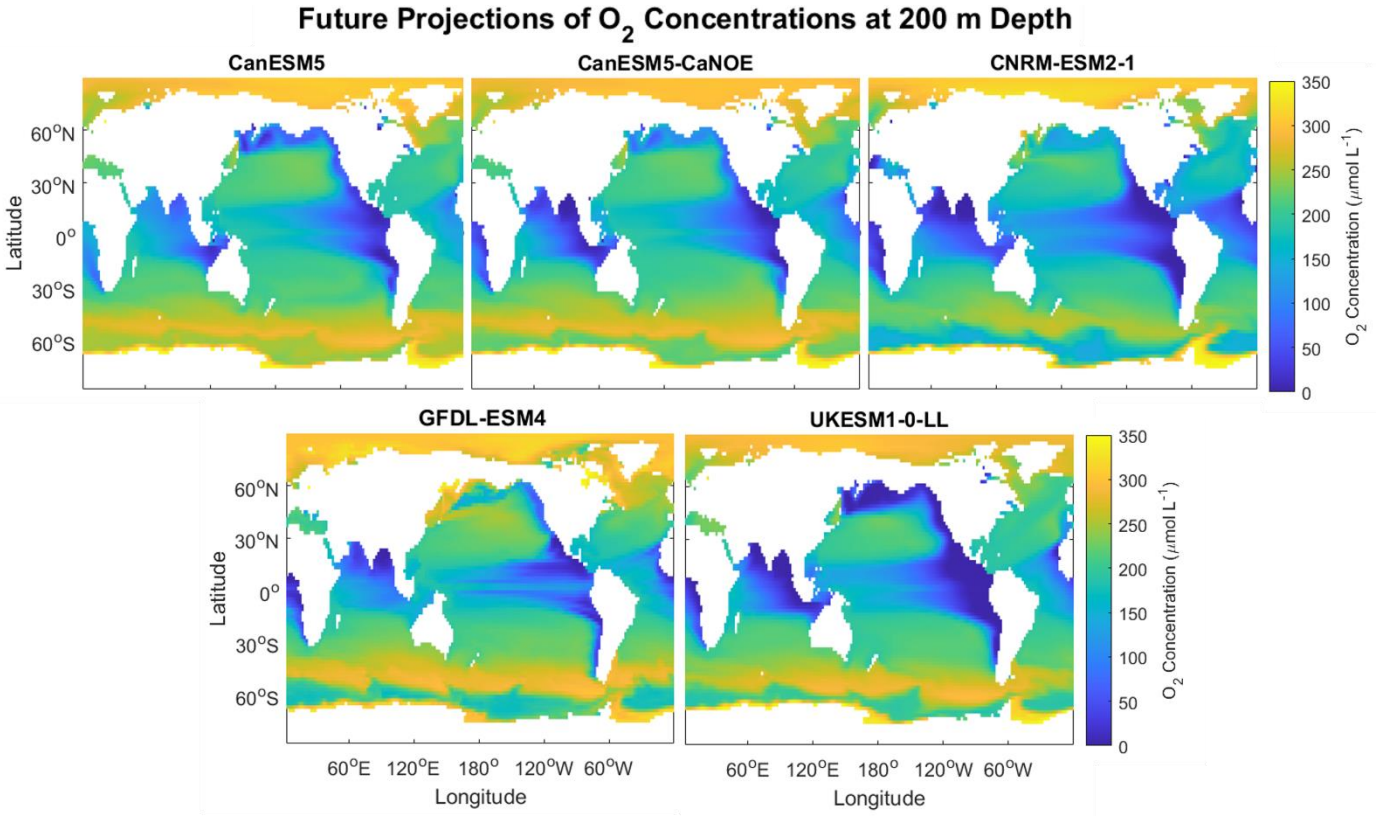

Figure 56: Future ESM Projections of O_2 at 200 m depth.

Global N_2O production rates using future projections of O_2 from the five ESMs (Figure 57) show that differences among models are somewhat maintained, e.g., UKESM1-0-LL remains the

highest due to low denitrification consumption rates. Top panel depicts all production and consumption processes, while bottom panel highlights the nitrification production rates from the top panel at a larger scale.

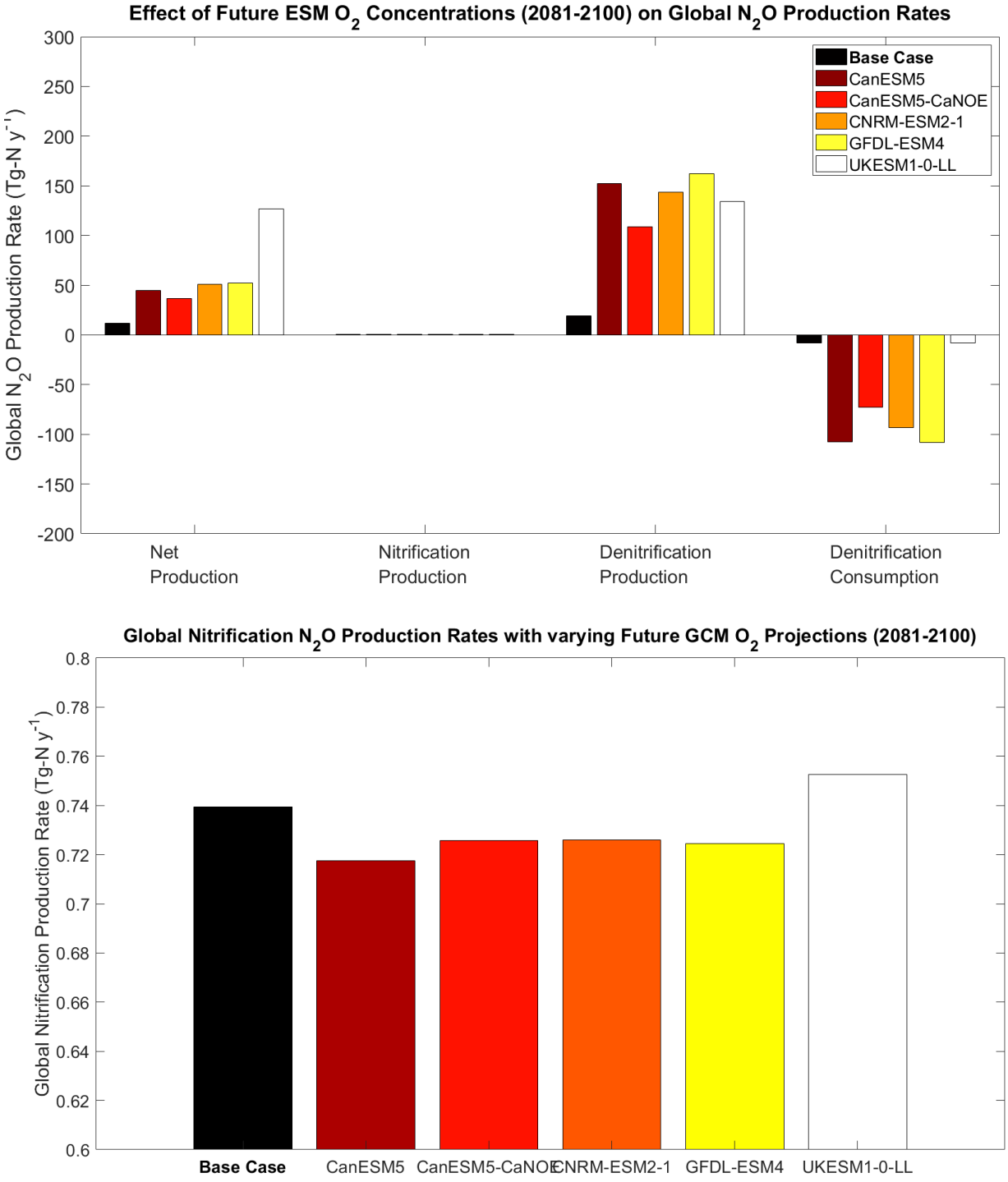

Figure 57: Global N_2O production and consumption rates based on future (2081-2100) O_2 concentrations from five ESMs.

Incorporating future O_2 data results in UKESM1-0-LL having the highest N_2O production rates by far, over twice the magnitude of any other ESM, due to extremely low N_2O consumption rates. The other four models are comparable in their net N_2O production rates, with CanESM5-CanOE having the lowest net production rates. Interestingly, while both CanESM5 and GFDL-ESM4 have similar denitrification production and consumption rates that are larger than those of CNRM-ESM2-1, CNRM-ESM2-1's net N_2O production rates are of near-equal magnitude to CanESM5 and GFDL-ESM4. This means that the net denitrification production rate (denitrification production minus consumption) is comparable for all three models despite differences in the magnitudes of denitrification production and consumption. Nitrification N_2O production rates are comparable across all ESMs, though UKESM1-0-LL has slightly higher rates. The base case scenario has nitrification rates close to an average between the UKESM1-0-LL and four other ESMs.

ΔO_2: Future Minus Historical O_2

The ΔO_2 (future minus historical from the five ESMs) is investigated here to assess projected future changes in N_2O production and consumption rates independently of model bias and to compare the magnitude of that future change with the model bias in the historical data. A visual representation of ΔO_2 is provided in Figure 58, where red indicates regions where O_2 decreases from historical to future (deoxygenation).

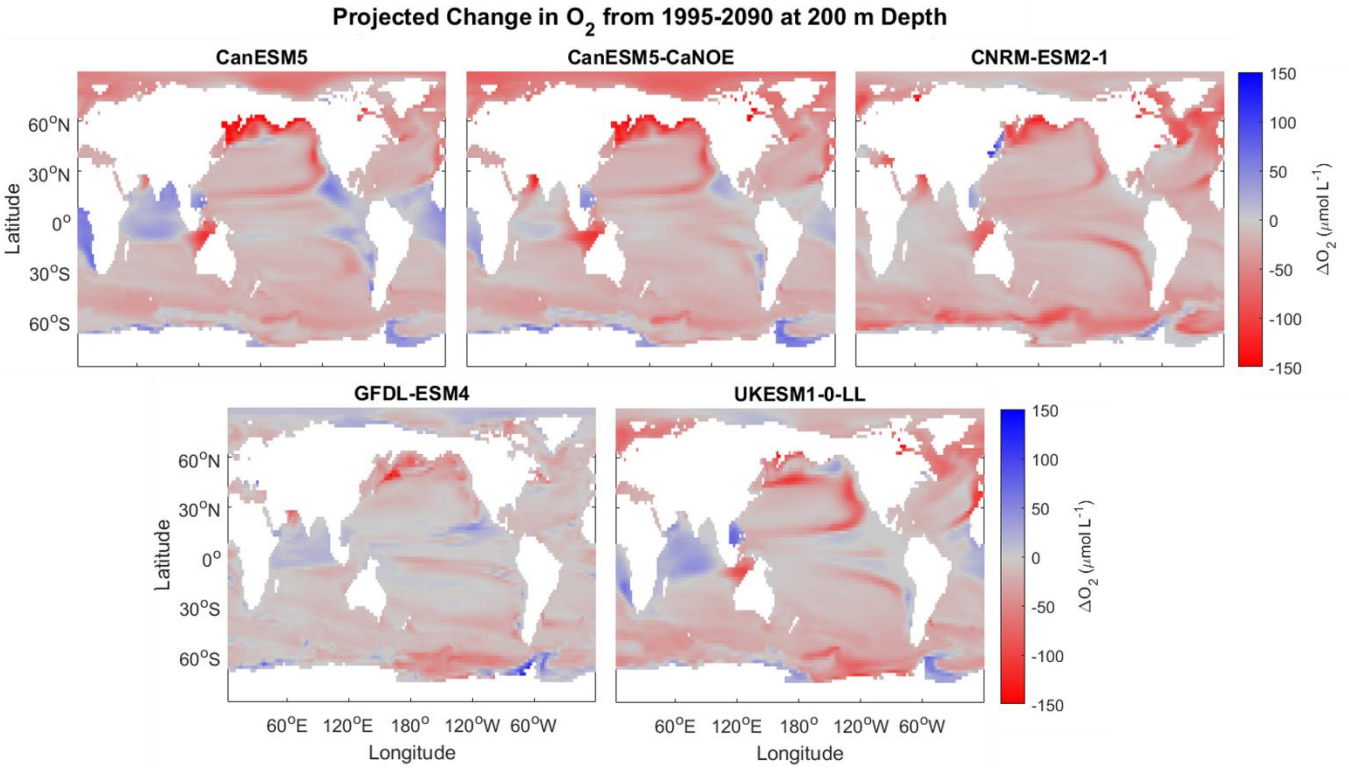

Figure 58: Projected change in O_2 (ΔO_2: future minus historical O_2 concentration) from 1986-2090 for each of the five ESMs from the ssp585 experiment at 200 m.

Interestingly, while the boundaries of ODZs in the North and South Pacific tend to experience a decrease in O_2, the ODZ cores experience an increase in O_2 for some of the ESMs (Figure 58). As N_2O production and consumption by denitrification increase from past to future (Figure 59, top panel), the expansion of ODZ regions seems to have a greater effect on N_2O than locally

increased O_2. There are multiple possible explanations for this. The ODZ region may expand, increasing the global volume of suboxic water and leading to more denitrification production of N_2O. Similarly, decreased O_2 in ODZs may increase denitrification production rates (as well as consumption rates), and could increase yield of N_2O from nitrification. Increased O_2 in the core of ODZs also decreases N_2O consumption, leading to a higher proportion of N_2O produced by denitrification versus N_2O consumed by denitrification. Denitrification production is similarly decreased with increased O_2, but the range of O_2 that permits denitrification production is larger than the range required for denitrification consumption, so elevated O_2 in ODZ cores still supports some denitrification production of N_2O while inhibiting consumption.

It is not clear which of these scenarios has the greatest effect on net N_2O production rates in these regions, but their net effect for each ESM is shown in Figure 59. ΔO_2 in the oxygenated waters has a minimal effect on nitrification N_2O production rates - as long as O_2 is above approximately 50 μmol-O_2 L^{-1}, neither nitrification rate nor nitrification N_2O yield will change substantially (see Figures 8-9, Section 2.1.1). Figure 59 provides a better look at how changing O_2 may affect N_2O production, where ΔO_2 from the future and historical ESM data products is added to the original WOA O_2 data product and input into the model.

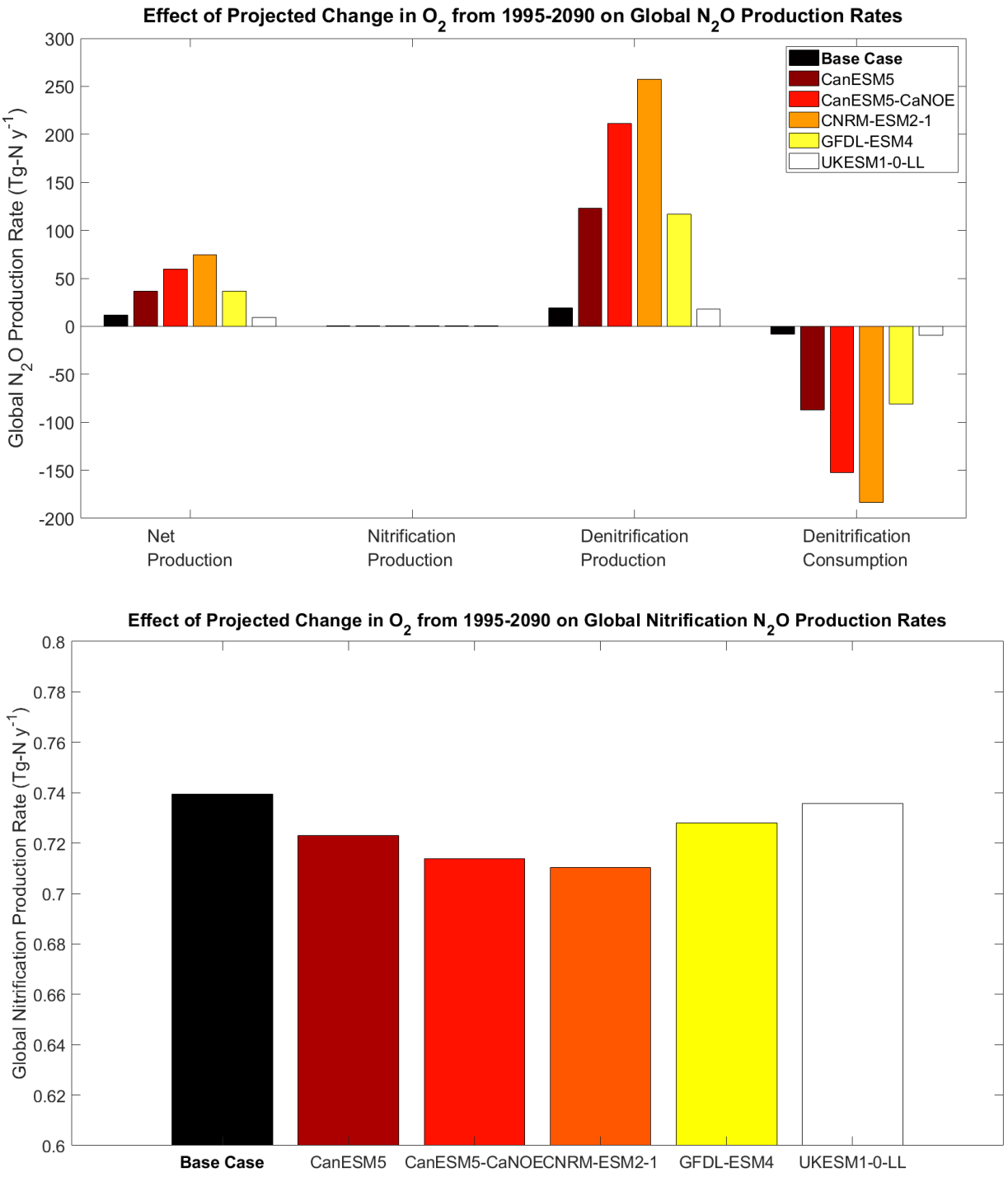

Figure 59: Global N_2O production and consumption rates ΔO_2 (future minus historical O_2) concentrations for five ESMs from the ssp585 experiment, where ΔO_2 is added to the base case O_2 data from World Ocean Atlas 2018.

With the exception of UKESM1-0-LL, global net N_2O production rates are much higher than in the base case of 11.5 Tg-N y^{-1}. Since O_2 input into the model uses WOA data plus the ESMs' ΔO_2, this means that the ΔO_2 decreases the O_2 strongly enough from past to future to greatly increase denitrification production and consumption rates. In other words, while there is some spatial variation among the ESMs that results in varying N_2O production and consumption, the

overall change between past and future produces a substantial increase in global net N_2O production rates. This change is due to larger denitrification net N_2O production rates: both denitrification production and consumption rates increase, but denitrification production rates remain higher than consumption rates.

While UKESM1-0-LL displayed high denitrification production rates and very low denitrification consumption rates in both historical and future data, this effect is mitigated in the ΔO_2 data. Essentially, the change between past and future O_2 for UKESM1-0-LL results in the smallest change in global N_2O production and consumption rates such that net global N_2O production rates are similar to the base case scenario that uses historical WOA data. This likely means that the extremely low denitrification consumption rates for UKESM1-0-LL is due to model bias, as it isn't reflective in the ΔO_2 data.

Conversely, CanESM5-CanOE and CNRM-ESM2-1 have very large changes in global N_2O production and consumption rates by denitrification to result in very high net N_2O production rates in comparison to the base case scenario. Both CanESM5 and GFDL-ESM4 see more moderate increases in net N_2O production rates, and UKESM1-0-LL sees very little change from past to future N_2O production rates.

Nitrification production rates are not substantially affected by ΔO_2, which is reasonable given that nitrification is much less sensitive to changes in O_2 than denitrification. Nevertheless, there is a small decrease in nitrification production rates across all ESMs in comparison to the base case scenario.

3.6.2 Organic Matter Flux

Organic matter input to the model will also be analyzed by comparing historical and future projections of EPC – export of particulate carbon at 100 m – from the five ESMs by using the ΔEPC (Figure 62). Unlike the above section with ΔO_2, where the ΔO_2 is added to the base case historical 2018 WOA data, the ΔEPC will not be added to the base case scenario. The organic matter (detritus) input for the base case scenario of the model uses historical EPC from CanESM5-CanOE, where a comparison of global N_2O production rates across the five ESMs for the historical EPC was presented in Section 3.3.1 (Figure 31). Historical EPC is normalized to 20 Pg-C y^{-1} as in the base case scenario, and the adjustment factor used for each model's historical EPC normalization is then applied to the future EPC projections for each ESM.

ΔEPC: Future Minus Historical Data Products

ΔEPC in this section involves the future minus historical data (Figures 60, 61). ΔEPC provides valuable information on how strongly the spatial patterns between ESMs may affect global N_2O production and consumption rates compared to the changes over time.

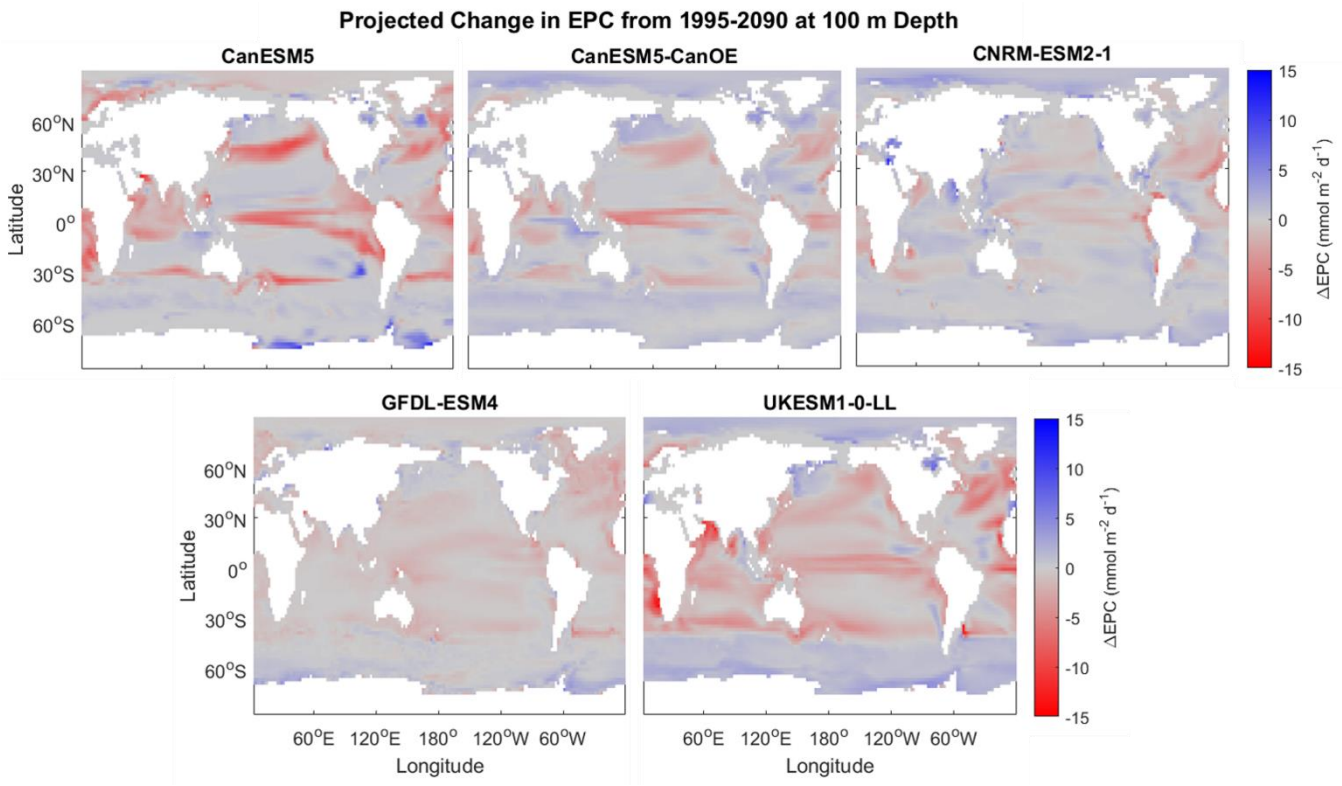

Figure 60: Change in EPC from 1995-2090 **(**ΔEPC: future minus historical) for each of the five ESMs at 100 m depth from the ssp585 experiment.

Compared to the maps for ΔO_2, the ΔEPC at 200 m in Figure 60 depicts less variation from past to future data for all five ESMs. CanESM5 and UKESM1-0-LL experience the greatest changes in EPC, especially in the Southern Ocean for CanESM5.

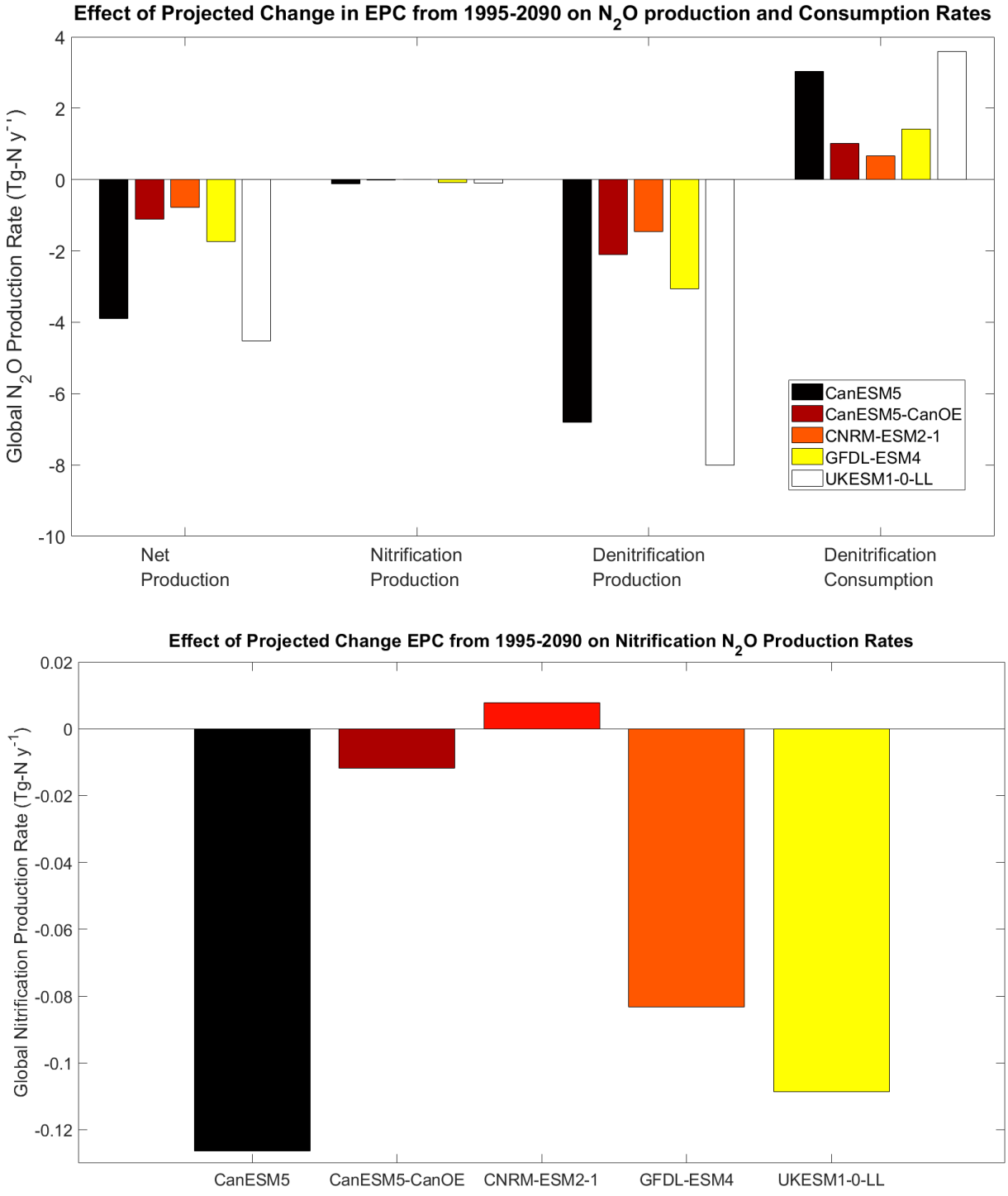

Figure 61: Changes in N_2O production and consumption rates due to changes in EPC (ΔEPC: future minus historical) for five ESMs from the ssp585 experiment.

It is important to note that Figure 61 differs from the above analysis for O_2 (Figure 59) in that the change in N_2O production and consumption rates is from future-minus-past EPC (ΔEPC) (Figure 61), while the change in N_2O production and consumption rates for O_2 uses future-minus-past O_2 added to the base case O_2 data from World Ocean Atlas ($\Delta O_2 + O_{2,WOA}$) (Figure 59).

Changes in EPC from past to future lead to a substantial decrease in N_2O production and consumption by denitrification, resulting in a net decrease in the global net N_2O production rate. This effect is strongest for CanESM5 and UKESM1-0-LL, while CanESM5-CaNOE (base case scenario), CNRM-ESM2-1, and GFDL-ESM4 experience a more moderate effect. This is reasonable, given that changes in EPC are most apparent for CanESM5 and UKESM1-0-LL (Figure 60). Globally, there is a net decrease in EPC from past to future model projections, which leads to a decrease in the amount of organic matter supplied to the system. Nitrification is more directly affected by total organic matter supply and so is more sensitive to changes in total EPC than denitrification, whereas denitrification is more sensitive to the spatial pattern. As a result, nitrification N_2O production rates also see a strong decrease from past to future - with the exception of CNRM-ESM2-1, which sees a small increase in nitrification production of N_2O. As EPC from CanESM5-CanOE is used for the base case of the model, the moderate decrease in net N_2O production as a result of denitrification and the small decrease in N_2O production from nitrification are most reflective of the data used for this model.

A similar experiment was conducted for ΔEPC, where both historical and future EPC were normalized to 20 Pg-C y^{-1}. This uniform normalization means there is no change from past to future in the global total EPC, although both methods can be used to compare spatial differences between models for ΔEPC. The uniform normalization also leads to a decrease in net N_2O production that is less than half of the magnitude of the above version in Figure 60. Interestingly, using the uniform normalization ΔEPC leads to a net *increase* in N_2O production by nitrification for all models except GFDL-ESM4. The effect on nitrification production rates by ΔEPC is much stronger than for ΔO_2, as nitrification is more sensitive to changes in organic matter supply than to changes in O_2. When using this method, CanESM5-CanOE (used in the base case model) and UKESM1-0-LL have the largest changes in net production due to decreased denitrification.

3.6.3 Temperature Increase

The base case scenario uses temperature from the 2018 World Ocean Atlas, but historical and future projection data can also be generated using the five ESMs. Using the same method as for ΔO_2, the spatial differences between models as well as between future and historical temperatures are evaluated by using the ΔT data added to the existing 2018 WOA T data (Figure 62).

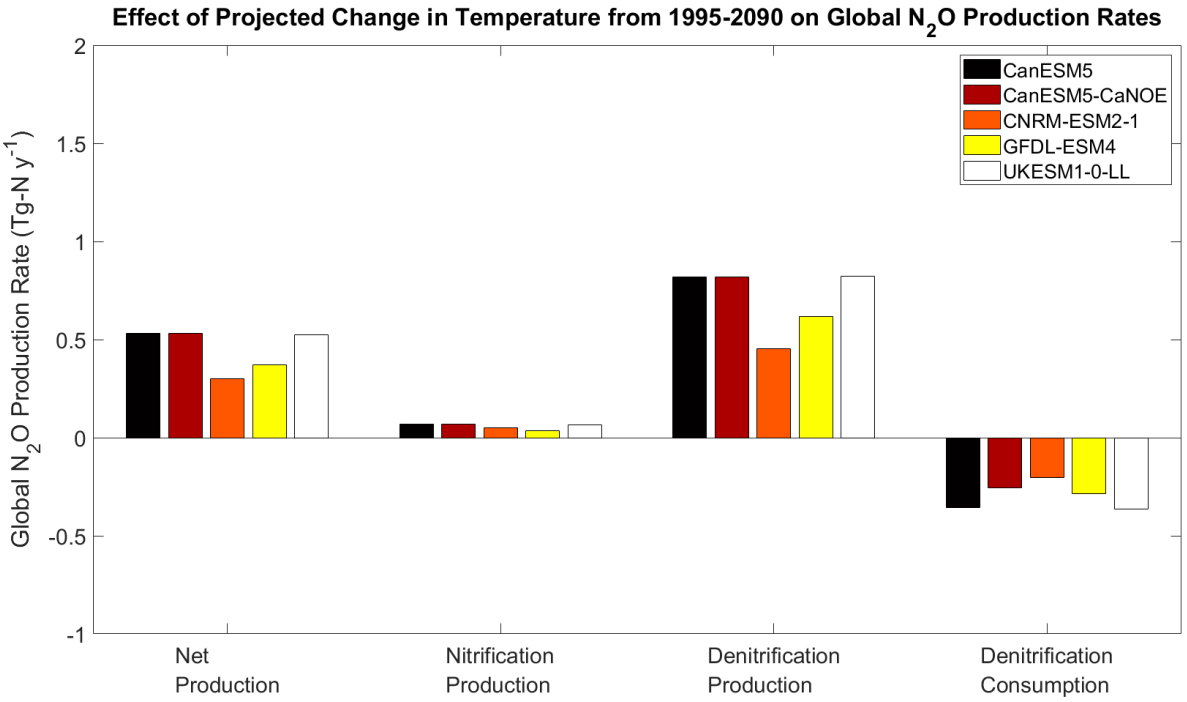

Figure 62: Changes in N_2O production and consumption rates from ΔT (future minus historical temperature) for the five ESMs from the ssp585 experiment.

The effect of changing temperature from past to future is negligible when considering N_2O production and consumption rates. ΔT itself is fairly small in comparison to ΔEPC and especially to ΔO_2, but more importantly the effect of variations in temperature on net N_2O production rates is minimal (<0.6 Tg-N y^{-1}). While warming of the oceans will likely have some effect on remineralization rates, it has very little effect on net global N_2O production rates.

4 Discussion

The aim of this research is to quantify and parameterize the main controls on N_2O production by nitrification and denitrification, and to determine how strongly model parameters and environmental conditions affect net global N_2O production. The uncertainty of many of these parameters necessitated evaluation of a range of values from existing model and observational literature, and the above results have highlighted which uncertainties are most important to N_2O production reactions. This section provides a discussion of these parameters and their significance to global net N_2O production rates as well as to nitrification and denitrification, how current estimates and future projections of environmental conditions influence ocean production of N_2O, and how the limitations of the model framework affect these results.

4.1 Significance of Uncertain Parameters

In order of most to least importance, the uncertain parameters and environmental conditions that have the greatest influence on global net N_2O production rates are: O_2 data products, thr_{O2} (the O_2 concentration that signifies the end of oxic remineralization and beginning of denitrification), the exponent c in Ω (the constant that controls how strongly oxic remineralization rates decrease and denitrification rates increase with O_2 in suboxic waters), α_{RLS} (the inverse remineralization length scale), spatial distribution of detritus flux (choice of Earth System Models used to generate EPC), $K_{O2,cons}$ (the O_2 concentration that signifies the start of N_2O consumption), $fNO_{3,remin}$ (the half-saturation threshold for denitrification/suboxic remineralization), and γ (the yield parameterization for N_2O production by nitrification).

In general, O_2 has the greatest control on N_2O production rates and so the input O_2 data product has substantial influence on model results, as do the parameters that control the proportions of oxic to suboxic remineralization (thr_{O2} and c) and the parameter that controls the proportion of N_2O production by denitrification to consumption by denitrification ($K_{O2,cons}$). $K_{O2,cons}$ has a substantial influence on net N_2O production, though its impact is relative to the strength of denitrification production and consumption as determined by thr_{O2} and c. N_2O yield (γ) has strong control over N_2O production by nitrification but does not have a very powerful impact on net N_2O production, as nitrification contributes a relatively small amount of the total net N_2O production. The accuracy of O_2 data products and the exact O_2 concentration of thr_{O2} and $K_{O2,cons}$ are essential when parameterizing N_2O production but are highly uncertain in past modelling and observational studies. In comparison, N_2O yield during nitrification is generally well-understood although the new parameterization of γ is still relatively recent (Ji et al. 2018).

4.1.1 Control by Oxygen

While the parameters thr_{O2}, c, $K_{O2,cons}$, and γ are both uncertain and highly influential to N_2O production and consumption, the largest control on ocean N_2O production is the accuracy of the O_2 data input to the model. To evaluate denitrification reactions that only occur in suboxic regions, it is essential that the gridded O_2 data is accurate in the 0-6 μmol range. Interpolation of O_2 data products to a uniform 3D grid or averaging of monthly data to an annual mean can 'smear out' suboxic O_2 data points, leading to severe underrepresentation of denitrification processes taking place and, consequently, underestimation of N_2O production and consumption by denitrification. As denitrification is responsible for a majority of net global N_2O production in this model, the relative control by parameters thr_{O2}, c, $K_{O2,cons}$, and γ cannot be properly assessed without accurate suboxic O_2 data.

Averaging monthly O_2 data products from World Ocean Atlas 2018 to an annual mean leads to loss of 75-100% of grid cells with O_2 concentrations below 4 μmol-O_2 L^{-1}. As this model has a thr_{O2} of 6 μmol-O_2 L^{-1} to signify the end of N_2O production by denitrification and a $K_{O2,cons}$ of 0.3 μmol-O_2 L^{-1} to control N_2O consumption, using this annually-averaged O_2 data leads to a 65% decrease in the global net N_2O production rate compared to using monthly O_2 data (note that monthly O_2 data is a relatively recent addition to the World Ocean Atlas). Newly developed O_2 data products (Kwiecinski and Babbin, 2021) have higher resolution due to using continuous depth profiles with higher resolution across depth layers as well as due to a greater amount of data points in total, which results in over ten times the fraction of suboxic data points as the World Ocean Atlas 2018. 11.6% of all data points lie in the 0-6 μmol-O_2 L^{-1} region for the Kwiecinski and Babbin data as opposed to 0.50% for the World Ocean Atlas data, though this number may be biased high as Kwiecinski and Babbin's (2021) data is not interpolated to a uniform grid and is focused on ODZ regions in the Pacific. As such, O_2 data for Kwiecinski and Babbin (2021) and the World Ocean Atlas can not be directly compared. However, many ODZ regions in the World Ocean Atlas do not reach the 6 μmol-O_2 L^{-1} threshold for denitrification at all, while it did in multiple locations in Kwiecinski and Babbin's (2021) data.

Furthermore, Kwiecinski and Babbin's (2021) O_2 data portrays the oxycline in ODZs as occurring at shallower depths than in the World Ocean Atlas for almost all locations. This has substantial influence on N_2O production rates, as there is higher organic matter availability in shallower waters. Overlap of higher organic matter supply in locations with suboxic O_2 provides a greater amount of substrate for suboxic remineralization, and so increases N_2O production and consumption by denitrification. In a location in the North Pacific ODZ (15°N, 110°W), O_2 concentrations reach as low as 2 μmol-O_2 L^{-1} for the Kwiecinski and Babbin (2021) data set compared to 4 μmol-O_2 L^{-1} for the World Ocean Atlas, and have an oxycline that begins at approximately 50 m as opposed to 150 m. These two factors lead to an increase in maximum net N_2O production of nearly 50-fold, from 0.028 nmol-N_2O L^{-1} (World Ocean Atlas) to 1.25 nmol-N_2O L^{-1} (Kwiecinski and Babbin, 2021), and so have large repercussions for modelling ocean N_2O production.

As far as O_2 control through parameter choices, thr_{O2} is one of the most impactful terms for modelling N_2O production through denitrification. This concentration is difficult to isolate due to the overlap of oxic remineralization and suboxic remineralization (denitrification) over a small range of suboxic O_2 concentrations. A difference of 1 μmol-O_2 L^{-1} can determine the difference between oxic and suboxic processes, and so measuring thr_{O2} would require extreme accuracy in sample measurement and analysis. The reaction rates of each of these processes can also vary widely due to influence by substrate availability and other environmental conditions, so while consumption of organic matter or electron acceptors (O_2 for oxic remineralization, NO_3^- for suboxic remineralization) can be measured *in situ*, the relative magnitude of contribution by oxic versus suboxic remineralization is challenging. In other words, a decrease in organic matter over time can be directly measured but determining whether this organic matter is consumed by the oxic pathway or suboxic pathway is more complicated as it is not solely dependent on O_2.

Isolating thr_{O2} is also complicated by simplification of past model's parameterization of these individual reaction mechanisms. Often, elevated N_2O production at ODZ oxyclines is represented by one term that signifies N_2O production in suboxic O_2 by both nitrification and denitrification, and N_2O consumption is represented simply as 'no production' after a certain low O_2 concentration is reached (Suntharalingam et al. 2000, Nevison et al. 2003, Bianchi et al.

2012). Because of this, the O_2 threshold that partitions oxic and suboxic remineralization in many models disregards denitrification's ability to simultaneously produce and consume N_2O and conflates the O_2 concentration for elevated N_2O yield with the O_2 concentration for the start of denitrification N_2O production.

For example, strong accumulation of N_2O at higher O_2 concentrations (such as 20 μmol-O_2 L^{-1}) has been measured in ODZ oxyclines that could indicate that the threshold for denitrification is higher than 6 μmol-O_2 L^{-1} (Farías et al. 2009, Sun et al. 2021), but it could also indicate elevated production by nitrification (Trimmer et al. 2016), or even the influence of other completely unrelated environmental conditions such as increased substrate supply or the effects of physical mixing at ODZ boundaries (Casciotti et al. 2018, Monreal et al. 2022). It is also uncertain whether elevated N_2O production is purely because of elevated N_2O production, or the absence of N_2O consumption.

Sun et al.'s (2021) model increased the O_2 threshold for oxic versus suboxic remineralization to 20 μmol-O_2 L^{-1} from the 1 μmol-O_2 L^{-1} used in Babbin et al. (2015), and the resultant high global N_2O production rates caused them to similarly increase the $K_{O2,cons}$ from 0.3 μmol-O_2 L^{-1} to 4.5 μmol-O_2 L^{-1} in order to lower net N_2O production rates through increased N_2O consumption. If Babbin et al. (2015) are correct, then N_2O production has smaller denitrification source and sink terms than represented by Sun et al. (2021) and yet, both models produce similar global net N_2O production rates (3-5 Tg-N y^{-1}).

The model developed for this thesis uses a commonly accepted thr_{O2} of 6 μmol-O_2 L^{-1} (e.g., Devol 2008) and has found that such a threshold leads to moderately high denitrification N_2O production rates, which are accompanied by moderate denitrification consumption rates. However, the model tests a thr_{O2} range from 1-20 μmol-O_2 L^{-1}, resulting in net N_2O production rates from 5.6 Tg-N y^{-1} to 57.9 Tg-N y^{-1}. In this model, a thr_{O2} of 20 μmol-O_2 L^{-1} results in denitrification production rates (without including N_2O consumption) as high as 65.8 Tg-N y^{-1}, compared to the 19.2 Tg-N y^{-1} produced when using a thr_{O2} of 6 μmol-O_2 L^{-1}.

While past model estimates of pelagic denitrification (total denitrification, including NO_3^- reduction to N_2) have reached much higher than 65 Tg-N y^{-1} (Gruber and Galloway 2008, Bianchi et al. 2012), estimates of N_2O production through denitrification reaching such high global totals are much less supported by past literature. Regardless, Sun et al.'s research posits an important question. Is there more denitrification – both incomplete (N_2O production) and complete (N_2O consumption) – occurring at higher O_2 concentrations than expected? The results from this research indicate that this is possible, as the high variability of net N_2O production rates from the sensitivity experiments may indicate very high production and consumption rates.

To further investigate the proportion of denitrification production to consumption, and the net production by denitrification compared to production by nitrification, two other parameters – c and $K_{O2,cons}$ – must also be considered. While thr_{O2} sets the upper limit for suboxic processes, the exponent c in Ω controls how quickly the proportion of suboxic remineralization increases (with respect to oxic remineralization) as O_2 decreases, and so influences net production by denitrification in combination with thr_{O2}. C is a term introduced by this model parameterization rather than a physical quantity that can be measured like O_2 concentration.

The value of $c = 3$ was chosen according to how c affects the shape of the Ω curve (Figure 49). Research by Devol (1978) and Dalsgaard et al. (2012) indicates that c should be greater than 1 – i.e., the curve should be 'convex' rather than 'concave' – as the fraction of oxic remineralization

decreases gradually in the upper range of suboxic concentrations (3-6 μmol-O_2 L^{-1}) and rapidly in the lower range (0-3 μmol-O_2 L^{-1}). Beyond this, there is not much literature that dictates the range of *c*. This model tests a range from 1.5 to 6, which generates substantially different global net N_2O production rates and denitrification N_2O production rates (Figure 50, 51). A lower c = 1.5 increases global net N_2O production rates to 20.5 Tg-N y^{-1} while a higher c = 6 decreases rates to 6.4 Tg-N y^{-1}, resulting in a range of approximately 70% (see Section 3.5.4, Figure 51). The base case scenario using c = 3 generates global net N_2O production rates of 11.5 Tg-N y^{-1}.

In order to narrow down the most likely value of *c* (or to create a similar parameterization that moderates control by O_2), modelling can be a useful complement to laboratory and *in situ* research. Trying to observe the proportion of oxic to suboxic remineralization is difficult to accomplish in a controlled laboratory environment, and nearly impossible to measure in the actual ocean across a consistent and small range of O_2 concentrations.

The magnitude of N_2O production by denitrification is controlled by both thr_{O2} and *c*, but the ratio of production by denitrification to consumption by denitrification is controlled by $K_{O2,cons}$. While thr_{O2} is a strict O_2 threshold for the upper limit of denitrification and is mediated by *c*, $K_{O2,cons}$ is not a threshold and is instead mediated by an exponential parameterization (*Equation 10*, Figure 9).

N_2O consumption, or complete denitrification through reduction of N_2O to N_2, is generally expected to occur at O_2 concentrations below 1 μmol-O_2 L^{-1} and for this reason the base case scenario of $K_{O2,cons}$ is 0.3 μmol-O_2 L^{-1} but a range from 0.3-4.5 μmol-O_2 L^{-1} was tested. This variation in $K_{O2,cons}$ generates global N_2O consumption rates between 8.4 and 13.9 Tg-N y^{-1}, with N_2O production rates by denitrification remaining the same at 19.2 Tg-N y^{-1}. The result is that net N_2O production rates can change by approximately 2.1 times over the range of $K_{O2,cons}$ values tested (Figure 53).

The base case where $K_{O2,cons}$ = 0.3 μmol-O_2 L^{-1} represents a scenario where denitrification consumption rates are slightly less than 50% of the denitrification production rate, while a higher $K_{O2,cons}$ would have consumption rates that are almost 75% of denitrification production rates. Essentially, if N_2O consumption occurs at higher O_2 concentrations then the global net N_2O production by denitrification will be smaller in proportion to N_2O production by nitrification. If N_2O consumption only occurs at near-anoxic O_2, then the net N_2O production rates by denitrification will remain high even when N_2O consumption is simultaneously occurring.

Unfortunately, the relative magnitude of thr_{O2} and $K_{O2,cons}$ is hard to determine from model results as three scenarios arise that are all plausible. Firstly, thr_{O2} could be in the higher range of values tested with a relatively low $K_{O2,cons}$, such as our base case scenario where thr_{O2} = 6 μmol-O_2 L^{-1} and $K_{O2,cons}$ = 0.3 μmol-O_2 L^{-1} that generates high denitrification production rates and high denitrification consumption rates to result in moderate net denitrification production of N_2O. Secondly, thr_{O2} could be lower (e.g., 3 μmol-O_2 L^{-1}) with a low $K_{O2,cons}$ ($K_{O2,cons}$ = 0.3 μmol-O_2 L^{-1}), which would generate moderate-to-low net denitrification production. Thirdly, thr_{O2} could be moderate with a high $K_{O2,cons}$ (such as both thr_{O2} and $K_{O2,cons}$ = 3 μmol-O_2 L^{-1}), which would result in nearly equal denitrification production and consumption rates for very low net denitrification production of N_2O. Determining which scenario is most likely is related to the relative production of N_2O by net denitrification production and by nitrification production, which is also uncertain in past literature. In this model, however, N_2O production by nitrification is always low, even at the boundaries of ODZs, and so moderate-to-high net production by

denitrification is the most likely choice as it reflects observations of high N_2O at ODZ boundaries.

The final O_2-relevant parameter that exhibits a moderate influence on global N_2O production rates is γ – yield of N_2O from nitrification. The constants *a* and *b* in γ determine how much N_2O is produced during nitrification. Therefore, the yield parameterization controls N_2O production through nitrification (*Equation 6*, Figure 45) and the proportion of N_2O produced by nitrification relative to denitrification. Varying parameterizations for γ generate a wide range of global nitrification N_2O production rates between 0.37-1.41 Tg-N y^{-1}. However, when this is considered in relation to global net N_2O production rates, this amounts to a maximum of 8.4% of global net production. Therefore, the choice of parameterization for γ has a large effect on nitrification production of N_2O but a modest effect on global net N_2O production rate.

If the proportion of N_2O produced by nitrification was much greater than in this model, as has occasionally been posited (Freing et al. 2012), then the N_2O yield would have much greater importance. However, the relative amount of global N_2O production from nitrification and denitrification is a still a question without a definitive answer. The results from this model suggest that denitrification production of N_2O is the dominant pathway in the global ocean and that N_2O production rates by denitrification have been underestimated in many past studies, but it is still uncertain exactly how much N_2O is produced by denitrification and by nitrification.

Regardless of the magnitude of N_2O production by nitrification in the global ocean, γ and N_2O production by nitrification need more scrutiny, especially in low O_2 regions and with the perspective of the full system of N_2O production and consumption mechanisms. While yield is increased at low O_2, nitrification rates are decreased at low O_2, and the cumulative effect of this on a global scale is uncertain. Specific instances of elevated N_2O production by nitrification at low O_2 (Goreau et al. 1980, Nevison et al. 2003) have been observed but often lack the necessary context. In other words, is observed elevated N_2O production by nitrification at a certain location purely due to an O_2 effect on yield and reaction rates, or is it due to other influences like organic matter supply?

If one assumes that nitrification is the dominant N_2O production pathway in the ocean, then the sensitivity of global net N_2O production to γ is of paramount importance. However, the results from this model have shown no scenario where global nitrification production of N_2O is higher than denitrification production of N_2O. Even with the N_2O yield parameterization that produces the highest nitrification N_2O production rates of 1.4 Tg-N y^{-1} (Figure 44), nitrification N_2O production only contributes up to 11.6% of global net N_2O production (Figure 45). Furthermore, scenarios that lower the net global denitrification production rate never approach the 1.5 Tg-N y^{-1} of nitrification N_2O production – the lowest net denitrification production rate is 4.8 Tg-N y^{-1} (Figure 48).

It should be noted that this research does not include contributions of nitrification within the euphotic zone. As this model does not include reaction in the euphotic zone or any depths above 100 m, it is likely that nitrification N_2O production rates are higher than estimated here. Nevertheless, this was considered an acceptable concession as N_2O production in the euphotic zone is expected to be low (Yool et al. 2007, Freing et al. 2012, Grundle 2012, Zamora and Oschlies 2014). Euphotic zone nitrification therefore is not expected to qualitatively change the proportion of nitrification N_2O production in terms of global net N_2O production.

4.1.2 Control by Organic Matter Supply

While O_2 controls the proportion of oxic versus suboxic processes and the rates of N_2O production by nitrification and denitrification, detrital organic matter serves as the initial 'fuel' for the system of reactions. The model input of detritus comes from particulate matter exported from the euphotic zone, and the amount of available organic matter dictates how much of all the reactions in the system (remineralization, nitrification, denitrification) occur. If there is a substantial amount of detritus exported from the euphotic zone, there will be ample substrate to be remineralized to NH_4^+ and consequently converted to N_2O and NO_3^- through nitrification (oxic pathway) or aiding in NO_3^- remineralization to N_2O (suboxic pathway). Since detritus is consumed in both oxic and suboxic pathways, it can affect N_2O production through nitrification and denitrification directly and indirectly. High availability of detritus generally implies higher N_2O production rates, although the exact magnitudes of the N_2O production and consumption rates are influenced by other environmental conditions such as O_2.

The influence of organic matter supply and remineralization was tested using EPC (export production of carbon) data generated by five different Earth System models – CanESM5, CanESM5-CaNOE, CNRM-ESM2-1, GFDL-ESM4, and UKESM1-0-LL – since observation-based estimates of EPC are highly uncertain and/or of low spatial resolution (e.g., Schlitzer 2000). The spatial variation of EPC can lead to substantial differences in global net N_2O production rates. This affects denitrification production and consumption rates in particular as the location of high organic matter supply in relation to suboxic O_2 concentrations is of particular importance.

Among the EPC data from the five Earth System models, there is a range of almost twofold in global net N_2O production rates, with GFDL-ESM4 providing the lowest (9.6 Tg-N y^{-1}) and UKESM1-0-LL the highest (17.3 Tg-N y^{-1}) global net N_2O production. This is reasonable given the variability in spatial distribution of EPC (Figure 31). In general, CanESM5, CanESM5-CaNOE, and UKESM1-0-LL show more organic matter availability in ODZ locations than CNRM-ESM2-1 and GFDL-ESM4. However, the interactions between high organic matter supply, suboxic O_2 that promotes N_2O production through denitrification, and the near-anoxic O_2 that allows N_2O consumption by denitrification results in UKESM1-0-LL having the highest global net N_2O production rate, with CNRM-ESM2-1 the second highest (Figure 32).

The attenuation of detritus flux with depth was parameterized in this model as a simple exponential decay. The inverse remineralization length scale, α_{RLS}, determines how quickly detritus flux decreases with depth (see *Equation 12*; Figure 33). The steepness of this curve determines availability of organic matter in relation to regions of suboxic O_2 concentrations, especially when considering that the upper oxycline of ODZs (where N_2O production rates are highest) frequently occurs at 100-300 m depth and that ODZs can persist to much greater depths ($\geq$ 1000 m).

Testing a range of α_{RLS} between 0.001 – 0.020 m^{-1} generated a substantial difference in global net N_2O production rates, and while it did not affect rates quite as strongly as spatial variation in the EPC, the model is still quite sensitive to α_{RLS}. In general, increasing α_{RLS} will decrease net N_2O production rates due to a strong effect on denitrification. This is once again related to not only how much detritus is available, but the location of where it is available – a higher α_{RLS} provides less organic matter to the regions where denitrification occurs. An exception to this is the lowest tested α_{RLS} of 0.001 m^{-1}. (Figure 33, bottom). In this case, input of organic matter is low at all depths. This includes the region above ODZs near the oxycline that normally generate high N_2O

production rates, as much of the detritus is instead transported to greater depths below the ODZ (Figure 33).

Notably, this model does not directly include the full effect of temperature and O_2 on remineralization rates. The consumption of detritus in the model's $d[D]/dt$ process equation is influenced by temperature using the Arrhenius equation (*Equation 1, 2*), but O_2 controls the partitioning of suboxic and oxic remineralization processes without influencing the rate magnitude. Since this model uses a constant remineralization length scale (α_{RLS}) for the flux of EPC exported from the euphotic zone, the effects of O_2 and temperature variations on the detrital input to the model are considered negligible. In other words, the change in detrital organic matter supply ([D]) with depth is assumed to be the same for all locations, with no difference between ODZ regions or other, better oxygenated regions, which is not true in the real world. If the effects of O_2 and temperature in ODZs were considered in terms of the supply of organic matter exported from the euphotic zone, it is most likely that the model estimates of denitrification would be lower as there would be less overall organic matter supplied in ODZ regions (Devol and Hartnett 2001, Cram et al. 2021). Although N_2O production by denitrification is high in this model compared to past model studies, overall denitrification as it pertains to the nitrogen budget is comparatively low (discussed further in Section 4.2).

While denitrification rates tend to decrease with higher α_{RLS}, nitrification N_2O production rates increase with higher α_{RLS}. This is because the location-specific interaction of detritus availability and O_2 concentration is much less relevant for nitrification than for denitrification. Nitrification occurs throughout the oxygenated ocean, so changes in the total amount of detritus input into the model from varying α_{RLS} will affect nitrification N_2O production rates more than localized detritus availability in suboxic regions.

The effect of varying α_{RLS} is slightly higher for nitrification than for denitrification: denitrification production rates vary by 36%, while nitrification rates vary by 39% for a total maximum effect on global net N_2O production rates of 35% as rates vary between 7.5-11.5 Tg-N y^{-1}. The global proportion of N_2O produced by nitrification compared to N_2O produced by denitrification remains small.

The combined influence of α_{RLS} and the spatial pattern of EPC at 100 m on detritus input into the model is large, and organic matter supply affects N_2O production rates not only by magnitude but by its location in relation to suboxic regions that permit denitrification and associated N_2O production.

4.1.3 Control by Other Parameters

As discussed earlier, denitrification requires both organic matter and low O_2 concentration; however, it also requires NO_3^-. To test whether NO_3^- limitation of suboxic remineralization can affect global N_2O production rate, the half-saturation constant $K_{NO3,remin}$ was varied between 0.1 – 30 μmol-NO_3^- L^{-1} (see Figure 42, 43). Increasing $K_{NO3,remin}$ will decrease N_2O production by denitrification as it raises the requirement for NO_3^- availability. Global net N_2O production rates ranged from 7.6-13.0 Tg-N y^{-1} from altering $K_{NO3,remin}$ alone for a maximum difference of 42% - a substantial difference that is on a scale comparable to the influence of O_2 and organic matter availability.

There is little literature that addresses the degree to which low NO_3^- concentrations affect denitrification rates through a parameter such as $K_{NO3,remin}$. This is in part because there are few studies that separate the denitrification reaction into two steps – reduction of NO_3^- to N_2O and

subsequent reduction of N_2O to N_2 – and it is difficult to accurately measure rate kinetics *in situ* across the multiple intermediates present in this multi-step reaction. Experimental studies indicate that enzymes used by each step of denitrification exhibit different reaction kinetics (see Figure 1, top panel) and are activated at different O_2 concentrations (Casciotti et al. 2018, Rees et al. 2021, Sun et al. 2021). Conflating the behaviour of these various reaction mechanisms may in part be responsible for the uncertainty of parameters and parameterizations for denitrification production and consumption of N_2O. For example, if denitrification is considered solely as reduction of NO_3^-, it would be reasonable to investigate reaction kinetics by measuring NO_3^- loss in suboxic waters. Unfortunately, doing so would ignore different reaction behaviours for reduction of NO_3^-, NO_2^-, NO, and N_2O to N_2, all of which use different enzymes, are activated at different O_2 concentrations, and can vary widely across microbial communities. Understanding how strongly these reaction steps differ is difficult to measure *in situ* and in laboratories due to the fast cycling rates of these reactions, but will be imperative to understanding the difference between production of N_2O (reduction of NO_3^- through NO_2^- and NO to N_2O) and consumption of N_2O (reduction of N_2O). Lacking more information, the base case scenario of $K_{NO3,remin}$ = 5 μmol-NO_3^- L^{-1} was chosen (see Section 2.1.1., Figure 6 and Section 3.5.1, Figure 42). Model sensitivity is low when comparing $K_{NO3,remin}$ values between 1-5 μmol-NO_3^- L^{-1}, as NO_3^- concentrations from the WOA are almost always much higher than 5 μmol-NO_3^- L^{-1}.

It is important to note that $fNO_{3,remin}$ also acts as a necessary 'fail-safe' for the model; without it, suboxic remineralization is only controlled by O_2. Exclusion of the $fNO_{3,remin}$ term can lead to scenarios with high suboxic remineralization rates that consume NO_3^- strongly enough for NO_3^- to become negative in the model. While NO_3^- is typically not a limiting reactant – there are no suboxic data points in World Ocean Atlas data where NO_3^- < 10 μmol-NO_3^- L^{-1} except in the Black Sea – extremely low NO_3^- concentrations do appear in ESM simulations.

The O_2 half-saturation constant for nitrification $K_{O2,AmOx}$ did not show strong influence on nitrification N_2O production rates or global net N_2O production rates. The influence of $K_{O2,AmOx}$ on global N_2O production rates is minimal except at very high half-saturation constants (such as $K_{O2,AmOx}$ = 30 μmol-O_2 L^{-1}) that severely restrict nitrification production of N_2O. The primary purpose of $fO_{2,AmOx}$ is to inhibit nitrification rates at very low O_2 concentrations, but the nitrification production of N_2O by O_2 is more influenced by the yield parameterization than by $fO_{2,AmOx}$. While $fO_{2,AmOx}$ decreases the rate of nitrification at very low O_2, γ controls the amount of N_2O produced by nitrification and increases at low O_2. Both terms are necessary to properly represent N_2O production rates by nitrification, but the sensitivity of global N_2O production to the yield is much greater (Figures 41, 45). Given a lack of literature data indicating otherwise, the base case scenario maintains a $K_{O2,AmOx}$ of 5 μmol-O_2 L^{-1}.

4.2 Model Evaluation

The steady state framework that serves as the basis of this model provides an in depth look into the individual mechanisms of nitrification and denitrification by maintaining simplicity and allowing for control of environmental conditions, substrate input, and reaction and dilution rates, within the framework of the global 3D distribution of oxygen, nitrate and other environmental conditions. However, this simple framework also has drawbacks. In this section, the validity of this model framework will be assessed.

Assuming steady state conditions permits a direct relationship between the chemostat's dilution rate and the reaction rate constants. As *in situ* nitrification and denitrification reaction rates are

extremely variable and the controls on the reaction rates are poorly understood, finding observation-based rate constants is challenging. The magnitude of the reaction rate constants used in the chemostat is determined by their relationship to the dilution rate rather than for their relationship to actual process rates.

While the simplicity of the model is its strength as it allows for better investigation of the individual reaction mechanisms in a controlled environment, there are a few terms that have been excluded due to the model scope and time constraints. Most significantly, the absence of transport mechanisms like advection and mixing may impact N_2O production and consumption rates, especially in the regions at the boundaries of ODZs. These physical mechanisms can affect the distribution of N_2O in and around ODZs, whether through the transport of N_2O itself, or the transport of O_2 and reaction substrates that have a strong control on N_2O production and consumption rates. For example, N_2O transported away from strong suboxic zones with high denitrification production and consumption rates could 'escape' consumption by mixing with more oxygenated waters. This would increase net N_2O production rates as well as increase N_2O concentrations at the oxic boundaries of ODZs that might otherwise be attributed to N_2O produced by nitrification. Incursions of oxygenated water into the ODZs could have effects on all three N_2O production and consumption mechanisms; nitrification N_2O yield would decrease even as nitrification rates increase, denitrification production could become elevated in relation to denitrification consumption, or both denitrification production and consumption could be inhibited.

4.2.1 Reaction Rates and Rate Constants

This research focuses on analyzing N_2O reaction rates rather than resulting N_2O concentrations, as N_2O concentrations in the chemostat effluent can not meaningfully be compared with observed concentrations. N_2O can remain in the ocean for very long timescales, and N_2O concentrations can accumulate substantially over time, especially in ODZ regions that are characterized by slow circulation of water masses. This model doesn't account for physical and biological processes over long timescales or the age of water masses and so can not reliably represent N_2O concentrations in real world conditions. As N_2O reaction rates are primarily influenced by the immediate conditions of the surrounding environment, they serve as a more dependable method of analysis. However, reaction rates are dependent on substrate concentrations – N_2O consumption rates, for example, are strongly influenced by the high N_2O concentrations produced by denitrification N_2O production – and so the influence of physical mechanisms that affect concentrations should not be ignored in future studies. While ODZ regions are characterized by weak circulation and slow movement of water masses, mechanisms such as eddy mixing at ODZ boundaries could have a substantial influence on N_2O production rates (Grundle et al. 2017, Monreal et al. 2022) and so would affect model analysis of the proportion of N_2O produced and consumed by denitrification and the proportion of N_2O produced by nitrification compared to denitrification.

Using the steady state parameterization, the remineralization rate constant (k_{remin}) is set to be equal to the dilution rate (DR = 0.25 d^{-1}) so that the rate of remineralization of detritus can be obtained from the attenuation of EPC flux from the euphotic zone.

Equation 13 helps to explain this and so is reiterated here:

$$\frac{d[\mathrm{X}]}{dt} = Source_X - Sink_X + DR([\mathrm{X}]_{in} - [\mathrm{X}]) = 0$$

At steady state, $d[X]/dt = 0$. This means that for detritus ([D]), the rate of remineralization has to equal $DR([D]_{in}-[D])$. [D] does not equal exactly $0.5[D]_{in}$, but the selected rate for *DR* and k_{remin} in combination with the EPC normalization to 20 Pg-C y^{-1} means it is quite close. This allows the chemostat to generate a scenario where approximately half of the total EPC input is remineralized (8.52 Pg-C y^{-1}), which reflects literature estimates of approximately 9 Pg-C y^{-1} of export from the euphotic zone. Remineralization of this quantity of EPC consequently leads to a global nitrification rate (not nitrification production of N_2O) of approximately 189 Tg-N y^{-1}.

As this is one of the few hard constraints to the model, k_{remin} and the dilution rate can not be arbitrarily adjusted without also ensuring that the changes result in a net of 9 Pg-C y^{-1}. The rate constants for nitrification (k_{AmOx}) and N_2O consumption (k_{cons}) are chosen to be high in relation to the *DR* and k_{remin} to simulate high reaction rates where most of the substrates for the reactions (NH_4^+ for k_{AmOx} and N_2O for k_{cons}) are consumed and little is left over in the chemostat effluent.

In the case of nitrification, this seems reasonable as very little NH_4^+ remains available in the ocean for a substantial amount of time and so NH_4^+ concentrations tend to be low. The rate constant for nitrification is constrained by NH_4^+ concentrations – if k_{AmOx} was ten times smaller than k_{remin}, for example, then the steady state concentration of NH_4^+ would be higher than what is observed *in situ* (typically < 0.1 μmol-NH_4^+ L^{-1}). A high rate constant for k_{AmOx} means that all of the NH_4^+ is ultimately oxidized to NO_3^-, which is true in most ocean waters below the euphotic zone, as there are not many competing processes that consume the NH_4^+ before it is oxidized. Within reasonable limits, this means that the exact rate at which nitrification occurs is unimportant in the steady state framework of the chemostat as long as it is high enough in relation to the remineralization rate to consume most of the NH_4^+. If there is leftover NH_4^+ in the chemostat effluent, the model will underestimate N_2O production by nitrification (Figure 63).

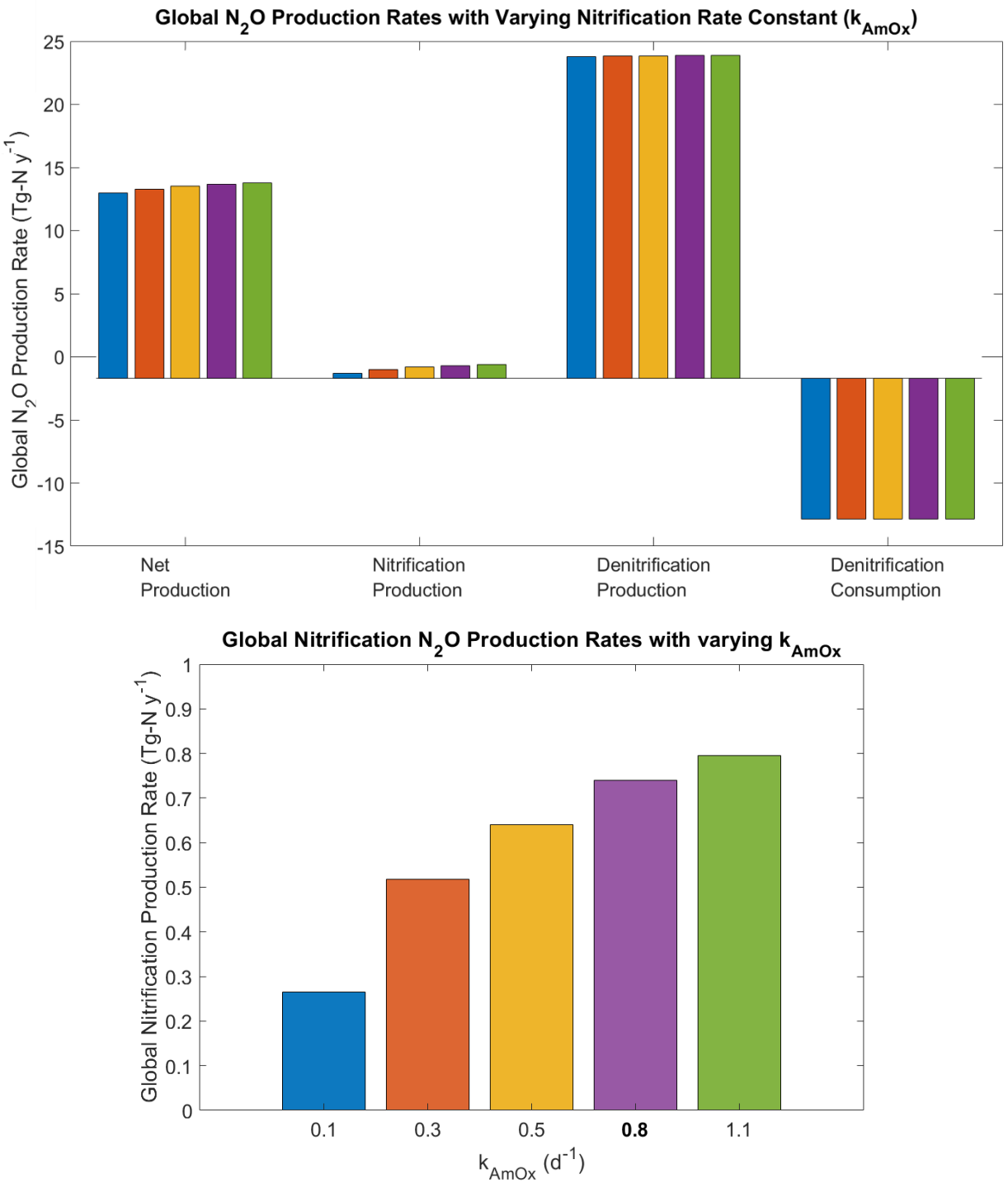

Figure 63: Global N_2O production and consumption rates with varying k_{AmOx}. Top panel depicts all production and consumption processes, bottom panel is a larger depiction of the nitrification production rates.

In Figure 63, k_{AmOx} was varied between 0.1-1.1 d^{-1}, showing strong control on the nitrification N_2O production rates which range from 0.27-0.80 Tg-N y^{-1}. However, the validity of the lower rate constants is dubious for the reasons stated above – they do not consume all of the available NH_4^+, and so underestimate N_2O production by nitrification in comparison to the base case scenario (k_{AmOx} = 0.8 d^{-1}). As the rate constants are directly constrained by the model setup the

rate constant k_{AmOx} is set to create realistic rates of N_2O production under the somewhat artificial conditions of the chemostat and should not be assumed to represent real world values.

For N_2O consumption during denitrification, there is little available data from which to determine whether most of the N_2O available in ODZs is rapidly consumed or slowly consumed. N_2O that is produced in ODZs has been observed at locations far from their origin (e.g., Popp et al. 2002), and this export of N_2O from ODZs suggests that contemporaneous N_2O consumption does not remove all of the N_2O produced by denitrification in suboxic waters.

For the purposes of this model, k_{cons} was set to be as high as k_{AmOx} (0.8 d^{-1}). The results demonstrate that even with a large k_{cons} (in viable conditions for N_2O consumption), N_2O production by denitrification remains higher than N_2O consumption by denitrification (Figure 64). The effect of the steady-state framework on the fraction of N_2O consumed is discussed further below.

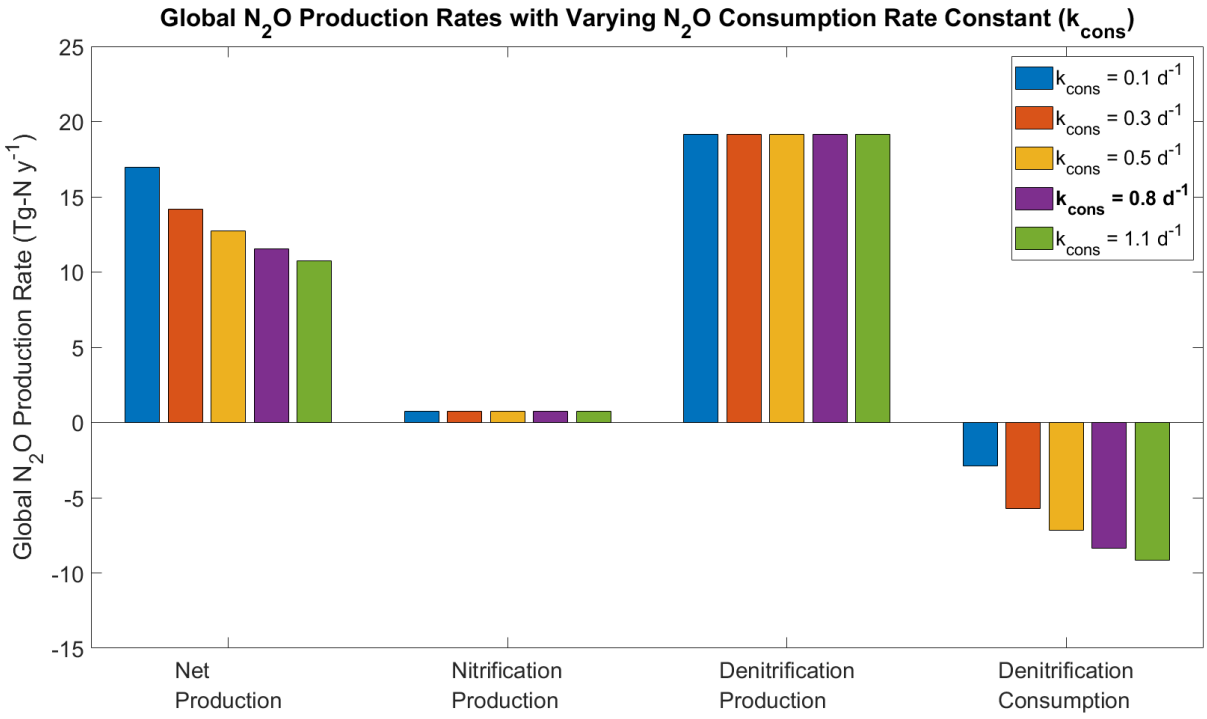

Figure 64: Global N_2O production and consumption rates with varying k_{cons}

Changes in the consumption rate by altering k_{cons} are substantial and have a large degree of control over net N_2O production rates (Figure 64). As N_2O production and consumption occurs rapidly and is controlled by a small range of O_2 – it is not known whether most of the N_2O should be consumed in each daily time step or if much of the N_2O produced should be left over in the effluent.

Even when k_{cons} is at its highest (1.1 d^{-1}) and the global consumption rate is increased to -9.1 Tg-N y^{-1}, N_2O production (especially by denitrification) still greatly exceeds consumption. This implies that there is a surplus of N_2O generated, and that denitrification production in ODZs exports more N_2O outside of its suboxic waters than is consumed within the ODZ boundaries. The experiments with $K_{O2,cons}$ – the O_2 concentration that controls when N_2O consumption

begins – also support this, as even increasing $K_{O2,cons}$ to a high O_2 concentration results in denitrification production that far exceeds consumption.

It should be noted, however, that the nature of the reaction pathway for N_2O consumption requires production of N_2O in order to provide a substrate for consumption, and therefore N_2O production by denitrification must be higher than consumption by denitrification – both in this model and in real world conditions. One exception to this would be if there was very high N_2O production by nitrification that provides ample N_2O as a substrate for high N_2O consumption rates, but it is very unlikely that nitrification N_2O production is this strong in the near-anoxic waters that are capable of N_2O consumption by denitrification. Another such exception would be mixing of waters with moderately-high suboxic concentrations (~3 μmol-O_2 L^{-1}) - that produce high N_2O concentrations due to denitrification production of N_2O - with near-anoxic waters (<1 μmol-O_2 L^{-1}) where N_2O consumption occurs. In both scenarios, N_2O consumption could exceed production by denitrification as a result of high N_2O concentrations that aren't directly related to denitrification N_2O production at that location, in a location with low enough O_2 to support N_2O consumption.

4.2.2 N_2O Residence Time

To further test the above hypothesis, the N_2O residence time with respect to the N_2O consumption rate is evaluated in locations with varying O_2 concentrations in order to see how much and how quickly N_2O is consumed according to O_2. Residence times were calculated for all 3D global locations as well as for a specific location in the North Pacific ODZ where O_2 is known to be low enough for N_2O consumption to take place. Additionally, an experiment was conducted to evaluate N_2O concentrations across steadily increasing O_2 concentrations as they are affected by the N_2O consumption rate alone. The intent of this experiment is to mimic the transport of a water parcel containing N_2O away from the ODZ and into more oxygenated waters.

Residence time is calculated by taking the N_2O concentration divided by the N_2O consumption rate at that location.

$$N_2O\ Residence\ Time = \frac{[N_2O]}{N_2O\ Consumption\ Rate}$$

Equation 15

The residence time for all global locations with relatively low O_2 concentrations (0-30 μmol-O_2 L^{-1}, using input O_2 from Bianchi-corrected World Ocean Atlas data rather than model-generated steady state O_2 concentrations) is shown in Figure 65.

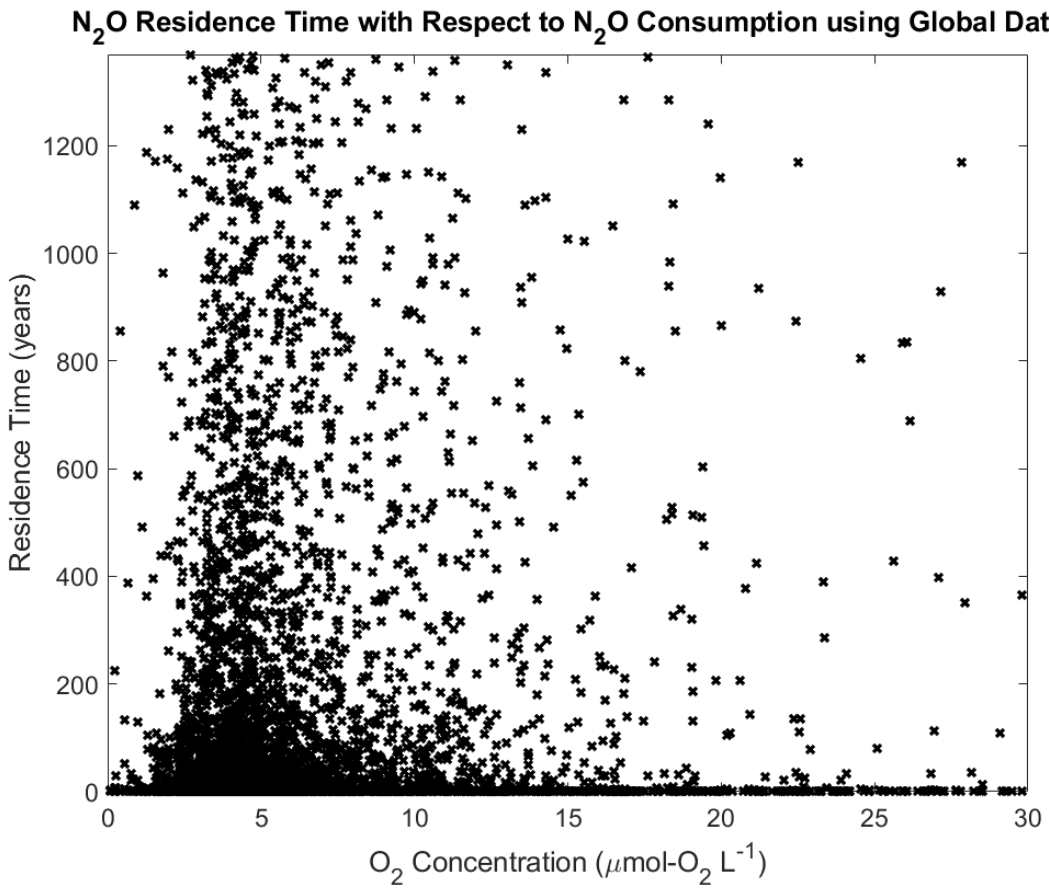

Figure 65: N_2O residence times with respect to N_2O consumption across multiple global locations.

Although Figure 65 mainly depicts residence times in the lower O_2 range, the model also calculates extremely high residence times at higher O_2 concentrations. The exponential parameterization for N_2O consumption is such that N_2O consumption occurs even in oxic waters, but at such low rates that they can be considered negligible. Such low consumption rates would lead to extremely high residence times for N_2O but are not relevant to the relationship between O_2 and N_2O consumption discussed here, nor to global net N_2O production rates. The residence times for N_2O in relation to the N_2O consumption rate as depicted by Figure 65 can help describe how N_2O consumption rates and N_2O concentrations relate at various O_2 concentrations, though the relationship is not always straightforward.

In the range of 0.3-3 μmol-O_2 L^{-1} where denitrification N_2O production is high and N_2O consumption is low, residence times are high. In the 3-10 μmol-O_2 L^{-1} range where denitrification production of N_2O is moderate but N_2O consumption is near zero, residence times are also high. Comparatively, in the small range between 0-0.3 μmol-O_2 L^{-1} where N_2O consumption is high, residence times are low.

To take a closer look at this interaction a location-specific investigation was conducted on residence times in the North Pacific ODZ (Figure 66), which includes O_2 and N_2O concentrations alongside N_2O production and consumption rates by denitrification for perspective.

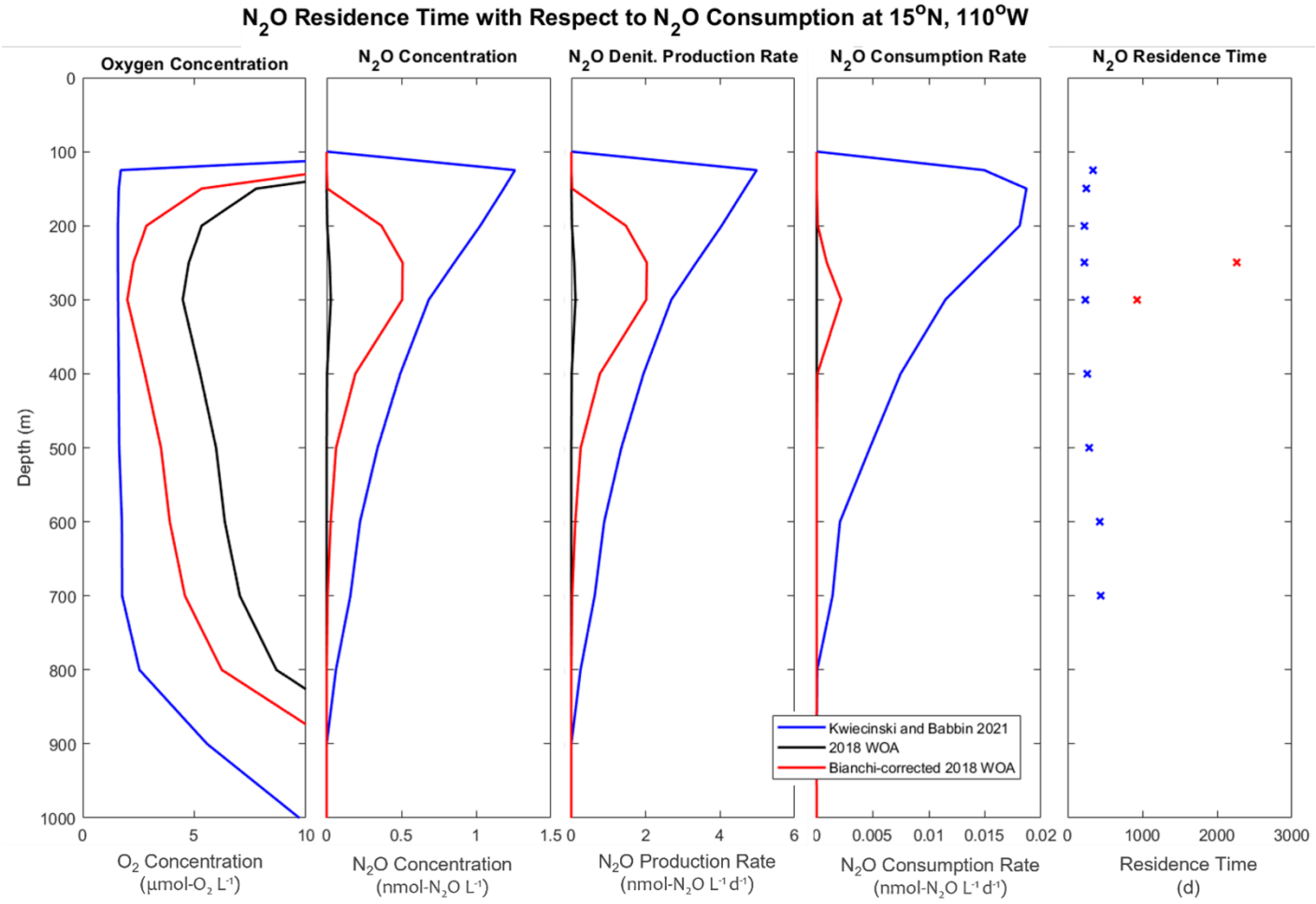

Figure 66: O_2 concentrations, N_2O concentrations, N_2O production and consumption rates by denitrification, and N_2O residence times with respect to N_2O consumption at a location in the North Pacific ODZ (15°N, 110°W) for three O_2 data sets: Kwiecinski & Babbin 2021 (blue), 2018 World Ocean Atlas (WOA) (black), and Bianchi-corrected WOA2018 (red).

As the 2018 WOA O_2 data products (black) do not reach concentrations low enough for substantial N_2O consumption at this location, only the Bianchi-corrected 2018 WOA data products (red) and Kwiecinski and Babbin 2021 data products (blue) residence times are calculated. The residence times for the Bianchi-corrected 2018 WOA data are larger than for the Kwiecinski and Babbin 2021 data because the N_2O consumption rates are lower. Residence time is shown for the Bianchi-corrected data for only two depths because these are the only ones with substantial consumption rates.

The residence times calculated for the Kwiecinski and Babbin data and the Bianchi-corrected 2018 WOA data at this location are plotted against O_2 concentration in Figure 67. The smaller residence times for the Kwiecinski and Babbin O_2 data occur at lower O_2 concentrations because lower O_2 allows for greater N_2O consumption rates. The change in N_2O consumption rates is more important than the change in N_2O concentrations because N_2O production by denitrification remains high.

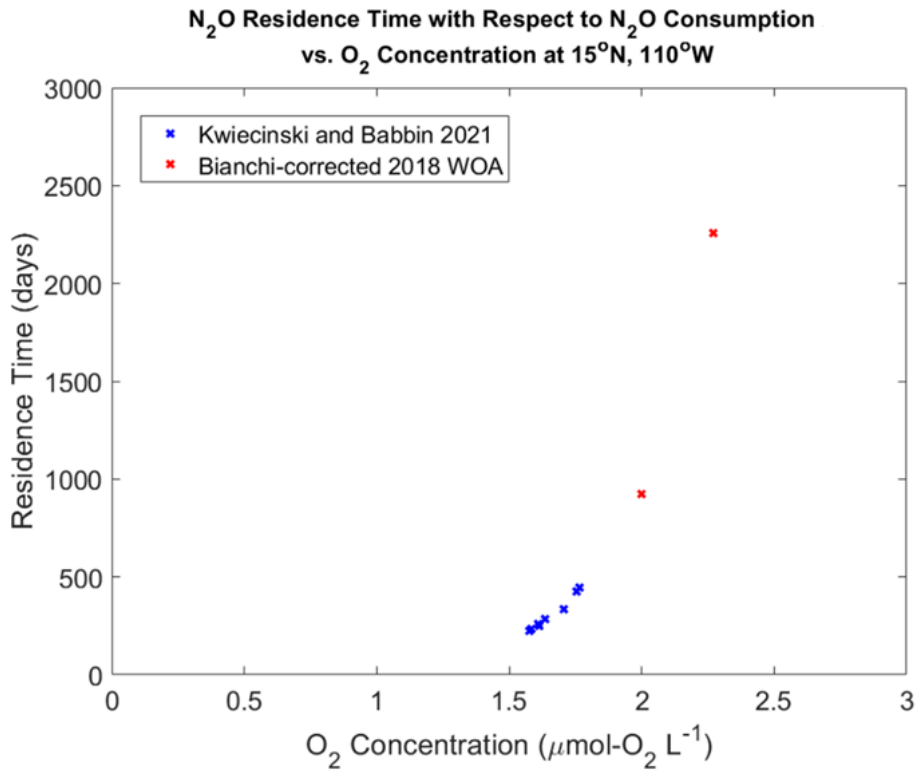

Figure 67: N_2O residence time with respect to N_2O consumption vs. input O_2 concentration at a location in the North Pacific ODZ (15°N, 110°W) for two O_2 data sets: Kwiecinski and Babbin 2021 (blue) and Bianchi-corrected 2018 World Ocean Atlas (WOA) (red).

In Figure 67, the residence times of N_2O with respect to the N_2O consumption rates decrease at lower O_2 concentrations and increase at higher O_2 concentrations. This is an expected conclusion when considering the shape of the curve for the N_2O consumption rate parameterization (*Equation 10*). While N_2O consumption rates can be large in near-anoxic waters, substantial consumption of N_2O is almost exclusively limited to ODZs. This means that any export of N_2O from ODZs will potentially remain in circulation for centuries until it is either released into the atmosphere or brought back to regions with extremely low O_2.

We can further investigate how N_2O is consumed by plotting N_2O consumption term over time (Figure 68). Since N_2O consumption rates change with O_2 concentrations, three 'starting points' of [O_2] are depicted: 1, 3, and 5 μmol-O_2 L^{-1}. All three experiments increase O_2 by 0.05% per day as a conservative estimate of how a water parcel might experience elevated O_2 by mixing with outside, more oxygenated waters. O_2 that starts at 1 μmol-O_2 L^{-1} will increase to 2.5 μmol-O_2 L^{-1} in 5 years and 6.2 μmol-O_2 L^{-1} in 10 years, O_2 that starts at 3 μmol-O_2 L^{-1} will increase to 7.5 μmol-O_2 L^{-1} in 5 years and 18.6 μmol-O_2 L^{-1} in 10 years, and O_2 that starts at 5 μmol-O_2 L^{-1} will increase to 12.4 μmol-O_2 L^{-1} in 5 years and 31.0 μmol-O_2 L^{-1} in 10 years.

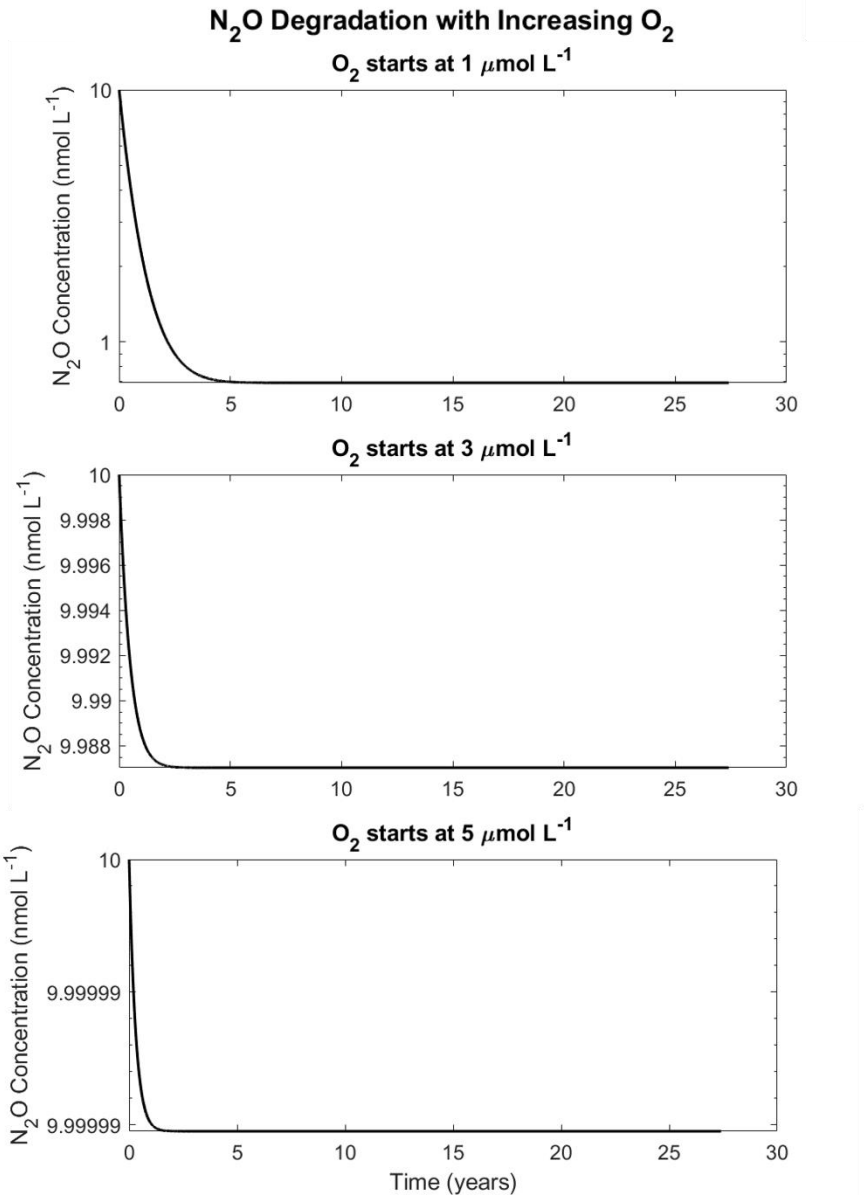

Figure 68: N_2O degradation through denitrification N_2O consumption over time with a range of different starting O_2 concentrations and a rate of increase of 0.05% d^{-1}.

Using the same starting concentration of N_2O but different starting concentrations of O_2 generates different asymptotic concentrations of N_2O. When O_2 is 3 μmol-O_2 L^{-1} or higher, the degradation of N_2O over time with increasing O_2 is extremely low, only decreasing N_2O

concentrations by less than 0.2% (Figure 68, middle and bottom). However, when O_2 starts at a near-anoxic concentration of 1 μmol-O_2 L^{-1} it is possible that N_2O could be consumed strongly enough to eliminate nearly all of the available N_2O, but *only if* N_2O consumption by denitrification is the only process acting on the N_2O (Figure 68, top). In other words, if a parcel of water at 1 μmol-O_2 L^{-1} remained at or near that concentration (only increasing by 0.05% per day) and there was no further N_2O production occurring, it could theoretically be possible that the N_2O could be consumed in a few years.

Regardless of differences between the proportion of N_2O concentration consumed, the residence times for N_2O are usually high and indicate that N_2O production by denitrification greatly exceeds N_2O consumption by denitrification. As mentioned previously, N_2O production must exceed N_2O consumption due to the nature of N_2O as an intermediate between these reaction steps. The results from measuring residence times are important in that they detail how N_2O production by denitrification *greatly exceeds* N_2O consumption by denitrification. However, as the O_2 data products used in this model overestimate suboxic concentrations in ODZs (even when applying the Bianchi correction to World Ocean Atlas 2018 data), the model may not account for all of the anoxic and near-anoxic water where $O_2 < 0.3$ μmol-O_2 L^{-1} in the cores of real-world ODZs. Because of this, there is a chance that global N_2O consumption is higher than estimated in this research – in such a case, smaller residence times could imply that N_2O consumption may be more comparable in magnitude to N_2O production by denitrification within ODZ cores.

The high residence times of N_2O with increasing O_2 in Figure 68 suggest that once N_2O is exported from ODZ regions – in particular, the ODZ cores where N_2O consumption can take place – the N_2O will stay in circulation for a very long time until it is either released to the atmosphere or encounters another region of water with near-anoxic concentrations. It is possible that there are N_2O sinks not investigated in this model (e.g., Rees et al. 2021) that are large enough to create regions with an N_2O deficit or to remove the N_2O before it is outgassed. As with other reaction pathways that are not included in this model (anammox, DNRA, bacterial vs. archaeal nitrification), further research is needed to understand and quantify the effects of these reactions and their biological relevance in the global ocean.

4.2.3 Relationship between Denitrification Production and Denitrification Consumption

The relationship between denitrification production rates and denitrification consumption rates has also been evaluated by their global rate estimates across a series of sensitivity tests. These rates are related as consumption rates depend on N_2O as a substrate and the majority of N_2O is produced by denitrification, especially in ODZs where both processes occur. High denitrification production rates can therefore produce high denitrification consumption rates, and past literature has often debated whether these processes are near-equal in magnitude (Babbin et al. 2015, Kelly et al. 2021, Sun et al. 2021).

To observe this relationship, global N_2O production and consumption rates by denitrification were compared using a ratio of the two for a series of sensitivity experiments (Figure 69). These experiments include varying the spatial distribution of detritus flux, the exponent c in Ω, the NO_3^- half-saturation constant for denitrification ($K_{NO3,remin}$), and the parameter that controls the O_2 concentration dependence of N_2O consumption ($K_{O2,cons}$).

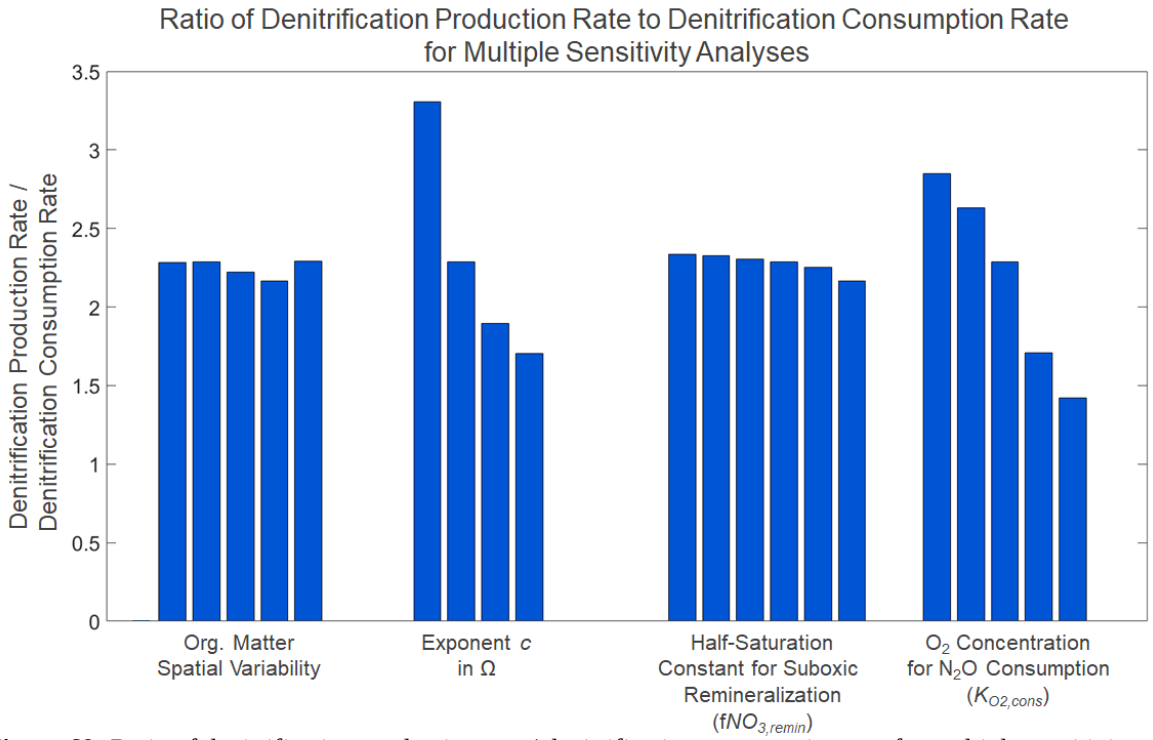

Figure 69: Ratio of denitrification production rate / denitrification consumption rate for multiple sensitivity analyses. These sensitivity analyses can be found in Figure 32 (organic matter spatial variability), Figure 51 (exponent *c* in Ω), Figure 43 (half-saturation constant for suboxic remineralization, $fNO_{3,remin}$), and Figure 53 (O_2 concentration for N_2O consumption, $K_{O2,cons}$)..

The ratio of global denitrification production rates to global denitrification consumption rates has a consistent value around 2.25. This is more apparent for parameters that affect both reactions (such as the spatial distribution of detritus data products, or $K_{NO3,remin}$) rather than parameters that cause changes in just one reaction (such as $K_{O2,cons}$). Varying the exponent *c* in **Ω** is an interesting case, as it would be expected that varying *c* would affect both denitrification production and consumption – the shape of **Ω** determines how much suboxic remineralization takes place in relation to O_2, which directly affects denitrification production and so indirectly affects denitrification consumption. The variability of the ratio of production rates to consumption rates by denitrification here is likely a result of how the range of *c* values tested shifts N_2O production towards the upper or lower region of the 0-6 μmol-O_2 L^{-1} O_2 range. More importantly, the ratio never approaches 1 – i.e., denitrification production always exceeds denitrification consumption by a large margin.

The relevance of the ratio of N_2O production by denitrification to N_2O consumption by denitrification relates to how denitrification and net N_2O production influence the nitrogen budget. N_2O is produced through incomplete denitrification while consumption of N_2O to N_2 occurs through complete denitrification, and both N_2O and N_2 production result in a loss of fixed nitrogen (fixed-N) from the ocean. As mentioned in Section 4.1, some past models do not explicitly separate denitrification production and consumption of N_2O, either assuming that N_2O production by denitrification becomes zero below a set O_2 threshold due to consumption becoming strong enough to be equal to production (Nevison et al. 2003, Bianchi et al. 2012), or assuming that N_2O production by denitrification decreases below an O_2 threshold without accounting for an individual consumption term (Suntharalingam et al. 2012, Ji et al. 2018). As

stated earlier, the overlap between these processes and their denotation and parameterization in models leads to considerable confusion in understanding and measuring these reactions.

The total estimated loss of fixed-N through pelagic denitrification – defined here as reduction of NO_3^- to N_2O and/or N_2 – is higher in past models than in this model, with estimates ranging from approximately 50-80 Tg-N y^{-1} (Gruber and Galloway 2008, Bianchi et al. 2012, DeVries et al. 2012, Eugster and Gruber 2012, Peters et al. 2018), as well as some estimates reaching higher than 150 Tg-N y^{-1} (Codispoti 2007). In comparison, the estimated loss of fixed-N only through N_2O production is lower in past models than in this model, at 2-12 Tg-N y^{-1} (see Table 1). In other words, this model projects lower fixed-N loss for total denitrification than past models, but a higher proportion of fixed-N loss attributed to N_2O production rather than N_2 production.

When accounting for all of the ocean source and sink terms for the nitrogen budget, there are concerns of a large 'missing source' term as nitrogen fixation may not provide enough fixed-N to match estimates of fixed-N loss from denitrification (Codispoti 2007). If global estimates for denitrification are smaller than projected by past models, as in this model, it could help reduce the gap between these sources and sinks of fixed-N. Past models that do not separate incomplete and complete denitrification adequately may not be able to account for this larger N_2O production term and so might be overestimating N_2 production and fixed-N loss through complete denitrification. This model does account for the partitioning of denitrification production and consumption of N_2O, and while this allows for more investigation into the controls of these two processes it is only the first step in understanding and parameterizing the reactions.

Narrowing down the uncertainties listed in the above sections will also require more accurate O_2 data products in order to reconcile model results and real-world observations. For example, the base case scenario of this model uses a $K_{O2,cons}$ of 0.3 μmol-O_2 L^{-1}, which leads to low N_2O consumption in relation to N_2O production by denitrification. Such a small O_2 concentration rarely occurs in gridded O_2 data and is difficult to accurately measure both *in situ* and in laboratory environments. Determining if this very low $K_{O2,cons}$ is accurate will have large repercussions for the proportion of N_2O production versus consumption by denitrification, and so affect the size of the sink terms for loss of fixed-N by N_2O production and N_2 production by denitrification.

Existing uncertainties such as $K_{O2,cons}$ are still not quantified by this research, which highlights the need for improved models with a focus on N_2O and denitrification as well as emphasizing the necessity of maintaining separate parameterizations for nitrification N_2O production, denitrification N_2O production, and denitrification consumption of N_2O. If denitrification occurs more strongly in the global ocean, as anticipated by this research, then better understanding of control by parameters thr_{O2}, c, and $K_{O2,cons}$ are pivotal to estimating fixed nitrogen loss through both N_2O production and N_2O reduction to N_2.

5 Conclusion

This research investigates possible parameterizations of global net N_2O production in the ocean and tests model sensitivity to uncertain parameters and environmental conditions. In doing so it has confirmed that O_2 has the greatest impact on N_2O production, followed by availability of organic matter. While the total amount of organic matter input into the model is the initial control on how much N_2O can be produced, the location of organic matter supply in relation to suboxic regions capable of high N_2O production rates by denitrification has a greater impact on global N_2O production estimates. Therefore, the most important influence on estimates of global N_2O production and consumption is the O_2 data input into the model, and inaccuracies in commonly used interpolated data sets such as World Ocean Atlas result in underestimation of the degree of suboxia and anoxia in the ocean and so the estimated proportion of N_2O produced and consumed through the denitrification pathway.

Aside from increased O_2 sampling with greater accuracy and precision (especially in and around oxygen deficient zones), future N_2O studies need to ensure that suboxic O_2 data are not lost to interpolation or to averaging of monthly O_2 data to an annual mean. Such methods can substantially decrease the global volume of suboxic waters capable of denitrification, and in some cases may remove all or most O_2 concentrations below approximately 4 μmol-O_2 L^{-1}. When investigating processes that exclusively occur at suboxic O_2 concentrations, such a loss of data is counterproductive to understanding the nature of these reactions.

Global N_2O production by denitrification was found to exceed N_2O consumption by denitrification in all tested scenarios, but the relative proportion of these rates are highly sensitive to changes in parameters such as the threshold for denitrification production of N_2O (thr_{O2}) and the parameter that determines N_2O consumption dependence on O_2 concentration ($K_{O2,cons}$). The ratio of N_2O production to consumption by denitrification remains uncertain. Nitrification production of N_2O in this model provided a very small amount of the total net N_2O production and is greatly exceeded by net production by denitrification in every scenario tested. While nitrification N_2O production rates were sensitive to the parameterization of the N_2O yield (γ), changes in O_2 or organic matter availability had more limited effects on nitrification N_2O production. Since the proportion of N_2O produced by nitrification in comparison to that produced by denitrification is minor, the sensitivity of global net N_2O production to parameters that primarily influence nitrification is also relatively minor.

The model's base case scenario suggests high N_2O production by denitrification (11.4 Tg-N y^{-1}) compared to past models (2-12 Tg-N y^{-1}, see Table 1). However, the model's estimates of total fixed-N loss by denitrification (19.2 Tg-N y^{-1}, including both N_2O and N_2 production) are low compared to past estimates of approximately 50-80 Tg-N y^{-1} (Gruber and Galloway 2008, Bianchi et al. 2012, DeVries et al. 2012, Eugster and Gruber 2012, Peters et al. 2018).

Low estimates of total denitrification in this model may be attributed to a lack of suboxic O_2 concentrations in O_2 data products, inaccurate spatial distribution of EPC (such that less organic matter is available for denitrification in suboxic regions), and/or uncertainties in parameters and parameterizations. The proportion of N_2O consumed vs. produced by denitrification could also

be underestimated due to a lack of mixing in the model that would transport N_2O to near-anoxic waters where N_2O consumption takes place. The high ratio of N_2O production to N_2 production may also be a result of O_2 data products or uncertainties in parameters such as $K_{O2,cons}$ that influence N_2O consumption. Any increases in total denitrification that would bring the global total closer to historical estimates, however, would also increase the amount of N_2O produced. Based on other literature estimates, it is likely that total denitrification is underestimated and N_2O production is overestimated in this model. The inaccuracies in the O2 data set underestimate the volume of suboxic water, which indicates that denitrification may be higher than modelled in the base case scenario. High model sensitivity to uncertain parameters provides a wide range of estimates for global N_2O and N_2 production by denitrification; however, it is not yet possible to isolate the specific terms that would lead to a resolution regarding the proportion of fixed-N loss to N_2O vs. N_2 production.

In summary, this research has found that a) global net N_2O production by denitrification greatly exceeds N_2O produced by nitrification, b) denitrification production greatly exceeds denitrification consumption in suboxic regions and in the global ocean, c) total denitrification in the ocean has probably been underestimated in this model due to underrepresentation of suboxic O_2 in oxygen deficient zones. To improve upon estimates of ocean production of N_2O and understanding of the nitrogen budget and cycling reactions, there is not only a need for more and better observational data, but also a need for future model investigations to maintain nitrification production, denitrification production, and denitrification consumption of N_2O as separate processes. Isolating uncertain parameters such as thr_{O2}, c, and $K_{O2,cons}$ will not be possible without research into the interactions among these individual mechanisms.

6 References

Anderson, B., Bartlett, K., Frolking, S., et al. (2010). Methane and nitrous oxide emissions from natural sources. *Office of Atmospheric Programs, US EPA, EPA* 530-R-10-001.

Arst, H., Mäekivi, S., Lukk, T., and Herlevi, A. (1997). Calculating irradiance penetration into water bodies from the measured beam attenuation coefficient. *Limnol. Oceanogr.* 42(2), 379-385. doi:10.4319/lo.1997.42.2.0379.

Austin, R.W. and Petzold, T.J. (1981). The determination of the diffuse attenuation coefficient of sea water using the coastal zone colour scanner. In: Gower, J.F.R. (ed.) Oceanography from Space. Marine Science, vol 13. Springer, Boston, MA. doi:10.1007/978-1-4613-3315-9_29.

Babbin, A.R., Bianchi, D., Jayakumar, A., and Ward, B.B. (2015). Rapid nitrous oxide cycling in the suboxic ocean. *Science* 348(6239), 1127-1129. doi:10.1126/science.aa8380.

Bange H.W., Arévalo-Martínez, D.L., de la Paz, M., et al. (2019). A harmonized nitrous oxide (N2O) ocean observation network for the 21st century. *Front. Mar. Sci.* 6. doi:10.3389/fmars.2019.00157.

Battaglia, G. and Joos, F. (2018). Marine N_2O emissions from nitrification and denitrification constrained by modern observations and projected in multimillennial global warming simulations. *Global Biogeochem. Cy.* 32(1), 91-121. doi:10.1002/2017GB005671.

Bianchi, D., Dunne, J.P., Sarmiento, J.L., and Galbraith, E.D. (2012). Data-based estimates of suboxia, denitrification, and N_2O production in the ocean and their sensitivities to dissolved O_2. *Global Biogeochem. Cy.* 26, GB2009. doi:10.1029/2011GB004209.

Bishop, J.K.B., Rossow, W.B., and Dutton, E.G. (1997). Surface solar irradiance from the International Satellite Cloud Climatology Project 1983-1991. *J. Geophys. Res. Atmos.* 102(D6), 6883-6910. doi:10.1029/96JD03865.

Breitburg, D., Levin, L.A., Oschlies, A., et al. (2018). Declining oxygen in the global ocean and coastal waters. *Science* 359(6371). doi:10.1126/science.aam7240.

Bristow, L.A., Dalsgaard, T., Tiano, L., et al. (2016). Ammonium and nitrite oxidation at nanomolar oxygen concentrations in oxygen minimum zone waters. *Proc. Natl. Acad. Sci. U.S.A.* 113(38), 10601-10606. doi:10.1073/pnas.1600359113.

Bunce, J. (2019). Variation in responses of photosynthesis and apparent Rubisco kinetics t otemperature in three soybean cultivars. *Plants* 8(11), 443. doi:10.3390/plants8110443.

Burdige, D.J. and Komada, T. (2011). Anaerobic oxidation of methane and the stoichiometry of remineralization processes in continental margin sediments. *Limnol. Oceanogr.* 56(5), 1781-1796. doi:10.4319/lo.2011.56.5.1781.

Capone, D.G., Bronk, D.A., Mulholland, M.R., and Carpenter, E.J. (2008). Nitrogen in the Marine Environment (Second Edition). Academic Press. 1445-1495. doi:10.1016/B978-0-12-372522-6.00033-5.

Casciotti, K.L., Forbes, M., Vedamati, J., et al. (2018). Nitrous oxide cycling in the Eastern Tropical South Pacific as inferred from isotopic and isotopomeric data. *Deep-Sea Res.* 156, 155-167. doi:10.1016/j.dsr2.2018.07.014.

Christian, J.R., Denman, K.L., Hayashida, H., et al. (2022). Ocean biogeochemistry in the Canadian Earth System Model version 5.0.3: CanESM5 and CanESM5-CanOE. *Geosci. Model Dev.* 15, 4393-4424. doi:10.5194/gmd-15-4393-2022.

Ciais, P., Sabine, C., Bala, G., & Peters, W. (2013). Carbon and Other Biogeochemical Cycles. In T. F. Stocker, D. Qin, G. K. Plattner, M. Tignor, S. K. Allen, J. Boschung, A. Nauels, Y. Xia, V. Bex, & P. M. Midgley (Eds.), *Climate Change 2013: The Physical Science Basis. Contribution of Working Group I to the Fifth Assessment Report of the Intergovernmental Panel on Climate Change* (465-570). Cambridge University Press. doi:10.1017/CBO9781107415324.015.

Coates, C.J. and Wyman, M. (2017). A denitrifying community associated with a major, marine nitrogen fixer. *Environ. Microbiol.* 19(12), 4978-4992. doi:10.111/1462-2920.14007.

Codispoti, L.A., Brandes, J.A., Christensen, J.P., et al. (2001). The oceanic fixed nitrogen and nitrous oxide budgets: Moving targets as we enter the anthropocene? *Sci. Mar.* 65(2), 85-105. doi:10.3989/scimar.2001.65s285.

Codispoti, L.A. (2007). An oceanic fixed nitrogen sink exceeding 400 Tg N a^{-1} vs the concept of homeostasis in the fixed-nitrogen inventory. *BG* 4, 233-253. doi:10.5194/bg-4-233-2007.

Codispoti, L.A. (2010). Interesting times for marine N_2O. *Science* 327(5971), 1339-13340. doi:10.1126/science.1184945.

Cram, J.A., Fuchsman, C.A., Duffy, M.E., et al. (2021). Slow particle remineralization, rather than suppressed disaggregation, drives efficient flux transfer through the eastern tropical North Pacific oxygen deficient zone. *Global Biogeochem. Cy.* 36(1), e2021GB007080. doi:10.1029/2021GB007080.

Dalsgaard, T., Stewart, F.J., Thamdrup, B., et al. (2014). Oxygen at nanomolar levels reversibly suppresses process rates and gene expression in anammox and denitrification in the oxygen minimum zone off Northern Chile. *mBio* 5(6), e01966-14. doi:10.1128/mBio.01955-14.

Dalsgaard, T., Thamdrup, B., and Canfield, D.E. (2005). Anaerobic ammonium oxidation (anammox) in the marine environment. *Microbiol. Res.* 156(4), 457-464. doi:10.1016/j.resmic.2005.01.011.

Dalsgaard, T., Thamdrup, B., Farías, L., and Revsbech, N.P. (2012). Anammox and denitrification in the oxygen minimum zone of the eastern South Pacific. *Limnol. Oceanogr.* 57(5), 1331-1346. doi:10.4319/lo.2012.57.5.1331.

Dekas, A.E., Poretsky, R.S., and Orphan, V.J. (2009). Deep-sea archaea fix and share nitrogen in methane-consuming microbial consortia. *Science* 326(5951), 422-426. doi:10.1126/science.1178223.

Devol, A.H. (1978). Bacterial oxygen uptake kinetics as related to biological processes in oxygen deficient zones of the oceans. *Deep-Sea Res.* 2, 137-146. doi:10.1016/0146-6291(78)90001-2.

Devol, A.H. and Hartnett, H.E. (2001). Role of the oxygen-deficient zone in transfer of organic carbon to the deep ocean. *Limnol. Oceanogr.* 46(7), 1684-1690. doi:10.4319/lo.2001.46.7.1684.

Devol, A.H. (2008). Denitrification including anammox. In D.G. Capone, D.A. Bronk, M.R. Mulholland, E.J. Carpenter (eds) *Nitrogen in the Marine Environment* (Second Edition, 263-301). Academic Press. doi:10.1016/B978-0-12-372522-6.00033-5.

DeVries, T., Deutsch, C., Primeau, F., et al. (2012). Global rates of water-column denitrification derived from nitrogen gas measurements. *Nat. Geosci.* 5, 547-550. doi:10.1038/ngeo1515.

Dore, J.E. and Karl, D.M. (1996). Nitrite distributions and dynamics at station ALOHA. *Deep-Sea Res.* 43(2-3), 385-402. doi:10.1016/0967-0645(95)00105-0.

Eugster, O. and Gruber, N. (2012). A probabilistic estimate of global marine N-fixation and denitrification. *Global Biogeochem. Cy.* 26(4). doi:10.1029/2012GB004300.

Eying, V., Bony, S., Meehl, G.A., et al. (2016). Overview of the Coupled Model Intercomparison Project phase 6 (CMIP6) experimental design and organization. *Geosci. Model Dev.* 9, 1937-1958. doi:10.5194/gmd-9-1937-2016.

Freing, A., Wallace, D.W.R., and Bange, H.W. (2012). Global oceanic production of nitrous oxide. *Philos. Trans.R. Soc. Lond. B. Biol. Sci.* 367(1593), 1245-1255. doi:10.1098/rstb.2011.0360.

Froelich, P.N., Klinkhammer, G.P., Bender, M.L., et al. (1979). Early oxidation of organic matter in pelagic sediments of the eastern equatorial Atlantic: suboxic diagenesis. *Geochim. Cosmochim. Acta*. 43(7), 1075-1090. doi:10.1016/0016-7037(79)90095-4.

Fuenzalida, R., Schneider, W., Garcés-Vargas, J., Bravo, L., and Lange, C. (2009). Vertical and horizontal extension of the oxygen minimum zone in the eastern South Pacific Ocean. *Deep-Sea Res.* 56(16), 992-1003. doi:10.1016/j.dsr2.2008.11.001.

Garcia, H.E., Weathers, K., Paver, C.R., et al. (2018). World Ocean Atlas 2018, Volume 3: Dissolved Oxygen, Apparent Oxygen Uitilzation, and Oxygen Saturation. A. Mishonov Technical Ed.; NOAA Atlas NESDIS 83, 38.

Garcia, H.E., Weathers, K., Paver, C.R., et al. (2018). World Ocean Atlas 2018, Volume 4: Dissolved Inorganic Nutrients (phosphate, nitrate, and nitrate+nitrite, silicate). A. Mishonov Technical Ed.; NOAA Atlas NESDIS 84, 35.

Garcia, H. E., Locarnini, R.A., Boyer, T.P., and Antonov, J.I. (2006). World Ocean Atlas 2005, Volume 3: Dissolved Oxygen, Apparent Oxygen Utilization, and Oxygen Saturation. S. Levitus Technical Ed.; NOAA Atlas NESDIS 63, 342.

Goreau, T.J., Kaplan, W.A., Wofsy, S.C., et al. (1980). Production of NO_2^- and N_2O by nitrifying bacteria at reduced concentrations of oxygen. *Appl. Environ. Microbiol.* 40(3), 526-532.

Gruber, N. and Galloway, J.N. (2008). An Earth-system perspective of the global nitrogen cycle. *Nature* 451, 293-296. doi:10.1038/nature06592.

Grundle, D.S. (2012). Upper water column nitrification processes and the implications of euphotic zone nitrification for estimates of new production. (Doctoral thesis, University of Victoria, BC, Canada). Retrieved from https://dspace.library.uvic.ca/bitstream/handle/1828/4395/Grundle_Damian_Ph.D._2012.pdf.

Grundle, D.S., Löscher, C.R., Krahmann, G., et al. (2017). Low oxygen eddies in the eastern tropical North Atlantic: implications for N_2O cycling. *Sci. Rep.* 7, 4806. doi:10.1038/s41598-017-04745-y.

Hall, D.O. and Rao, K.K. (1999). Photosynthesis (Sixth Edition). Cambridge University Press.

Jayakumar, A., Chang, B.X., Widner, B., et al. (2017). Biological nitrogen fixation in the oxygen-minimum region of the eastern tropical North Pacific ocean. *ISME J.* 11, 2356-2367. doi:10.1038/ismej.2017.97.

Ji, Q., Babbin, A.R., Jayakumar, A., Oleynik, S., and Ward, B.B. (2015). Nitrous oxide production by nitrification and denitrification in the Eastern Tropical South Pacific oxygen minimum zone. *Geophys. Res. Lett.* 42(24), 10755-10764. doi:10.1002/2015GL066853.

Ji, Q., Buitenhuis, E., Suntharalingam, P., Sarmiento, J.L., and Ward, B.B. (2018). Global nitrous oxide production determined by oxygen sensitivity of nitrification and denitrification. *Global Biogeochem. Cy.* 32(12), 1790-1802. doi:10.1029/2018GB005887.

Kalvelage, T., Jensen, M.M., Contreras, S., et al. (2011). Oxygen sensitivity of anammox and coupled N-cycle processes in oxygen minimum zones. *PLoS One* 6(12): e29299. doi:10.1371/journal.pone.0029299.

Kanter, D.R., Ogle, S.M., and Winiwarter, W. (2020). Building on Paris: integrating nitrous oxide mitigation into future climate policy. *Curr. Opin. Environ. Sustain.* 47, 7-12. doi:10.1016/j.cosust.2020.04.005.

Keeling, R.F., Körtzinger, A., and Gruber, N. (2010). Ocean deoxygenation in a warming world. *Ann. Rev. Mar. Sci.* 2, 199-229. doi:10.1146/annurev.marine.010908.163855.

Kelly, C.L., Travis, N.M., Baya, P.A., and Casciotti, K.L. (2020). Quantifying nitrous oxide cycling regimes in the eastern tropical North Pacific ocean with isotopomer analysis. *Global Biogeochem. Cy.* 35(2), e2020GB006637. doi:10.1029/2020GB006637.

Kirk, J.T.O. (1994). Light and Photosynthesis in Aquatic Ecosystems. Cambridge University Press, Cambridge. doi:10.1017/CB09780511623370.

Könneke, M., Bernhard, A.E., de la Torre, J.R., et al. (2005). Isolation of an autotrophic ammonia-oxidizing marine archaeon. *Nature* 437(7058), 543-546. doi:10.1038/nature03911.

Kriest, I. and Oschlies, A. (2015). MOPS-1.0: towards a model for the regulation of the global oceanic nitrogen budget by marine biogeochemical processes. *Geosci. Model Dev.* 8, 2929-2957. doi:10.5194/gmd-8-2929-2015.

Kwiecinski, J.V. and Babbin, A.R. (2021). A high-resolution atlas of the Eastern Tropical Pacific Oxygen deficient zones. *Global Biogeochem. Cy.* 35(12), e2021GB007001. doi:10.1029/2021GB007001.

Lam, P. and Kuypers, M.M.M. (2011). Microbial nitrogen cycling processes in oxygen minimum zones. *Ann. Rev. Mar. Sci.* 3, 317-345. doi:10.1146/annurev-marine-120709-142814.

Laufkötter, C., John, J.G., Stock, C.A., and Dunne, J.P. (2017). Temperature and oxygen dependence of the remineralization of organic matter. *Global Biogeochem. Cy.* 31(7), 1038-1050. doi:10.1002/2017GB005643.

Locarnini, R.A., Mishonov, A.V., Antonov, J.I., Boyer, T.P., and Garcia, H.E. (2010). World Ocean Atlas 2009, Volume 1: Temperature. S. Levitus, Ed.; NOAA Atlas NESDIS 68, 184.

Locarnini, R.A., Mishonov, A.V., Baranova, O.K., et al. (2018). World Ocean Atlas 2018, Volume 1: Temperature. A. Mishonov Technical Ed.; NOAA Atlas NESDIS 81, 52.

Löscher, C.R., Kock, A., Könneke, M., et al. (2012). Production of oceanic nitrous oxide by ammonia-oxidizing archaea. *BG* 9, 2419-2429. doi:10.5194/bg-9-2419-2012.

Makowski, D. (2019). N2O increasing faster than expected. *Nat. Clim. Chang.* 9(12), 909-910. doi:10.1038/s41558-019-0642-2.

Marsay, C.M., Sanders, R.J., Henson, S.A., et al. (2014). Attenuation of sinking particulate organic carbon flux through the mesopelagic ocean. *Proc. Natl. Acad. Sci. U.S.A.* 112(4), 1089-1094. doi:10.1073/pnas.1415311112.

Martens-Habbena, W., Berube, P.M., Urakawa, H., de la Torre, J.R., and Stahl, D.A. (2009). Ammonia oxidation kinetics determine niche separation of nitrifying archaea and bacteria. *Nature* 461, 976-979. doi:10.1038/nature08465.

Martinez-Rey, J., Bopp, L., Gehlen, M., Tagliabue, A., and Gruber, N. (2015). Projections of oceanic N_2O emissions in the 21^{st} century using the IPSL earth system model. *BG* 12, 4133-4148. doi:10.5194/bg-12-4133-2015.

Martiny, A.C., Vrugt, J.A., and Lomas, M.W. (2014). Concentrations and ratios of particulate organic carbon, nitrogen, and phosphorus in the global ocean. *Sci. Data*. 1, 140048. doi:10.1038/sdata.2014.48.

Marsay, C.M., Sanders, R.J., Henson, S.A., et al. (2015). Attenuation of sinking particulate organic carbon flux through the mesopelagic ocean. *Proc. Natl. Acad. Sci. U.S.A.* 112(4), 1089-1094. doi:10.1073/pnas.1415311112.

Medlyn, B.E., Dreyer, E., Ellsworth, D., et al. (2002). Temperature response of parameters of a biochemically based model of photosynthesis. II. A review of experimental data. *Plant Cell Environ.* 25(9), 1167-1179. doi:10.1046/j.1365-3040.2002.00891.x.

Monreal, P.J., Kelly, C.L., Travis, N.M., and Casciotti, K.L. (2022). Identifying the sources and drivers of nitrous oxide accumulation in the eddy-influenced Eastern Tropical North Pacific

oxygen-deficient zone. *Global Biogeochem. Cy.* 36(6), e2022GB007310. doi:10.1029/2022GB007310.

Müller, C., Franke, J., Jägermey, J., et al. (2021). Exploring uncertainties in global crop yield projections in a large ensemble of crop models and CMIP5 and CMIP6 climate scenarios. *Environ. Res. Lett.* 16(3), 034040. doi:10.1088/1748-9326/abd8fc.

Naqvi, S.W.A., Bange, H.W., Farías, L., et al. (2010). Marine hypoxia/anoxia as a source of CH_4 and N_2O. *BG* 7, 2159-2190. doi:10.5194/bg-7-2159-2010.

Nevison, C., Butler, J.H., and Elkins, J.W. (2003). Global distribution of N_2O and the ΔN_2O-AOU yield in the subsurface ocean. *Global Biogeochem. Cy.* 17(4), 1119. doi:10.1029/2003GB002068.

Newell, S.E., Fawcett, S.E., and Ward, B.B. (2013). Depth distribution of ammonia oxidation rates and ammonia-oxidizer community composition in the Sargasso Sea. *Limnol. Oceanogr.* 58(4), 1491-1500. doi:10.4319/lo.2013.58.4.1491.

Nowicki, M., DeVries, T., and Siegel, D.A. (2022). Quantifying the carbon export and sequestration pathways of the ocean's biological carbon pump. *Global Biogeochem. Cy.* 36(3), e2021GB007083. doi:10.1029/2021GB007083.

Pajares, S. and Ramos, R. (2019). Processes and microorganisms involved in the marine nitrogen cycle: Knowledge and gaps. *Front. Mar. Sci.* 6. doi:10.3389/fmars.2019.00739.

Paulmier, A. and Ruiz-Pino, D. (2009). Oxygen minimum zones (OMZs) in the modern ocean. *Prog. Oceanogr.* 80(3-4), 113-128. doi:10.1016/j.pocean.2008.08.001.

Peters, B., Horak, R., Devol, A., et al. (2018) Estimating fixed nitrogen loss and associated isotope effects using concentration and isotope measurements of NO_3^{--}, NO_2^{-}, and N_2 from the Eastern Tropical South Pacific oxygen deficient zone. *Deep Sea Res.* 156, 121-136. doi:10.1016/j.dsr2.2018.02.011.

Portmann, R.W., Daniel, J.S., and Ravishankara, A.R. (2012). Stratospheric ozone depletion due to nitrous oxide: influences of other gases. *Philos. Trans.R. Soc. Lond. B. Biol. Sci.* 367(1593), 1256-1264. doi:10.1098/rstb.2011.0377.

Rahmstorf, S. (2002). Ocean circulation and climate change during the past 120,000 years. *Nature* 419, 207-214. doi:10.1038/nature01090.

Rassamee, V., Sattayatewa, C., Pagilla, K., and Chandra, K. (2011). Effect of oxic and anoxic conditions on nitrous oxide emissions from nitrification and denitrification processes. *Biotechnol. Bioeng.* 108(9), 20136-20145. doi:10.1002/bit.23147.

Raven, J.A. and Geider, R.J. (1988). Temperature and algal growth. *New Phytol.* 110(4), 441-461. doi:10.1111/j.1469-8137.1988.tb00282.x.

Ravishankara, A.R., Daniel, J.S., and Portmann, R.W. (2009). Nitrous oxide (N_2O): The dominant ozone-depleting substance emitted in the 21st century. *Science* 325, 123-125. doi:10.1126/science.1176985.

Redfield, A.C. (1958). The biological control of chemical factors in the environment. *AmSci* 46, 205-22.

Rees, A.P., Brown, I.J., Jayakumar, A., Lessin, G., Somerfield, P.J., and Ward, B.B. (2021). Biological nitrous oxide consumption in oxygenated waters of the high latitude Atlantic Ocean. *Commun. Earth Environ.* 2(36). doi:10.1038/s43247-021-00104-y.

Resplandy, L., Lévy, M., and McGillicuddy Jr., D.J. (2019). Effects of eddy-driven subduction on ocean biological carbon pump. *Global Biogeochem. Cy.* 33(8), 1071-1084. doi:10.1029/2018GB006125.

Revsbech, N.P., Larsen, L.H., Gundersen, J., et al. (2009). Determination of ultra-low oxygen concentrations in oxygen minimum zones by the STOX sensor. *Limnol. Oceanogr.* 7(5), 371-381. doi:10.4319/lom.2009.7.371.

Santoro, A.E., Buchwald, C., Knapp, A.N., et al. (2021). Nitrification and nitrous oxide production in the offshore waters of the Eastern Tropical South Pacific. *Global Biogeochem. Cy.* 34, e2020GB006716. doi:10.1029/2020GB006716.

Schlitzer, R. (2000). Electronic atlas of WOCE hydrographic and tracer data now available. *Eos* 81(5), 45. doi:10.1029/00EO00028.

Schmidtko, S., Stramma, L., and Visbeck, M. (2017). Decline in global oceanic oxygen content during the past five decades. *Nature* 542(7641): 335. doi:10.1038/nature21399.

Schwing, F., Parrish, R., and Mendelssohn, R. (1998). Recent trends in the spatial structure of wind forcing and SST in the California Current System. In: Global versus Local Changes in Upwelling Systems. Editions de L'Orstom. 101-125.

Séférian, R., Nabat, P., Michou, M., et al. (2019). Evaluation of CNRM Earth System Model, CNRM-ESM2-1: Role of Earth System Processes in Present-Day and Future Climate. *J. Adv. Model. Earth Syst.* 11(12), 4182-4227. doi:10.1029//2019MS001791.

Smith, J.M., Chavez, F.P., and Francis, C.A. (2014). Ammonium uptake by phytoplankton regulates nitrification in the sunlit ocean. *PLoS One*, 9(9), e108173. doi:10.1371/journal.pone.0108173.

Snider, D.M., Venkiteswaran, J.J., Schiff, S.L., and Spoelstra, J. (2015). From the ground up: Global nitrous oxide sources are constrained by stable isotope values. *PLOS ONE* 11(2), e0149290. doi:10.1371/journal.pone.0149290.

Stock, C.A., Dunne, J.P., Fan, S., et al. (2020). Ocean biogeochemistry in GFDL's Earth system model 4.1 and its response to increasing atmospheric CO_2. *J. Adv. Model. Earth Syst.* 12(10), e2019MS002043. doi:10.1029/2019MS002043.

Stramma, L., Johnson, G.C., Sprintall, J., and Mohrholz, V. (2008). Expanding oxygen-minimum zones in the tropical oceans. *Science* 320, 655-658. doi:10.1126/science.1153847.

Sun, X., Jayakumar, A., Tracey, J.C., Wallace, E., Kelly, C.L., Casciotti, K.L., and Ward, B.B. (2021). Microbial N_2O consumption in and above marine N_2O production hotspots. *ISME J.* 15, 1434-1444. doi:10.1038/s41396-020-00861-2.

Sun, X., Ji, Q., Jayakumar, A., and Ward, B.B. (2017). Dependence of nitrite oxidation on nitrite and oxygen in low-oxygen seawater. *Geophys. Res. Lett.* 44, 7883-7891. doi:10.1002/2017GL074355.

Suntharalingam, P., Sarmiento, J.L., Toggweiler, J.R. (2000). Global significance of nitrous-oxide production and transport from oceanic low-oxygen zones: A modeling study. *Global Biogeochem. Cy.* 14(4), 1353-1370. doi:10.1029/1999GB900100.

Suntharalingam, P., Buitenhuis, E., Le Quéré, C., et al. (2012). Quantifying the impact of anthropogenic nitrogen deposition on oceanic nitrous oxide. *Geophys. Res. Lett.* 39(7), L07605. doi:10.1029/2011GL050778.

Thamdrup, B. (2012). New pathways and processes in the global nitrogen cycle. *Ann. Rev. Mar. Sci.* 43, 407-428. doi:10.1146/annurev-ecolsys-102710-145048.

Thamdrup, B., Dalsgaard, T., and Revsbech, N.P. (2012). Widespread functional anoxia in the oxygen minimum zones of the Eastern South Pacific. *Deep Sea Res.* 65, 36-45. doi:10.106/j.dsr.2012.03.001.

Tian, H., Xu, R., Canadell, J.G., et al. (2020). *Nature* 586(7828), 248-256. doi:10.1038/s41586-020-2780-0.

Trimmer, M., Chronopooulou, P., Maanoja, S.T., Upstill-Goddard, R.C., Kitidis, V., and Purdy, K.J. (2016). Nitrous oxide as a function of oxygen and archaeal gene abundance in the North Pacific. *Nat. Commun.* 7(13451). doi:10.1038/ncomms13451.

Ulloa, O., Canfield, D.E., DeLong, E.F., et al. (2012). Microbial oceanography of anoxic oxygen minimum zones. *Proc. Natl. Acad. Sci. U.S.A.* 109(40), 15996-16003. doi:10.1073/pnas.1205009109.

Voss, M., Bange, H.W., Dippner, J.W., et al. (2013). The marine nitrogen cycle: recent discoveries, uncertainties and the potential relevance of climate change. *Philos. Trans. R. Soc.* 368, 20130121. doi:10.1098/rstb.2013.0121.

Yool, A., Martin, A.P., Fernández, C., and Clark, D.R. (2007). The significance of nitrification for oceanic new production. *Nature* 447, 999-1002. doi:10.1038/nature05885.

Yool, A., Palmiéri, J., Jones, C.G., et al. (2021). Evaluating the physical and biogeochemical state of the global ocean component of UKESM1 in CMIP6 historical simulations. *Geosci. Model Dev.* 14, 3437-3472. doi:10.5194/gmd-14-3437-2021.

Zamora, L.M. and Oschlies, A. (2014). Surface nitrification: A major uncertainty in marine N_2O emissions. *Geophys. Res. Lett.* 41(12), 4247-4253. doi:10.1002/2014GL060556.

Zhou, Y., Gong, H., and Zhou, F. (2022). Responses of horizontally expanding oceanic oxygen minimum zones to climate change based on observations. *Geophys. Res. Lett.* 49(6), doi:10.1029/2022GL0097724.